



RADON GENERATION, ENTRY AND ACCUMULATION INDOORS

PhD thesis

Lluís Font Guiteras

Grup de Física de les Radiacions

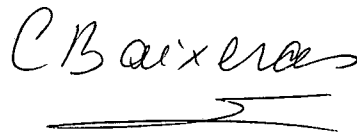
Universitat Autònoma de Barcelona

CARMEN BAIXERAS DIVAR, professora titular del departament de Física de la Facultat de Ciències de la Universitat Autònoma de Barcelona

CERTIFICA:

Que la tesi doctoral "Radon generation, entry and accumulation indoors", realitzada sota la seva direcció per en Lluís Font Guiteras, llicenciat en Ciències Físiques, reuneix les condicions necessàries per a ser llegida davant el tribunal que a tal efecte s'anomeni.

I per a que així consti, signo el present document a Bellaterra, disset de juny de mil nou-cents noranta set.



C. Baixeras



RADON GENERATION, ENTRY AND ACCUMULATION INDOORS

PhD thesis

Lluís Font Guiteras

Grup de Física de les Radiacions

Universitat Autònoma de Barcelona

TABLE OF CONTENTS

1. Introduction and objectives	1
2. Relevant parameters and processes	5
2.1 Radon generation and migration.	5
2.1.1 Soil	5
2.1.1.1 Radon generation	5
2.1.1.2 Radon migration	7
2.1.2 Building materials	15
2.2 Radon entry into houses.	18
2.2.1 Radon entry from soil	19
2.1.1.1 Advective entry	19
2.1.1.2 Diffusive entry	22
2.2.2 Radon entry from building materials	22
2.2.3 Radon entry from water and gas supplies	25
2.2.4 Sum up of all radon entry contributions	26
2.3 Radon accumulation indoors.	28
3. The dynamic sectorial model RAGENA	31
3.1 The Stella II software.	31
3.1.1 Generalities.	31
3.1.2 Software elements.	32
3.1.3 The simulation algorithms.	33
3.1.4 Application of Stella II software to indoor radon dynamic modelling.	33
3.2 Review of the existing radon models.	34
3.2.1 Radon entry into houses.	34
3.2.2 Indoor radon accumulation and its time-evolution.	35
3.3 The RAGENA model.	36
3.3.1 Global structure: sectors.	37
3.3.2 Soil sector.	39
3.3.2.1 Undisturbed soil	43
3.3.2.2 Disturbed soil	43
3.3.3 Building materials sector.	46
3.3.4 Outdoors sector.	47
3.3.5 Water and gas sectors.	48
3.3.6 Indoors sector.	48
3.3.7 Environmental parameters and occupant behaviour sectors.	50
3.3.7.1 Environmental parameters sector	50
3.3.7.1.1 Atmospheric pressure	50
3.3.7.1.2 Indoor-oudoor temperature differences	51
3.3.7.1.3 Wind	51
3.3.7.1.4 Soil temperature	51
3.3.7.1.5 Rainfall	52
3.3.7.2 Occupant behaviour sector	52
3.3.7.2.1 Opening windows and doors pattern	52
3.3.7.2.2 Use of Heating, Ventilating and Air-conditioned Systems (HVAC)	53
3.3.7.3 Equations	53

4. Modelling a reference configuration.	55
4.1 Description of the reference configuration.	55
4.1.1 Building design.	55
4.1.2 The building materials.	56
4.1.3 Soil.	57
4.1.4 Steady-state radon entry.	58
4.1.5 Dynamic radon entry.	59
4.2 Steady-state results.	61
4.2.1 Simulation results.	61
4.2.2 Variability analysis.	66
4.2.2.1 Soil parameters	69
4.2.2.1.1 Radium content and emanation fraction	69
4.2.2.1.2 Water saturation fraction and soil type	69
4.2.2.1.3 Gas-permeability	72
4.2.2.2 Concrete parameters	73
4.2.2.3 Soil-house interface parameters	74
4.2.2.4 Ventilation and air-exchange parameters	75
4.2.3 Sensitivity analysis	76
4.2.3.1 Step functions	76
4.2.3.2 Pulses	78
4.2.3.3 Sinwave	81
4.2.4 Uncertainty analysis	84
4.3 Dynamic results.	85
4.4. Discussion	88
5. Experimental study.	91
5.1 The EU project.	91
5.2 Experimental site.	92
5.2.1 General description	92
5.2.1.1 Test house	92
5.2.1.2 Previous radon studies in the region	93
5.2.2 Equipment.	94
5.2.2.1 Soil radon detectors	94
5.2.2.1.1 Track-etch detector: LR-115	94
5.2.2.1.2 Clipperton	96
5.2.2.2 Indoor radon detectors	99
5.2.2.2.1 Prassi	99
5.2.2.2.2 Makrofol	100
5.2.2.3 Weather station	101
5.2.2.4 Difference pressure sensor	101
5.2.2.5 Permeability device	102
5.3 Calibration and intercomparison activities	104
5.3.1 Radon detectors.	104
5.3.1.1 Passive detectors	104
5.3.1.2 Active detectors	105
5.3.2 Weather station.	110
5.3.3 Pressure differential transducer and permeability device.	110

6. Experimental results.	113
6.1 Time integrated data.	113
6.1.1 Indoor radon data.	113
6.1.2 Soil radon data.	114
6.2 Time-resolved data.	115
6.2.1 Indoor radon data.	116
6.2.2 Soil radon data.	118
6.2.3 Weather station data.	120
6.2.4 Soil-indoor pressure difference data.	122
6.3 Soil characterization data	123
6.3.1 Texture.	123
6.3.2 Permeability.	123
6.3.3 Radium and uranium content.	125
6.4 Discussion	125
7. Model-experiment comparison.	127
7.1 Adaptation of RAGENA model to the test-house.	127
7.1.1 Geometry of the room	128
7.1.2 Soil parameters	128
7.1.3 Soil-indoor pressure difference and ventilation rate	129
7.1.4 Water saturation fraction	131
7.2 Comparison of RAGENA predictions with experimental results.	132
7.2.1 Steady-state results.	132
7.2.2 Dynamic results.	133
8. Conclusions.	137
8.1 Results obtained.	137
8.2 Perspectives for future work.	141
References	143
List of Figures and Tables	149
Glossary of the principal symbols	157
Annexes	161

1

Introduction and objectives

Since indoor radon (^{222}Rn) has been identified as the largest single source of radiation exposure to population, an increasing number of programs have been developed to reduce this exposure (Henschel 1994, Cliff et al. 1994, Ennemoser et al. 1995, Fisk et al. 1995, Bonnefous et al. 1996). It is of special importance to understand the processes of radon generation in the sources, transport in the source media, entry into the dwelling, and accumulation indoors in order to i) Locate houses with high radon levels, ii) Determine the most effective mitigation methods, and iii) Improve building design and practises to avoid high radon levels in new dwellings.

Radon generation, transport, entry and accumulation indoors depend on a lot of parameters most of which are time-dependent. This complexity has led to many theoretical and/or experimental studies focused on a partial aspect like for instance, radon entry from soil, radon exhalation from building materials, indoor radon dynamics, etc. As a consequence of these studies, it exists a general understanding on the processes involved from radon generation in the source media to its accumulation indoors and on the parameters that affect these processes as well. However, up to now there has not been any effort to integrate all these knowledge on a global radon dynamic model.

The main objectives of this study are:

- 1) To establish a generic dynamic model on radon generation, entry and accumulation indoors that takes into account simultaneously all the parameters and processes involved, having the possibility of being easily applied to different sites.
- 2) To carry out variability, sensitivity and uncertainty analysis around a generic reference configuration in order to i) determine the most relevant parameters affecting indoor radon from the generic point of view, ii) check the response of the model when the system is hardly stressed in different ways with the aim to identify any limitation of the model, and iii) obtain the uncertainty associated to the model predictions when the input parameters follow a given distribution.
- 3) To carry out an experimental study in a real inhabited house typical for the Mediterranean climate, to characterise the radon levels in the house and in the soil underneath.

4) To adapt the model to the data available from the experimental site to check the model predictions in a real site and to characterise the relevant radon sources, entry processes, and factors affecting its accumulation indoors.

Conceptually, this report is structured into four parts:

The first part (chapter 2) consists of a review on the relevant parameters and processes involved in the field of radon in houses, and contains a representative summary of experimental data collected from the literature, given in tables.

The second part (chapters 3 and 4) constitutes the theoretical work, which is divided into two chapters: In chapter 3 we describe in detail the global dynamic model of radon generation, entry and accumulation indoors (RAGENA). This model has a sectorial structure that allows the integration of all the radon sources and processes affecting indoor radon dynamics in a multi-zone house from the dynamic point of view, and constitutes a new integrated approach to model indoor radon dynamics by means of a simple numerical method. The model is applied in chapter 4 to a generic reference configuration corresponding to a mixture of basement and slab-on-grade house. The reference configuration has been determined by assigning to the parameters common values from the literature, and the behaviour of the model is explored by uncertainty, variability and sensitivity analysis.

The third part is the experimental work (chapters 5 and 6) carried out in this study. Chapter 5 outlines the EU project within which the work has been performed and describes the experimental site and the quality assurance efforts. This work presents, for the first time in Spain, a characterisation of a real inhabited and typical house from the radon diagnosis point of view; indoor radon, soil radon, weather parameters and other complementary information has been collected continuously for a period of one year within the frame of the EU project. The experimental data obtained is presented and discussed in chapter 6.

The fourth part of the report (chapter 7) is the adaptation of the model to the experimentally studied house (test-house), showing how the model can be adapted to the information available in a given site; this is an important feature of the model: its conceptual simplicity allows the user to adapt it to different situations easily, without the need of a very detailed description of the site. The model predictions in both the steady-state and the dynamic state are compared with the experimental data.

The report finishes in chapter 8 with the conclusions obtained and outlines the perspectives for future work opened with this study.

2

Relevant parameters and processes

The purpose of this chapter is to give an overview of the parameters and processes related to indoor radon dynamics. We have divided the processes by which radon atoms accumulate indoors into three steps: the first one is radon generation and migration in the source medium, the second is its entry into the houses and the third is its accumulation indoors. The chapter is divided into three sections, each corresponding to a given step. Special attention is given to the time-dependence of the parameters and processes. An excellent review of the parameters and processes affecting radon generation, entry into houses and its accumulation is given in the Nazaroff and Nero "Radon and its decay products in indoor air" (Nazaroff and Nero, 1988).

Radon is generated from the radioactive decay of radium in the earth's crust, and indoor radon concentrations depend on the access of this radon to indoor environments. Radon enters into dwellings from different sources, such as the soil or rock under or surrounding the dwellings, building materials, water supplies, natural gas, and outdoor air. It is believed that the most important radon source is the soil underneath or surrounding the building shell and that the second is the building materials, which can have high levels of radium content (UNSCEAR, 1993). Although water and natural gas can constitute an important radon source in some specific cases, they normally do not contribute significantly to indoor radon levels (UNSCEAR, 1993). Outdoor air usually has low radon concentration due to the radon dilution in the atmosphere.

2.1 Radon generation and migration

In this section we describe briefly radon generation and migration in soil and building materials. We do not consider water and natural gas because they simply carry the radon gas, which is dissolved in the fluid medium.

2.1.1 Soil

2.1.1.1 Radon generation

Soil can be treated as a porous medium consisting of organic matter, soil grains and pores filled with water and soil gas. Radon is generated from the radioactive decay of radium which is fixed in

the soil grains. Thus, an important parameter is the radium content of the medium (A_{Ra}) which is typically given as activity per unit mass ($Bqkg^{-1}$). Due to the long half-life of ^{226}Ra (1600 y) the soil radium content can be considered as constant for most of radon studies. When created, the radon atom has a kinetic energy of 86 keV owing to the conservation of the linear momentum and may reach the pore volume of the soil. The fraction of radon atoms generated in the soil grains that reach the pore volume is known as the “emanation coefficient”, “emanating fraction” or “emanating power” and we denote it as f . This emanation coefficient depends basically on the soil grain-size distribution, porosity, and water content. The geometry and size of the soil grains and pores determine the “static” emanation coefficient in the sense that they do not change in time. Water content has a large impact on the emanation coefficient, increasing it when water content increases (Nazaroff and Nero 1988, Markkanen and Arvela 1992, Strong and Levins 1982.). This is due to the lower recoil range for radon in water (0.1 μm) than in air (63 μm): when a radon atom reaches the pore volume, if there is only soil gas, it may reach the next soil grain, but if there is water, the radon atom will be kept in the liquid phase of the soil fluid.

The partition of radon between the gas and liquid phases is given by the coefficient of solubility of radon in water (L), which depends on the temperature as specified in table 2.1. The effect of outdoor air temperature on soil gas temperature is reduced on account of the fact that soil has a low thermal conductivity and therefore, strongly attenuates short-period air temperature variations; only the most strongly variations of air temperature and the seasonal changes may influence on soil air temperature.

$$C_w = LC_g \tag{2.1}$$

where C_w is the radon activity concentration in the liquid-phase of the soil pores (Bqm^{-3}).
 C_g is the radon activity concentration in the gas-phase of the soil pores (Bqm^{-3}).

Table 2.1: Radon solubility in water as function of temperature (from Andersen 1992 p.9)

Temp K	L -
273.15	0.5249
278.15	0.4286
283.15	0.3565
288.15	0.3016
293.15	0.2593
298.15	0.2263
303.15	0.2003
308.15	0.1797

The equilibrium of radon between both phases is achieved rapidly; a characteristic time of 0.1 sec for transport from water to air is estimated in Nazaroff and Nero 1988, p.78.

2.1.1.2 Radon migration.

Once radon is in the pore volume of the soil, it migrates, basically through the larger pores, by two principal mechanisms: diffusive and advective flows. The first one is governed by the Fick's law, which relates a concentration gradient to a flow through the diffusion coefficient. Depending on whether bulk or pore volume is used to determine concentration and bulk or pore area to determine flow density, different diffusion coefficient result: the "bulk" diffusion coefficient (D) relates the gradient of the interstitial concentration to the flow density across a geometric or bulk area; the "effective" or "interstitial" diffusion coefficient (D_e) relates the gradient of the interstitial concentration to the flow density across the pore area. Both coefficients are related by the porosity of the soil ε

$$D = D_e \varepsilon \quad (2.2)$$

then the Fick's law can be written as

$$\Phi_d = -D_e \nabla C_{Rn} \quad (2.3)$$

where

- Φ_d is the diffusive flow density of radon activity per unit of pore area of the soil ($\text{Bqm}^{-2}\text{s}^{-1}$).
- D_e is the effective diffusion coefficient (m^2s^{-1}).
- C_{Rn} is the interstitial radon activity concentration (Bqm^{-3}).

A parameter equivalent to the effective diffusion coefficient is the diffusion length l_d (m). They are related through the expression

$$l_d = \sqrt{D_e \lambda_{Rn}^{-1}} \quad (2.4)$$

where λ_{Rn} is the radon decay constant (s^{-1}).

The advective flow follows the Darcy's law, which relates the apparent velocity of fluid flow through the soil to the pressure gradient

$$v = -\frac{k}{\mu} \nabla P \quad (2.5)$$

where

- v is the superficial velocity vector (ms^{-1}), that is, the flow per unit geometrical area defined over an element of volume large relative to individual pores but small relative to the overall dimensions of the soil (Nazaroff 1988).
- k is the gas-permeability of the soil (m^2) and shows how easily a gas may flow through the soil.
- P is the pressure field (Pa).
- μ is the dynamic viscosity of the gas-phase of the soil pores (Pa.s).

The advective flow density or radon activity across the pore area is then calculated by multiplying the Darcy's velocity by the radon activity concentration in the soil pores and dividing by the soil porosity

$$\Phi_a = \frac{C_{Rn}}{\varepsilon} v = -\frac{C_{Rn}}{\varepsilon} \frac{k}{\mu} \nabla P \quad (2.6)$$

The total radon flow is a combination of diffusive and advective flows

$$\Phi = \Phi_d + \Phi_a = -D_e \nabla C_{Rn} - \frac{C_{Rn}}{\varepsilon} \frac{k}{\mu} \nabla P \quad (2.7)$$

When trying to relate soil physical parameters to the effective diffusion coefficient and the soil permeability, it has been found that the effective diffusion coefficient depends basically on the soil porosity and water content and that the permeability depends on the soil type (size and shape of the pores), porosity, and water content (Nazaroff and Nero, 1988; Nielson et al. 1994).

The effective diffusion coefficient has an upper bound given by the diffusion coefficient of radon in open air (D_0), $1.2 \times 10^{-5} \text{ m}^2\text{s}^{-1}$. Experimental measurements of D_e over one thousand soil samples ranging from sandy gravel to fine clays and from dried to saturated soils ranged from 10^{-10} to $10^{-5} \text{ m}^2\text{s}^{-1}$ (Nielson et al. 1994). The diffusion coefficient for radon in dry materials is four orders of magnitude greater than that through saturated materials, showing that water content within the porous media is the most important variable affecting the diffusion coefficient (IAEA 1992).

The soil gas-permeability is a very important parameter because of the very broad range of values it assumes, as shown in Fig. 2.1, where it can be seen that permeability can span up to 10 orders of magnitude. Due to the fact that soil normally is neither isotropic nor homogeneous, permeability

may have privileged directions and might be described by a 3 x 3 matrix. In addition to the soil type, porosity, and water content, other factors may change the soil permeability like, for instance: in clay soils, permeability is governed by fracture patterns developed as the soil dries out (Scott, 1994); the type of vegetation may influence on permeability by the root channelling (Morris and Fraley, 1994). It has also been seen that soil permeability depends on the spatial scale; Garbesi (1993) developed a new technique for measuring soil permeability to air (dual-probe dynamic pressure technique) that has the possibility of making measurements over a significant range of length scales and that allows unambiguous detection of anisotropy of permeability.

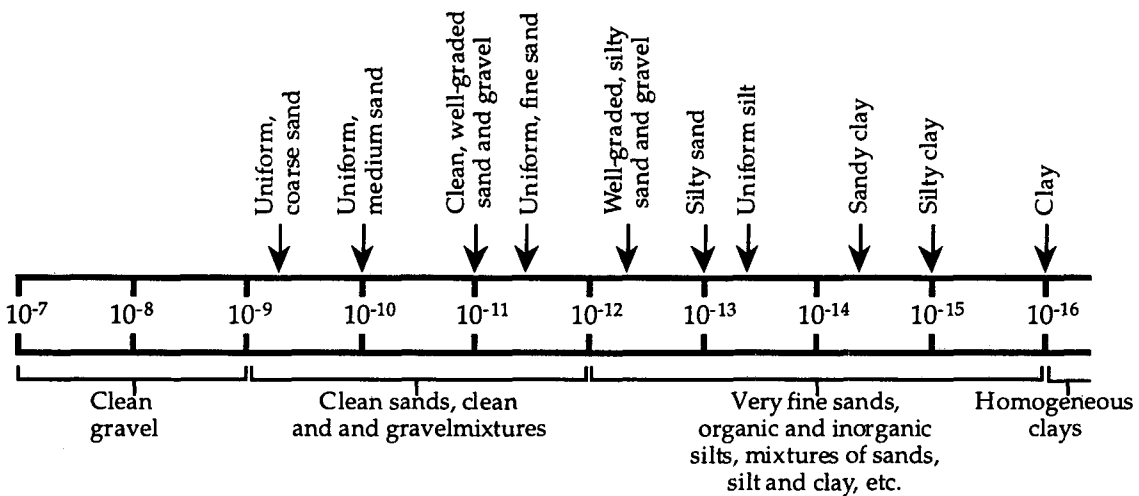


Fig. 2.1: Typical soil permeability values (m^2) (from Nazaroff and Nero 1988 p.62).

Summing up, radon migration in soil is driven by two independent processes, the movement of radon atoms as a response to a gradient of radon concentration (diffusion) independently of a soil gas flow due to a pressure gradient (advection). These two processes are described by the parameters D_e , k , ϵ , and μ and by the concentration and pressure gradients. The dynamic viscosity and the porosity are constant, but the effective diffusion coefficient and the permeability are time-dependent: in a given site, they change because of the change on the water content (due to rainfall and irrigation) and in the case of permeability, also because of other dynamic processes (developing of fracture patterns, root channelling,...). Pressure and concentration gradients may change in time as well. Of particular importance is the effect of barometric pressure changes, which usually have an inverse influence on the movement of soil gases to the atmosphere: When barometric pressure decreases, gas flux from soil to the atmosphere increases because the air-pumping phenomenon; increasing pressures tend to force atmospheric air into the soil (Chen and Thomas 1995).

In order to describe the migration of radon in the soil, a transport equation is required. The derivation of the transport equation implies the assumption of some simplifications. Several

examples of soil radon transport equations can be obtained from the literature (Andersen 1992, Loureiro 1987, Nazaroff and Nero 1988, etc.). They are all basically equivalent; the differences are due to the different approximations and specially to whether water content is considered or not. Normally the equation does not have analytical solution and numerical techniques are needed. Perhaps the most general transport equation is given in Nazaroff and Nero (1988)

$$\frac{1}{\varepsilon} \frac{\partial (C_g \varepsilon_g + C_w \varepsilon_w)}{\partial t} = \nabla \cdot D'_e \nabla C_g - \nabla \cdot C_g \frac{v'}{\varepsilon_g} + f' \rho_{gr} \frac{1-\varepsilon}{\varepsilon} A_{Ra} \lambda_{Rn} - \frac{1}{\varepsilon} \lambda_{Rn} (C_g \varepsilon_g + C_w \varepsilon_w) \quad (2.8)$$

where

- ε is the soil porosity (dimensionless).
- C_g is the radon activity concentration in the gas-filled volume of the soil pores (Bqm^{-3}).
- ε_a is the gas-porosity, defined as the ratio between the gas-filled volume of the soil pores and the total soil pore volume.
- C_w is the radon activity concentration in the water-filled pore volume of soil (Bqm^{-3}).
- ε_w is the water-porosity, defined as the ratio between the water-filled volume of the soil and the total soil pore volume, so that $\varepsilon = \varepsilon_g + \varepsilon_w$
- D'_e is the effective diffusion coefficient (m^2s^{-1}) corrected by the effect of the water content.
- v' is the superficial velocity vector of soil gas (ms^{-1}).
- f' is the emanation coefficient (dimensionless) corrected by the effect of the water content.
- ρ_{gr} is the density of the soil grains (kgm^{-3}).
- A_{Ra} is the radium activity concentration in the soil (Bqkg^{-1}).

In the right hand of the Eq. (2.8), the first term corresponds to the diffusive transport, the second to the advective transport, the third to the radon generation and the fourth to the radon radioactive decay. Eq. (2.8) is obtained from a conservation-of-mass equation and has the following implicit approximations:

- 1) Any transport of radon that may result from the diffusion of another species in air is neglected.
- 2) As in open air, all the kinetic interactions of the radon atoms occur with gas molecules. This assumption is reasonable when the pores are large relative to the mean free path of the radon atoms, $0.065 \mu\text{m}$ at 25°C .
- 3) Any possible adsorption of radon on the surfaces of the soil grains is neglected.
- 4) Any moisture migration and any migration of radon within the water are neglected.

Eq. (2.8) can be simpler by considering the following additional assumptions:

- 5) The water content is negligible.
- 6) The superficial velocity vector is described by Darcy's Law.
- 7) The soil is isotropic and homogeneous with respect to the diffusion coefficient, permeability, porosity, emanation coefficient, radium content, and bulk density.
- 8) Soil gas is incompressible for the range of pressures of interest.

Then, Eq. (2.8) can be written

$$\frac{\partial(C_g)}{\partial t} = D_\epsilon \nabla^2 C_g + \frac{k}{\epsilon \mu} \nabla P \cdot \nabla C_g + G - \lambda_{Rn} C_g \quad (2.9)$$

$$\text{where } G = f \rho_{gr} \frac{1-\epsilon}{\epsilon} A_{Ra} \lambda_{Rn} \text{ is the generation term (Bq}\cdot\text{m}^{-3}\cdot\text{s}^{-1}\text{)} \quad (2.10)$$

Many studies suggest that diffusion is the dominant mechanism by which radon enters the atmosphere from uncovered soil (Nazaroff and Nero 1988)). Much of the early research on radon transport focused on its applications in the earth and atmospheric sciences, and diffusion plays a central role in many of these applications. The steady state solution of Eq. (2.9) for a semi-infinite, and homogeneous soil layer is easy to obtain in one-dimensional form. In the case of being diffusion the dominant mechanism, the solution is

$$C_g(x) = C_\infty (1 - \exp(-\frac{x}{l_d})) \quad (2.11)$$

where $C = G / \lambda_{Rn}$ is the deep-soil radon activity concentration, which corresponds to the concentration in secular equilibrium with radium, and the atmospheric radon concentration has been set to zero. The diffusion length corresponds then to the distance at which radon concentration is reduced a factor $(1-e^{-1})$ with respect to the deep-soil radon concentration.

The solution of an advection-dominated soil layer is also easy to obtain if we consider a constant Darcy's velocity of the gas in the soil layer and we set the atmospheric radon concentration to zero

$$C_g(x) = C_\infty (1 - \exp(-\frac{x}{l_a})) \quad (2.12)$$

where, by analogy, we have defined the “advection length” as that at which radon concentration is reduced a factor $(1-e^{-1})$

$$l_a = \frac{v}{\varepsilon} \frac{1}{\lambda_{Rn}} = \frac{v}{\varepsilon} \tau_{Rn} \quad (2.13)$$

where τ_{Rn} is the radon mean-life (s). This definition is the one to be expected considering the apparent velocity vector across the pore area (that is, divided by the porosity).

In the case of being both diffusion and advection relevant radon transport mechanisms, the one-dimensional steady-state solution of Eq. 2.9 under the previous boundary conditions is

$$C_g(x) = C_\infty \left\{ 1 - \exp \left[\frac{1}{2l_d^2} \left(l_a - \sqrt{l_a^2 + 4l_d^2} \right) x \right] \right\} \quad (2.14)$$

and we define therefore the “migration distance” as a typical distance that radon can migrate in the soil and in which radon concentration is reduced a factor $(1-e^{-1})$ compared with the deep soil radon concentration

$$M_d = \frac{1}{2} \left(l_a + \sqrt{l_a^2 + 4l_d^2} \right) \quad (2.15)$$

To obtain expression 2.15 we have assumed that the atmospheric radon concentration is zero, which is a very reasonable assumption. However, when we consider the interface between the soil and the indoors instead of the soil and the outdoors, the value of the indoor radon concentration might be taken into account. Then, expressions (2.14) and (2.15) can be corrected by imposing as boundary condition that radon concentration is C_0 at $x=0$. The radon profile and the migration distance obtained are

$$C_g(x) = (C_0 - C_\infty) \exp \left[\frac{1}{2l_d^2} \left(l_a - \sqrt{l_a^2 + 4l_d^2} \right) x \right] + C_\infty \quad (2.16)$$

$$M_d = \left(1 - \frac{C_0}{C_\infty} \right) \frac{1}{2} \left(l_a + \sqrt{l_a^2 + 4l_d^2} \right) \quad (2.17)$$

Expressions (2.11), (2.12), (2.14), (2.15), (2.16) and (2.17) have been obtained by standard methods to solve ordinary differential equations and their derivation is given in Annex 1. Since the pressure

gradient, the permeability, and the diffusion coefficient of the soil may change in time, we expect the migration distance to have a high time-dependence.

Tables 2.2 summarizes this section showing all the parameters related with radon generation and migration in soil.

Table 2.2: Parameters related with radon generation and migration in soil.

Parameter	Definition	Units	Factors affecting it	Time-behaviour
Radium content	Radium activity concentration per dry mass	Bqkg ⁻¹		Ctant
Emanation coefficient	Fraction of Rn atoms generated that reach the pore volume		Water content Porosity Grain-size distribution	Dynamic
Emanation rate	Number of Rn atoms that emanate into the pores per unit time and mass.	atoms kg ⁻¹	Water content Porosity Grain-size distribution	Dynamic
Effective diffusion coefficient	Relates interstitial gradient with pore area: Fick's law	m ² s ⁻¹	Water content Porosity	Dynamic
Gas-permeability	Relates apparent velocity through the soil with pressure gradient: Darcy's law	m ²	Water content Grain-size and shape distribution Porosity	Dynamic
Solubility of Rn in water	Ration between water and gas radon concentrations when equilibrium		Temperature	Dynamic
Dynamic viscosity		Pa s		Ctant

In table 2.3 a literature review of experimental soil data is given.

Table 2.3: Literature review of soil radon generation and migration parameters data

Parameter	Common value	Range	Remarks	Reference
Radium content (Bqkg ⁻¹)	41	9-155	USA surface soils	Nazaroff et al. (1988)
	37	2.4-430	China surface soils	UNSCEAR (1993)
		5-25	Nordic countries: sand and silt	UNSCEAR (1993)
		20-120	Nordic countries: clay	"
		20-80	Nordic countries: moraine	"
		100-1000	Nordic countries: soils with alum shale	"
	3.68±0.13		Dried homogeneous sand	Van der Graaf et al. (1994)
		176-216	Dense glacial till - site 1	Holkko and Liukkonen (1993)
	77.5		Dense glacial till - site 5	"
	75		Esker sand	Markkanen and Arvela (1992)
78	50% in (61-92)	Clay	"	

	52	50% in (38-63)	Silt	"
	54	50% in (31-61)	Sand	"
	81	50% in (53-100)	Gravel	"
	126	50% in (56-95)	Till	"
		720-1760	Shale bearing soil	Stranden et al. (1984)
		67-98		Washington and Rose (1992)
	54±4			Gadd and Borak (1994)
	30			Robinson and Sextro (1995)
Emanation	0.2	0.02-0.7	Literature review up to 1988	Nazaroff et al. (1988)
coefficient	0.23	0.02-0.83	Various soil types	UNSCEAR (1993)
	0.13±0.02		Sand	Van der Graaf et al. (1994)
	0.13	0.15-0.24	Dense glacial till - site 1	Holkko and Liukkonen (1993)
	0.19		Dense glacial till - site 5	"
	0.24		Esker sand	"
	0.18	50% in (0.17-0.31)	Clay	Markkanen and Arvela (1992)
	0.17	50% in (0.11-0.24)	Silt	"
	0.19	50% in (0.11-0.22)	Sand	"
	0.20	50% in (0.15-0.23)	Gravel	"
		50% in (0.12-0.25)	Till	"
	0.26			Rogers and Nielson (1991)
	0.38		Gravelly sandy loam	Schery et al. (1984)
		0.18-0.25		Washington and Rose (1992)
	0.10±0.02			Gadd and Borak (1994)
		0.31-0.45		Robinson and Sextro (1995)
Eman. rate	9.7±0.5	2.5-20	Sand and sandy clay	Andersen (1992)
(atoms kg⁻¹s⁻¹)	15	50% in (9-18)	Clay	Markkanen and Arvela (1992)
	11	50% in (8-14)	Silt	"
	6	50% in (4-8)	Sand	"
	7	50% in (4-8)	Gravel	"
	10	50% in (5-9)	Till	"
Effect. diff.	10 ⁻⁶	10 ⁻¹⁰ -10 ⁻⁵	Literature review up to 1988	Nazaroff et al. (1988)
coeff. (m²s⁻¹)	8.6·10 ⁻⁶			Rogers and Nielson (1991)
	9·10 ⁻⁷		Gravelly sandy loam	Schery et al. (1984)
		7.99·10 ⁻⁷ -6.61·10 ⁻⁶		Washington and Rose (1992)
		10 ⁻¹⁰ -10 ⁻⁵	From sandy gravel to fine clays	Nielson et al. (1994)
Mean grain		60-2000	Sand	Nazaroff et al. (1988)
diameter (µm)		2-60	Silt	"
		<2	Clay	"
	3000		Dense glacial till - site 1	Holkko and Liukkonen (1993)
	1300		Dense glacial till - site 5	"
	800		Esker sand	"
Porosity	0.5	0.2-0.6		Nazaroff et al. (1988)
	0.53	0.46-0.57	Sand and sandy clay	Andersen (1992)
	0.36±0.02		Sand	Van der Graaf et al. (1994)
	0.41			Rogers and Nielson (1991)
	0.35		Gravelly sandy loam	Schery et al. (1984)
		0.45-0.49		Washington and Rose (1992)
	0.39			Gadd and Borak (1994)

		0.25-0.45	Gas-filled porosity	Robinson and Sextro (1995)
Water saturation fraction	0.1	0.05-0.15	Sand	Nazaroff et al. (1988)
	0.35	0.1-0.58	Silt	"
	0.58	0.48-0.68	Clay	"
	0.32	0.21-0.37	Sand and sandy clay	Andersen (1992)
	0.19			Rogers and Nielson (1991)
		0.06-0.97	From gravely sands to fine clays	Nielson et al. (1994)
Gas permeability (m ²)	10 ⁻¹²	10 ⁻¹⁶ -10 ⁻⁷	All soil types	Nazaroff et al. (1988)
	3·10 ⁻¹²	2·10 ⁻¹⁵ -1.4·10 ⁻¹¹	Sand and sandy clay	Andersen (1992)
	5.45·10 ⁻¹¹		Sand	Van der Graaf et al. (1994)
	10 ⁻¹⁴		Dense glacial till - sites 1 and 5	Holkko and Liukkonen (1993)
	4·10 ⁻¹¹		Esker sand (dried)	"
	1.1·10 ⁻¹¹		Gravely sandy loam	Schery et al. (1984)
		1.6·10 ⁻¹² -9.5·10 ⁻¹¹		Washington and Rose (1992)
		10 ⁻¹⁶ -10 ⁻¹⁰	From gravely sands to fine clays	Nielson et al. (1994)
	10 ⁻¹¹		Sandy clay, loam	Ward et al. (1993)
Solubility of Rn in water	0.30	0.18-0.52		Andersen (1992)
Dynamic viscosity (Pa s)	18·10 ⁻⁶			Andersen (1992)

2.1.2 Building materials.

The principles of radon production and migration in the building materials are the same as in the soil, as building materials can be treated as porous media with a given radium content. An important difference between building materials and soil is that the water content of the building materials do not change in time in the same way as in soil. Emanation and transport processes within the building materials do not change in time as suddenly as in the soil. In the case of concrete, its water content decreases during its first years until it reaches a steady value. This fact explains that different radon diffusion coefficients found in new and old concrete samples (Rogers at al. 1994, 1995). It is believed that the dominant transport mechanism in the building materials is diffusion because most materials that produce radon have very low permeability (Stranden 1988). Then, the steady-state one-dimensional transport equation for radon in the building materials, considering only diffusion and using the diffusion length parameter is

$$\frac{d^2 C_m}{dx^2} - \frac{1}{l_{a,m}^2} C_m = -\frac{G_m}{\lambda_{Rn}} \frac{1}{l_{a,m}^2} \quad (2.18)$$

where

G_m is the generation term in the material, defined by expression (2.10) taking the values corresponding to the building material (Bq·m⁻³·s⁻¹).

$l_{d,m}$ is the diffusion length of the material (m).

C_m is the interstitial radon activity concentration field in the material ($\text{Bq}\cdot\text{m}^{-3}$).

The solution of Eq. (2.18)* depends on the boundary conditions. In case of assuming that radon concentration is zero at both sides of the building material, the solution is given by the expression

$$C_m(x) = \frac{G_m}{\lambda_{Rn}} \left[1 - \frac{\cosh\left(\frac{x}{l_{d,m}}\right)}{\cosh\left(\frac{w_{1/2}}{l_{d,m}}\right)} \right] \quad (2.19)$$

where $w_{1/2}$ is the half-width of the building material and x is the distance from its centre.

In order to be more realistic, we have considered the case in which radon activity concentrations at both sides of the building material are neither zero nor equal. Calling them at the left and right sides C_L and C_R respectively, we obtain the following expression

$$C_m(x) = \frac{C_R}{2} \left[\frac{\cosh\left(\frac{x}{l_{d,m}}\right)}{\cosh\left(\frac{w_{1/2}}{l_{d,m}}\right)} + \frac{\sinh\left(\frac{x}{l_{d,m}}\right)}{\sinh\left(\frac{w_{1/2}}{l_{d,m}}\right)} \right] + \frac{C_L}{2} \left[\frac{\cosh\left(\frac{x}{l_{d,m}}\right)}{\cosh\left(\frac{w_{1/2}}{l_{d,m}}\right)} - \frac{\sinh\left(\frac{x}{l_{d,m}}\right)}{\sinh\left(\frac{w_{1/2}}{l_{d,m}}\right)} \right] + \frac{G_m}{\lambda_{Rn}} \left[1 - \frac{\cosh\left(\frac{x}{l_{d,m}}\right)}{\cosh\left(\frac{w_{1/2}}{l_{d,m}}\right)} \right] \quad (2.20)$$

The derivation of expressions (2.19) and (2.20) is given in Annex 1. Table 2.4 reviews experimental data collected from the literature.

Table 2.4: Building material data from literature

Parameter	Material	Common value	Range	Remarks	Reference
Radium content (Bqkg^{-1})	Concrete		10-80	Literature review	Stranden (1988)
	Clay brick		20-200	up to 1988	"
	Cement		10-50		"
	Granite		100-200		"
	Tuff		100-600		"
	Natural gypsum		5-20		"
	Alum-shale-based lightweight concrete		300-2500		"
	Concrete	62±4			Gadd and Borak (1995)
	Concrete		11-26		Roelofs and Scholten (1994)
	Phosphogypsum		610-1160		Rutherford et al. (1995)
Cement	36±5			Tso et al.. (1994)	

	Sea sand	7			"
	River sand	44±6			"
	Aggregate	136±66			"
	Granite chip	180±31			"
	Concrete block	98±12			"
	Red brick	78±11			"
	Fly ash	164			"
	Bottom ash	82			"
	Gypsum	26			"
	Concrete	18	13-98	Literature review	"
	Brick	40	18-78	Literature review	"
	Concrete	62±4			Ward et al. (1993)
	Concrete		36-87		Rogers and Nielson (1993)
Emanation coefficient	Concrete		0.1-0.4	Literature review	Stranden (1988)
	Brick		0.02-0.1	up to 1988	"
	Gypsum		0.03-0.2		"
	Cement		0.02-0.05		"
	Fly ash		0.002-0.02		"
	Concrete	0.15	0.1 - 0.4		UNSCEAR (1993)
	Brick (clay)	0.04	0.02 - 0.1		"
	Concrete		0.17-0.21		Gadd and Borak (1995)
	Phosphogypsum		0.19-0.20		Rutherford et al. (1995)
	Concrete	0.10±0.03			Tso et al. (1994)
	Light weight concrete	0.31			"
	Red brick	0.08±0.03			"
	Sand brick	0.11±0.02			"
	Bottom ash block	0.07			"
	Granite	0.01±0.02			"
	Concrete		0.01-0.28	Literature review	"
	Brick	0.02	0.005-0.08	Literature review	"
Concrete		0.02-0.09		Rogers and Nielson (1993)	
Emanation rate (10 ⁻⁶ Bq kg ⁻¹ s ⁻¹)	Concrete	21±0.6			Tso et al. (1994)
	Light weight concrete	22			"
	Red brick	13±5			"
	Sand brick	16±6			"
	Bottom ash block	12			"
	Granite	34±15			"
	Concrete	4.0	1.4-21	Literature review	"
	Brick	1.0	0.2-13	Literature review	"
Porosity	Concrete	0.13±0.02			Gadd and Borak (1995)
	Building materials	0.15	0.01 - 0.7		UNSCEAR (1993)
	Concrete		0.13-0.27	Residential concrete	Rogers et al. (1994)
	Concrete		0.16-0.24	Aged concrete	Rogers et al. (1995)
	Concrete	0.21	0.17-0.25		Tso et al. (1994)
	Red brick	0.25	0.24-0.26		"
	Concrete		0.12-0.20		Renken and Rosenberg (1995)
	Concrete		0.17-0.26		Rogers and Nielson (1993)
Bulk density	Concrete	2.1			Gadd and Borak (1995)

(10 ³ kgm ⁻³)	Concrete	1.93-2.26	Residential concrete	Rogers et al. (1994)
	Concrete	1.96-2.12	Aged concrete	Rogers et al. (1995)
Effect. diffusion coeff. (m ² s ⁻¹)	Concrete	7.6·10 ⁻⁹ -8.4·10 ⁻⁸	Literature review	Stranden (1988)
	Brick	8.4·10 ⁻⁸ -3.4·10 ⁻⁷		"
	Gypsum	(1.3-3.6)·10 ⁻⁶		"
	Concrete	(1.13-1.91)·10 ⁻⁷		Gadd and Borak (1995)
	Concrete	7.2·10 ⁻⁹ -5.4·10 ⁻⁷		Renken and Rosenberg (1995)
	Concrete	1.1·10 ⁻⁷ -2.1·10 ⁻⁶		Rogers and Nielson (1993)
	Concrete	2.1·10 ⁻⁸ -5.2·10 ⁻⁷	Residential concrete	Rogers et al. (1994)
	Concrete	(1.5-5.5)·10 ⁻⁷	Aged concrete	Rogers et al. (1995)
Permeability	Concrete	(1.4-5.0)·10 ⁻¹⁶		Renken and Rosenberg (1995)
	Concrete	(3.4-8.7)·10 ⁻¹⁶		Rogers and Nielson (1993)
Water content (% weight)	Concrete	0.0-7.4		Roelofs and Scholten (1994)

2.2 Radon entry into houses.

In this section we discuss the mechanisms and the routes by which radon enters into houses. In the early work on indoor radon it was believed that radon levels in houses were generally low, relatively constant, and that a high radium activity source close to the house was required to account for high indoor radon levels. Radium-rich soil and building materials (specially those having uranium mill tailings) were supposed to be the major sources and radon from these sources was believed to diffuse to the house because of a permanent high concentration gradient. However, the discovering of elevated indoor radon levels in houses built on rock or soil with normal levels of radium and that had not had uranium mill tailings used in the building materials led to the search for other entry processes (Scott, 1994; Scott, 1988). Detailed studies showed that concrete, which is a very common building material, is essentially impermeable to air (Rogers and Nielson 1993), so that radon gas in the soil flows into an structure primarily through cracks, gaps, holes and other penetrations through the building's foundation. Fig. 2.2 shows the entry routes of soil gas into a house. Now it is widely accepted that high entry rates of radon into structures occur through pressure-driven flow processes. Small underpressurization of the house with respect to a normal soil underneath (few Pascals) is enough to provide all the radon needed to give the observed levels in houses. Therefore, there was no longer need to search for an exceptional source, and radon might be a more general problem than initially expected. Following we describe briefly the entry from soil, building materials, and water and gas supplies.

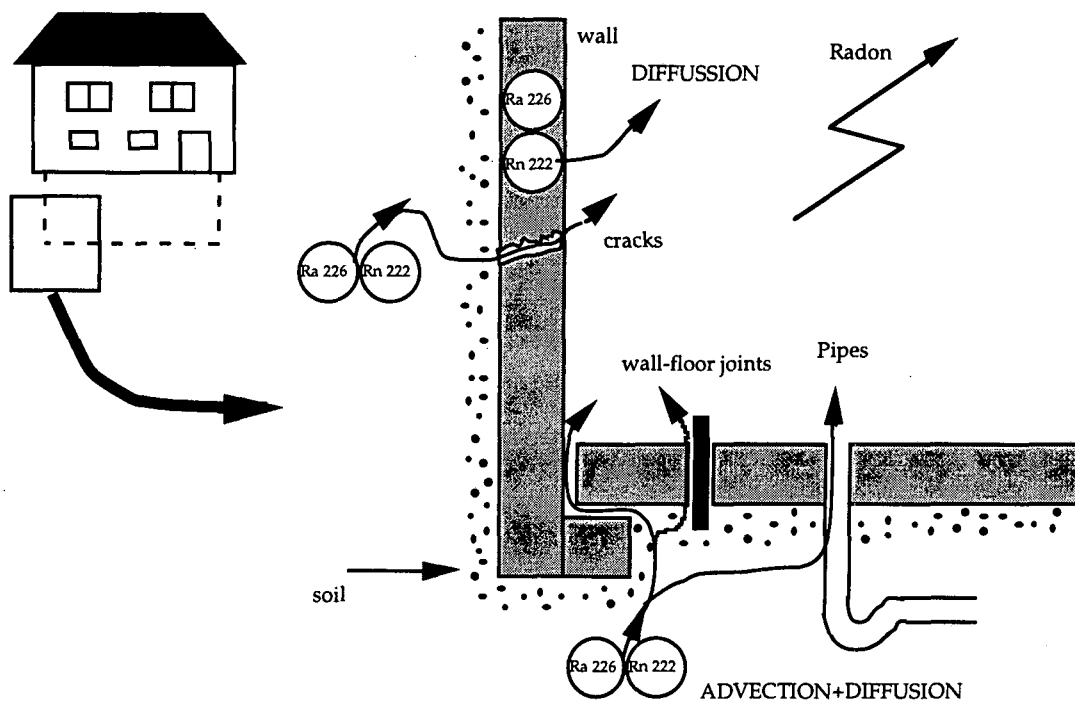


Fig. 2.2: Soil gas entry routes into a house, (from Font 1993 p.19)

2.2.1 Radon entry from soil

As we have said above, soil is normally the major source of indoor radon. A very important factor affecting the radon entry is the design and construction of the building substructure, which controls the degree of movement between the air in the soil and the air in the building. The total cross-sectional area of all penetrations through a foundation is defined as the open area, and has been found to play a complicate role on radon entry into houses (Robinson and Sextro 1995). The presence of the house disturbs the soil underneath: i) compresses the soil and therefore might change its porosity and the size-distribution of the pores, ii) changes the spatial distribution of the moisture content; protecting the soil from the rainfall, so that emanation and transport parameters are affected, and iii) generates a perturbative pressure gradient. The soil underneath the house may have also been brought from other places by the construction company and/or include rests of building materials.

2.2.1.1 Advective entry

The advective entry of soil gas into the houses is driven by indoor-soil pressure differences which are caused by different mechanisms. The first sources of house depressurization investigated were those that generate indoor-outdoor pressure differences and that, assuming the soil has the same pressure that outdoors, induce indoor depressurization with respect to the soil. These sources are 1) wind, 2) indoor-outdoor temperature differences (stack effect) and 3) the use of mechanical systems

such as exhaust fans and Heating, Ventilating and Air-Conditioned systems (HVAC). All these sources generate an underpressurization of few Pascals (normally less than 5 Pa) (Nazaroff et al. 1988; Ward et al. 1993, Cavallo et al. 1994; Hintenlang and Al-Ahmady 1994). The total indoor-outdoor pressure difference across the lower part of a building (ΔP_f) can be written as the sum of the 3 pressure-generating mechanisms (Nazaroff et al 1988)

$$\Delta P_f = \rho_a g(z-z_0) \frac{T_0 - T_i}{T_0} + \beta_p \rho_a \frac{u^2}{2} + \Delta P_{mv,u} \quad (2.21)$$

where

- ρ_a is the air density (kgm^{-3})
- g is the acceleration of gravity (ms^{-2}).
- z is the height of the lower part of the building (m).
- z_0 is the reference height at which the pressure difference due to the stack effect is zero (m).
- T_0 is the outdoor air temperature (K).
- T_i is the indoor air temperature (K).
- β_p is the so-called drag or pressure coefficient (dimensionless).
- u is the wind speed (ms^{-1}).
- $\Delta P_{mv,u}$ is the pressure difference (Pa) generated by the unbalanced mechanical ventilation.

However, the observation that indoor-soil and indoor-outdoor pressure differences were not well coupled in an research house from Florida, led to the conclusion that each of these pressure differences originate from independent mechanisms and must therefore be considered separately in any model of radon entry into houses: indoor-soil pressure differences can result from the slow response of the soil air to outdoor barometric pressure changes compared to the indoor response (Hintenlang and Al-Ahmady, 1992). These pressure differences are often called transient pressure differences. The inertia of soil gas to transmit barometric pressure changes depends mainly on the soil gas-permeability. For a 1 m distance, the characteristic time τ_p for propagation of pressure disturbance in soil can range from 0.01 s for high a permeability soil like gravel up to 10 days for a very low permeability soil as clay and can be estimated from equation (Nazaroff et al. 1988)

$$\tau_p = \frac{l_p^2}{D_p} \quad (2.22)$$

where

- l_p is the distance that the pressure disturbance is propagated (m).
- $D_p = kP_a(\mu\varepsilon)^{-1}$ is a "diffusion coefficient" for pressure disturbances (m^2s^{-1}).

k	is the gas-permeability of the soil (m^2).
P_a	is the atmospheric pressure (Pa).
μ	is the dynamic viscosity of soil gas (Pas-s).
ε	is the soil porosity (dimensionless).

The effect of periodic atmospheric pressure variations on radon entry into buildings has also been studied by Tsang and Narasimhan (1992); they investigated the consequences of the presence of time-dependent periodic variations of barometric pressure as well as a persistent small steady depressurization of about 5 Pa within the basement of a house. From experimental atmospheric pressure data, they found two frequencies and amplitudes of barometric pressure: one with a short period of 0.5 hour and amplitude 50 Pa, and the other with a period of 24 hours and typical amplitude of 250 Pa. They predicted that atmospheric pressure changes can provide transient pressure differences which increase 120% the steady radon entry into the structure. All these studies lead to the conclusion that only time-dependent modelling can try to describe properly radon entry into houses, specially when placed on low-permeability soil.

We have seen in section 2.1.1.2 that the advective flow of radon in the soil follows the Darcy's law and therefore it is a laminar flow. This is a good hypothesis for the soil underneath the house when common values of natural depressurization (5 Pa) are driving the advective transport. However, if high velocities of soil gas occur (up to 1 ms^{-1}) when operating subslab ventilation systems used as mitigation methods, this description is no longer valid; inertial losses, which are proportional to the velocity squared, cannot be neglected and the Darcy-Forchheimer law is required (Bonnefous et al. 1992)

$$\nabla P = -\left(\frac{\mu}{k}\right)(1 + h|v|)v \quad (2.23)$$

where h is the Forchheimer term ($\text{s}\cdot\text{m}^{-1}$) and the other symbols are defined in Eq. (2.5).

The advective soil-gas entry into a building is proportional to $(\Delta P)^v$ where v is a factor to be determined and that ranges from 0.5, corresponding to a turbulence flow, to 1, corresponding to a laminar flow (Cavallo et al. 1994). Turbulence flow may dominate when it is a flow through an opening with a large width-to-depth ratio and for high-velocity air-flow, while laminar flow may dominate for long and narrow openings and when the air-velocity is low. The soil gas entry into a building is a combination of both types of flows. Nielson et al. (1994) used $v = 1$ because they predicted a low-velocity air-flow; Hintenlang and Al-Ahmady (1994) found experimentally $v = 0.69 \pm 0.04$, and the range $0.66 < v < 1$ is given theoretically in Nazaroff et al. (1988).

2.2.1.2 Diffusive entry

Common values of radon concentration of the soil gas are 20 - 80 kBq·m⁻³, which are about 3 orders of magnitude higher than indoor radon levels. Thus, a permanent concentration gradient drives soil radon gas into the house. The diffusive radon entry into the house is approximately constant, constituting a baseline entry rate over which a more time-dependent advective entry rate is added. Even though high entry rates can not be explained only with diffusive entry, in some cases diffusion has been found as the most important entry process (Ward et al. 1993) and its contribution increases with the crack density. Holub and Killoran (1994) analysed the relative importance of diffusion and advection as a function of the crack density, finding that when both flows are plotted as a function of it, a crossover occurs where diffusion starts to dominate. Therefore, both diffusive and advective entries must be considered when modelling radon entry into houses.

2.2.2 Radon entry from building materials

The importance of building materials as radon source is given by the exhalation rate, defined as the amount of radon activity released per unit surface and time from the material, and expressed in Bqm⁻²s⁻¹. Exhalation rate has been found to depend on atmospheric pressure, moisture content and temperature. Experimental evidence shows that a sudden pressure drop results in increased radon exhalation from building materials (Stranden 1988); increasing its temperature increases radon exhalation as well: Tso et al. (1994) reported a factor 4 increase of exhalation when heating building materials from 20°C to 50°C.

Exhalation rate can be obtained from expressions (2.19) and (2.20) by applying the Fick's law, multiplying the effective diffusion coefficient by the porosity because the exhalation is given per unit geometrical surface. The exhalation rate obtained in case of being radon concentration zero at both sides of the material is

$$E(x = w_{1/2}) = E(x = -w_{1/2}) = \lambda_{Rn} A_{Ra,m} \rho_m f_m l_{d,m} \tanh\left(\frac{w_{1/2}}{l_{d,m}}\right) \quad (2.24)$$

where

- λ_{Rn} is the decay constant of ²²²Rn (s⁻¹).
- $A_{Ra,m}$ is the ²²⁶Ra activity concentration in the material (Bqkg⁻¹).
- ρ_m is the density of the material (kgm⁻³).
- f_m is the emanation coefficient (dimensionless).
- $l_{d,m}$ is the diffusion length (m).

$w_{1/2}$ is the material half-thickness (m).

The exhalation rate is equal at each side. This symmetry disappears when radon concentration at the left and right sides of the material (C_L and C_R) are not equal; the exhalation rate at the left and right sides are then

$$\begin{aligned}
 E(x = w_{1/2}) &= \\
 &= \lambda_{Rn} A_{Ra,m} \rho_m f_m l_{d,m} \tanh\left(\frac{w_{1/2}}{l_{d,m}}\right) - l_{d,m} \lambda_{Rn} \epsilon_m \left[\left(\frac{C_R + C_L}{2}\right) \tanh\left(\frac{w_{1/2}}{l_{d,m}}\right) + \left(\frac{C_R - C_L}{2}\right) \cot \operatorname{anh}\left(\frac{w_{1/2}}{l_{d,m}}\right) \right]
 \end{aligned}
 \tag{2.25}$$

$$\begin{aligned}
 E(x = -w_{1/2}) &= \\
 &= \lambda_{Rn} A_{Ra,m} \rho_m f_m l_{d,m} \tanh\left(\frac{w_{1/2}}{l_{d,m}}\right) - l_{d,m} \lambda_{Rn} \epsilon_m \left[-\left(\frac{C_R + C_L}{2}\right) \tanh\left(\frac{w_{1/2}}{l_{d,m}}\right) + \left(\frac{C_R - C_L}{2}\right) \cot \operatorname{anh}\left(\frac{w_{1/2}}{l_{d,m}}\right) \right]
 \end{aligned}
 \tag{2.26}$$

The derivation of expressions (2.24), (2.25) and (2.26) is given in Annex 1. Fig. 2.3 shows the radon concentration profile and the exhalation rate at both sides of a concrete sample for three different boundary conditions: i) $C_R=C_L=0$; ii) $C_R= 100$, $C_L=30000$ and iii) $C_R= 500$, $C_L=100000$ (all the concentrations are expressed in $\text{Bq}\cdot\text{m}^{-3}$). In this Fig. the effect of having different C_R and C_L values is clearly seen: when radon concentration at both sides is negligible, the radon concentration profile inside the building material is symmetric, reaching its maximum value at the centre, and consequently the exhalation rate is equal at both sides (case i)). However, when C_R and C_L are very different, the maximum of the radon concentration inside the material shifts towards the side with higher radon concentration and the exhalation rate at the lower concentration side increases (case ii)). This situation might be found in the wall of a basement in direct contact with a soil having a radon concentration value of $30000 \text{ Bq}\cdot\text{m}^{-3}$ and with an indoor atmosphere having $200 \text{ Bq}\cdot\text{m}^{-3}$. More important this effect is in case iii), where soil radon concentration is higher than the value corresponding to the radon in equilibrium with radium in the building material; now, radon atoms from the soil enter into the building material from the left side and there is not any maximum of radon concentration in the material. As a result, radon exhalation at the right side is raised a lot compared with case i). This situation can be interpreted as a net flow of radon occurring from the soil through the building material into the basement. This result shows that in some cases radon entry into a basement through the foundations by diffusion might not be negligible. In fact, Gadd and Borak (1994) found that 40% of radon entering into a structure came from the soil through the concrete wall.

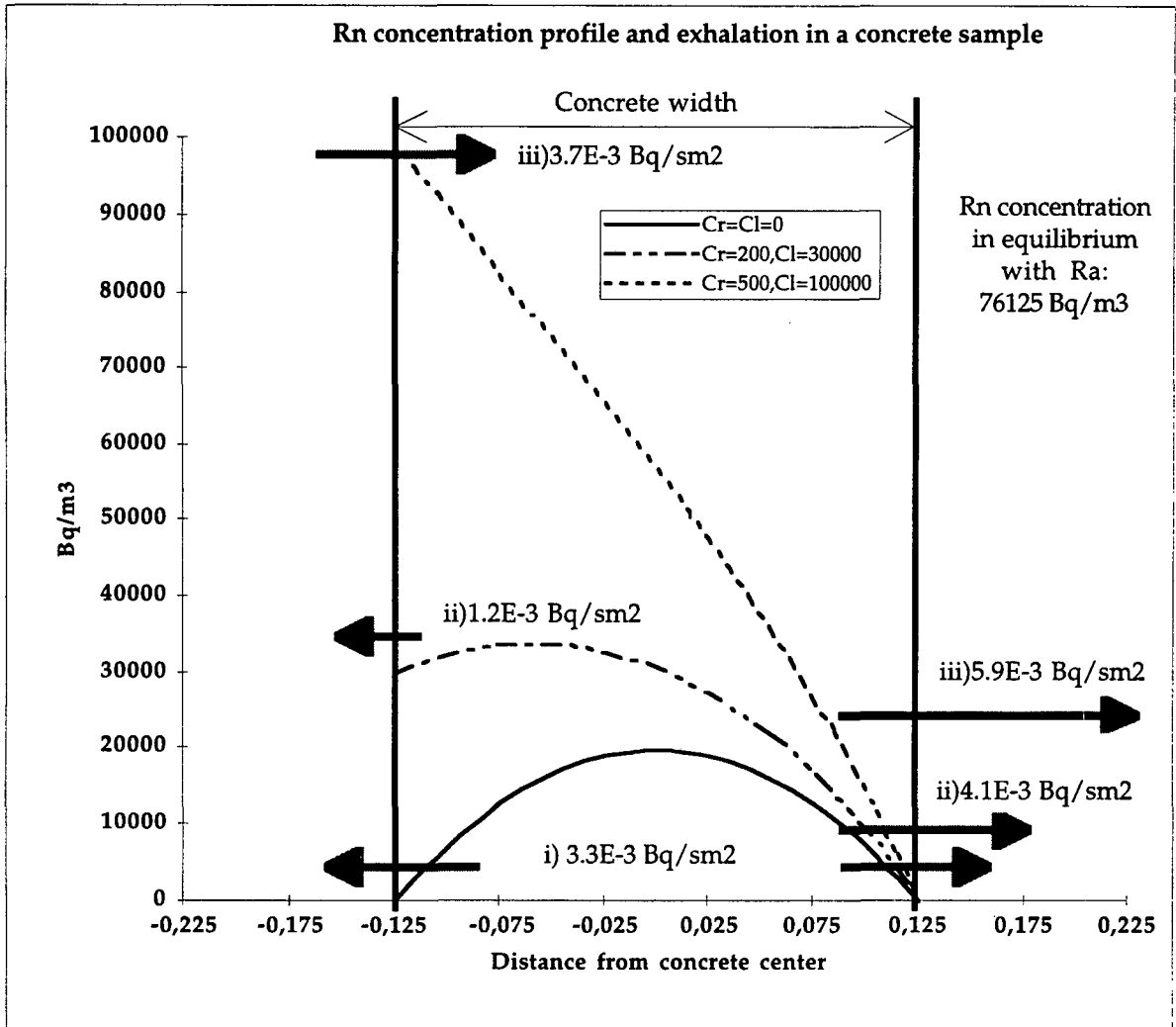


Fig. 2.3: Radon concentration profile in a concrete sample that has the parameter values given in table 2.5. C_L and C_R are the value of the radon concentration at the left and right side of the material respectively. Horizontal arrows represent the exhalation rate at the surface in the cases i) $C_R=C_L=0$, ii) $C_R=200, C_L=30000$ and iii) $C_R=500, C_L=100000$. The concentrations are expressed in $Bq \cdot m^{-3}$.

Table 2.5 shows the exhalation rates obtained from expressions (2.25) and (2.26) in several boundary conditions for a given concrete material.

Table 2.5: Radon exhalation rate from concrete for different boundary conditions

Parameter	Symbol	Value	Boundary conditions ($Bq \cdot m^{-3}$)	Exhalation rate at left side ($Bq \cdot m^{-2} \cdot s^{-1}$)	Exhalation rate at right side ($Bq \cdot m^{-2} \cdot s^{-1}$)
Radium content	A_{ra}	$50 Bq \cdot kg^{-1}$	$C_R = C_L = 0$	$-3.301 \cdot 10^{-3}$	$3.301 \cdot 10^{-3}$
Emanation fraction	f	0.15	$C_R = C_L = 40$	$-3.299 \cdot 10^{-3}$	$3.299 \cdot 10^{-3}$
Porosity	ϵ	0.2	$C_R = 10, C_L = 40$	$-3.298 \cdot 10^{-3}$	$3.301 \cdot 10^{-3}$
Half-width	$w_{1/2}$	0.125 m	$C_R = 200, C_L = 30000$	$-1.204 \cdot 10^{-3}$	$4.088 \cdot 10^{-3}$
Eff. diff. coefficient	D_e	$5 \cdot 10^{-8} m^2 \cdot s^{-1}$	$C_R = 500, C_L = 100000$	$3.692 \cdot 10^{-3}$	$5.936 \cdot 10^{-3}$
Density	ρ	$2030 kg \cdot m^{-3}$			
Equil. Rn concentration	C_{eq}	$76125 Bq \cdot m^{-3}$			

The exhalation of radon from building materials is affected by the type of surface coating used in the house. Tso et al. (1994) and Yu (1993) investigated the effect of material covering on exhalation from building materials. They found that the percentage of reduction can span from 2% up to more than 85.5%.

2.2.3 Radon entry from water and gas supplies

Water and gas supplies constitute the less important radon source in general, but in some specific cases their contribution can be important. Normally the contribution of each supply to the total indoor radon concentration can be estimated from the source radon concentration, the supply-use rate and the transfer efficiency from the source to the air. Very high radon concentration in the water and natural gas are required to mean a significance contribution to the total radon entry rate; this situation might be found when using private wells and when the natural gas has been collected close to the place where is consumed. The distance that water has to travel in public supplies is long enough to allow the decay of most of its radon; the same thing happens when the natural gas has to travel from very far until reaching the house.

The contribution of water supplies is normally more important than that from gas supplies: Stranden (1988) estimates the average increase in indoor radon concentration resulting from water use as

$$C_{av} = \frac{C_w W_r t_w}{V_r \lambda_v} \quad (2.27)$$

where:

- C_{av} is the average increase in indoor radon activity concentration ($\text{Bq}\cdot\text{m}^{-3}$).
- C_w is the radon activity concentration in water ($\text{Bq}\cdot\text{m}^{-3}$).
- W_r is the water-use rate per resident ($\text{m}^3\cdot\text{person}^{-1}\cdot\text{s}^{-1}$).
- t_w is the use-weighted average transfer efficiency of radon from water to air (dimensionless).
- V_r is the volume per resident of the dwelling ($\text{m}^3\cdot\text{person}^{-1}$).
- λ_v is the ventilation rate of the residence (s^{-1}).

Eq. (2.27) can be re-written in terms of a transfer factor t

$$C_{av} = tC_w \quad t = \frac{W_r t_w}{V_r \lambda_v} \quad (2.28)$$

The most common value of t is in the vicinity of 10^{-4} and its range is $(10^{-5}-10^{-3})$. Radon concentrations in the USA. ground water range from 10^3 up to 10^6 Bq·m⁻³, so that in special cases when ground water concentration is in the high range of values, its contribution to the total indoor air concentration might be important. Measurements on USA single-family houses yield lognormal distributions of radon concentration in public and private (including wells) ground water with the following geometric mean (GM), geometric standard deviation (GSD) and range (R). Public water: $5.2 \cdot 10^3$ Bq·m⁻³ (GM), $3.53 \cdot 10^3$ Bq·m⁻³ (GSD), $(1-100) \cdot 10^3$ Bqm⁻³ (R). Private water: $36 \cdot 10^3$ Bq·m⁻³ (GM), $6.5 \cdot 10^3$ Bq·m⁻³ (GSD), $(1-1000) \cdot 10^3$ Bq·m⁻³ (R). Stranden (1988).

2.2.4. Sum up of all radon entry contributions.

Table 2.6 gives a literature review of the contribution of each source and transport mechanism to the radon entry into structures.

Table 2.6: Radon entry data from literature. The entry flow from building materials correspond to the so-called exhalation rate.

Radon source	Reference	Entry mechanism	Entry rate (Bq s ⁻¹)	Entry flow (Bq m ⁻² s ⁻¹)	Remarks
Soil	Cavallo et al. (1992)	Advection	56-83		Basement windows open
		Advection	347-458		Basement windows closed
	Cavallo et al. (1994)	Advection	606		Basement windows opened
		Advection	4306		Basement windows closed
	UNSCEAR (1993)	Diff + Adv	2		
	Gadd and Borak (1994)	Diff. + Adv	0.13-0.20		71% of global entry
			0.07-0.11	$(2.4-3.6) \cdot 10^{-3}$	Entry through concrete wall
			0.011-0.017	$(1.0-1.5) \cdot 10^{-3}$	Entry through concrete floor
	Hintenlang and Al-Ahmady (1994)	Diffusion	10		
	Hintenlang and Al-Ahmady (1992)		6.8		
	Robinson and Sextro (1995)	Advection	0-0.8		Normalised entry rate (Bq s ⁻¹ Pa ⁻¹)
	Revzan et al. (1993)	Diff + Adv.	0.67-44.4		Theoretical results: simulation
	Tsang and Narashiman (1992)	Diffusion	0.011-0.167		Theoretical results: simulation
		Advection	0-0.818		Theoretical results: simulation
Ward et al. (1993)	Diffusion	0.26±0.06			
	Advection	0-0.43			
Building materials	Gadd and Borak (1994)	Exhalation	0.053-0.081		29% of global entry
			0.040-0.061	$(1.3-2.0) \cdot 10^{-3}$	Entry from concrete wall
			0.013-0.019	$(1.2-1.8) \cdot 10^{-3}$	Entry from concrete floor
	Stoop et al. (1993)	Exhalation	0.0069	$7.22 \cdot 10^{-5}$	From living-room wall
		Exhalation	0.0181	$3.72 \cdot 10^{-4}$	From living-room floor

Stranden (1988)	Exhalation (data from Nordic countries)	(5.6-83)·10 ⁻⁴	Concrete
		(1.4-11)·10 ⁻³	By-product gypsum
		(1.4-5.6)·10 ⁻²	Alum shale concrete
		(2.8-8.3)·10 ⁻⁴	Lightweight concrete
		(5.6-14)·10 ⁻⁴	Brick
Chen et al. (1993)	Exhalation from Building material samples	(0.06-0.10)·10 ⁻⁴	Marble
		(0.06-0.13)·10 ⁻⁴	Red floor brick
		(0.10-0.25)·10 ⁻⁴	Quartz brick
		(0.13-0.19)·10 ⁻⁴	Floor brick
		(0.10-0.27)·10 ⁻⁴	Black schist
		(0.10-0.18)·10 ⁻⁴	Black fragmentary stone
		(0.15-0.24)·10 ⁻⁴	Artificial stone
		(0.26-0.35)·10 ⁻⁴	Red brick
		(0.60-1.60)·10 ⁻⁴	Concrete slab
		(0.21-28.5)·10 ⁻⁴	Granite
	Exhalation from building surfaces	(0.03-0.06)·10 ⁻⁴	Sheet vinyl
		(0.12-0.29)·10 ⁻⁴	Floor brick
		(0.21-0.54)·10 ⁻⁴	Polished concrete floor
		(0.30-0.62)·10 ⁻⁴	Rough concrete floor
		(0.48-1.69)·10 ⁻⁴	Concrete ground floor
Tso et al. (1994)	Exhalation	(0.50-0.92)·10 ⁻⁴	Inner wall (brick, plaster, paint)
		(0.76-1.68)·10 ⁻⁴	Outer wall (concrete, plaster, paint)
		(1.75-3.00)·10 ⁻⁴	Polished floor with aggregates
		(2.0-3.0)·10 ⁻³	Red brick
		(3.1-3.9)·10 ⁻³	Concrete
Yu et al. (1995)	Exhalation	(1.0-45)·10 ⁻³	Inner wall surfaces from 32 buildings

Effect of material

	covering on exhalation:	% reduction	Surface coating
Tso et al. (1994)		2	Plastering
		27	Pearl glow (latex paint)
		36	Latex paint
		40	Wall paper without gloss undercoat
		42	Latex vinyl paint
		47	Chlorinated rubber paint
		53	Weather shield
		60	Gloss undercoat
		62	Wall paper with gloss undercoat
		68	Brushing lacquer
Yu (1993)		>66.4->80.0	Plastic lined wallpaper
		21.0-27.3	Plaster
		16.2-23.8	Ceramic mosaics
			Glazed ceramics:
		>68.3->85.5	no gap
		38.1-55.4	with gap

Water supply	Parameter	Common value	Range	Literature review
	Use-rate:			
Stranden (1988)	m ³ ·person ⁻¹ ·d ⁻¹	0.19	0.10-0.38	

Transfer efficiency	0.95	0.90-0.98	Dishwasher
	0.66	0.63-0.71	Shower
	0.42	0.3-0.5	Bath
	0.3	0.29-0.3	Toilet
	0.92	0.9-0.95	Laundry
	0.34	0.1-0.5	Drinking and cleaning
Radon concentration	5.2	1-100	Public ground water in the USA
10^3 Bqm^{-3}	36	1-1000	Private ground water in the USA

2.3 Radon accumulation indoors.

Because of being radon a noble gas, its atoms do not interact with other air components and no rate of chemical transformation is required. Thus, the time-behaviour of indoor radon concentration is given by the mass-balance between the entry rate and the removal rate. Given the entry rate, the accumulation of radon in a room depends on three factors: room volume, ventilation rate, and inter-zone flows. The radon decay might be considered as well, but radon decay constant (0.0076 h^{-1}) is much smaller than common values of air-exchange rates (0.5 h^{-1}). We have already described the parameters and processes affecting radon entry into a room and in this section we will describe those affecting the air-exchange rates.

The total ventilation rate of a given room can be separated into three components:

- i) Infiltration: this is the rate at which air is exchanged through small openings or imperfections in the building shell.
- ii) Air exchange through windows or doors that are partially or temporally open.
- iii) Ventilation supplied mechanically by exhaust fans or other systems.

Each of this components vary with time and space, being possible to detect relevant changes at almost any time-scale and therefore, the total ventilation rate has a very important time-dependence. Infiltration is the dominant mechanism when windows and doors are kept closed, and it is generated by the wind speed and the indoor-outdoor temperature differences. Energy-saving efforts trying to reduce the infiltration can lead to high indoor radon concentrations. The infiltration component of the ventilation rate can be estimated from the simple model (Nero 1988)

$$\lambda_{v,i} = A_0 \left[(y_w u)^2 + (y_s \Delta T^{1/2})^2 \right]^{1/2} \quad (2.29)$$

where

A_0 is the effective "leakage area".

y_w is the "wind" parameter, accounting for local and terrain shielding effects, the distribution of the leakage area around the building envelope, and the height of the building relative to the height at which the wind speed is measured.

y_s is the "stack" parameter, accounting for the building height and the distribution of the leakage area.

Common values of infiltration rates are within the range 0.1 - 1 h⁻¹. The opening and closing of windows and doors may have a large impact on the total ventilation rate. This component of the ventilation rate is very difficult to control because it depends strongly on inhabitants habits, in addition to the meteorological parameters (mainly the wind speed). Cavallo et al. (1994) found an increase on ventilation rate from 0.64 to 1.13 h⁻¹ when opening the windows of a basement. The mechanical ventilation rate depends on the characteristics of the given mechanical system and its mode of operation.

Another useful way to classify the total ventilation rate is differentiating between the so-called "balanced" and the "unbalanced" ventilation rates. The first one is independent on the pressure difference across the building shell and includes i) any mechanical ventilation system that provides equal supply and exhaust flows and ii) the effect of opening and closing windows and doors. The second one depends on the pressure difference and includes infiltration and mechanical ventilation that provides only supply or exhaust. The unbalanced ventilation component is related to the average indoor-outdoor pressure difference across the building shell by a power-law relationship (Nazaroff et al 1988)

$$\lambda_{v,u} = \frac{A_0(2/\rho_a)^n}{V} (\Delta P)^n \quad 0.5 < n < 1.0 \quad (2.30)$$

where ρ_a is the air density (kgm⁻³)

V is the volume of the room (m³)

ΔP is the average indoor-outdoor pressure difference across the building shell (Pa)

Measurements of n yield values in the range 0.5-0.75. At this point it is important to note that unbalanced ventilation rate depends directly on the mean indoor-outdoor pressure differences generated by the wind, the stack effect, and the unbalanced mechanical ventilation, while the advective radon entry is related to the indoor-soil pressure differences, which may be induced not only by the previous generating mechanisms, but also by the transient effects due to the

atmospheric pressure tides. The fact that both entry and ventilation may be dependent on some meteorological parameters can lead to surprising results as for instance, increasing advective entry rate results in a decrease of indoor radon concentration. Certainly, this phenomenon has been observed experimentally (Ward et al. 1993): a rise in wind speed generates indoor-soil pressure differences, increasing advective entry rate, but also increases ventilation rate; as a consequence, indoor radon concentration can decrease.

3

The dynamic sectorial model RAGENA

In this chapter we describe the generic and dynamic model of Radon Generation, Entry, and Accumulation indoors (RAGENA) that has been set up in this work. RAGENA solves a set of coupled first order differential equations by the 4th order Runge-Kutta numerical method. It takes into account the radon sources and processes affecting indoor radon dynamics, and has the possibility of incorporating time-dependent data experimentally collected or patterns of behaviour assumed.

The chapter is divided into 3 sections. First, we describe briefly the software used for building the model (for more detailed information, see the software manual, High Performance Systems, 1994). A good set of examples is given in Hannon and Ruth (1994). Second, we review the existing models on radon and finally, we give a detailed description of the RAGENA model with all the assumptions considered.

3.1 The STELLA II software

3.1.1 Generalities

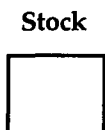
Stella II software (High Performance Systems Inc.) was developed to model Dynamic Systems by the finite difference equations technique. It consists of an expansive, clean-slate construction site, a set of building blocks, tools for manipulating the building blocks and objects to be used in organising the construction site. With this software it is possible to construct operational multi-compartment maps that make explicit a model of how something works. Once the operational maps are built, it is possible to define easily the equations that describe the dynamic behaviour of the system and also it is possible to incorporate directly the experimental time-series data obtained for the simulation running.

The Stella II language is built around a progression of structures which allows the user to define several sectors (groups of functionally-related elements). When running a simulation, it is possible to run only one sector of the model, a selected group of sectors or the entire model.

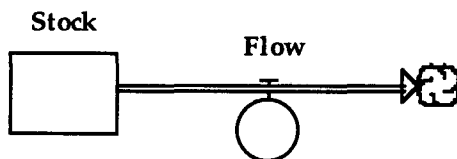
3.1.2 Software elements.

The basic components of Stella II are the building blocks. There are four different types of building blocks: Stocks, flows, converters and connectors.

- **Stocks** represent accumulations. They reflect the state of the system at any point in time and can be understood as the compartments of the model.



- **Flows** represent activities or entities in motion. They fill and/or drain stocks, i.e., they transport material or non-material entities. The units of the flows must be the units of the related stocks *per unit time*.



- **Converters** convert inputs into outputs. They are used to elaborate the detail of the stock and flow structure; providing an alternative way to measure the magnitude of a stock (typically converting an absolute measure given by a stock to a relative measure), combining several flow processes, detailing the steps of the logic sequence which feed a particular flow and entering external inputs into the model (typically time series inputs).



- **Connectors** reflect the assumptions about what depends on what in the model. They allow the user to establish relationships between the objects of the model.



Combining all these building blocks, different structural levels can be achieved. Even though there are an infinity of possibilities, the handbook of the software gives us a set of five basic flow process templates that can be used to define the majority of flows we will need when modelling. At the highest structure level in Stella II models, it is possible to group functionally-related elements by creating a sector.

3.1.3 The simulation algorithms.

When n flows are attached to a stock, the Stella II software generates a finite difference equation for each stock as follows

$$Stock_t = Stock_{t-\Delta t} + \sum_{i=1}^n (Flow_i) \cdot \Delta t \quad (3.1)$$

Where Δt (step size) is the discretised time interval used in Stella II computation. Step size can be selected by the user. The smaller step size, the higher time-resolution and accuracy of the model and the longer time needed for simulation.

The relationship between differential equations and the software's diagram components is that flows represent time derivatives of stocks, stocks are the integrals (or accumulations) of flows over time and converters contain the micro-logic of flows.

Stella II software allows the user to choose between three standard numerical methods to solve the system of equations comprised in the model: Euler's method, 2nd order Runge-Kutta and 4th order Runge-Kutta.

3.1.4 Application of Stella II software to indoor radon dynamic modelling.

There are three main reasons why we chose Stella II software to model indoor radon dynamics:

- First, due to its sector structure, it is possible to develop an integrated approach to the problem, modelling from radon generation in the sources to radon accumulation indoors.

- Second, in addition to being a dynamic model instead a steady-state one, all the parameters of the model that change in time can be incorporated directly from experimental data collected by means of the time series inputs very easily.

- Finally, it is possible, starting with a very simple model, to add gradually more detail and thus going deeply into the processes that describe indoor radon dynamics while keeping the generic approach.

Since Stella II was developed to model the dynamic behaviour of a system, it has no spatial resolution and thus it is not possible, for instance, to obtain the soil radon concentration field underlying the house as it can be obtained with other numerical methods (Loureiro 1987, Andersen 1992). However, using Stella II brings another approach to the indoor radon problem that could increase the general understanding on indoor radon dynamics.

3.2 Review of the existing radon models

So far, efforts to understand indoor radon concentration can be divided into two groups: i) studies focused on radon entry into houses, which depends on three factors: radon generation availability of the source, transport properties of the source and of the interface between it and indoor air, and the driving forces, ii) studies that try to understand indoor radon accumulation indoors, which also depends on three factors: house volume, ventilation rate, and inter-zone flows. In this section we give a literature review of both types of studies.

It is worthwhile to remark that all the studies contributing to the understanding of radon behaviour are useful for the development of appropriate long-term mitigation methods (Cavallo et al. 1992; Cavallo et al. 1994; Hintenlang and Al-Ahmady 1994, Bonnefous et al. 1992, Bonnefous et al. 1994)

3.2.1 Radon entry into houses.

An excellent review of the existing models of radon entry into houses, is given by Gadgil (1992). There are three different approaches to model radon entry: analytical models, lumped parameter models and numerical methods. All of them may be useful depending on their purposes. Most of these models describe the steady-state entry of radon into a structure from the soil underneath the house, which is commonly accepted as the major source of indoor radon concentration (Loureiro 1987, Revzan et al. 1993, Scott 1994, Nielson et al. 1994). The increasing awareness of the importance of transient effects of atmospheric pressure (Tsang and Narashiman, 1992, Hintenlang and Al-Ahmady, 1992) and the water content (Markkanen and Arvela 1992, Morris and Fraley, 1994, Washington and Rose, 1992), which is related to rainfall, has led to the conclusion that it is

very important to develop dynamic models which could incorporate the time variation of all the time-dependent parameters. Andersen (1992) modelled the dynamics of the advective radon entry into houses varying the pressure difference with a sinwave, keeping all the other parameters constant. Cripps (1996) developed a mixture of analytical and numerical model to look at the time varying effects caused by the changing atmospheric pressure or by the development of a landfill site over time. Perhaps the most complete dynamic model of radon transport in soil has been developed by Chen and Thomas (1995); where all primary factors affecting gas transport through unsaturated soil are considered: barometric pressure changes, rainfall events, water content changes, emanation rate changes, etc. showing an agreement with field-measured values.

The research efforts concerning the models of radon entry from other sources (building materials, water and natural gas) are basically limited to the equations given in the chapter 2. Only Sun (1995) simulated radon emanation from dry building materials by a Monte Carlo method. Even though there are relevant investigations showing the dependence of radon exhalation from building materials on the barometric pressure (Stranden 1988), on the humidity (Roelofs and Scholten 1994), and on their age (Roelofs and Scholten 1994, Rogers et al. 1995, Yu and Young 1995), we have not found any attempt to model these effects in our literature research.

3.2.2 Indoor radon accumulation and its time-evolution.

In relation to the efforts to understand indoor radon accumulation, the models usually consider mass-balance equations to describe indoor radon dynamics. The time dependence of radon concentration in a room is given by the balance between the entry rate (also called production rate or radon source strength) and the removal rate. This removal rate is due to the air-exchange rate with outdoors (ventilation rate) or with other rooms (inter-zone flows). Investigations normally focus on one of this two balance terms, studying the influence of a given process or parameter on it, without considering any generation or transport parameter from the source. Hubbard et al. (1992) developed a model to explain indoor radon dynamics for a given constant entry rate as a function of the infiltration produced by the stack effect. Capra et al. (1994) investigated the effect of ventilation rate on indoor radon concentrations keeping the entry rate constant. Arvela et al. (1988) predicted the variations of indoor radon concentrations with a simple model which considers a constant diffusion entry and a pressure driven entry due to the stack effect. De Meijer et al. (1992) calculated air-exchange flows and measured indoor radon concentrations to determine the relative contribution of radon flows and sources. Peter et al. (1994) used a set of linear differential equations to describe the radon transport between the atmosphere and the rooms of a multi-room building. Stoop et al. (1993) used source strengths and dynamic variables as input for a

multi-room model to describe the variations and interrelations of radon concentrations in various compartments.

3.3 The RAGENA Model

We have seen in chapter 2 that radon generation, transport, entry and accumulation indoors depends on a lot of parameters most of which are time-dependent. This complexity has led to different approaches to understand the problem; each facing a partial aspect of radon and/or being site-specific, considering a given source or process related with radon in a given site. Sophisticated models of radon transport and entry into houses from soil use physical transport parameters, but either a very detailed knowledge of the site or important simplifications are required: the models need, to be validated, a test structure in which the maximum number of parameters are controlled and monitored. Therefore, it is difficult to extrapolate their results to real inhabited houses, where detailed knowledge of the soil parameters underneath the house, the building structure and cracks, the inhabitants habits, etc. is not available. On the other hand, indoor radon models with mass-balance equations are usually far from the physical processes that emanate radon and drive it into houses. An integrated approach, taking into account all the parameters that affect the processes of generation, transport, entry and accumulation indoors at the same time, and taking advantage of the lots of studies already performed, is necessary to try to fully understand indoor radon dynamics.

In this section we describe in detail the generic sectorial model of Radon Generation, Entry, and Accumulation indoors (RAGENA). This model might be considered as a global integrated model of indoor radon dynamics because of three reasons:

i) It takes into account all the radon sources and processes affecting indoor radon dynamics, being able to relate experimental data with the physical parameters that influence radon generation, transport, entry, and accumulation indoors. In this sense, it simulates indoor radon time-behaviour from the point of view of a multi-parameter analysis.

ii) It intends not to be very site-specific; the simple conceptual model allows its adaptation to different situations easily, without the need of a very detailed description of the site.

iii) It is adaptable to any time-scale. The time-unit of the model can be fixed, depending on the purpose of the study, from seconds up to years.

Since it is almost impossible to apply partial studies in different types of real inhabited houses; a model that might be useful for predicting indoor radon concentration and to determine the main entry rates in very different types of real houses must be simple enough to run with only the information available in each site. Rather than a complete description of the system, the RAGENA model is more concerned with the integration of the knowledge collected from partial studies paying attention to the dynamic behaviour of the system. The model mass-balances the inflows and outflows of radon atoms in different compartments without any spatial resolution. This approach requires the use of averaged-over-macroscopic-volume or "effective" parameter values which may include the parameters' anisotropy and simplifies very much the mathematical treatment. Therefore, the model, in contrast with other studies (Loureiro 1987, Andersen 1992, Revzan et al. 1993) cannot describe radon transport in the source media and give as an output the soil radon concentration field under the house, but it doesn't need, for example, the knowledge of the soil permeability matrix and of the cracks distribution and geometry. An important characteristic of the model is that it is possible to incorporate step by step not only more detail to it, but also to add any missing aspect or any linked problem like, for instance, indoor radon short-lived daughters.

3.3.1 Global structure: sectors

RAGENA is divided into eight sectors, each corresponding to a relevant radon-related process. Fig. 3.1 shows the global structure of the RAGENA model. There are the sectors related with the radon sources: *soil*, *building materials*, *water* and *gas*. Each source sector is constituted by a partial model that gives one or more radon flows from the source into indoors. The soil sector produces a net diffusion flow into indoors which is unidirectional as a permanent positive gradient concentration between soil and indoors is assumed; this sector also produces a bi-directional pressure-driven flow allowing the pressure difference that drives it to change its sign. The building materials sector yields an unidirectional exhalation flow because it is assumed that diffusion is the mechanism of exhalation. The water and gas sectors produce a release unidirectional flow. The *outdoors* sector describes the air-exchange rate flow due to ventilation; this flow is bi-directional because an eventual radon concentration outdoors higher than indoors can produce a net input of radon atoms from outdoors into indoors. All the cited flows are balanced in the *indoors* sector to give the time profile of indoor radon concentration in a single or multi-zone house. The parameters used by the model in these sectors are those that actually influence on radon generation, entry and accumulation indoors like, for example, soil and building material emanation factors, soil permeability, soil and building material effective diffusion constant, indoor-soil pressure difference, etc. We call these parameters "primary" parameters. For a given configuration of values of these primary parameters the system tends to an steady-state. Indoor

radon levels in a house change in time because of the change in the environmental parameters and the occupants' behaviour that affect the generation and transport parameters, the entry processes, and the ventilation of the rooms of the house. Therefore, there are two additional sectors that drive the dynamics of the system: the *environmental parameters* and the *occupants' behaviour* sectors. The environmental parameters sector hosts five sub-sectors, each corresponding to a relevant environmental parameter: barometric pressure, rainfall, soil temperature, indoor and outdoor temperatures, and wind. Each sub-sector describes the effect of the corresponding environmental parameter on a given generation, entry, and accumulation process. For instance, rainfall increases the soil water content, which in turn increases the emanation factor and decreases the soil permeability and the diffusion transfer coefficient; a rise in wind speed generates indoor-soil pressure differences but also increases ventilation rate. The occupants' behaviour sector takes into account the habits of the occupants, like the patterns of occupancy, use of Heating, Ventilation and Air-Conditioning systems (HVAC), and opening and closing windows and doors. All the parameters of these two last sectors are called "secondary" parameters. Thus, radon generation, transport, entry and accumulation indoors depend on the primary parameters, which change in time because of the secondary parameters' changes. The complete diagram of the RAGENA model is given in annex 3.

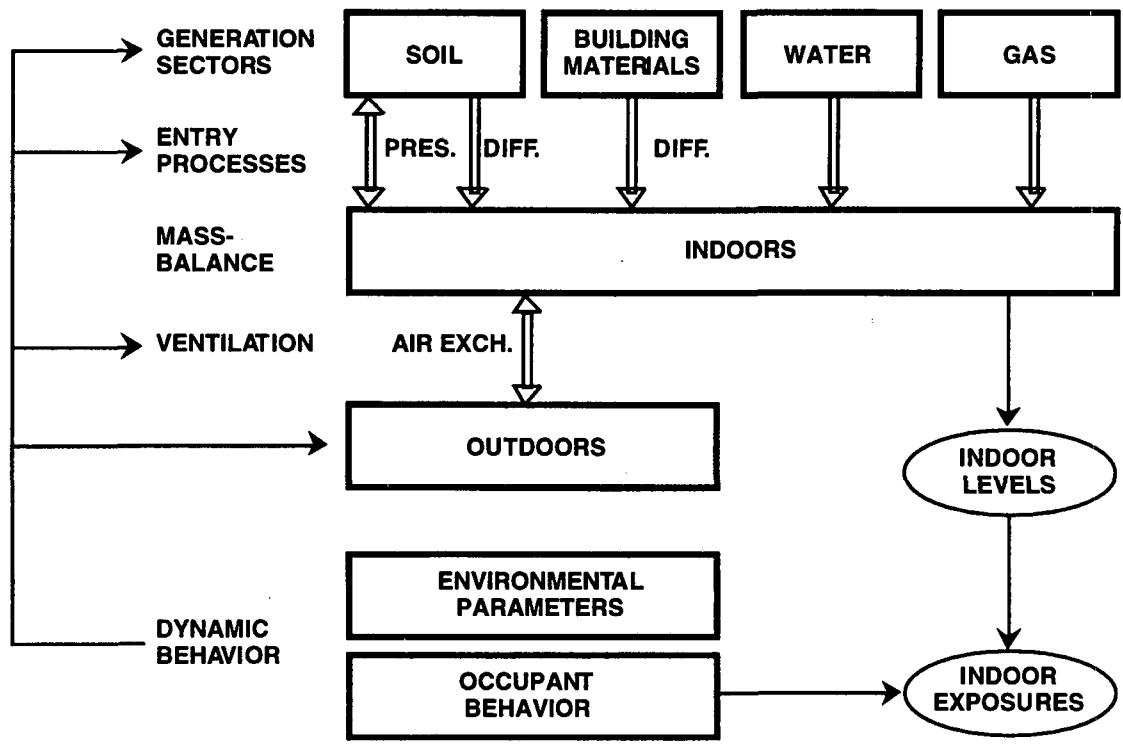


Fig. 3.1: Global structure of the RAGENA dynamic model of radon generation, entry, and accumulation indoors.

The outputs of the model are the soil radon concentration, the different entry rates and the indoor radon levels. The model can be used to estimate the contribution of a given entry process to the indoor radon concentration. The values of the parameters needed for running the model can be either experimental data time series, constant values, assumed distributions or reference patterns obtained from the literature. In case of using one month or one year as a time-unit, the meteorological patterns typical for the region where the study is performed could be more appropriate than direct measurements, so that the model could be useful for mean radon exposure estimation and risk assessment. The occupancy pattern together with the indoor radon levels calculated in the indoors sector allows the model to estimate the indoor radon exposure.

3.3.2 Soil sector

This sector is divided into two compartments, the disturbed soil (DS) and the undisturbed soil (US). The disturbed soil is the volume of the soil underneath the house from which radon generated within it can reach the basement of the house by diffusion and pressure driven flows. The undisturbed soil is the soil attached to the disturbed soil that is not influenced by the presence of the house. Due to the entry of radon from the disturbed soil into the basement, a radon concentration gradient between both soil types could arise. In that case, a diffusion flow from the undisturbed soil is assumed. Fig. 3.2 shows the separation of the soil sector into two compartments.

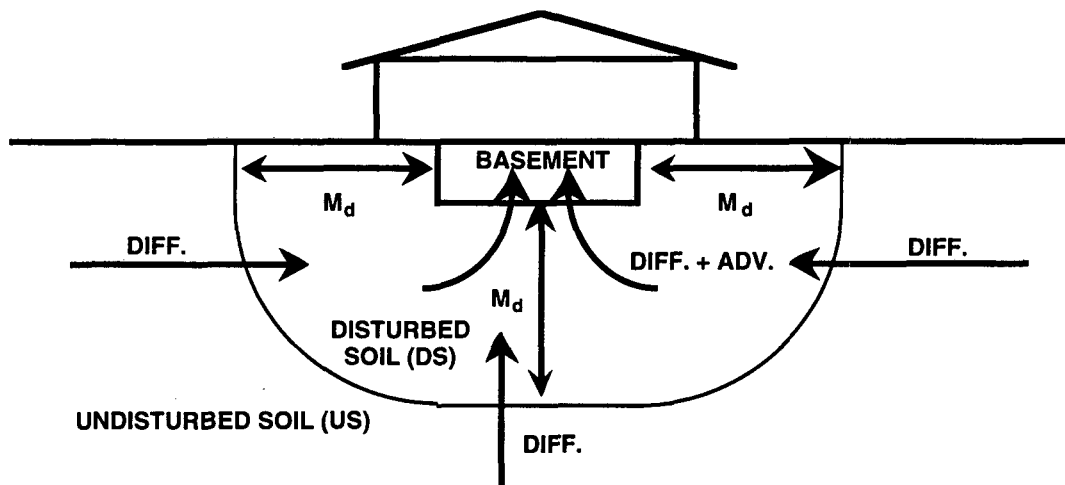


Fig. 3.2: Separation of the soil underneath the house into the disturbed and the undisturbed soils. M_d is the radon migration distance, defined in equation 2.17.

In each compartment, we treat the soil as a porous medium consisting of soil grains and pores filled with water and soil gas. We consider the values of soil properties as the values averaged

over the macroscopic volume (V) of the soil. The pore volume (V_p) of the soil is divided into a gas-filled volume (V_g) and a water-filled volume (V_w) such that

$$V_p = V_g + V_w \quad (3.2)$$

and then, the porosity (ε), gas-porosity (ε_g), water-porosity (ε_w) and the fraction of water saturation (m) are defined as

$$\varepsilon = \frac{V_p}{V} \quad \varepsilon_g = \frac{V_g}{V} \quad \varepsilon_w = \frac{V_w}{V} \quad m = \frac{V_w}{V_p} = \frac{\varepsilon_w}{\varepsilon} \quad (3.3)$$

Since we do not consider organic matter, the density of the wet soil (ρ_{ws}) can be obtained from

$$\rho_{ws} = (1 - \varepsilon)\rho_{gr} + \varepsilon_w\rho_w = (1 - \varepsilon)\rho_{gr} + m\varepsilon\rho_w \quad (3.4)$$

where ρ_{gr} is the soil grain density ($\text{kg}\cdot\text{m}^{-3}$).

ρ_w is the water density ($\text{kg}\cdot\text{m}^{-3}$).

Radon generated in the soil grains emanates into the gas-filled and water-filled part of the pores. The partition of radon between the gas and the liquid phases is given by the coefficient of solubility of radon in water given in chapter 2 (Eq. 2.1). We have considered the partition of radon between both phases to be permanently in equilibrium because the mass transfer from air to water is fast: a characteristic time of 0.1 s is estimated in Nazaroff et al. (1988). The radon emanation rate (E) of the soil, given in atoms s^{-1} entering into the pore space, can be expressed as

$$E = A_{Ra} f V \rho_{ws} \quad (3.5)$$

where A_{Ra} is the radium activity concentration of the soil expressed in $\text{Bq}\cdot\text{kg}^{-1}$.

f is the emanation coefficient.

It is well known that increasing the water saturation fraction increases the emanation fraction mainly because of the lower recoil range for radon in water than in air. We assume that for a saturated soil the emanation fraction is maximum, and as the soil dries out it decreases down to a 20% of the maximum value (f_{max}) following the expression

$$f = f_{max} [0.2 + 0.8\{1 - \exp(-qm)\}] \quad (3.6)$$

The factor q increases with the mean soil diameter, with values comprised between 6 and 14, and takes into account that emanation fraction reaches its saturation value for lower water saturation fractions when the grain size increases (Markkanen and Arvela 1992). Even though this expression has not been fitted to a set of experimental data, it reproduces a behaviour of the emanation fraction as a function of the water saturation fraction similar to that obtained experimentally by Strong and Levins (1982) and by Markkanen and Arvela (1992).

Considering that radon migrates basically through the gas-filled pores, we are only interested on radon atoms in the gas-filled volume. Thus, we have to multiply the emanation rate (E) by the fraction of radon atoms emanated into the pore volume that reach the gas volume. This fraction, denoted as F , is given by the equation

$$F = \left(1 + \frac{mL}{1-m}\right)^{-1} \quad (3.7)$$

Therefore, we define the effective emanation rate (E') as the number of radon atoms that reach the gas volume per unit time

$$E' = E \cdot F \quad (3.8)$$

The water saturation fraction has also a great influence on the effective diffusion constant and on the soil permeability (Nazaroff et al. 1988). The RAGENA model uses the following empirical expressions to estimate the effective diffusion constant (D_e) and the gas-permeability (k) of the soil (Nielson et al. 1994)

$$D_e = D_0 \varepsilon \exp(-6m\varepsilon - 6m^{14}\varepsilon) \quad (3.9)$$

$$k = 10^2 \left(\frac{\varepsilon}{500}\right)^2 d^{4/3} \exp(-12m^4) \quad (3.10)$$

where D_0 is the diffusion constant of radon in air ($\text{m}^2 \cdot \text{s}^{-1}$).

d is the mean soil particle diameter (m).

Relationships (3.9) and (3.10) give a range of values from 10^{-10} to $10^{-6} \text{ m}^2 \cdot \text{s}^{-1}$ and from 10^{-19} to 10^{-8} m^2 for the effective diffusion constant and the permeability respectively, depending on the fraction of water saturation, when porosity and mean particle diameter range from 0.4 to 0.6 and from 10^{-7} to 10^{-3} m respectively.

Expressions (3.6), (3.9) and (3.10) are estimations that may be useful when no experimental data are available. The effect of the water saturation fraction on the soil parameters k , D_e and f obtained for clay, silt and sand is shown in Fig. 3.3, where the values chosen for porosity and grain diameter are, respectively, 0.6 and 10^{-6} m for clay, 0.5 and 10^{-5} m for silt and 0.4 and 10^{-4} m for sand.

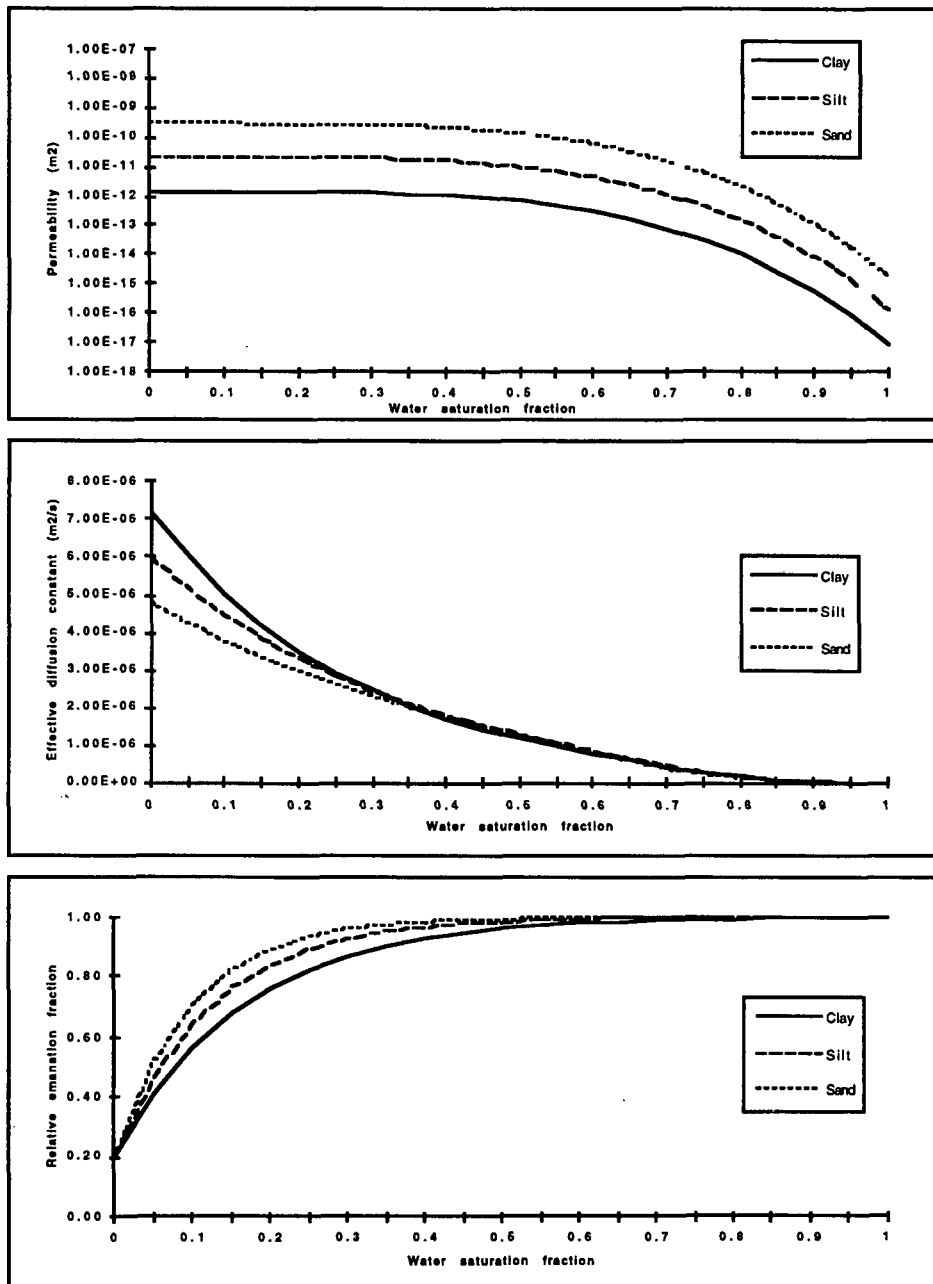


Fig. 3.3: Dependence of gas-permeability, effective diffusion constant and relative emanation fraction on the water saturation fraction for clay, silt and sand, where the values of porosity and mean grain diameter are, respectively, 0.6 and 10^{-6} for clay, 0.5 and 10^{-5} for silt, and 0.4 and 10^{-4} for sand.

3.3.2.1 Undisturbed Soil.

The time variation of the number of radon atoms in the undisturbed soil gas is calculated from the equation

$$\frac{dN_{US}}{dt} = E'_{US} - K_{US}(c_{US} - c_{DS}) - \lambda_{Rn}N_{US} \quad (3.11)$$

where

- N_{US} is the number of radon atoms in the undisturbed soil (US) gas-filled volume ($V_{US,g}$).
- K_{US} is the US transfer coefficient ($m^3 \cdot s^{-1}$).
- c_{US} is the US radon concentration in $V_{US,g}$ ($atoms \cdot m^{-3}$).
- c_{DS} is the disturbed soil (DS) radon concentration in the disturbed soil gas-filled volume $V_{DS,g}$ ($atoms \cdot m^{-3}$).
- λ_{Rn} is the radon decay constant in s^{-1} .
- E'_{US} is the US effective emanation rate expressed in $atoms \cdot s^{-1}$.

Equation (3.11) balances the processes of generation, transfer to the disturbed soil, and decay. The transfer term is assumed to be proportional to the difference of radon concentration between the disturbed and the undisturbed soils.

3.3.2.2 Disturbed Soil.

The equation that describes the time-variation of the number of radon atoms in the disturbed soil (DS) gas-filled volume takes into account, in addition to the generation, transfer to the undisturbed soil (US), and decay terms, the entry into the house terms: one corresponding to the diffusive entry and the other corresponding to the pressure driven entry. Diffusive entry is proportional to the difference of radon concentration between the DS and the basement of the house. Pressure driven entry is assumed to be proportional to the soil radon concentration and to the soil-indoor pressure difference ($v=1$, see section 2.2.1.1), but a turbulence entry could be considered as well. Thus. The equation used is

$$\frac{dN_{DS}}{dt} = E'_{DS} + K_{US}(c_{US} - c_{DS}) - K_D(c_{DS} - c_i) - K_{ACDS} \Delta P_{S-in} - \lambda_{Rn}N_{DS} \quad (3.12)$$

where

- N_{DS} is the number of radon atoms in the disturbed soil (DS) gas-filled volume ($V_{DS,g}$).

- K_D is the DS diffusion transfer coefficient ($\text{m}^3 \cdot \text{s}^{-1}$).
 c_i is the indoor radon concentration of room i ($\text{atoms} \cdot \text{m}^{-3}$).
 K_A is the DS advection transfer coefficient ($\text{Pa}^{-1} \cdot \text{s}^{-1} \cdot \text{m}^3$).
 $\Delta P_{s-in} = P_s - P_{in}$ is the soil-indoor pressure difference (Pa).
 E'_{DS} is the DS effective emanation rate in $\text{atoms} \cdot \text{s}^{-1}$.

The DS volume (V_{DS}) is obtained from the geometry of the house surface in direct contact with soil and the radon migration distance in soil (M_d), defined in Eq. (2.17). In case of a house with a rectangular basement of sides L_1 (m) and L_2 (m) and a depth below the ground level H (m), the DS volume is estimated from the expression

$$V_{DS} = 2HM_d(L_1 + L_2 + M_d) + L_1L_2M_d + \pi M_d^2 \left(\frac{L_1}{2} + \frac{L_2}{2} + \frac{4}{3}M_d \right) \quad (3.13)$$

According to expression (2.13), the advection length is obtained by the product between the superficial velocity vector, the radon mean life (the inverse of the radon decay constant) and the inverse of soil gas-porosity. Assuming a Darcy's flow we obtain

$$l_a = \frac{k}{\mu \varepsilon_g} \nabla P \frac{1}{\lambda_{Rn}} \quad (3.14)$$

The averaged pressure gradient driving the soil gas from the DS into the house is estimated as the pressure difference between the DS and indoor room in contact with soil divided by the distance that separate both volumes, which is called foundations width (w_f)

$$\nabla P = \frac{\Delta P_{s-in}}{w_f} \quad (3.15)$$

It is necessary to define an upper bound to the migration distance, denoted as M , because when the permeability is high (10^{-9} m^2), the migration distance can raise, depending on the pressure gradient values, up to several thousand meters, which has no physical sense. Fig. 3.4 shows the dependence of the migration distance on the permeability for different pressure gradients, taking an effective diffusion constant of $10^{-6} \text{ m}^2 \cdot \text{s}^{-1}$ and a dynamic viscosity of $18 \times 10^{-6} \text{ Pa} \cdot \text{s}$. It can be seen that in general, pressure-driven flow dominates radon migration in soil for permeability values higher than 10^{-12} m^2 , and that for lower values diffusion is the dominant flow, tending the migration distance to the diffusion length (0.69 m). This behaviour is very similar to that obtained by Tanner (1991).

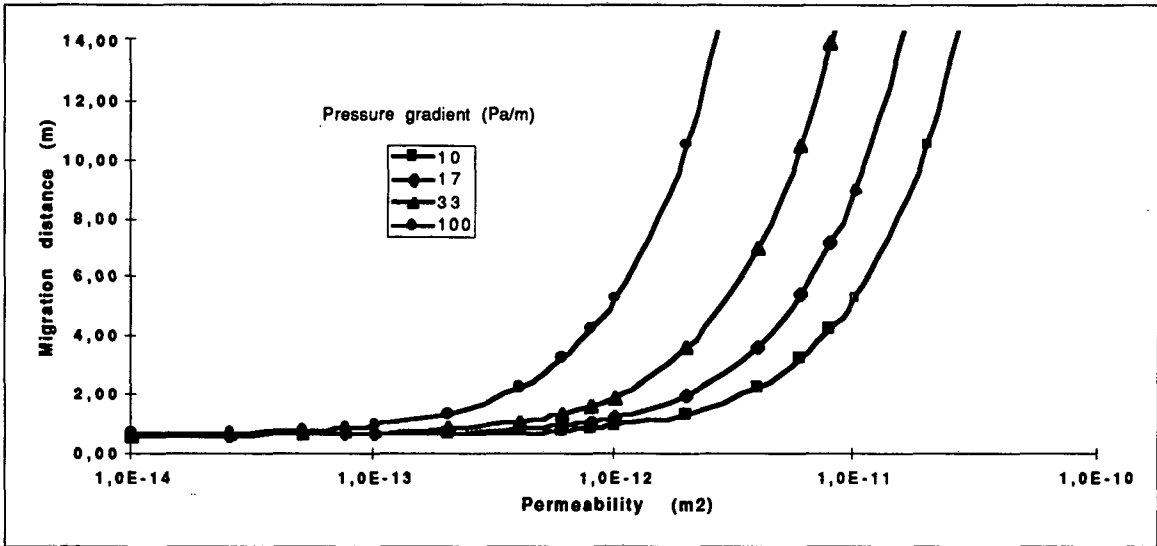


Fig. 3.4: Radon migration distance in the soil as a function of the gas-permeability for pressure gradients of 10, 17, 33 and 100 Pa m⁻¹. Soil effective diffusion constant, porosity and dynamic viscosity have been taken respectively, as 10⁻⁶ m²s⁻¹, 0.5, and 18 x 10⁻⁶ Pa s. The radon concentration in the deep soil and in the basement are respectively 30000 and 200 Bq·m⁻³.

The model assumes that diffusive radon entry is proportional to the radon concentration difference between the DS and the indoor room in contact with it. The coefficient of proportionality is the DS diffusion transfer coefficient, which is related to the effective diffusion constant of the DS. An estimation of their relationship can be obtained from the Fick's law and the assumption that solid building material in contact with soil is essentially impermeable to air (Rogers and Nielson 1993), so that soil radon gas flows into the room primarily through the open area.

The diffusive entry rate (DER, given in atoms s⁻¹) obtained with the model is given by

$$DER = K_D(c_{DS} - c_i) \quad (3.16)$$

The Fick's law relates the gradient of the interstitial soil radon concentration to the flow density across the pore area (see equation (2.3)). Therefore, the number of atoms entering the indoor room in contact with soil per unit time and surface, called diffusion entry flow (DEF) and given in atoms·s⁻¹·m², might be

$$DEF = D_{e,s} \nabla c_{Rn} = D_{e,s} \frac{c_{DS} - c_i}{w_f} \quad (3.17)$$

where $D_{e,s}$ is the effective radon diffusion coefficient in the DS (m²·s⁻¹).

Defining σ as the fraction of the open area (dimensionless), and S_{is} as the indoor surface in direct contact with soil (m^2), so that the product $S_{is}\sigma$ is the open area, and noting that DEF is the DER divided by the open area, the following relationship is obtained from equations (3.16 and 3.17)

$$K_D = D_{e,s} \frac{S_{is}\sigma}{w_f} \quad (3.18)$$

The advective radon entry is assumed to be proportional to the soil radon interstitial concentration and to the soil-indoor pressure difference, being the coefficient of proportionality the advection transfer coefficient K_A ($Pa^{-1}\cdot s^{-1}\cdot m^3$). This coefficient has the same units as the inverse of the so-called radon resistance parameter, which is widely used in lumped parameter models by considering the simple analogy to an equivalent electronic circuit (pressure differences are represented as voltage differences and gas flows as currents). Proceeding in a similar way as to obtain relationship (3.18), and using the Darcy's law, we obtain

$$K_A = \frac{1}{R_{soil}} = \frac{k}{\mu} \frac{S_{is}\sigma}{\epsilon_g w_f} \quad (3.19)$$

where we have assumed that foundations' resistance (R_{found}) is negligible compared to soil resistance (R_{soil}), according to previous studies (Turk et al. 1992, Scott 1994).

Even though the relations (3.18) and (3.19) are only approximate, they allow to interpret physically the diffusion and convection transfer coefficients and to make proper use of the values of effective diffusion constant and permeability reported in the literature.

3.3.3 Building materials sector

Building materials are treated as dried porous media. The evolution of the number of radon atoms in the pore volume of the building materials is described by the balance of three processes: generation, entry into the room, and decay. The entry into the room is assumed to be diffusive and therefore proportional to the difference between indoor radon concentration and building material interstitial radon concentration. The equation describing this balance is

$$\frac{dN_{BM}}{dt} = E_{BM} - K_{D,BM}(c_{BM} - c_i) - \lambda_{Rn} N_{BM} \quad (3.20)$$

where N_{BM} is the number of radon atoms in the building material (BM) pores.
 $K_{D,BM}$ is the BM diffusion transfer coefficient ($m^3\cdot s^{-1}$).

- c_{BE} is the BM interstitial radon concentration (atoms·m⁻³)
 E_{BM} is the BM emanation rate in atoms·s⁻¹

The BM volume has been calculated as the product of the BM surface (S_{BM}) by the minimum between the BM width (w_{BM}) and the BM diffusion length (l_{BM}) in order to take into account that the diffusion length can be larger than the BM width.

It is also possible to establish a relationship between the BM diffusion transfer coefficient and the effective diffusion constant of the BM, as we do for the soil sector

$$K_{D,BM} = gD_{e,BM} \frac{S_{BM}}{w_{CL}} \quad (3.21)$$

- where $D_{e,BM}$ is the effective BM diffusion constant in m²·s⁻¹.
 g is the BM covering factor.
 w_{CL} is the width (m) of the BM covering layer.

The BM covering factor (g), equal or lower than one, takes into account that covering materials can reduce strongly the exhalation from building materials (Yu 1993).

It is necessary to consider several types of BM in this sector because in most of the houses a diversity of BM may be found. This diversity may be encountered even in a given room, where for instance, some walls could be made from concrete (building shell) and some from bricks (thin walls). Each type of building material is characterised by a given set of values of the parameters affecting radon exhalation, and should be treated independently. Therefore, expressions (3.20) and (3.21) with their corresponding set of parameter values are introduced for each type of BM.

3.3.4 Outdoors sector

This sector accounts for the radon exchange rate between indoors and outdoors. Denoting q_{io} as the air current (m³·s⁻¹) from room i to outdoors, and noting that the number of radon atoms going from room i to outdoors per unit time is given by the product of q_{io} by the i -room radon atoms concentration ($c_i = N_i V_i^{-1}$), the net radon atoms exchange rate between room i and outdoors (F_{io}) is obtained from

$$F_{io} = q_{io} c_i - q_{oi} c_o = -F_{oi} \quad (3.22)$$

The air current from room i to outdoors can be expressed as

$$q_{io} = \lambda_{io} V_i \quad (3.23)$$

where λ_{io} is the ventilation rate of room i (s^{-1}).

In case of being the air current from room i to outdoors exactly the same as the current from outdoors to room i , the net radon atoms exchange rate between room i and outdoors is

$$F_{io} = \lambda_{io} V_i (c_i - c_o) \quad (3.24)$$

3.3.5 Water and gas sectors

This sectors are described by the water and gas radon entry rates, which are obtained from the expressions

$$F_w = c_w W_{ur} t_w \quad (3.25)$$

$$F_g = c_g G_{ur} t_g \quad (3.26)$$

where F_w is the radon atoms entry rate from water supply ($\text{atoms}\cdot\text{s}^{-1}$).

c_w is the water radon concentration ($\text{atoms}\cdot\text{m}^{-3}$).

W_{ur} is the water-use rate ($\text{m}^3\cdot\text{s}^{-1}$).

t_w is the transfer efficiency of radon from water to indoor air (dimensionless).

F_g is the radon atoms entry rate from gas supply ($\text{atoms}\cdot\text{s}^{-1}$).

c_g is the natural gas radon concentration ($\text{atoms}\cdot\text{m}^{-3}$).

G_{ur} is the gas-use rate ($\text{m}^3\cdot\text{s}^{-1}$).

t_g is the transfer efficiency of radon from natural gas to indoor air (dimensionless).

3.3.6 Indoors sector

In this sector all the inflows and outflows corresponding to the previous sectors are mass-balanced. The model has the possibility of incorporating as many rooms as the house has. The air-exchange rates between the considered room i and other joined rooms are defined as ij rates λ_{ij} (s^{-1}). The air current from room i to room j , denoted as q_{ij} , can be expressed as

$$q_{ij} = \lambda_{ij} V_i \quad (3.27)$$

where:

- q_{ij} is the air current from room i to room j ($\text{m}^3 \cdot \text{s}^{-1}$).
- λ_{ij} is the air-exchange rate from room i to room j (s^{-1})
- V_i is the effective volume of room i (m^3)

Proceeding in a similar way as in the outdoors sector (section 3.3.4), the net balanced radon exchange rate between rooms i and j is obtained from

$$F_{ij} = q_{ij} c_i - q_{ji} c_j = \lambda_{ij} N_i - \lambda_{ji} N_j = -F_{ji} \quad (3.28)$$

where

- N_i is the number of radon atoms in room i (atoms).
- F_{ij} is the net radon atoms exchange rate from room i to room j ($\text{atoms} \cdot \text{s}^{-1}$).

The parameters λ_{ij} and λ_{ji} depend on the complex pattern of air movement inside a structure and present in general different values (Cavallo et al. 1994). However, in case of assuming that the air current from room i to room j is exactly the same as that from j to i , we have the following relation between both air-exchange rates

$$\lambda_{ij} = \frac{V_j}{V_i} \lambda_{ji} \quad (3.29)$$

and the net radon exchange rate between rooms i and j is

$$F_{ij} = \lambda_{ij} V_i (c_i - c_j) = -F_{ji} \quad (3.30)$$

In each room, the corresponding inflows and outflows are considered. The time behaviour of the number of indoor radon atoms in a room i in direct contact with soil, built up with n different types of building materials, in contact with outdoors, joined to m rooms, and having water and gas supplies is given by the mass-balance equation

$$\begin{aligned} \frac{dN_i}{dt} = & K_D (c_s - c_i) + K_C c_s \Delta P_{s-in} + \sum_{i=1}^n K_{D,BM}^i (c_{BM}^i - c_i) + c_w W_{ur} t_w + c_g G_{ur} t_g \\ & - (q_{io} c_i - q_{oi} c_o) - \sum_{j=1}^m (q_{ij} c_i - q_{ji} c_j) - \lambda_{Rn} N_i \end{aligned} \quad (3.31)$$

It can be seen from equation (3.31) that the model takes into account the processes of radon entry from soil by diffusive and pressure driven flows, radon exhalation from building materials, radon entry from water and natural gas supplies, air-exchange with outdoors, air-exchange with joined rooms, and decay.

3.3.7 Environmental parameters and occupant behaviour sectors

As we said in section 3.3.1, for a given set of values of all the parameters considered in the above sections (primary parameters), the system tends to the steady-state. The changes of these parameters are caused by the influence of the environmental parameters and occupants' behaviour (secondary parameters). The objective of the following sectors is to model the influence of a given environmental or occupant behaviour parameter on the primary parameters. However, in the case of having one of these parameters directly measured, it is better to use the experimental results rather than these sectors. For instance, the soil-indoor pressure difference is modelled from the atmospheric pressure, the soil permeability, the indoor-outdoor temperature differences, the wind speed, and the use-pattern of HVAC systems. All the expressions used to obtain the final pressure difference are approximate, so that an important uncertainty is associated with, and consequently, if experimental time-series data are available they are used directly without running the corresponding sectors.

3.3.7.1 Environmental parameters sector.

3.3.7.1.1 Atmospheric pressure

The variations of atmospheric pressure are supposed to influence the indoor-soil pressure difference and the exhalation rate from building materials. It is also possible to incorporate a dependence of outdoor radon concentration on it, as it is well-known that decreasing atmospheric pressure increases exhalation from uncovered soil. However, due to the fact that the effects of atmospheric pressure changes on the radon exhalation from building materials and on outdoor radon concentration are of less importance than the effect on transient soil-indoor pressure differences, they are not considered in this work and will be faced in future research work.

The effect of atmospheric pressure changes on the soil-indoor pressure differences (called transient pressure differences) $\Delta P_{s-in,t}$ is estimated from the following expressions

$$\Delta P_{s-in,t}(t) = P_s(t) - P_{in}(t) \quad (3.32)$$

where as a first, approximation, we assume that indoor pressure follows instantaneously the atmospheric pressure

$$P_{in}(t) = P_{at}(t) \quad (3.33)$$

and that the soil pressure follows the atmospheric pressure with a delay time (τ_p) given by expression (2.22) taking as a typical distance to be the pressure propagated half of the migration distance

$$P_s(t) = P_{at}(t - \tau_p) \quad (3.34)$$

3.3.7.1.2 Indoor-outdoor temperature differences

Indoor-outdoor temperature differences generate both indoor-soil pressure difference and infiltration rate. The contribution of indoor-outdoor temperature differences to the soil-indoor pressure difference is obtained from expression (2.21), and the contribution to the infiltration rate from expression (2.29). Indoor-outdoor temperature difference is considered positive when indoors is warmer than outdoors, yielding a positive soil-indoor pressure difference, that is, soil pressure higher than indoor pressure.

3.3.7.1.3 Wind

Wind speed generates both indoor-soil pressure differences and infiltration rate. The effect of wind direction might be considered in a specific site by multiplying the pressure difference and infiltration rates generated by a correction factor depending on the wind direction. For the generic model, we only consider the effect of the wind speed on the pressure difference and on the infiltration rate by using the corresponding terms of equations (2.21) and (2.29) respectively. The effect of the wind speed on outdoor radon concentration will modelled in future research work.

3.3.7.1.4 Soil temperature

There are no relevant effects of soil temperature on soil radon at short-term studies, as soil acts as a good isolator. At 1 meter depth, the daily temperature fluctuations are very diminished. The effects of soil temperature on radon emanation and soil-gas concentration are important only at a long-time scale when the seasonal variations are recorded. In this case, RAGENA model uses a graphical relationship between the soil temperature and the coefficient of solubility of radon in

water (L) obtained with data from table 2.1 to model the effect of soil temperature variations on radon entry into a house from soil.

3.3.7.1.5 Rainfall

As we have seen in section 2.1, the fraction of water saturation in soil is a very important parameter affecting radon generation and transport in soil. It changes mainly because of the rainfall and the artificial irrigation. The relationship between the rainfall and the fraction of water saturation in soil is not simple; there are several studies and models already developed to determine the fraction of water saturation in an unsaturated soil versus time for a given constant rainfall rate (Geneviève, 1994). Current efforts are focused on the coupling of one of these type of models to our model in order to incorporate directly experimental or typical for the region under study rainfall rates.

As a first approximation, we developed a very simple model to relate rainfall to water saturation fraction: We assume that in case of no rainfall for a long period of time, the soil keeps a remaining amount of water corresponding to the hygroscopic and capillary fractions of the soil water. This amount of water is considered as the remaining water saturation fraction (m_r). In case of a rainfall event, the initial inflow of water into the soil is used to fill the empty pores, depending on the intensity and duration of the rainfall, up to the saturation. After the rainfall, downward infiltration takes place due to gravity forces. Then, we roughly estimate the change of water volume in the soil, that is, the drying process, by a constant called "drying rate" (λ_{dr}) which must be fitted for each type of soil. We assume that the drying process follows an exponential decay down to the remaining water saturation fraction.

3.3.7.2 Occupant behaviour sector

3.3.7.2.1 Opening windows and doors pattern

The pattern of opening windows and doors is very important because when opened, the ventilation rate increases very much; infiltration doesn't dominate the total ventilation rate and a sudden removal of radon can be observed. We define the "manual" component of the ventilation rate, $\lambda_{v,m}$ as the air-exchange rate due to the opening of windows and doors. Assuming a given sudden increase of $\lambda_{v,m}$ when windows and doors are open, RAGENA model has the possibility to incorporate easily the corresponding pattern of $\lambda_{v,m}$ for a given site.

3.3.7.2.2 Use of Heating, Ventilating and Air-Conditioned Systems (HVAC)

The effects of HVAC systems on radon entry and accumulation indoors strongly depend on the specific characteristics of the system in a given site and on the operation mode and pattern. Therefore, these effects are not considered in the generic model. However, RAGENA has been developed to have the possibility of incorporating the contribution of HVAC systems in two ways: first, the use of unbalanced HVAC systems can generate a few Pascal underpressurization at the lower part of the building ($\Delta p_{mv,u}$), and second, they can induce also an air-exchange rate called "mechanical" ventilation $\lambda_{v,me}$.

3.3.7.3 Equations

At this point it is worthwhile to summarise the effect of the environmental parameters and occupants behaviour sectors on the primary parameters.

The total soil-indoor pressure difference is obtained from the contribution of atmospheric pressure changes, the indoor-outdoor temperature differences, the wind speed, and the use of unbalanced mechanical ventilation

$$\Delta P_{S-in} = \Delta P_{S-in,t} + \rho g(z-z_0) \frac{T_i - T_o}{T_o} + c_f \rho \frac{u^2}{2} + \Delta P_{mv,u} \quad (3.35)$$

The total ventilation rate is obtained from the contribution of indoor-outdoor temperature differences, wind speed, the pattern of opening windows and doors and the use of mechanical ventilation

$$\lambda_v = A_0 \left[(y_w u)^2 + (y_s (T_i - T_o)^{1/2})^2 \right]^{1/2} + \lambda_{v,m} + \lambda_{v,me} \quad (3.36)$$

4

Modelling a reference configuration

In the preceding chapter we have presented a generic dynamic sectorial model that provides a frame to integrate the current knowledge of radon generation, entry, and accumulation indoors from a global and dynamic point of view. In this chapter we apply the model to a reference configuration corresponding to a generic single family house, which tries to have features realistic enough to be representative of a real inhabited house. The chapter contains four sections: First, we describe in detail the reference configuration, giving values of the parameters corresponding to the building design, the building materials, the soil, the steady-state radon entry and the dynamic radon entry. The values chosen correspond to typical average values taken from the literature. Second, we analyse the steady-state entry results by means of variability, sensitivity and uncertainty analysis which are described in detail. Thereafter, we present the results of the dynamic radon entry and accumulation in each room. Finally, we discuss the results obtained in this chapter.

4.1 Description of the reference configuration

4.1.1 Building design

We consider a single-family detached house with a simple geometry. It has a single-zone basement of dimensions $5 \times 5 \times 2 \text{ m}^3$ without any window. There are a ground floor and a first floor, both having two rooms, each with the same dimensions: $5 \times 5 \times 2.5 \text{ m}^3$. Thus, the surface of the above-ground building shell is $5 \times 10 \text{ m}^2$. Fig. 4.1 shows a diagram of the reference configuration house. Rooms 1 and 2 are in the ground floor and 3 and 4 in the first floor. A 1 mm-width crack along all wall joints in direct contact with soil is present, such that the total crack surfaces in the basement and in room 2 are, respectively, 0.028 m^2 and 0.020 m^2 . Each room has a $1.5 \times 1 \text{ m}^2$ window. In addition, room 1 has the entrance door ($2 \times 1 \text{ m}^2$). The rooms are interconnected in the following way: Rooms 1,2 and 3,4 are connected through a $2 \times 1 \text{ m}^2$ door; rooms 2,3 and 2, basement are connected through steps and a $1 \times 1 \text{ m}^2$ trapdoor. We have chosen a single-room basement of size half of the house surface in order to analyse simultaneously two very typical situations: i) A house with a basement that has no direct ventilation with outdoors and ii) A slab-on-grade house. Soil radon enters into the ground floor room 2 through the basement, while in the case of the ground floor room 1, it enters directly from soil. The values of

the parameters needed to run the model corresponding to the building design are given in table 4.1. The effective volume is the same for all the rooms because we have not considered any furniture in the house and steps do not have a significant volume. Room 4 has water supply available. We do not consider either any Heating, Ventilating and Air-Conditioning (HVAC) system or any gas supply.

Table 4.1: Building design parameters

Parameter	Symbol	Value
Basement volume	V_b	50 m ³
Volume of rooms 1,2,3 and 4	$V_1 V_2 V_3 V_4$	62.5 m ³
Basement surface in contact with soil	S_{bs}	65 m ²
Fraction of the basement open area	σ_b	0.00043
Room 1 surface in contact with soil	S_{1s}	25 m ²
Fraction of the room 1 open area	σ_1	0.0008

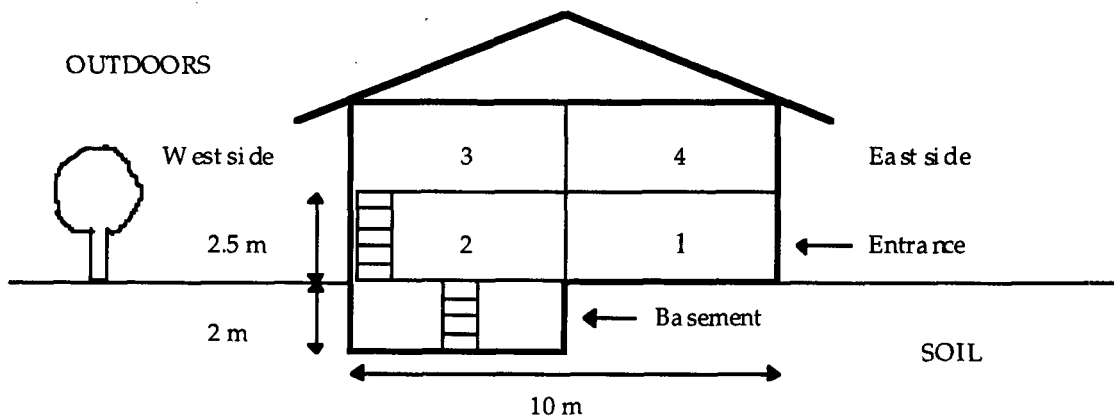


Fig. 4.1: Diagram of the reference configuration house

4.1.2 The building materials

There are two main types of building materials. The building shell and the floors are made from concrete. The thin walls are made from bricks. All brick and concrete surfaces are covered with a 0.05 m layer of plaster and paint. The values of the parameters corresponding to concrete and brick are given in table 4.2. The effect of the layer of plaster and paint is characterised by the "Building materials covering factor" (see equation 3.21). Doors and trapdoors are made from wood with no significant radium content.

Given these types of the building materials and the building design introduced in section 4.1.1, the values of the building material surfaces for each room and each building material construction type obtained are shown in table 4.3.

Table 4.2: Building materials' parameters

PARAMETER	MATERIAL	
	Concrete	Brick
Width (m)	0.25	0.20
Porosity	0.20	0.25
Density (Kg·m ⁻³)	2030	2000
Radium content (Bq·kg ⁻¹)	50	60
Emanation coefficient	0.15	0.05
Effective diffusion coefficient (m ² ·s ⁻¹)	5·10 ⁻⁸	10 ⁻⁷
Covering layer width (m)	0.05	0.05
Building materials covering factor	0.7	0.7

Table 4.3 Building material surface values for the reference configuration. All walls made from brick have the same surface (S_{br}).

Building material	Room	Symbol	Value
Concrete	Basement	S_{bc}	89 m ²
	1	S_{1c}	84 m ²
	2	S_{2c}	84 m ²
	3	S_{3c}	85 m ²
	4	S_{4c}	86 m ²
Brick	1, 2, 3, 4	S_{br}	10.5 m ²

4.1.3 Soil

In table 4.4 all the soil parameter values are given: Both disturbed and undisturbed soil are assumed to have the same physical characteristics, so that no distinction is made for the values of their parameters. We have also included in table 4.4 the parameters calculated from the input parameters according to their corresponding equations from chapter 3.

The map of the RAGENA model adapted to the reference configuration is given in annex 3, together with an example of the "results sheet", a sheet in which the results of a single simulation are summarised.

Table 4.4: Soil parameters

Input parameter	Symbol	Value
Soil grain density	ρ_{gr}	2700 kg·m ⁻³
Mean soil grain diameter	d	20 x 10 ⁻⁶ m
Water saturation fraction	m	0.35
Soil-gas dynamic viscosity	μ	18 x 10 ⁻⁶ Pa·s
Soil porosity	ϵ_S	0.5
Radon diffusion coefficient in air	D_0	1.2 x 10 ⁻⁵ m ² ·s ⁻¹
Soil radium activity concentration	$A_{Ra,S}$	50 Bq kg ⁻¹
Soil maximum emanation coefficient	$f_{S,max}$	0.3
Soil maximum migration distance	M	6 m
Coefficient of solubility of radon in water	L	0.302
Radon decay constant	λ_{Rn}	2.098 x 10 ⁻⁶ s ⁻¹

Calculated parameter

Wet soil density	ρ_{us}	1525 kg m ⁻³
Soil-gas porosity	ϵ_g	0.33
Fraction of emanated radon atoms that reach gas-filled volume	F	0.86
Soil emanation fraction	f_s	0.29
Soil gas-permeability	k	4.53 × 10 ⁻¹¹ m ²
Effective diffusion constant of soil	$D_{e,s}$	2.09 × 10 ⁻⁶ m ² ·s ⁻¹
Migration distance	M_d	6 m

4.1.4 Steady-state radon entry

The steady-state entry of radon into a house depends, in addition to all the previous parameters, on the mean values of soil-basement and soil-room 1 pressure difference, ventilation rate of each room, inter-zone flows, outdoor radon concentration and water sector parameters.

We assume that the mean value of air current from room i to room j is equal to the air current from room j to room i , and that the same happens from room i to outdoors and viceversa, so that

$$q_{ij} = q_{ji}$$

$i, j = 0, b, 1, \dots, 4$ (0 and b mean outdoors and basement respectively)

and, according to sections 3.3.4 and 3.3.6, we only need the values of the λ_{ij} rates instead of both λ_{ij} and λ_{ji} . The mean values chosen are given in table 4.5.

Table 4.5: Mean value of steady-state entry parameters

Parameter	Symbol	Value
Soil-basement pressure difference	$\Delta P_{s,b}$	5 Pa
Soil-room 1 pressure difference	$\Delta P_{s,1}$	5 Pa
Ventilation rates (indoor-outdoor air-exchange-rates)		
Rooms 1 and 2	$\lambda_{1o}, \lambda_{2o}$	1.0 h ⁻¹
Rooms 3 and 4	$\lambda_{3o}, \lambda_{4o}$	0.6 h ⁻¹
Inter-zone rates (inter-room air-exchange rates)		
Basement - room 2	λ_{b2}	0.2 h ⁻¹
Rooms 2-3	λ_{23}	0.2 h ⁻¹
Rooms 1-2 and 3-4	$\lambda_{12}, \lambda_{34}$	0.4 h ⁻¹
Outdoor radon concentration	C_{out}	5 Bq·m ⁻³
Water supply (only in room 4)		
Use rate	W_r	0.032 m ³ ·h ⁻¹
Radon concentration	C_w	5·10 ³ Bq·m ⁻³
Transfer efficiency	t_w	0.7

4.1.4 Dynamic radon entry

In order to describe the dynamics of radon entry, a period of one week has been chosen, using one hour as a time-unit. This time-interval and resolution seems reasonable on account of the fact that the parameters that affect indoor radon dynamics (meteorological parameters and the habits of the inhabitants) have normally a 12 h or 24 h period. Thus, a resolution of one hour is good enough and an interval of one week provides several periods to analyse. Of course, changes of indoor radon at higher frequency may occur, but this argument applies to almost any time-resolution.

We assume that we know the time-behaviour of those "primary" parameters (see section 3.3.7) that are time-dependent, and therefore, the environmental parameters and occupant behaviour sectors are not used when running the model. As we said in sections 3.3.7 and 3.3.8, these sectors are to be used when no direct knowledge of the primary parameters is available.

Fig. 4.2 shows the pattern of behaviour assumed for the following parameters: Soil-basement and soil-room 1 pressure difference (we assume that both are equal), ventilation and air-exchange rates of each room, soil water saturation fraction, and the water supply use rate. The mean value of these parameters over the week correspond to their mean value considered in the steady-state entry. We have assumed that soil temperature and outdoor radon concentration do not change in the week and that no HVAC systems are in use during the week.

The variation of the water saturation fraction and the soil-basement pressure difference produces, according to equations (3.6), (3.7), (3.9) and (3.10), a variation of the soil emanation fraction, the fraction of emanated radon atoms that reach the gas-filled volume, the soil effective diffusion constant, and the soil permeability. Fig. 4.3 shows their time-behaviour.

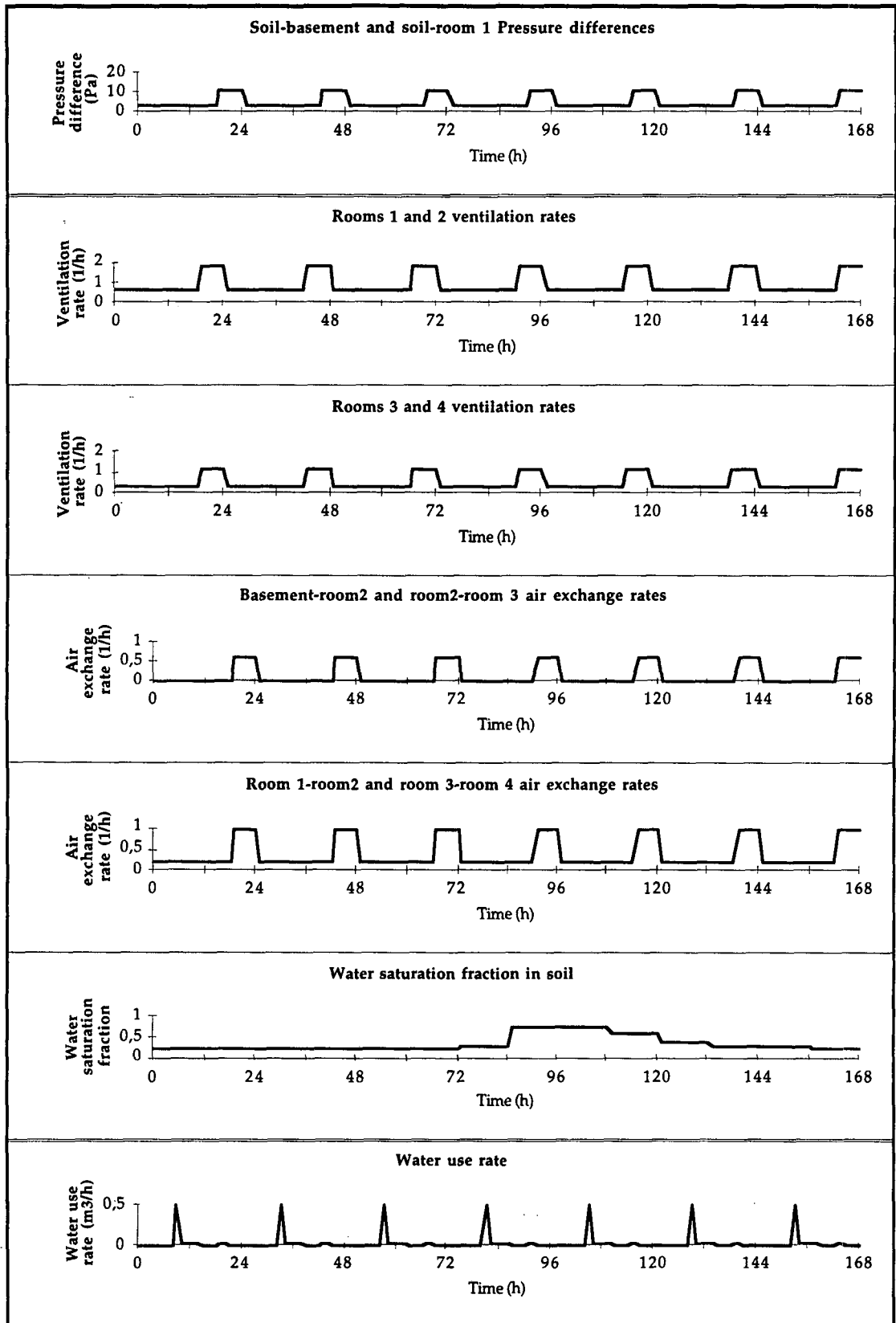


Fig 4.2: Patterns of one week dynamics of soil-basement and soil-room 1 pressure differential, ventilation rates of rooms 1 and 2, and rooms 3 and 4, inter-zone air exchange rates between basement and room 2 and between rooms 2 and 3, inter-zone air exchange rates between rooms 1 and between rooms 3 and 4, soil water saturation fraction, and water use rate.

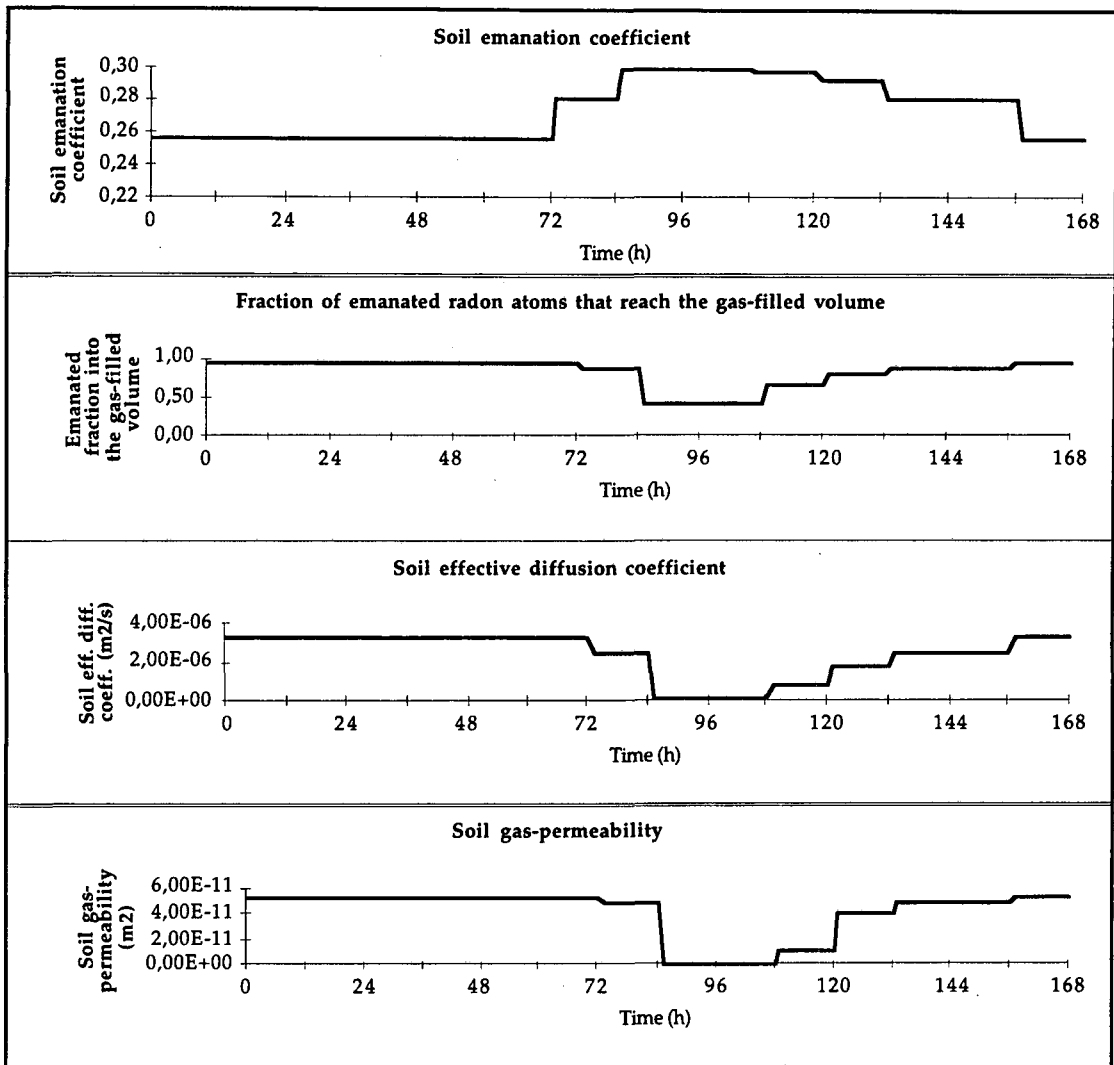


Fig. 4.3: Variation of soil emanation fraction, fraction of emanated radon atoms that reach the gas-filled volume, soil effective diffusion constant and soil permeability, during the one-week simulation period..

4.2 Steady-state results

4.2.1 Simulation results

Since all parameters are kept constant when running the model with the reference configuration, the system tends to an steady-state as shown in Figs. 4.4a and 4.4b, where the evolution of the indoor radon concentration of the basement and of each of the four rooms of the house, the disturbed soil radon concentration and the undisturbed soil radon concentration are presented. When the steady-state is reached, in each compartment of the model the sum of all inflows is equal to the sum of all outflows. The undisturbed soil radon concentration tends to the value corresponding to the radioactive equilibrium with radium for the given default input parameter values as might be expected. The disturbed soil radon concentration tends to a value slightly lower than that corresponding to equilibrium because of radon entry into the house.

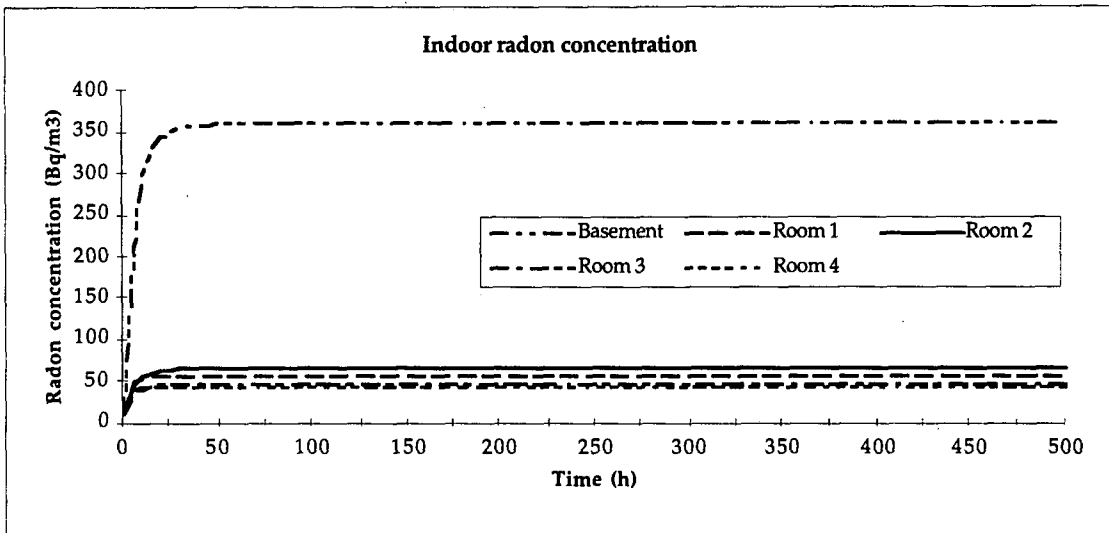


Fig. 4.4a: Evolution of basement and rooms, radon concentration obtained for the reference configuration under steady conditions.

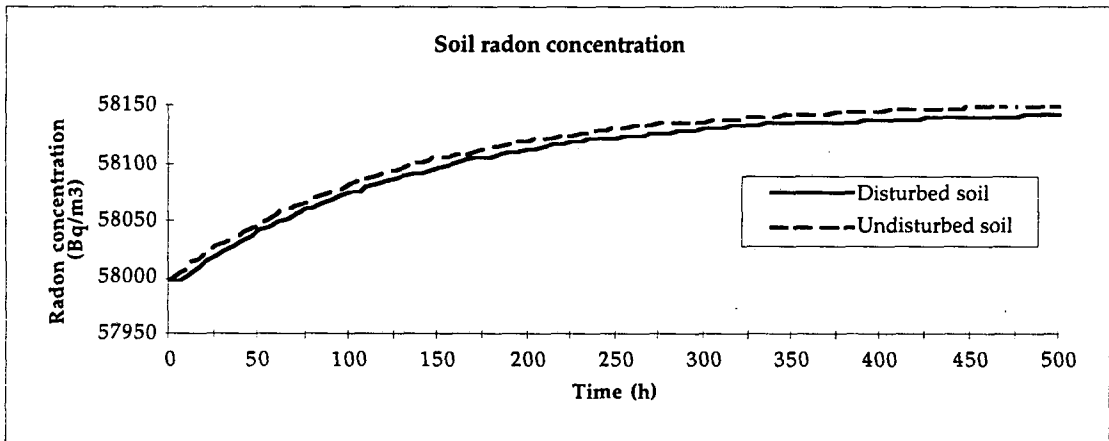


Fig. 4.4b: Evolution of disturbed soil and undisturbed soil radon concentrations obtained for the reference configuration under steady conditions.

Table 4.6 presents the values of the soil and indoor radon concentrations, the different radon entry rates and flows, and the inter-zone rates obtained with the reference configuration. In the steady-state, the sum of the radon entry rates equals the sum of the removal rates in each room. The sign of the inter-zone rates (radon exchange rates) defines the direction of the net radon activity flow from one room into the other: a positive exchange rate between i and j means a net flow from room i to j . Thus, the radon exchange between rooms 1 and 2 gives a net radon flow from room 2 into room 1. The highest indoor radon concentration is achieved in the basement because of two reasons: i) it is in direct contact with soil and ii) it has not a direct ventilation with outdoors. As it can be seen in table 4.7, the maximum entry rate is obtained in room 2 ($1.2086 \text{ Bq}\cdot\text{s}^{-1}$), which is not in direct contact with soil. This is due to the contribution of radon atoms entering into room 2 from the basement (67.6% of the total radon entry into room 2). Room 2 has not the maximum radon concentration because of its ventilation with outdoors.

Table 4.6 The steady-state results of the model for the reference configuration

Parameter		Value obtained
Indoor concentrations ($\text{Bq}\cdot\text{m}^{-3}$)	Basement	360.7
	Room 1	57.1
	Room 2	66.5
	Room 3	47.2
	Room 4	44.6
Building materials entry rates ($\text{Bq}\cdot\text{s}^{-1}$)		
Concrete walls	Basement	$4.00\cdot 10^{-1}$
	Room 1	$3.79\cdot 10^{-1}$
	Room 2	$3.79\cdot 10^{-1}$
	Room 3	$3.83\cdot 10^{-1}$
	Room 4	$3.88\cdot 10^{-1}$
Brick walls	Room 1	$1.28\cdot 10^{-2}$
	Room 2	$1.26\cdot 10^{-2}$
	Room 3	$1.27\cdot 10^{-2}$
	Room 4	$1.27\cdot 10^{-2}$
Soil entry rates ($\text{Bq}\cdot\text{s}^{-1}$)		
Advective	Basement	$4.32\cdot 10^{-1}$
	Room 1	$4.32\cdot 10^{-1}$
Diffusive	Basement	$2.32\cdot 10^{-2}$
	Room 1	$2.33\cdot 10^{-2}$
Water entry rate	Room 4	$6.53\cdot 10^{-8}$
Radon exchange rates ($\text{Bq}\cdot\text{s}^{-1}$)		
	Outdoors - Room 1	$-9.05\cdot 10^{-1}$
	Outdoors - Room 2	-1.07
	Outdoors - Room 3	$-4.39\cdot 10^{-1}$
	Outdoors - Room 4	$-4.13\cdot 10^{-1}$
	Basement - Room 2	$8.17\cdot 10^{-1}$
	Room 1 - Room 2	$-6.52\cdot 10^{-2}$
	Room 2 - Room 3	$6.71\cdot 10^{-2}$
	Room 3 - Room 4	$1.78\cdot 10^{-2}$
Building materials entry flows ($\text{Bq}\cdot\text{m}^{-2}\cdot\text{s}^{-1}$) (Exhalation rate)		
Concrete walls	Basement	$4.49\cdot 10^{-3}$
	Rooms 1 - 4	$4.51\cdot 10^{-3}$
Brick walls	Room 1	$1.22\cdot 10^{-3}$
	Room 2	$1.20\cdot 10^{-3}$
	Rooms 3 - 4	$1.21\cdot 10^{-3}$
Soil entry flows ($\text{Bq}\cdot\text{m}^{-2}\cdot\text{s}^{-1}$)		
Advective	Basement	$6.65\cdot 10^{-3}$
	Room 1	$1.73\cdot 10^{-2}$
Diffusive	Basement	$3.57\cdot 10^{-4}$
	Room 1	$9.32\cdot 10^{-4}$

The entry rates and flows obtained are comparable to the results obtained in the literature (see table 2.6) and the radon concentration values correspond to the mean values obtained around the world (UNSCEAR, 1993). The equation used in the model to obtain the exhalation rate from building materials is an approximation; however, the values obtained in each room are of the same order of those obtained from the exact solution of the diffusion transport equation if the same building material parameter values are taken (see table 2.5 in section 2.2.2.).

Table 4.7 shows the total entry rates in each room and the contribution in percentage of each source-process. It can be seen that the major source to radon entry into the basement and into room 1 is the soil underneath, being advection the dominant mechanism as it might be expected from the value of the permeability (see table 4.3). The contribution of the concrete walls is of the same order as the soil in these rooms and becomes the main one at the first floor. Of special relevance is the contribution of the radon exchange between the basement and room 2, which indicates that the contribution of the soil affects indirectly the radon concentration in room 2 even at higher degree than in the case of room 1 (in direct contact with soil): from table 4.6 we can see that radon entry rate from soil into room 1 is around $0.45 \text{ Bq}\cdot\text{s}^{-1}$, while radon entry from basement into room 2 is $0.82 \text{ Bq}\cdot\text{s}^{-1}$. Water supply contribution is absolutely negligible.

These results show that using reasonable input parameters, the model gives reasonable outputs, having the possibility of analysing all the processes involved in radon generation in the source, entry into the house and redistribution and accumulation indoors.

Table 4.7: Contribution of each source to the radon concentration in each room.

Room	Total entry rate ($\text{Bq}\cdot\text{s}^{-1}$)	Source-process	Contribution (%)
Basement	0.8552	Soil - advection	50.5
		Soil - diffusion	2.7
		Concrete - diffusion	46.8
Room 1	0.9123	Soil - advection	47.4
		Soil - diffusion	2.6
		Concrete - diffusion	41.5
		Brick - diffusion	1.4
		Room 2 - air exchange	7.1
Room 2	1.2086	Concrete - diffusion	31.3
		Brick - diffusion	1.0
		Basement - air exchange	67.6
Room 3	0.4628	Concrete - diffusion	82.8
		Brick - diffusion	2.7
		Room 2 - air exchange	14.5
Room 4	0.4185	Concrete - diffusion	92.7
		Brick - diffusion	3.0
		Room 3 - air exchange	4.3
		Water supply - release	$1.56\cdot 10^{-5}$

The radon concentration values obtained in the two soil volumes and in the building materials of the different rooms are given in table 4.8.

Table 4.8: Radon concentration in soil and building materials for the reference configuration.

Media	Volume description	Radon concentration (Bq.m ⁻³)
Soil	Undisturbed Soil	58151
	Disturbed Soil	58144
Concrete	Basement	6778
	Room 1	6500
	Room 2	6509
	Room 3	6491
	Room 4	6489
Brick	Rooms 1 - 2	926
	Rooms 3 - 4	911

When running a simulation it is necessary to define an initial value of radon concentration in each compartment; that is, in the disturbed and undisturbed soil volumes, in each room, in each building material, and outdoors. Independently of the initial values chosen, the system tends to the same steady-state. In Figs. 4.5a and 4.5b we present, respectively, the evolution of the basement radon concentration when different initial values of soil and concrete radon concentration are taken. The transient discrepancy between the different curves depends on how far from the steady-state value the initial soil and concrete radon concentration are; the closer to the value, the sooner the steady-state is reached. Thus, the only effect of choosing different initial values is to delay or to speed up the achievement of the steady-state. The initial soil radon concentration can produce the longest delay, while the initial concrete radon concentration can produce high discrepancies, but the steady-state is reached in less than 100 h. The impact of initial outdoor, brick, and room radon concentrations has been found negligible. Therefore, in order to save computing time, the value of the soil radon concentration in equilibrium with radium is calculated before running the model for a given configuration, and is used as initial soil radon concentration.

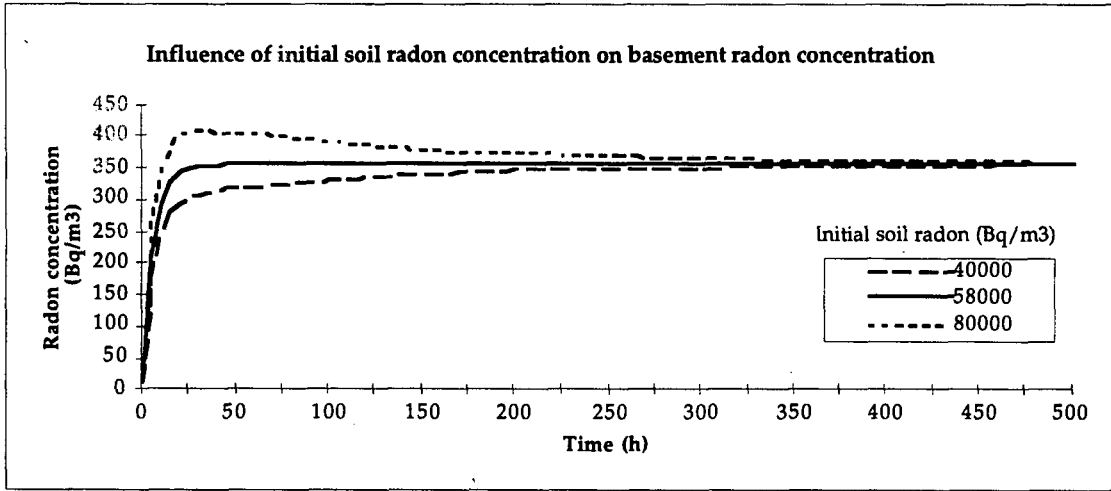


Fig. 4.5a: The influence of initial soil radon concentration on basement radon concentration.

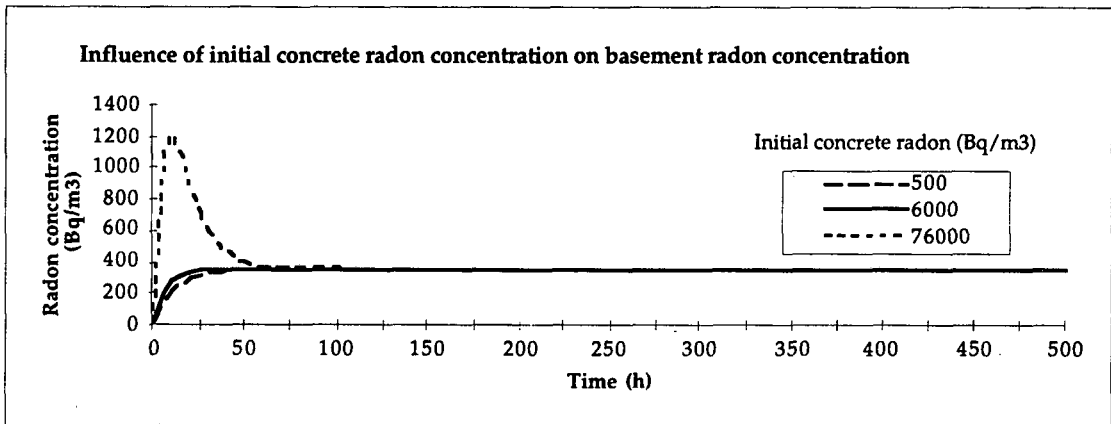


Fig. 4.5b: The influence of initial concrete radon concentration on basement radon concentration.

4.2.2 Variability analysis

The RAGENA model has been designed to be generic, as opposite to site-specific, in order to have the possibility of being easily adapted to a wide range of situations. The exploration of the applicability of the model to different situations has been performed in two steps by means of a variability analysis. This analysis focuses on the consequences of the difference in values of the input parameters across several situations, allowing the identification of the most important parameters from the generic point of view. Following the methodology given by Schell et al. (1996), we have investigated the response of the model to the variation of one of the input parameters within a wide range, holding the other parameters constant at the default value (that corresponding to the reference configuration).

It is worthwhile to distinguish a variability analysis from sensitivity and uncertainty analysis: the first one is concerned with the applicability of the model to several situations,

while the second one explores the response of the system to small and/or sudden fluctuations of a parameter around a given value and therefore, it is appropriate when studying a specific site or configuration. An uncertainty analysis accounts for the fact that the values of the parameters within a system are never precisely defined and are best described by a probability distribution. A sensitivity and uncertainty analysis around the reference configuration are the subject of sections 4.2.3. and 4.2.4 respectively.

The minimum (C_{min}) and maximum (C_{max}) indoor radon concentrations obtained with the model in each room when changing the parameter value have been used to calculate the Variability Index (VI) of the studied parameter, defined as:

$$VI = \left| 1 - \frac{C_{min}}{C_{max}} \right| \quad (4.1)$$

The ranges of variation of the model parameters and their corresponding VI for each room are given in table 4.8. The influence of the room dimensions has been analysed only in one room -the basement- from the ratio of the surface to the volume of the room. Two additional basements have been considered: a small squared room 1 meter deep and 2 meters in side and a bigger rectangular room 2 meters deep and sides of 5 and 10 meters. Table 4.8 allows to see which parameters are more relevant for the reference configuration and in which room their variation is more important as well. The VI ranges from 0 to 1; a value close to 1 means that the parameter has a large impact, while a value close to 0 means a low impact.

The determination of the most relevant parameters for each room depends on the value of the VI considered as high. Taking as a "first order in importance" those parameters with the VI value higher than 0.800, we see from table 4.9 that:

- i) The mean soil grain diameter has a large impact on all the rooms of the house, mainly in the basement and in the ground-floor. This is consequence of its range of variation and its influence on the soil permeability (see Eq. (3.10) and Fig. (3.3)).
- ii) The concrete radium content and emanation coefficient have also a large influence, specially in the first floor rooms, where the influence of the soil parameters is diminished.
- iii) The soil-indoor pressure difference and the fraction of the open area, that is, the soil-house interface parameters affect basically the basement and the ground-floor rooms.

iv) Ventilation rates, as the main responsible for radon removal, are very important parameters, affecting specially the room considered.

v) The most important inter-zone flow is that between the basement and room 2, which affects very much room 2 radon concentration.

Table 4..9: The range of variation and the Variability Index in each room corresponding to each parameter around the reference configuration.

Code	Parameter	Range	Variability index				
			Basement	Room			
				1	2	3	4
1	Mean soil grain diameter (m)	[10 ⁻⁶ - 10 ⁻³]	0.994	0.992	0.989	0.946	0.872
2	Soil grain density (kg·m ⁻³)	[2650 - 2750]	0.016	0.014	0.010	0.004	0.002
3	Soil water saturation fraction	[0.01 - 0.99]	0.496	0.436	0.335	0.091	0.038
4	Soil porosity	[0.2 - 0.6]	0.261	0.235	0.189	0.057	0.024
5	Soil radium content (Bq·kg ⁻¹)	[10 - 150]	0.698	0.653	0.563	0.214	0.098
6	Soil maximum emanation coeff.	[0.02 - 0.7]	0.677	0.627	0.526	0.182	0.081
7	Maximum migration distance (m)	[2 - 15]	0.000	0.000	0.000	0.000	0.000
8	Radon coeff. of solubility in water	[0.180 - 0.525]	0.074	0.067	0.050	0.015	0.007
9	Concrete width (m)	[0.1 - 0.4]	0.486	0.444	0.334	0.102	0.258
10	Concrete porosity	[0.12 - 0.27]	0.032	0.029	0.037	0.050	0.052
11	Concrete density (kg·m ⁻³)	[1930 - 2260]	0.075	0.072	0.088	0.117	0.123
12	Concrete radium content (Bq·kg ⁻¹)	[10 - 100]	0.590	0.570	0.660	0.790	0.814
13	Concrete emanation coefficient	[0.01 - 0.4]	0.700	0.680	0.766	0.883	0.904
14	Concrete eff. diff. coeff. (m ² ·s ⁻¹)	[7.6·10 ⁻⁹ - 2.1·10 ⁻⁶]	0.503	0.484	0.568	0.694	0.719
15	BM covering layer width (m)	[0.01 - 0.1]	0.071	0.069	0.085	0.114	0.121
16	BM covering factor	[0.15 - 0.98]	0.126	0.121	0.151	0.204	0.213
17	Brick width (m)	[0.10 - 0.25]	0.001	0.007	0.008	0.015	0.016
18	Brick porosity	[0.24 - 0.26]	0.000	0.000	0.000	0.000	0.000
19	Brick density (kg·m ⁻³)	[1950 - 2030]	0.000	0.000	0.000	0.002	0.000
20	Brick radium content (Bq·kg ⁻¹)	[20 - 200]	0.006	0.037	0.034	0.068	0.076
21	Brick emanation coefficient	[0.02 - 0.1]	0.003	0.021	0.019	0.037	0.041
22	Brick eff. diff. coeff. (m ² ·s ⁻¹)	[8.4·10 ⁻⁸ - 3.4·10 ⁻⁷]	0.000	0.000	0.000	0.000	0.000
23	Soil - indoor pressure diff. (Pa)	[-5 - 15]	0.973	0.909	0.781	0.295	0.134
24	Fraction of open area	[0.00001 - 0.1]	0.994	0.993	0.990	0.415	0.220
25	Rooms 1 and 2 vent. rates (h ⁻¹)	[0.1 - 1]	0.405	0.837	0.794	0.508	0.305
26	Rooms 3 and 4 vent. rates (h ⁻¹)	[0.1 - 1]	0.039	0.071	0.191	0.779	0.820
27	Air-exchange basement-2 (h ⁻¹)	[0.1 - 1]	0.703	0.251	0.999	0.085	0.078
28	Air-exchange 2-3 (h ⁻¹)	[0.1 - 1]	0.003	0.128	0.412	0.302	0.074
29	Air-exchange 1-2 (h ⁻¹)	[0.1 - 1]	0.007	0.379	0.473	0.086	0.045
30	Air-exchange 3-4 (h ⁻¹)	[0.1 - 1]	0.000	0.000	0.003	0.025	0.038
31	Outdoor Rn concentr. (Bq·m ⁻³)	[0 - 10]	0.026	0.159	0.137	0.190	0.198
32	Water use-rate (m ³ ·h ⁻¹)	[0.017 - 0.064]	0.000	0.000	0.000	0.000	0.000
33	Water transfer efficiency	[0.1 - 0.98]	0.000	0.000	0.000	0.000	0.000
34	Water Rn concentr. (Bq·m ⁻³)	[1 - 1000·10 ³]	0.000	0.000	0.000	0.000	0.000
35	Basement S/V ratio (m ⁻¹)	[1.10 - 3.75]	0.766	-	-	-	-

A closer view to the table 4.9 shows that in general, the importance of the soil parameters decreases with height while the importance of concrete parameters increases, as might be expected. The contribution of the brick building material is low compared to the concrete contribution. Considering as "second order in importance" those parameters with VI in the range [0.400 - 0.800], we obtain the soil water saturation fraction, radium content, and maximum emanation coefficient, the air-exchange between rooms, and the S/V ratio of the room. All the VI values higher than 0.400 in table 4.7 are in bold. Then, we can see that from a set of 35 parameters, the single parameter variation analysis has allowed to determine the relevant parameters for each room: 12 for the basement, room 1 and 2, 7 for room 3, and 5 for room 4.

We have separated the important parameters into 4 groups: i) Soil parameters (codes 1,3,5,6,9), ii) Concrete parameters (codes 12,13,14), iii) Soil-house interface and geometry parameters (codes 23,24), and iv) Ventilation and air-exchange parameters (25,26,27,28,29,30). A more detailed study of these parameters is following.

4.2.2.1 Soil parameters

The relevant soil parameters have been separated into three subgroups:

4.2.2.1.1 Radium content and maximum emanation fraction

We have analysed the parameters that influence radon emanation into the gas-filled volume of the soil keeping the soil type and the water saturation fraction constant. These parameters are the radium content and the maximum emanation fraction; their variations produce changes on soil radon concentration and therefore, their high VI evidences the importance of soil radon level on indoor radon concentration. Being the basement the room more influenced by soil parameters, we have plot the basement radon concentration as a function of the disturbed soil radon concentration in Fig. 4.6, where a linear relationship has been found with a slope of 0.31%. This slope shows the efficiency of soil radon to enter into the house and has been called Radon Entry Efficiency (REE); typical values for houses with basement would theoretically be in the range 0.3 - 0.7% (A. Tanner, 1994), in agreement with our result.

4.2.2.1.2 Water saturation fraction and soil type

We have analysed the effect of the water saturation fraction and the soil type on the basement radon levels. The soil type in the RAGENA model is characterised by its mean grain diameter, with high VI, and its porosity, having a much smaller VI. Considering clay, silt and sand with

the mean particle diameter and porosity values given in Fig. 3.3, the diffusive and advective radon entry from soil are plotted in Fig. 4.7 as a function of the water saturation fraction.

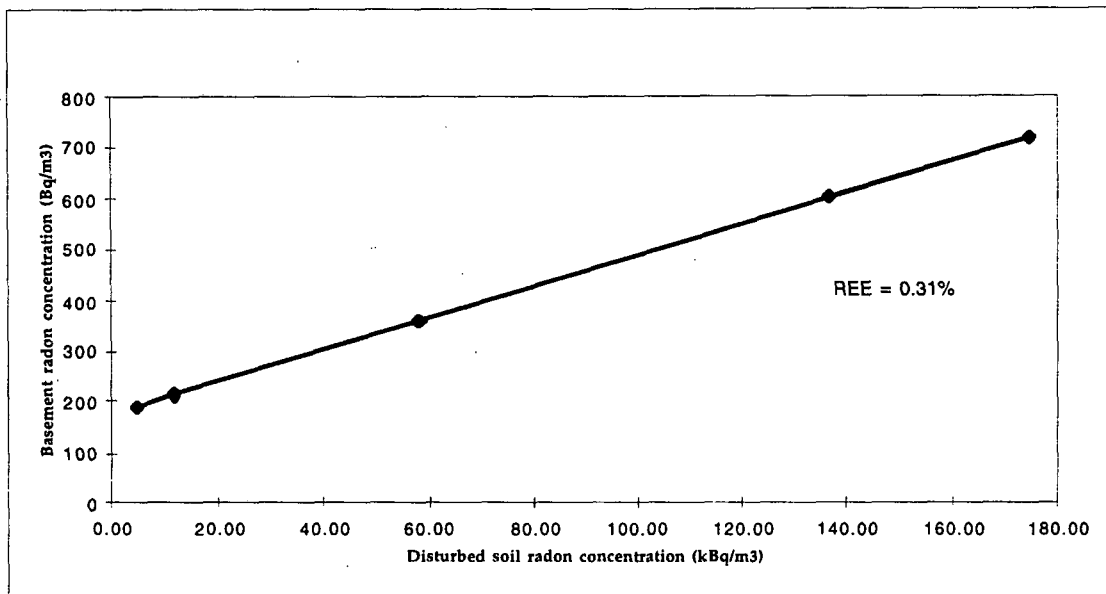


Fig. 4.6: Basement radon concentration as a function of soil radon concentration when soil-type and water saturation fraction are kept constant. The Radon Entry Efficiency (REE) is the slope (in percentage) of the line.

It is observed in the three plots that the maximum radon entry rate is achieved for an intermediate value of the water saturation fraction. This behaviour can be explained as follows: when the soil is dry, even though permeability and diffusivity are high, the emanation fraction is very low; an increase of the water content fills first the small pores and the emanation fraction is increased while the transport properties are only slightly reduced - as transport takes place mainly through large pores-, and when the soil is wet, the emanation fraction is higher but permeability and diffusivity are greatly reduced. The maximum entry rate is achieved sooner in clayey than in silty and sandy soils. It is observed that the relative importance of the entry processes depends strongly on the soil type and the water saturation fraction. Diffusion dominates radon entry into the basement for a clayey soil because of its low permeability, but for silty and sandy soils, advection is the dominant radon entry mechanisms. In any case, the model results show that the highest radon entry rates are achieved when the advective entry dominates, in accordance with previous studies (Loureiro 1987, Andersen 1992). It is worthwhile noting that these results correspond to the reference configuration and that the importance of a given parameter depends on the values of the other parameters; for example, choosing other soil parameter values (mean diameter and porosity), will change the relative importance of entry mechanisms.

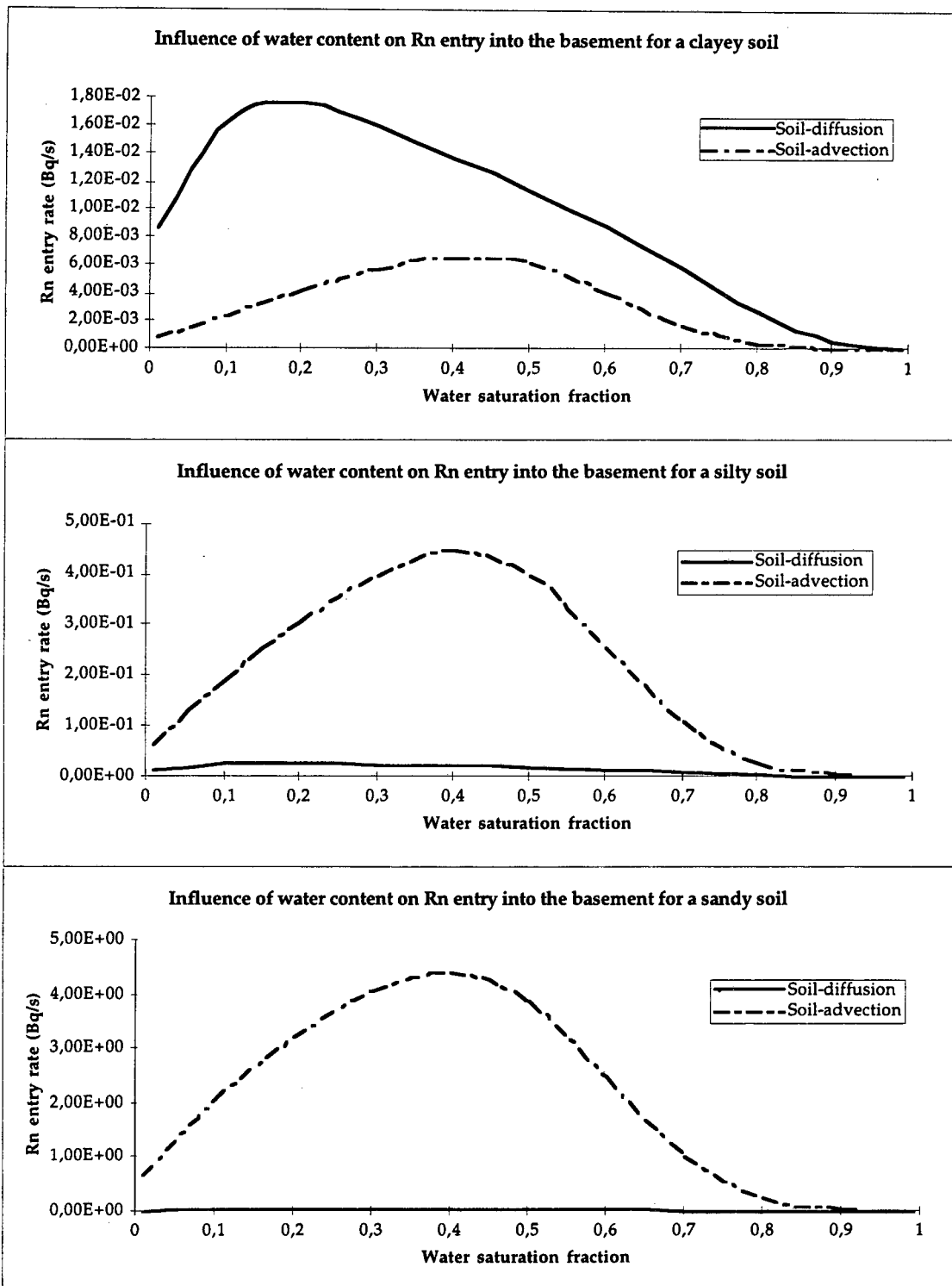


Fig. 4.7: Diffusive and advective radon entry from soil into the basement as a function of the water saturation fraction, where clay, silt and sand correspond to those given in Fig. 3.3.

Soil and indoor radon concentrations have been plotted as a function of water saturation fraction for the three mentioned soil types in Figs. 4.8 and 4.9. High indoor radon concentrations are obtained with a sandy soil, which has the highest permeability. The influence of the water

saturation fraction on soil radon concentration also manifests the importance of the rainfall: during precipitation events, water content increases at the expense of pore space available for radon transport. There is a reduction in the gas-filled soil porosity that reduces transport parameters, increases emanation fraction, and forces a redistribution of radon between gas and liquid phases. The result of these effects is an increased radon concentration in the gas-filled volume of the soil. We see then that even though soil radon concentration increases, the indoor radon concentration diminishes because of the reduction on soil radon transport parameters.

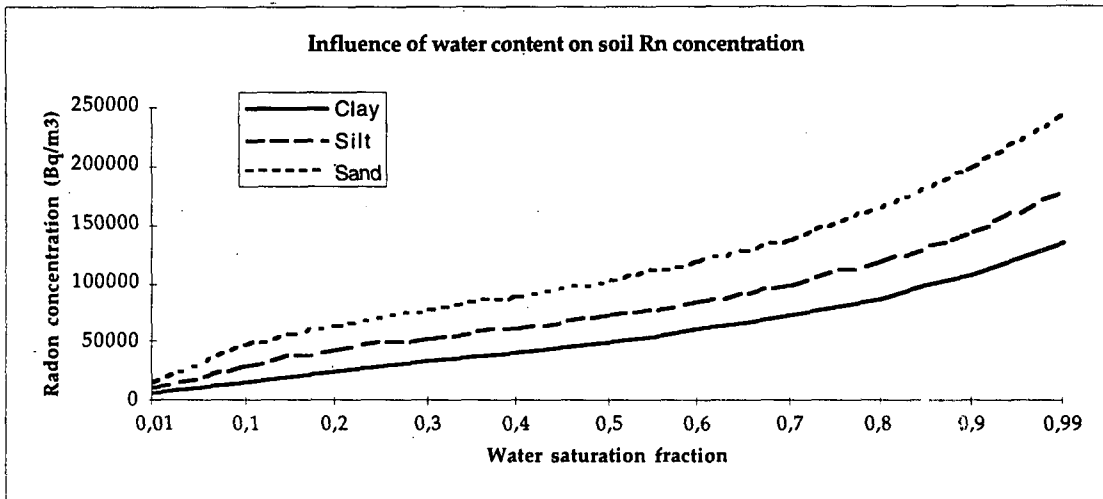


Fig. 4.8: Soil radon concentration as a function of the water saturation fraction, where clay, silt and sand correspond to those given in Fig. 3.3.

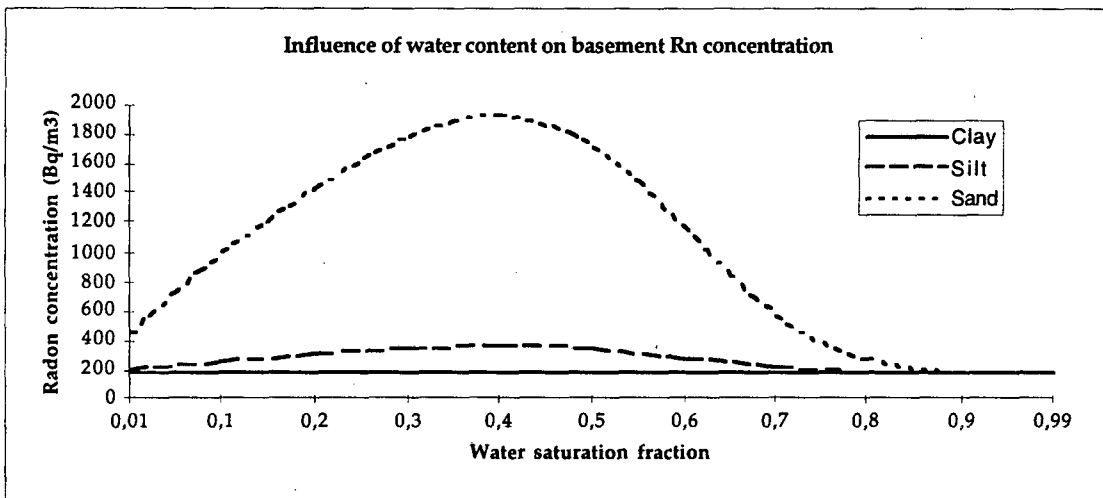


Fig. 4.9: Basement radon concentration as a function of the water saturation fraction, where clay, silt and sand correspond to those given in Fig. 3.3.

4.2.2.1.3 Gas-permeability

Variations on mean grain diameter, water saturation fraction, and soil porosity produce, according to Eq. (3.10), changes on soil gas-permeability. Owing to the importance of this

parameter, we have plotted in Fig. 4.10 the basement radon concentration as a function of soil gas-permeability considering the different values of soil gas-permeability obtained in the variability analysis. We observe that the effect of the soil gas-permeability on the indoor radon levels can be appreciated from the value $1 \cdot 10^{-12} \text{ m}^2$ approximately, and that high gas-permeability values correspond to high indoor radon concentrations. For values smaller than $1 \cdot 10^{-12} \text{ m}^2$, changes on gas-permeability do not influence on basement radon levels.

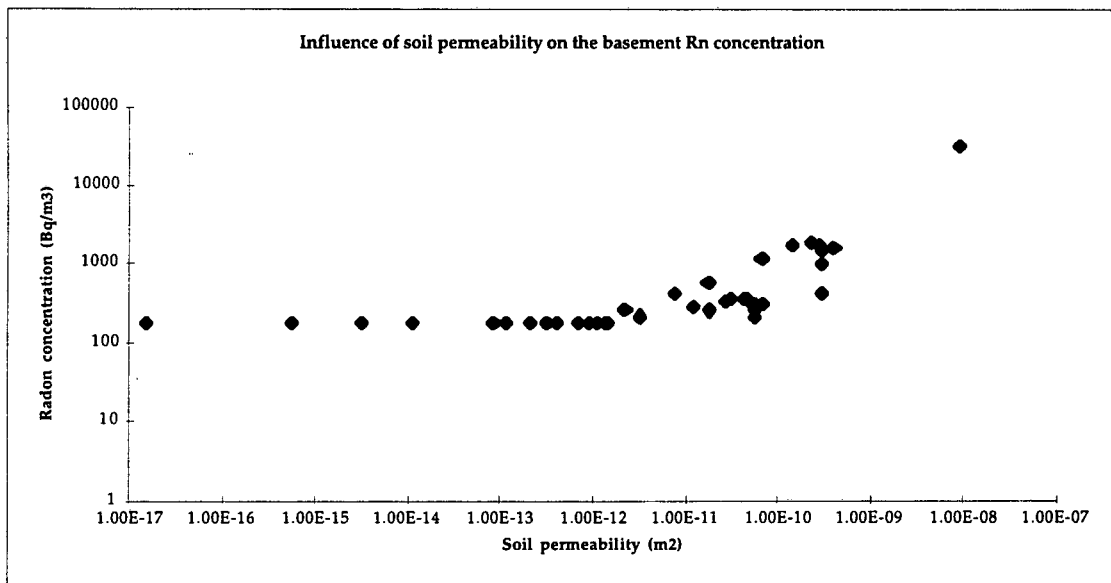


Fig. 4.10: Basement radon concentration as a function of soil gas-permeability

4.2.2.2 Concrete parameters.

The most relevant concrete parameters found with the variability analysis are the concrete radium content, emanation coefficient and effective diffusion coefficient. The concrete width has been found important only in basement and room. Since the exhalation mechanism is assumed to be diffusive, the radon concentration gradient between concrete and indoors and the effective diffusion coefficient are expected to be the most important parameters. Our results confirm this statement because the radon concentration gradient depends on the radon concentration difference between indoors and the concrete, being concrete concentration proportional to the radium content and the emanation coefficient. The importance of concrete width in the basement and room 1 can be explained easily by noting that in our reference configuration, the concrete width and the foundations width are equal, so that a change on the concrete width changes the advection transfer coefficient between soil and indoor according to Eq. (3.19) and thus, affects the advective radon entry rate.

In Fig. 4.11 we have plotted the radon concentration in each room of the reference configuration as a function of the concrete radon concentration. Even though a linear relationship is observed in all the rooms, the slope is different in each case, specially in the basement. The highest slope in the basement is due to the fact that the basement is the room that has the lowest ventilation and the larger concrete surface. Thus, this room is more sensitive to an increase on the concrete concentration.

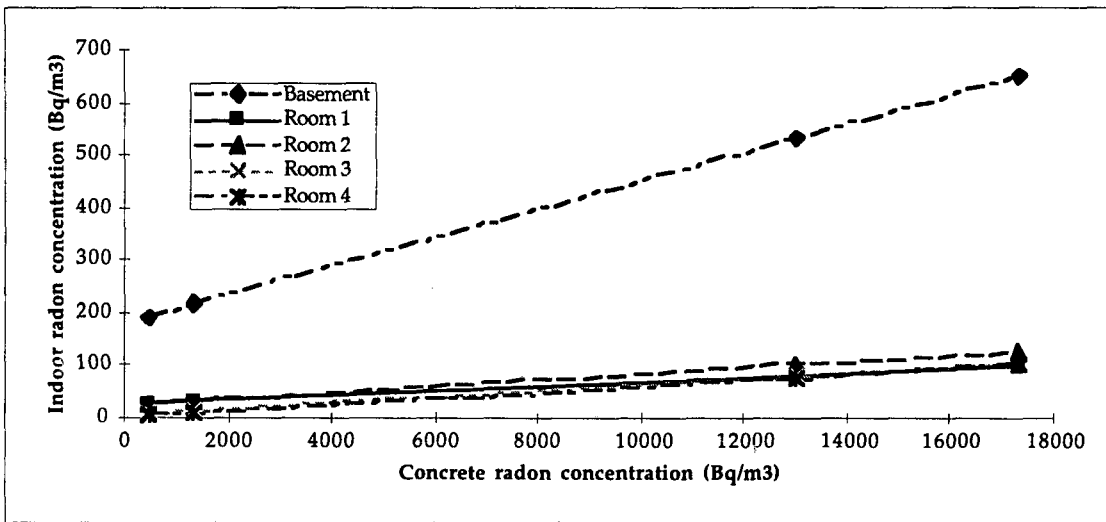


Fig. 4.11: Indoor radon concentrations as a function of the concrete radon concentration.

4.2.2.3 Soil-house interface and geometry parameters

The soil-house interface parameters are the fraction of the open area and the soil-indoor pressure difference. In our model, we describe the interface only with these two parameters, but in an specific site, a more detailed description can be attempted, considering, for example, the piping structure and design.

According to the assumptions of the RAGENA equations, we obtain a linear relationship between the open area and the radon entry rate from soil and between the soil-indoor pressure difference and the advective radon entry from soil. The results of the variability analysis show that decreasing the fraction of the open area down to $1 \cdot 10^{-5}$ (0.001%) reduces the basement radon concentration down to $185 \text{ Bq} \cdot \text{m}^{-3}$, and that an overpressure of 5 Pa reduces the basement radon concentration to $19 \text{ Bq} \cdot \text{m}^{-3}$. This results support crack sealing and indoor overpressuring as effective mitigation methods. As we said in section 3.3, the RAGENA model is more concerned to the dynamic behaviour of the system than have an space resolution: the values of the parameters correspond to space-averaged values. Other studies have showed a more complex dependence between the open area and the radon entry rate: from theoretical considerations, Holub and Killoran (1994) found that when diffusive and advective flows are plotted as a

function of the number of cracks per unit length, a crossover occurs where diffusion starts to dominate; Robinson and Sextro (1995) found both theoretically and experimentally that the response of the radon entry rate as a function of the open area strongly depends on the soil permeability and/or the presence of a subslab gravel layer: when the medium underneath the house has a high permeability, most of the large pores are connected and then, only a few percentage of cracks opened allows the radon entry into the structure; consequently, crack sealing is in this case an ineffective mitigation method because it is virtually impossible to seal all the cracks of a house; on the other hand, where the permeability is low, the radon entry gradually increases with the open area, ore in accordance with our results. Owing to the structure of the RAGENA model, this different dependence of the radon entry as a function of the open area for different permeability values can not be described.

Finally, the ratio of the surface to the volume of the basement has been found very important as well; keeping all the other parameters constant and just changing the dimensions of the basement room, we have found that radon concentration ranges from 319 to 1365 Bq·m⁻³ when changing the surface-volume ratio from 1.10 m⁻¹ to 3.75 m⁻¹. This result, which must be expected in any room, shows the importance of the geometry of the room when analysing its radon level.

4.2.2. Ventilation and air-exchange parameters

The ventilation rate between the room and outdoors is a key parameter, as we have seen in chapter 2. The balance between entry and removal by ventilation gives the final radon concentration in the house. The air-exchange between the rooms of the house governs the redistribution of the radon in the rooms: high air-exchange rates tend to homogenise the indoor air and then, a single-zone house might be considered; small air-exchange rates isolate the different rooms of the house, allowing high radon concentration differences between the rooms.

In Fig. 4.12 we have plotted the radon concentration of the basement, room 1 and room 2 as a function of ventilation rate of rooms 1 and 2, to see the dependence of indoor radon concentration on ventilation rate. Even though the basement does not have direct contact with outdoors, its air-exchange with room 2 makes it sensitive to room 2 ventilation rate. We have increased the range of variation of the ventilation rate in order to see better its influence on indoor radon levels. It is observed that varying the ventilation rate when it is low (<1 h⁻¹) has a large impact on radon levels and can reduce them very much. However, for ventilation rates higher than 2 h⁻¹, radon concentration is almost not influenced by an increase of them. This behaviour has been found in the other rooms as well. Therefore, the results indicate that increasing ventilation rate can be a good mitigation method when the initial ventilation rate is low.

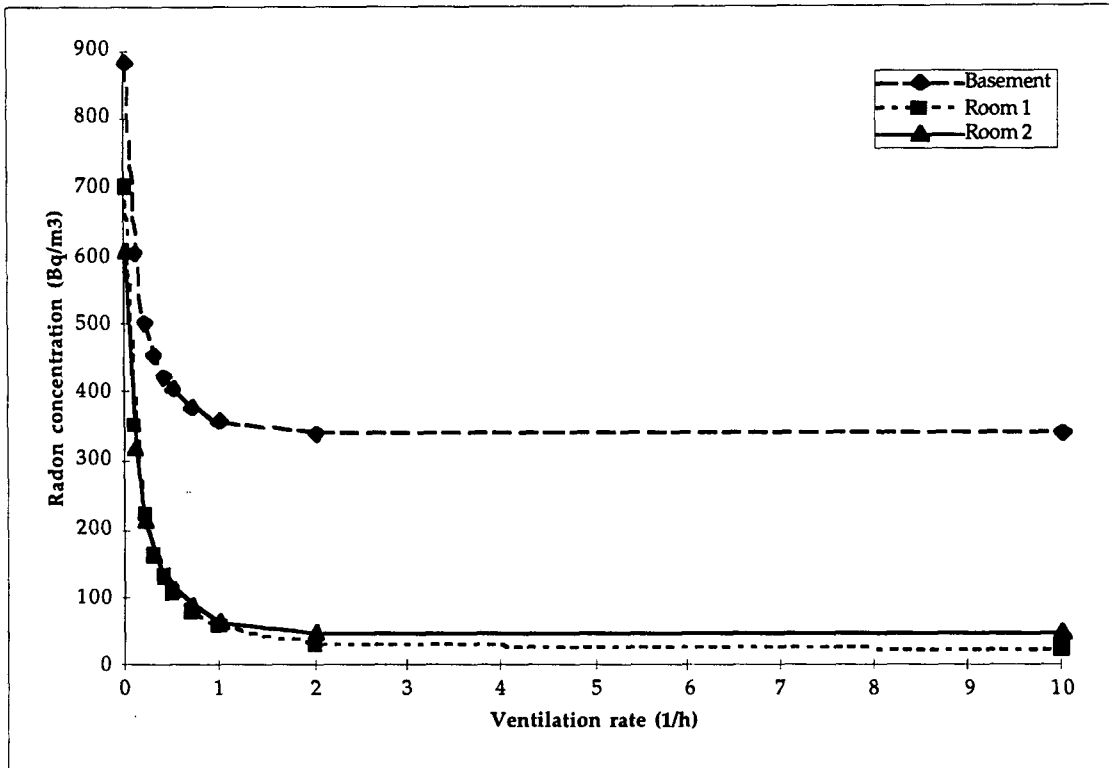


Fig. 4.12: Influence of the ventilation rate of rooms 1 and 2 on the radon concentration in the basement and in rooms 1 and 2.

4.2.3 Sensitivity analysis.

The variability analysis performed in the preceding section has allowed the determination of the most relevant parameters that affect indoor radon concentration, exploring the response of the model to a wide range of different situations around the type of house corresponding to the reference configuration. In this section we present the results of the sensitivity analysis performed in this work. The objective of such an analysis, as we said in the previous section, is to study the response of the system to sudden and/or small fluctuations of the parameter values around the default value. This analysis has been performed by stressing the system in three different ways: i) Step function: the studied parameter suddenly changes its value to a new one at which is kept. ii) Pulses: the parameter value experiments periodic instantaneous raises and descents, and iii) Sinwave: the parameter changes in time following a sinwave of a given frequency and amplitude.

4.2.3.1 Step functions

The parameters chosen for the step function are those expected to change suddenly in a given site: water saturation fraction, soil-indoor pressure difference, ventilation rates, air-exchange rates, and outdoor radon concentration. In each case, we have multiplied the value of the parameter by a factor of 2 at the instant $t=150$ h; the parameter is kept at the new value for the

rest of the simulation (until $t=500$ h). After the change, the system tends to a new steady-state. The effect of water saturation fraction step on the indoor radon levels is shown in Fig. 4.13, where it can be seen that the increase of the water saturation fraction from 0.35 to 0.70 results in a decrease of indoor radon levels. The time needed to reach the new steady state is different for each room. We characterise the dependence of the system to the sudden fluctuation of the parameter value by the longest time needed to reach the 95% of the radon concentration corresponding to the new steady-state (we call it "response time") and by the percentage of variation of the new steady-state with respect to the old one.

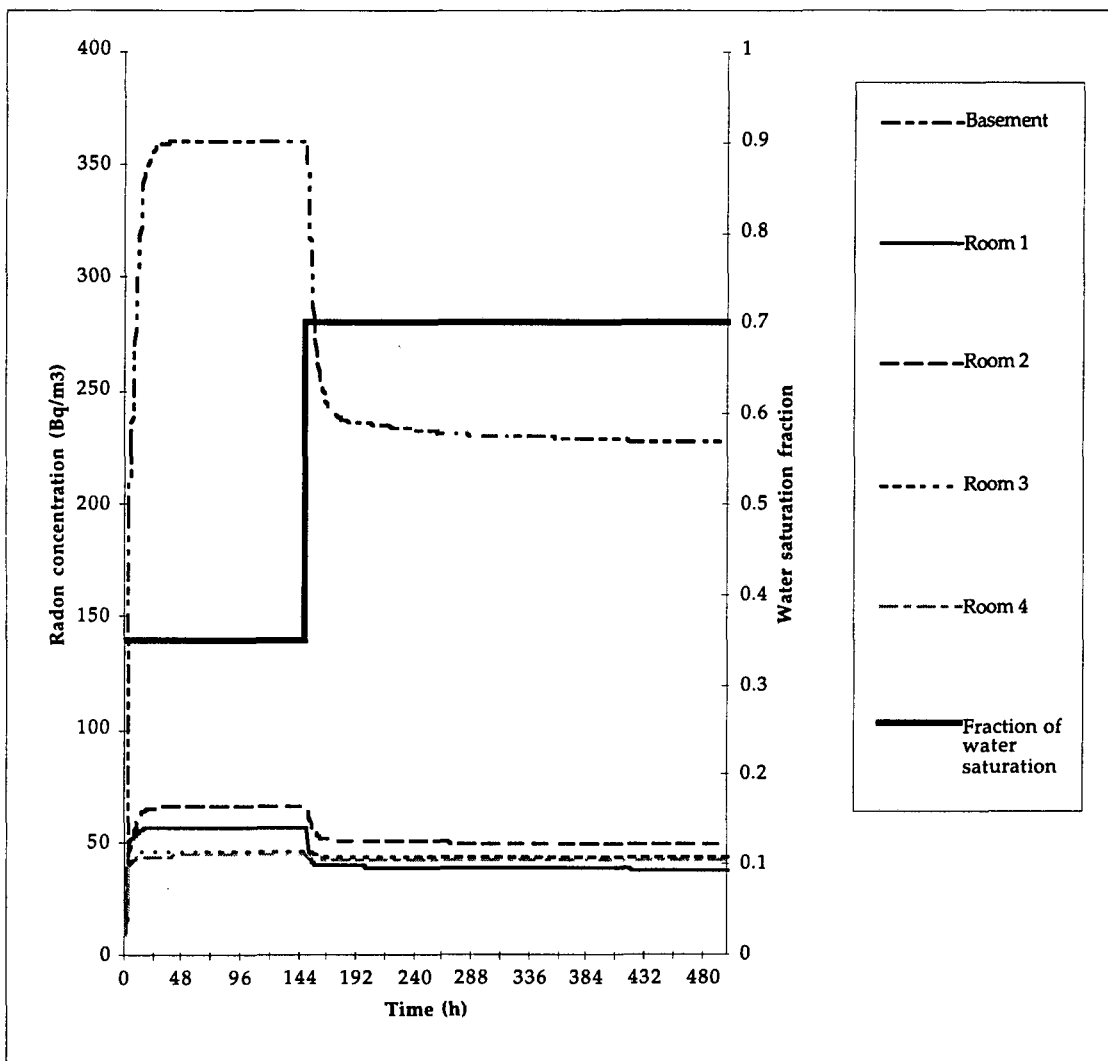


Fig. 4.13: Response of the indoor radon concentrations to a sudden change of the soil water saturation fraction.

In table 4.10 the response time and the percentage of variation obtained for a 100% sudden rise of the parameters is given. It can be seen that in all cases the response time is not so long: the

longest one (25 h) corresponds to the water saturation fraction in the soil. The effect of the 100% rise on the indoor radon levels is different for each parameter. The water saturation fraction and the soil-indoor pressure difference affect all the rooms of the house, although its impact decreases with height as it might be expected. The outdoor radon concentration affects all the rooms in direct contact with outdoors, and the air exchange rates basically only affect the two rooms involved. These results are very reasonable and show that the model presents a good behaviour when a sudden change of the parameters occurs.

Table 4..10: Response time (RT), new steady-state values of radon concentration C (in Bq·m⁻³) and percentage of variation (PV) obtained with the step functions for each studied parameter in each room. The PV is calculated as

$$PV = (New\ value - old\ value) * 100 / old\ value.$$

Parameter	RT (h)	Basement		Room 1		Room 2		Room 3		Room 4	
		C	PV	C	PV	C	PV	C	PV	C	PV
Water sat. frac.	25	228.2	-36.7	38.6	-32.4	50	-24.8	44	-6.8	43.4	-2.7
Pressure diff.	10	530.7	47.1	80.8	41.5	87.7	31.9	51.2	8.5	46.2	3.6
Vent. rate 1 and 2	3	333.8	-7.46	30.8	-46.1	38.5	-42.1	41.8	-11.4	42.5	-4.7
Vent. rate 3 and 4	3	358.4	-0.64	56.4	-1.23	64	-3.76	28.6	-39.4	25.2	-43.5
Air-exchange b-2	4	217.1	-39.8	57.3	0.35	67.1	0.9	47.3	0.2	44.7	0.2
Air-exchange 2-3	1	359.1	-0.44	56.6	-0.9	64.8	-2.6	49.7	5.3	45.6	2.2
Air-exchange 1-2	0	359.5	-0.33	58.6	2.63	65.2	-1.95	46.9	-0.64	44.5	-0.22
Air-exchange 3-4	0	360.7	0.00	57.1	0.00	66.5	0.00	46.8	-0.85	45.1	1.12
Outdoor Rn conc.	2	365.5	1.33	62.1	8.8	71.4	7.4	52.1	10.4	49.5	11.0

4.2.3.2 Pulses

Some parameter values can experiment periodical raises and descends in a house. This is the case, for example, of the ventilation rate in a room; it is very common that each morning the inhabitants open the window for half an hour or one hour to ventilate the room. This periodic behaviour produces a sudden increase and descend of the ventilation rate of the given room. The periodic use of Heating, Ventilating and Air-Conditioning systems may produce such a dynamic pattern as well. Therefore, the parameters chosen to follow this pattern are the soil-indoor pressure difference, the ventilation rates and the air-exchange rates. For each parameter, we have assumed a pulse pattern of a 8 unit increase, of one hour duration and a frequency of 1 pulse each 24 hours, starting at the instant t=100h.

In Fig. 4.14 we present the time evolution of indoor radon levels when the rooms 1 and 2 ventilation rate follows the described pulse pattern. It can be observed that when the system is disturbed by the high change of the parameter value, the radon concentration in each room decreases down to a given value and then goes back to the initial steady-state value, which is

reached before the following pulse occurs because the response time is shorter than the period between pulses. The pulse pattern of rooms 1 and 2 ventilation rates affects the radon levels of all rooms, being rooms 1 and 2 those most affected, as might be expected. In the case of ventilation of rooms 3 and 4, also radon concentration decreases and goes back to the initial steady-state in each room, being rooms 3 and 4 the most affected, but the impact on the basement and on rooms 1 and 2 is much smaller than the previous case.

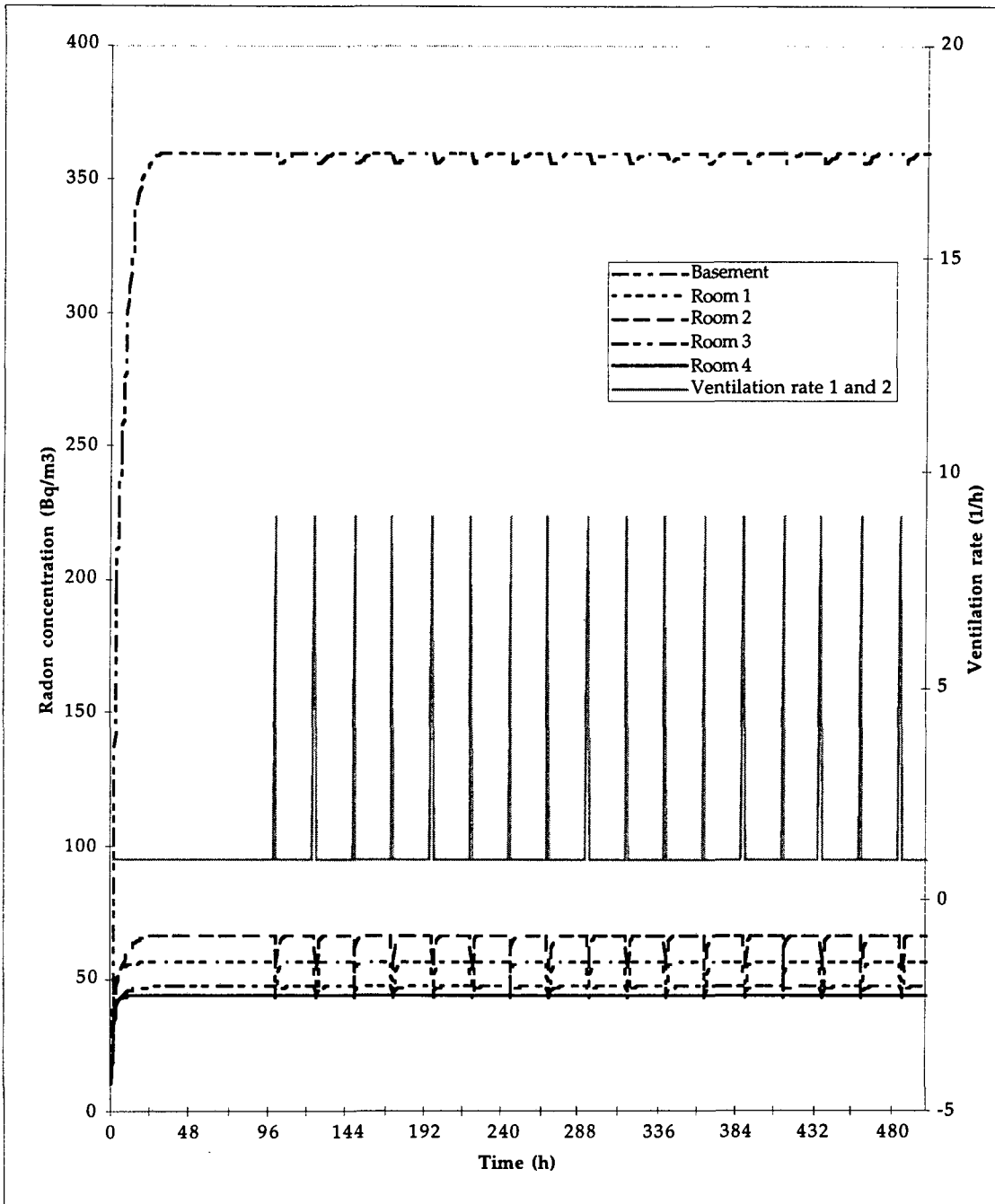


Fig. 4.14: Response of the indoor radon concentrations to a pulse pattern of rooms 1 and 2 ventilation rates: beginning at the instant $t=100$ h, a sudden raise and descend of ventilation rate from 1 to 9 (1/h) happens every 24 hours.

A similar behaviour has been obtained for the rest of parameters chosen: the pulse pattern of the pressure difference produces a sudden increase on indoor radon concentration, specially on the basement, followed by a decrease to the initial steady-state, which is reached before the following pulse as well. When the pulse corresponds to an air-exchange rate parameter, then radon concentration in a given room increases or decreases depending on whether the attached room has a higher or lower radon level respectively. This behaviour, which reproduces the "indoor room air redistribution" role of the air exchange rates, can be observed in Fig. 4.15, where the response of the system to an air exchange rate pulse between basement and room 2 is given.

In all the cases analysed, the system has had enough time to reach the initial steady-state. This behaviour depends on the intensity of the pulses and on their frequency. We have considered an increase of 8 units as a high enough to be representative of extreme cases: the ventilation rates have been increased from 0.6-1 to 8.6-9 h⁻¹, the air-exchange rates from 0.2-0.4 to 8.2-8.4 h⁻¹, and the soil-indoor pressure difference from 5 to 13 Pa.

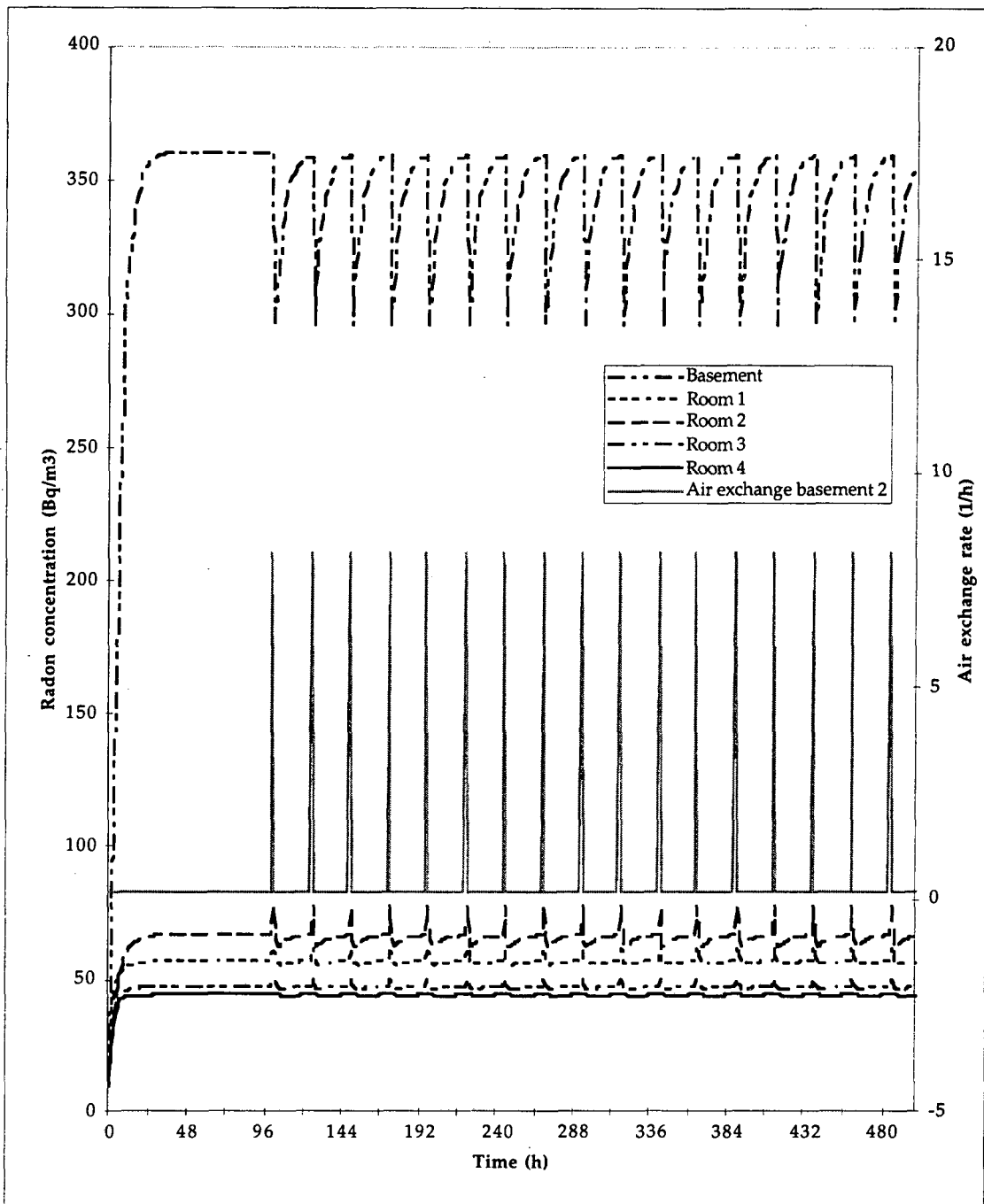


Fig. 4.15: Response of the indoor radon concentrations to a pulse pattern of the air-exchange rate between the basement and the room 2: beginning at the instant $t=100$ h, a sudden raise and descend of the air-exchange rate from 0.2 to 8.2 (1/h) occurs every 24 hours.

4.2.3.3 Sinwave

We have restricted this analysis to the soil-indoor pressure parameter, which is the most likely to follow a sinwave time-behaviour. We have assumed a constant baseline of 2 Pa pressure difference over which a sinwave of 2 Pa amplitude and 24 hour frequency has been added. The indoor radon dynamics of each room obtained is given in Fig. 4.16.

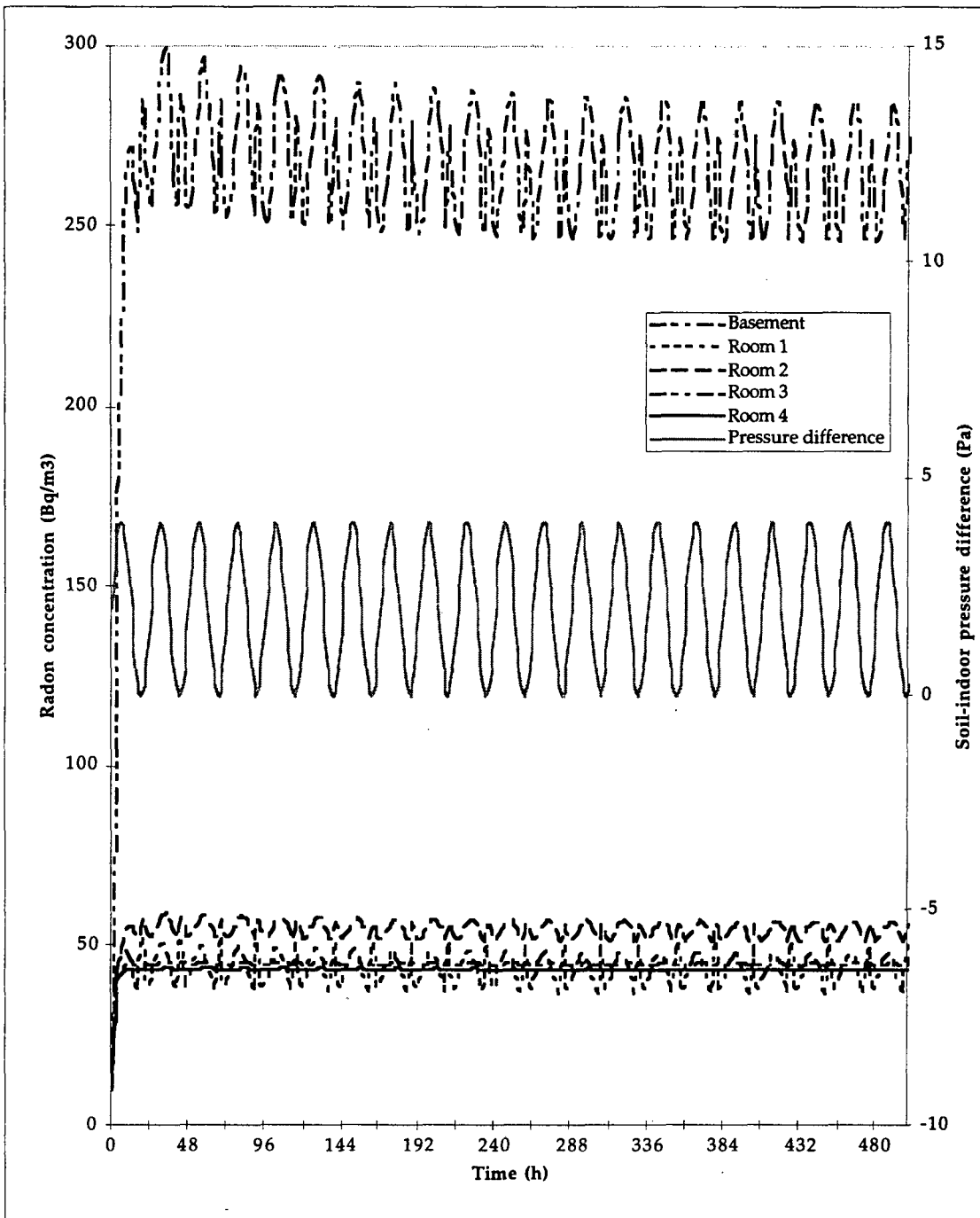


Fig. 4.16: Response of the indoor radon concentrations to a sinwave pattern of the soil-indoor pressure difference, with an amplitude of 2 Pa and a period of 24 hours, which has been added to a constant baseline of 2 Pa.

It can be seen from Fig. 4.16 that the room most affected by the harmonic behaviour of the soil-indoor pressure difference is the basement of the house and that the impact on rooms 3 and 4 radon levels is negligible. In all the rooms but the basement, a steady fluctuating state is reached immediately, while in the basement it is reached after a previous maximum of $300 \text{ Bq}\cdot\text{m}^{-3}$. Thus, after few hours, the radon concentration in each room oscillates around an average value, which is given in table 4.11. Each 24 hours we observe two different peaks in the indoor radon behaviour: the first one, with the higher amplitude and width, follows the frequency

given by the pressure difference sinwave and corresponds to the maximum advective radon entry into the house; the second one appears when the pressure difference, and consequently, the advective radon entry, are minimum. The presence of the last peaks can be explained as follows: the decrease of the soil-indoor pressure difference produces a reduction of the advective radon entry, which in turn, decreases indoor radon level and increases soil radon concentration. As a result, the soil-indoor radon concentration gradient increases, leading to an increment of the radon entry by diffusion that produces the cited peaks. Therefore, minimum pressure difference peaks correspond to the maximum diffusive entry rate. In Fig. 4.17 we have plotted the same parameters as in Fig. 4.16 when the period of the pressure sinwave is reduced to 12 hours and the same behaviour is observed. However, due to the higher frequency, the amplitude of indoor radon concentration fluctuations is lower, while the averaged radon values obtained in both cases are very similar. Table 4.11 shows these values together with those corresponding to an steady-state with a permanent soil-indoor pressure difference of 2 Pa. We can observe that even though the steady-state values and the averaged values of the dynamic patterns are similar, the last ones are higher than the first ones. The difference, which is lower than 3%, is interpreted as caused by the contribution of diffusive peaks found when the pressure difference is minimum. Even though the presence of the diffusive peaks can be reasonably explained, and their effect on the averaged indoor radon concentration is small, their amplitude manifests that the soil radon concentration underneath the house is very sensitive to the soil-indoor pressure difference. In fact, we have found that, up to now, the RAGENA model is limited to positive soil-indoor pressure differences because a negative soil-indoor pressure difference, that is, the room is overpressured with respect to the soil, produces a very high increase on soil radon concentration.

Table 4.11: Mean radon concentrations (in Bq·m⁻³) obtained with a constant 2 Pa indoor underpressurisation and with two sinwave pressure difference patterns, added to a constant baseline of 2 Pa. Notation: in the sinwave function, the first number in brackets is the amplitude (in Pa) and the second is the period (in hours).

Room	Pressure difference (Pa) pattern:		
	2 (Steady-state)	2 + sinwave (2,24)	2 + sinwave (2,12)
Basement	258.7	266.0	265.7
Room 1	42.9	43.9	43.8
Room 2	53.8	54.7	54.6
Room 3	44.7	44.9	44.9
Room 4	43.6	43.7	43.7

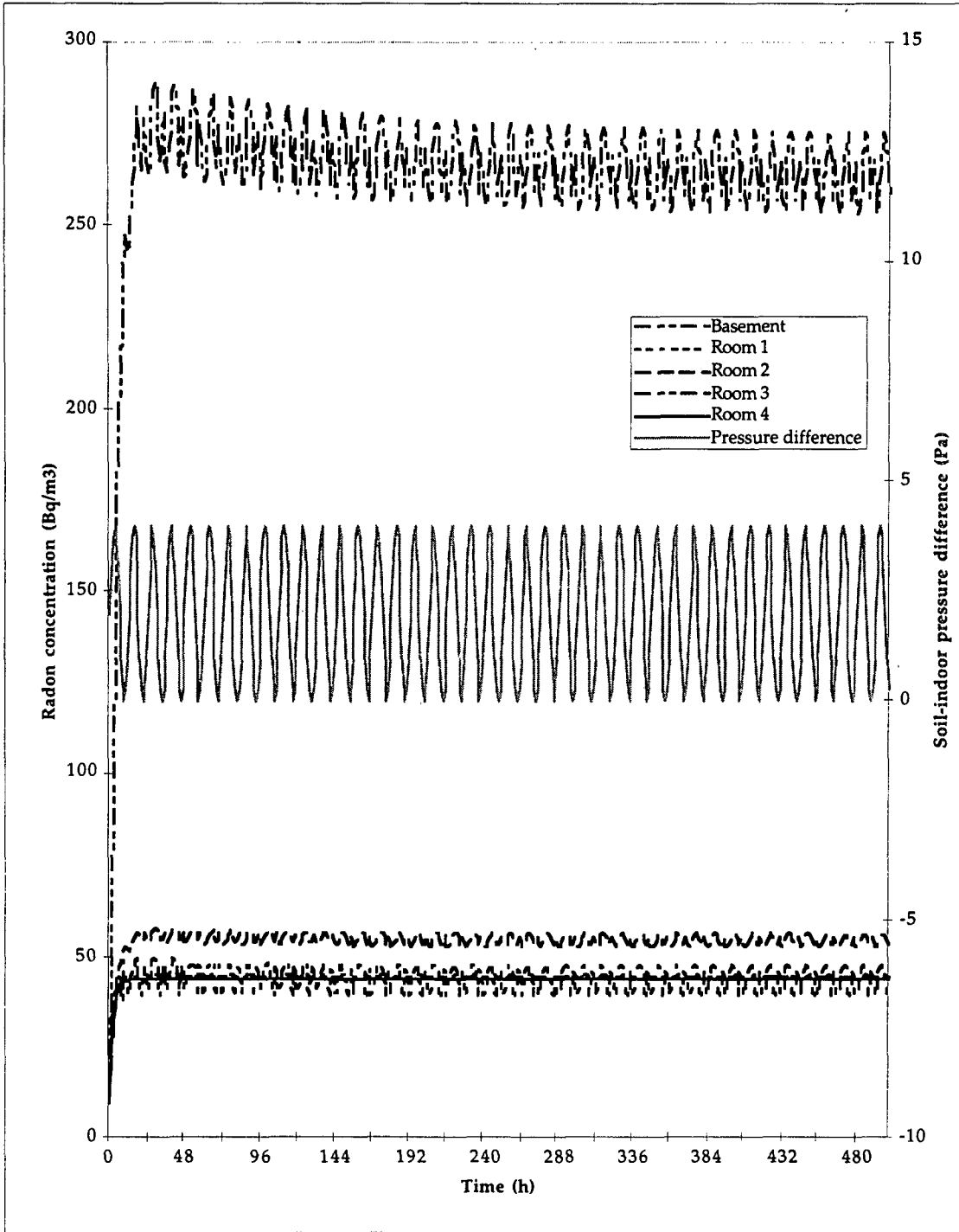


Fig. 4.17: Response of the indoor radon concentrations to a sinwave pattern of the soil-indoor pressure difference, with an amplitude of 2 Pa and a period of 12 hours, which has been added to a constant baseline of 2 Pa.

4.2.3 Uncertainty analysis.

In addition to the previous variability and sensitivity analysis, an uncertainty analysis is necessary to account for the fact that the values of the parameters within a system are never precisely defined and are best described by a probability distribution. Thus, an uncertainty analysis allows the estimation of the uncertainty associated with the model prediction values

when the probability distribution of the input parameters is given. In this section we have carried out an uncertainty analysis in which we have assumed that all the model input parameters are described by a normal distribution around their default value (that corresponding to the reference configuration), with a relative standard deviation of 10%. A descriptive statistics of the indoor radon levels obtained is given in table 4.12, where it can be seen that an uncertainty of 10% of all parameters produces an uncertainty on the model outputs in the range (16.7-21.9%) under steady-state conditions. Taking into account the uncertainty, the mean radon concentrations obtained are in agreement with the reference configuration results (see table 4.6).

Table 4.12: Descriptive statistics of the indoor radon concentrations (in Bq·m⁻³) obtained when all the input parameters are given by a normal distribution of 10% relative standard deviation around the reference configuration value.

	Basement	Room 1	Room 2	Room 3	Room 4
Mean	370.4	59.7	69.0	48.0	45.8
Median	363.5	57.3	67.6	47.9	44.9
Mode	401.5	50.3	68.7	54.3	35.8
Standard Deviation (SD)	62.7	10.0	11.6	8.7	10.0
Relative SD (%)	16.9	16.7	16.9	18.2	21.9
Minimum	259.7	42.0	47.1	34.0	30.4
Maximum	577.8	89.0	98.0	66.9	79.7

4.3 Dynamic results

In this section we present the indoor radon dynamics obtained with the RAGENA model in the basement and in the four rooms of the reference configuration house when the pressure difference, ventilation rates, inter-zone air-exchange rates, water saturation fraction, and water use rate follow the one-week patterns given in Fig. 4.3. To better differentiate the behaviour of each room, we present the results in three Figs.: 4.18, 4.19 and 4.20, which show, respectively, the radon dynamics in the basement, rooms 1 and 2, and rooms 3 and 4. As a consequence of the variability analysis, we know that the influence of the water use rate variations on indoor radon levels are negligible in our reference configuration and therefore, we do not consider this parameter in the following discussion.

The basement radon dynamics, starting at a steady-state value, presents from the instant at which pressure difference, ventilation and air-exchange rates start changing, a fluctuating behaviour in which the minimum radon concentration is reached when the air exchange between the basement and room 2, the soil-basement pressure difference, and the room 2 ventilation rate are maximum. We have seen in the sensitivity analysis that, in the basement, when the pressure difference is maximum, radon concentration tends to increase because of the advective

entry flow rise and that when room 2 ventilation rate and basement-room 2 air-exchange rate increase, it decreases. Thus, in our case these competitive effects have led to a decrease of the basement radon concentration when the advective radon entry dominates. This behaviour was found experimentally (Ward et al. 1993), as we said in section 2.3, and shows the importance of considering simultaneously the different parameter dynamics. After the decrease, basement radon concentration has not enough time to reach again the initial steady-state. Although the effect of the rainfall on the basement radon concentration dynamics is of less importance, it can be observed as well: just after the initial increase of the water saturation fraction in the soil underneath the house, the radon concentration reaches a new maximum higher than the previous ones, because at that water saturation fraction value, the emanation is increased and the transport parameters are only slightly reduced. When the water saturation fraction is high enough, the transport parameters are greatly reduced and consequently, basement radon concentration falls to an absolute minimum.

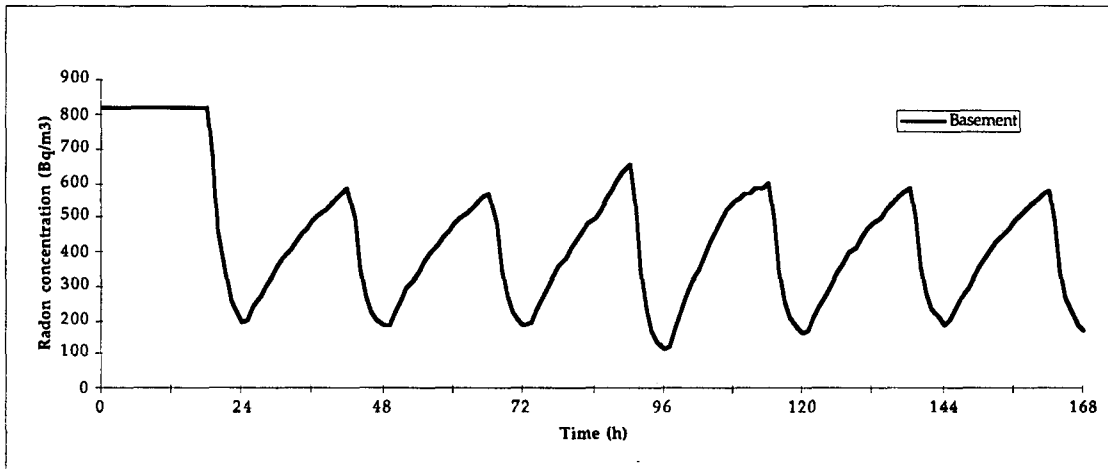


Fig. 4.18: One-week dynamics of the basement radon concentration when the soil-basement pressure difference, ventilation rates, inter-zone air-exchange rates, water saturation fraction of the soil, and water use rate follow the patterns given in Fig. 4.3

The dynamics of rooms 1 and 2 are shown in Fig. 4.19. It can be seen that the room 2 radon concentration presents narrow peaks corresponding to a sudden rise due to the increase of the air-exchange rate with the basement, and a fast decrease due to the rise of the ventilation rate. As in the case of the basement, the radon concentration has not enough time to reach the steady-state. The behaviour of room 1 radon concentration is very different: it has time to reach the steady-state between two consecutive fluctuations, and its variations are smoother than those of room 2. The periodic decreases are due to the pulses of its ventilation rate. The effect of the rainfall is again visible in both rooms, specially in room 1, which is in direct contact with soil.

The dynamics of rooms 3 and 4, which are in the first floor of the reference house, follow the characteristic pattern associated with periodic ventilation rate pulses. The radon

concentrations have enough time to fully reach the steady-state and only decrease when their corresponding ventilation rate increases according to Fig. 4.3.

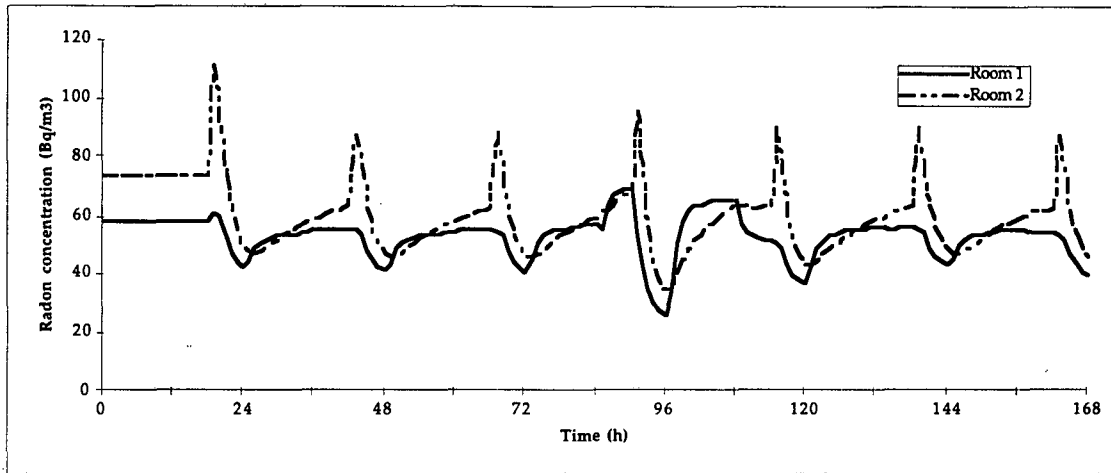


Fig. 4.19: One-week dynamics of rooms 1 and 2 radon concentration when the soil-basement pressure difference, ventilation rates, inter-zone air-exchange rates, water saturation fraction of the soil, and water use rate follow the patterns given in Fig. 4.3

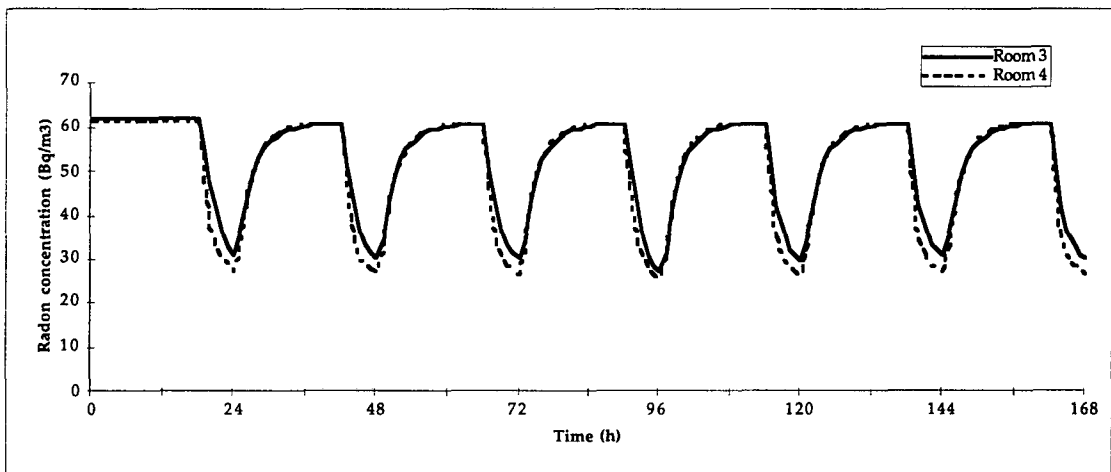


Fig. 4.20: One-week dynamics of rooms 3 and 4 radon concentration when the soil-basement pressure difference, ventilation rates, inter-zone air-exchange rates, water saturation fraction of the soil, and water use rate follow the patterns given in Fig. 4.3

Summing up, we have seen that under the one-week dynamic conditions given in Fig. 4.3, the parameters that drive the dynamics of the basement are the pressure difference, the air-exchange between the basement and room 2, the room 2 ventilation rate, and the water saturation fraction in the soil. Room 2 radon dynamics is driven by the air-exchange with the basement and by its ventilation rate. For the room 3, the relevant parameters are its ventilation rate and the water saturation fraction of the soil. Finally, rooms 3 and 4 radon concentration dynamics are driven only by their respective ventilation rate.

As we said in section 4.1.4, the mean value of the parameters assumed to follow the patterns given in Fig. 4.3, correspond to their steady-state entry values. In table 4.13 we present the mean radon concentration values obtained in the one-week dynamic radon entry compared with the steady-state values. It can be seen that the dynamic behaviour of some input parameters has led to an averaged-over-one-week basement radon concentration higher than that corresponding to the steady-state. In the house, we observe an increase of the mean radon concentration in the first floor rooms and a decrease in the ground floor rooms, as if the dynamic behaviour of the air-exchange rates results in a major mixture of the indoor air.

*Table 4.13: Radon concentration values (in Bq·m⁻³) averaged over the one-week dynamics compared with the steady-state results. The relative difference is defined as (averaged value - steady-state value)*100/steady-state value.*

	Basement	Room 1	Room 2	Room 3	Room 4
Averaged value	439	53.3	60.1	52.5	51.3
Relative Standard Deviation (%)	44	14	20	21	25
Steady-state value	360.7	57.1	66.5	47.2	44.6
Relative difference (%)	21.7	-6.7	-9.6	11.1	15.0

4.4 Discussion

In this chapter we have applied the RAGENA model to a generic single family house under static and dynamic conditions to check the response of the model to very different situations. The results obtained in the reference configuration are very reasonable and show how the model can be used to characterise the radon generation, entry and accumulation in a multi-zone house taking into account all the parameters and processes involved. Variability, sensitivity, and uncertainty analysis have been performed around the reference configuration, and the results obtained and discussed below show how important is to consider simultaneously the relevant parameters.

In the variability analysis, we have seen that the model can describe a very wide range of situations and therefore, can be considered as a global model, as opposite to a site-specific model. The variability index has allowed us to determine the most relevant parameters for the reference configuration. A more detailed study of that parameters have shown that the model describes satisfactorily most of the previous findings from theoretical and experimental studies: the relative importance of the radon entry processes, of the ventilation and inter-zone air-exchange rates, of the soil permeability and water content, etc. Only in the case of the open area, we have seen that the model cannot describe the complicate relationship between radon entry from soil and the open area, but this fact is basically due to the lack of spatial resolution of the model. It is worthwhile to consider also the conceptual simplicity of the model and the

amount of information it can give as outputs. In general, the results obtained have shown the importance of considering simultaneously all the relevant parameters when trying to model indoor radon dynamics; any partial model which only describes a given radon source or entry process will be useful only in case of being the given source or entry process clearly the dominant one.

In the sensitivity analysis, we have stressed the model with different types of sudden time-variations of the parameter values, choosing in each case the parameters most likely to follow the given variation. We have observed in all the cases a good behaviour of the model in the sense that the model predictions can be imputed to the physical system rather than to any mathematical problem. This is a consequence of the algorithm used to solve numerically the coupled first order differential equations: 4th order Runge-Kutta. This method is very well known, widely used, and presents no problems of stability and convergence. Only in one case we have found a strange behaviour: the soil radon concentration is very sensitive to the soil-indoor pressure difference. This problem will hopefully be solved in the future work.

The uncertainty analysis performed in this work has allowed us to estimate the uncertainty of the model predictions in the steady-state when the input parameters follow a normal distribution of 10% standard deviation, and has manifested that, given an assumed probability distribution of the inputs, the RAGENA model gives a probability distribution of outputs .

Finally, the results of the one-week dynamic radon entry and accumulation in the house, demonstrate that the model is appropriate to describe the indoor radon dynamics of a multi-zone house.

5 Experimental study

This chapter describes the experimental study performed in one inhabited house typical for the Barcelona area with a Mediterranean climate. This study has been carried out within the frame of an European Union (EU) project in which six laboratories from five European countries are involved. The chapter is divided into three sections. First, we outline the project with its objectives and methodology. Then, we describe in detail the experimental site and the equipment used. Finally, we report on the calibration and intercomparison activities performed to check the quality of the measurements.

5.1 The EU project

In 1994, the research project on radon "Criteria for indoor radon concentration - An experimental study considering especially the Leipzig-Hall brown coal area" was initiated within the EU program Human Capital and Mobility (ERB-CHRX-CT 930422). The project intends to improve the understanding of the specific behaviour of the radon gas and it is being carried out by six research groups belonging to five European countries (Jönsson et al. 1995).

A coordinated survey on six different sites, located in the Lund-Kiel-Leipzig-Montpellier-Barcelona-Roma areas is running according to an identical pattern to find criteria in common for the presence of radon gas in the indoor air in the different European areas. Each site has its own meteorological, geological and environmental conditions, and different types of houses as well. In each site a house typical for the region and normally inhabited has been selected as a "test house" and equipped to monitor:

- Indoor radon concentration with both passive (time integrated) and active (time resolved) detectors.
- Soil radon concentration with both passive and active detectors.
- Weather parameters.
- Soil-basement pressure differences.

In addition, the soil of the house garden has been characterised by measuring its porosity, texture, permeability and radium and uranium content.

Ten houses in the vicinity of the test house have been selected as control houses in which indoor and soil radon have been measured only with passive detectors. Some results of the project have been already published (Baixeras et al. 1996a, Baixeras et al. 1996b, Jönsson et al. 1996, Climent 1996). In this study we report on the experimental results obtained in the Barcelona test house for a one year cycle.

5.2 Experimental site

5.2.1. General description

5.2.1.1 Test house

The Barcelona test house is placed in Cerdanyola del Vallés, a town with a population over 50,000 inhabitants at 15 km far from Barcelona and 1 km from the Autonomous University of Barcelona. The Barcelona area belongs to the Catalonia "autonomia" and is one of the high density population areas in Europe (more than 1100 inhabitants per km²). The house is the last of a row of terraced houses, so that it shares only one wall with the neighbour's house. This type of single-family house is very common in the Barcelona area. The distribution of the rooms in the three floor levels present in the house is given in table 5.1 together with the surface of each room. In Figs. 5.1 and 5.2 top-view and lateral diagrams of the house respectively are shown.

Table 5.1: Distribution of the rooms in the three floor levels of the test house. The level 0 corresponds to the ground-floor.

Level	Room	Surface (m ²)	Remarks
-1	Garage	40.3	
-1	Laundry room	4.7	Heating system (natural gas + water)
-1	Basement room	10.9	Now used as office
0	Kitchen	9.5	Natural gas and water supplies
0	Lavatory	2.0	Water supply
0	Living-room	28.2	A French door communicates with the garden
0	Garden	135	Automatic irrigation system available. Covered with grass
1	Bedroom	12.5	
1	Bathroom-1	5.2	Inside the bedroom. Water supply
1	Bathroom-2	4.8	Water supply
1	Room 1	9.2	Used as office
1	Room 2	6.5	Used as office
2	Guest-room	27.3	Single-zone floor

The house is inhabited by a young married couple with no children. The floors are connected through an open staircase of 3.4 m² cross-sectional area. The total house shell in contact with soil has a surface of 60 m².

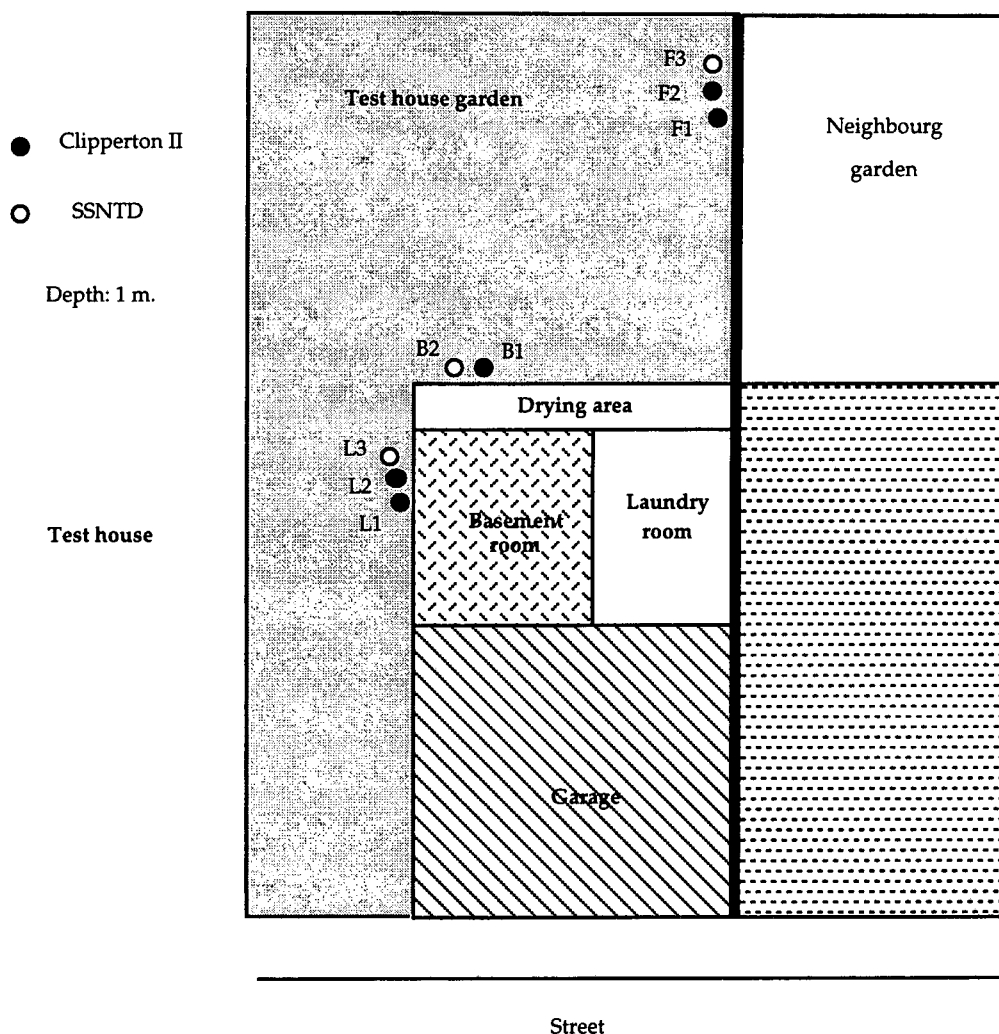


Fig. 5.1: Distribution of soil radon detectors in the test house garden (top view). The rooms of the test house are those placed at the basement level.

The test-house site belongs to the "Vallés Occidental" region, in the pre-littoral zone of Catalonia, which is mainly constituted by sedimentary soil. The climate is typically Mediterranean, with warm summers, soft winters and a mean rainfall of 600 mm per year. The area has a high industrial activity, comprising chemistry, metallurgic, building materials production, etc.

5.2.1.2 Previous radon studies in the region.

Radon concentration in dwellings from the Barcelona area was measured in a survey carried out by the Grup de Física de les Radiacions (GFR) of the UAB in collaboration with the Spanish institution CIEMAT (Baixeras et al. 1996c) in the period June 1991 - June 1992. The annual average of indoor radon concentration in the Barcelona area was $34 \text{ Bq}\cdot\text{m}^3$, with a geometric mean of $28 \text{ Bq}\cdot\text{m}^3$, a geometric standard deviation of $1.86 \text{ Bq}\cdot\text{m}^3$, and a range (2-622) $\text{Bq}\cdot\text{m}^3$. A total number of 204 dwellings was monitored in the Barcelona area, measuring radon

concentration in both living-room and bedroom by means of track etch detectors exposed for two consecutive periods of six months. The fraction of dwellings monitored represents more than 1 in 10000 of the housing stock, according to the suggestion of the UNSCEAR (1993) report. Due to its proximity to the UAB, several dwellings from Cerdanyola del Vallés were monitored in preliminary studies to perform the very first measurements in dwellings (Baixeras et al. 1991) and to carry out a preliminary survey (Gutiérrez et al. 1992).

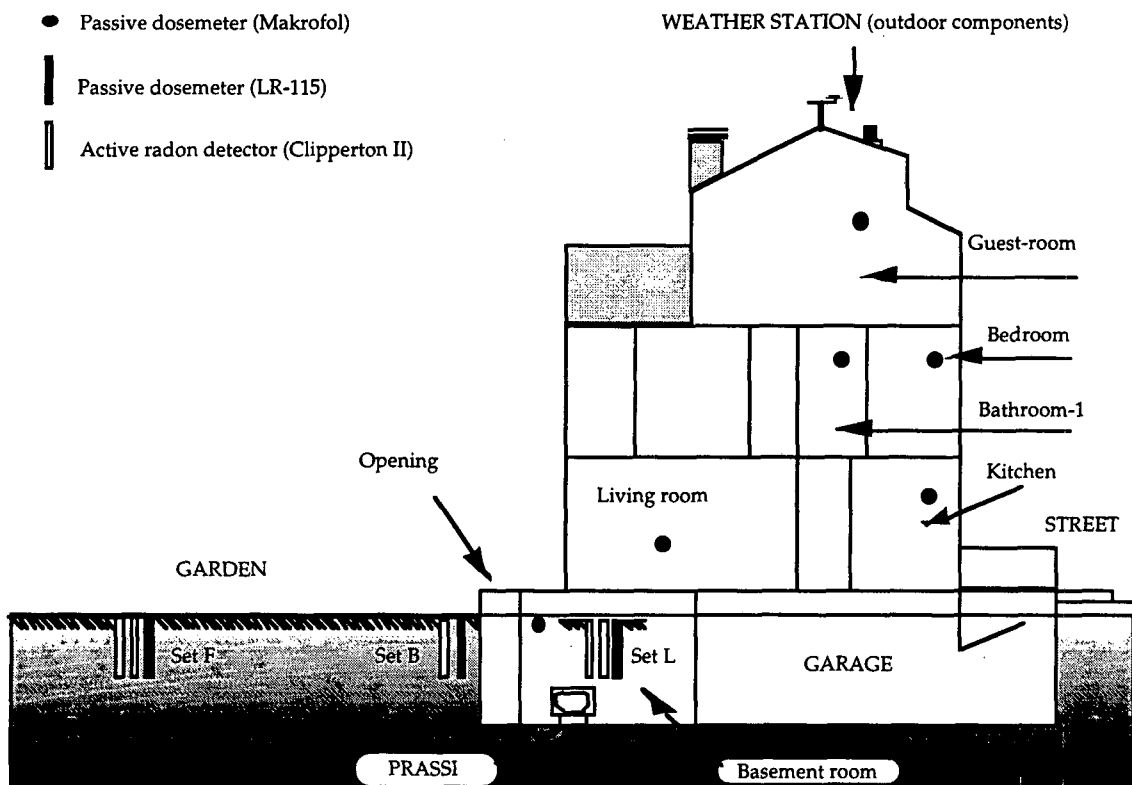


Fig. 5.2: Distribution of the different equipment installed in the test house for the experimental study.

In addition to this study, the test house participated in a campaign carried out by the GFR of the UAB and the "Institut de Tècniques Energètiques" (INTE) of the "Universitat Politècnica de Catalunya" in which radon concentration was measured with three different passive radon dosimeters: two of track-etched type and the other was a canister with diffusion barrier (Novell and Font, 1997). Sixty houses were monitored, exposing in each the three different types of dosimeters placed in the same site according to an exposure pattern: closed-type track-etched dosimeters based on Makrofol were exposed for two periods of three months; open-type track-etched dosimeters based on LR-115 type II strippable were exposed for four periods of 10 days, and canisters were exposed for eight 3-4 day periods. These measurements were performed in the period November 1993 - April 1995, and the mean values obtained in the test house with Makrofol, LR-115 and canisters were, respectively, 48, 43 and 24 Bq·m⁻³. All the radon concentration values were comprised within the range (16 - 128)Bq·m⁻³.

Finally, indoor radon concentration was measured in 78 houses of Catalonia as a part of a national survey conducted in 1990 by the Cátedra de Física Médica of the Universidad de Cantabria (Ródenas 1995); the measurements were obtained with a modified Lucas cell with the grab-sampling methodology. The arithmetic and geometric mean obtained were, respectively, 41 and 23 Bqm⁻³.

5.2.2. Equipment

5.2.2.1. Soil radon detectors

Soil radon levels were measured with passive, track-etched detectors of type LR-115 and with active electronic devices (Clipperton II). Following we describe briefly each type of soil radon detector.

5.2.2.1.1. Track-etch detector: LR-115

The dosimeter used to measure radon concentration in the soil consists of a cut cone of diameters $d_1 = 4.5$ cm and $d_2 = 6$ cm and a height of 7 cm used as a diffusion chamber. A squared foil LR-115 type II non strippable (2×2 cm²) is stuck in the inner side of the small disc. A fibreglass filter placed in the bigger disc and protected with a leaky screw top allows only the entry of radon gas into the diffusion chamber. A diagram of the LR-115 soil radon dosimeter is given in Fig. 5.3. In the EU-project, each participating group used its own type of passive radon detectors, so that this dosimeter has been used only by the Barcelona group in the test-house.

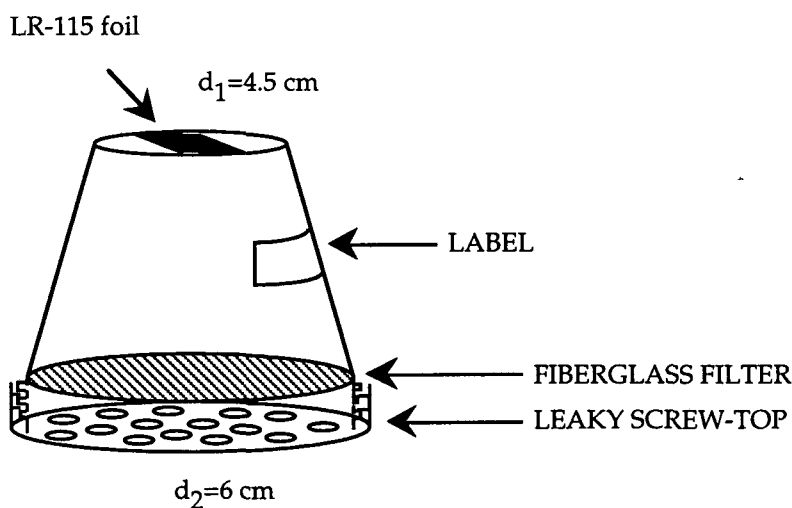


Fig. 5.3: Diagram of the LR-115 soil radon dosimeter

Soil radon concentration has been measured in three points of the test house garden (see Fig. 5.1). In each point, the dosimeter has been exposed for two weeks approximately, at one meter depth. A diagram of the installation of the dosimeter in the soil is given in Fig. 5.4. A PVC tube of 10 cm diameter and 1 m long is placed in the soil. The dosimeter is put in the bottom in direct contact with the soil, and a fishing-line allows its removal. The tube is then filled with an isolator bag and covered with a screw top. The isolator diminishes the outdoor temperature variations that would lead to water condensation in the detector surface. After being exposed, the LR-115 foils are etched for 120 minutes at 60° C in a solution of NaOH 2.5 N, sunken in distilled water, and dried.

The track counting is performed with the semiautomatic counting system available in our laboratory, which consists of the following components:

- Optical Microscope LEITZ coupled to a Video camera CCD SONY.
- Photo Video camera SONY PHV-A7E.
- Monitor SONY TRINITON Super fine pitch.
- Personal Computer based on processor 386/387.
- Monitor SVGA TAXAN.
- Digitiser card MATROX VIP1024.
- VISILOG™ 3.6 Software.

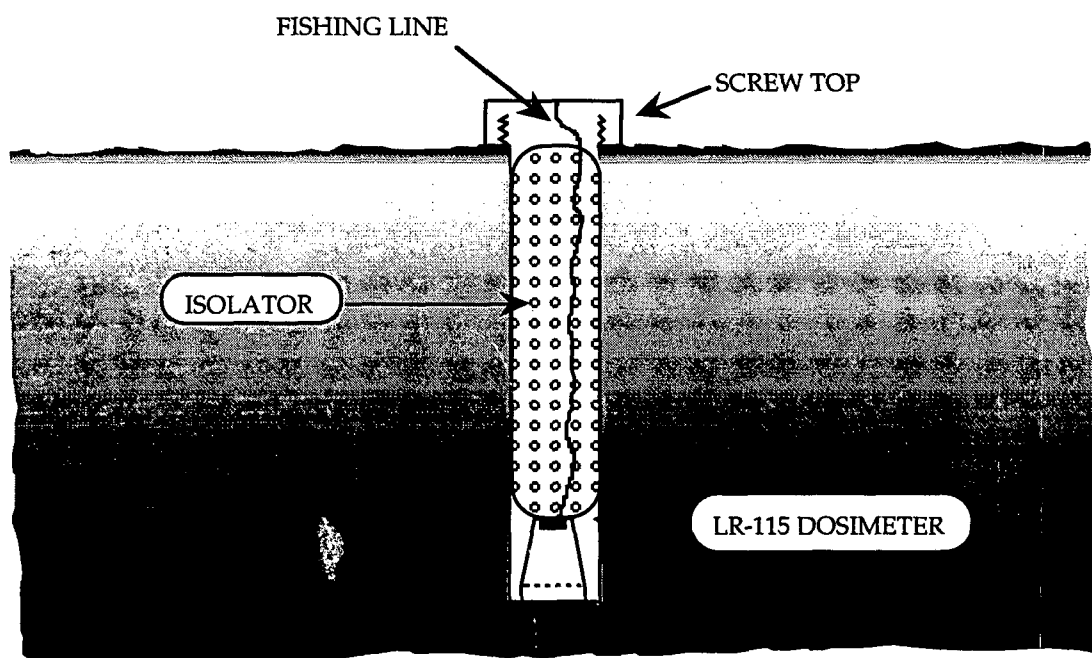


Fig. 5.4: Exposure of the LR-115 soil radon dosimeter

The VISILOG™ 3.6 Software is a powerful Computer Vision software package developed by NOSES S.A.R.L. that has over 200 already defined functions and that allows the user to program sets of linked functions called macros. We have programmed several macros for adapting the VISILOG software to counting tracks developed in both LR-115 foils and in the Makrofol foils used to measure indoor radon concentration. In the case of LR-115 foils, the optical microscope coupled to the Video camera is necessary because of the small size of the tracks. In contrast, when counting the tracks developed in the Makrofol foils, the image is acquired directly from the Photo Videocamera (see section 5.2.2.2). A diagram of the semiautomatic system is shown in Fig. 5.5.

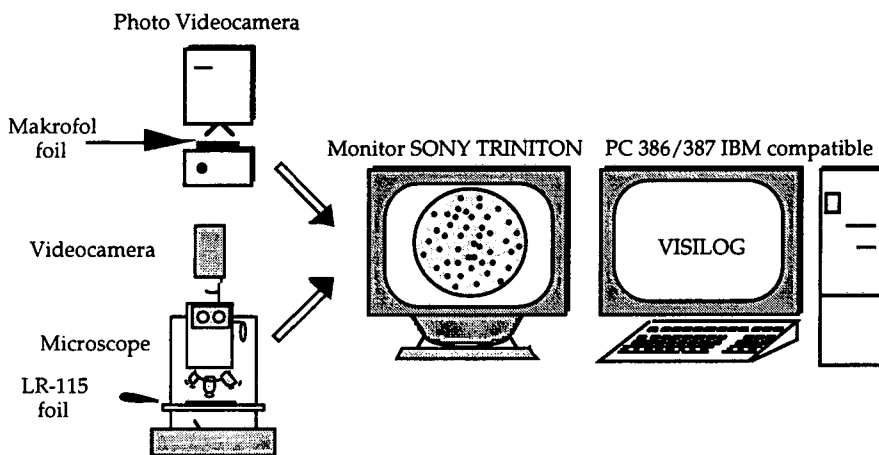


Fig. 5.5: Diagram of the semiautomatic counting system. The Microscope is used for track counting the LR-115 foils, while the Photo Videocamera is used for the Makrofol foils.

5.2.2.1.2. Clipperton

The "Clipperton II radon probe" is an active radon detector that was designed by the Montpellier group and that has been used for all the EU project groups to measure the evolution of soil radon concentration with a time resolution of one hour. The dosimeter is based on a solid-state detector without polarisation, which is protected by special layers against friction and water (both gas and liquid phase). A black 30 cm plastic tube fixed to the detector avoids the detection of thoron (^{220}Rn) and light photons. The data processing and storing is performed by a NSC810A microprocessor. The probe is operated by a Psion-organiser computer for initialisation and data transfer (Morin et al. 1993). The operating power (5-6 Volts) is supplied by external batteries that are placed in a box with two connectors; one giving the supply to the probe and the other to be plugged to the psion-organiser computer. Five clippertons were installed in the garden of the test house, at different locations as shown in Fig. 5.1. Each dosimeter was placed

at one meter depth using the same PVC tubes and isolator type as in the case of LR-115 detectors. Fig. 5.6 shows a diagram of the clipperton II probe placed in the soil.

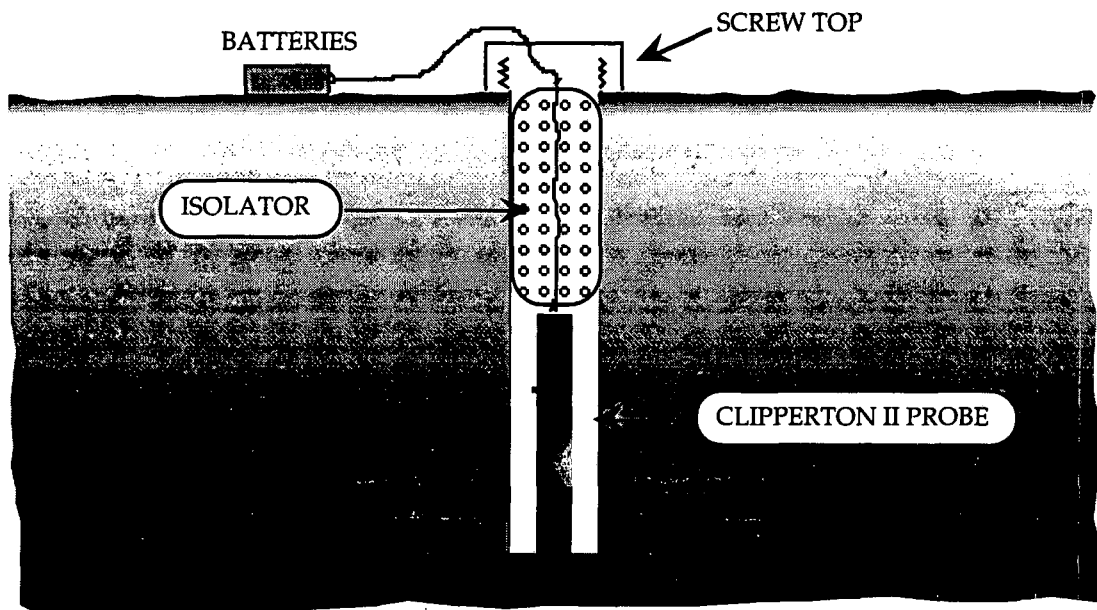


Fig. 5.6: Exposure of the Clipperton II probe to measure soil radon.

The operation of the probe is defined with three parameters: reading cycle, sampling frequency and discrimination level. The reading cycle defines the interval of time between two consecutive pulse readings, these readings are averaged every interval of time defined with the sampling frequency. The data transferred from the probe to the psion-organiser computer only includes these averaged values. In order to avoid the contribution of electronic background or other possible sources of sudden peaks, the discrimination value algorithm deletes the readings in each averaging period that present a fluctuation higher than a given percentage when compared with the others. In all the groups of the project, the following configuration was adopted:

- Reading cycle: 10 s.
- Sampling frequency: 1 h.
- Discrimination level: 10000%.

In order to minimise moisture problems, it is possible to protect the probes by means of a membrane or a polythene bag. The effect of this protection on the probe sensitivity is studied in section 5.3.1.2.

Fig. 5.1 shows the distribution of the soil radon detectors in the test house garden, where the house rooms drawn correspond to the basement level. The dosimeters are grouped in three sets, of codes L, B and F. The first set (L) corresponds to the dosimeters placed in the lateral wall of the

house, very close to the basement-room, which is the room at the basement level that we have monitored. The second set (B) of dosimeters is placed also near the house, but in the backward side, where an opening (drying area) is present. A door from the laundry room allows the access to this opening at the basement level, which is used to hang out the washing. The presence of a window in the basement room allows an air-exchange with outdoors through the opening. Finally, the third set (F) denotes the dosimeters placed at the right corner of the garden, far from the building shell. Therefore, detector sets L and B measure radon concentration in a soil that has been disturbed by the house and detectors from set F measure radon concentration in a less disturbed soil.

5.2.2.2. Indoor radon detectors

5.2.2.2.1. Prassi

The PRASSI portable radon monitor is a commercial monitor manufactured by the Italian company SILENA¹. This monitor is suitable for radon gas continuous or grab sampling measurements with the scintillation cell technique. It basically consists of a 1.83 liter cell coated with Zinc Sulphide activated with Silver [ZnS(Ag)] coupled to a low gain-drift photomultiplier. The sampled air is pre-filtered before reaching the measure chamber and the sampling flow-rate is electronically regulated to compensate for filter clog-up. A computation algorithm allows to compensate for the counts coming from radon daughters plate-out. We use this monitor to measure continuously radon concentration in the indoor air, with a time-resolution of one hour. The noise it produces when operating is very inconvenient for the inhabitants and therefore, it can not be used in a occupied room for 24 hours. This problem is typical for an inhabited house: it is not possible to use the instrumentation as easily as in a test structure or in the laboratory. Then, we have had the monitor under operation for a period of few months in the basement room, when it was not occupied, and eventually we have measured radon concentration in other rooms of the house. Fig. 5.7 shows the PRASSI radon monitor.

5.2.2.2.2. Makrofol

This dosimeter consists of a hemispherical cup (internal radius $r=1.5$ cm) of electrically conductive material as a diffusion chamber with a fiberglass filter and a 300 μm Makrofol DE foil (polycarbonate), covered with aluminised Mylar as an etched-track detector (Urban 1986). This dosimeter has been widely used by the GFR to measure indoor radon (Gutiérrez et al. 1992, Font 1993, Baixeras et al. 1995, Baixeras et al. 1996c, Baixeras et al. 1996d) and can be exposed

¹ SILENA Società per l'Elettronica Avanzata SpA. Via Firenze,3; I-20063 s/N. Italy.

for several months (3-6) to obtain the mean radon concentration. Fig. 5.8 shows the dosimeter and its components.

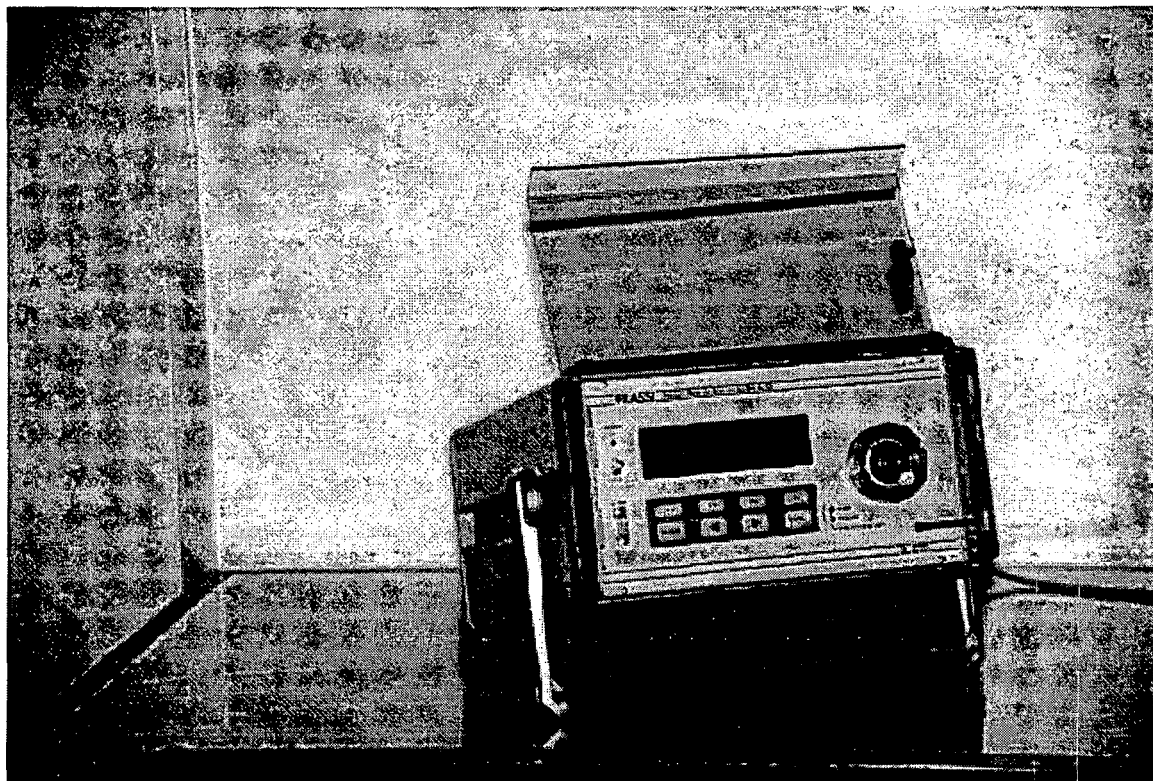


Fig. 5.7: The portable radon monitor PRASSI.

The etching conditions optimised for the diffusion chamber size were obtained in a previous study (Baixeras et al. 1991) and were: a) chemical etching for 4 h, and b) electrochemical etching (frequency: 3 kHz, voltage: 1000 V_{rms}) during 1.5 h, at 40 °C, using a mixture of 50% 6N KOH and 50% ethanol as the etching solution. The track counting is performed with the semiautomatic counting system described in section 5.2.2.1.1 (Fig. 5.5). The size of the tracks obtained with the electrochemical etching is big enough to allow the use of the Photo Videocamera to acquire the image without the need of a microscope.

5.2.2.3. Weather station.

The weather station used by all the groups of the project is manufactured by DAVIS INSTRUMENTS², and consists of a control unit, called Weather Monitor II, that must be installed indoors and that controls the data collection, and the outdoor components: rain collector, anemometer, and external temperature and humidity sensor . This control unit has temperature and pressure sensors incorporated. The parameters monitored are: indoors and

² Davis Instruments Corp. 3465 Diablo Ave., Hayward, CA 94545. U.S.A.

outdoors temperature and humidity, atmospheric pressure, dew point, daily and accumulated rainfall, wind direction and speed, and wind chill. The Weather Monitor II is linked to an IBM compatible PC through the Weatherlink hardware and software, which allows the user to store the data at a given frequency, create graphs, calculate average weather conditions, analyse trends, etc. The outdoor sensors of the weather station were placed on the roof of the house, and the indoor control unit was installed in the guest room, at the second floor. The time resolution chosen was one hour, as in the case of all the other time-resolved detectors or sensors used in the project.

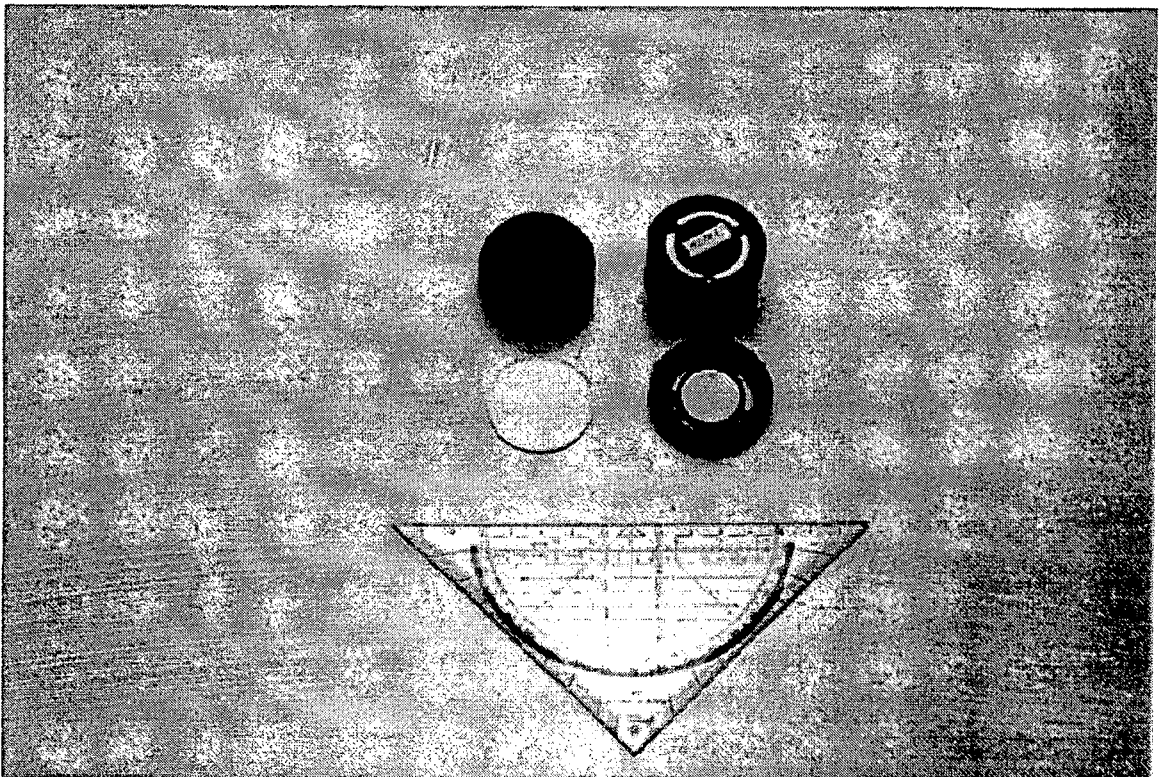


Fig. 5.8: The indoor radon dosimeter (based on Makrofol ED) and its components

5.2.2.4. Difference pressure sensor.

The soil-indoor pressure difference was measured with the differential pressure transmitter effa SK1T12, manufactured by the French company EFFA³. This sensor allows the measurement of pressure differences in the range (-100,100) Pa with an accuracy of 0.5%. It is based on the measurement of the movement of a membrane under pressure by an Eddy current detector with no mechanical contacts. The sensor was installed to measure the pressure difference between the basement room and the soil present at the other side of the wall; that is, close to the set L of soil radon detectors, as it can be seen in Fig. 5.9. Two plastic tubes connected to the pressure ports

³ EFFA. 116, avenue du Belvédère. 93310 Le Pré Saint-Gervais. France.

allow the selection of the pressure difference measurement points. We have installed the sensor and the tubes in such a way that the difference measurement points in both the soil and the basement room are at the same height.

A datalogger allowing the storage of the pressure difference data and their transfer to both a PC and to the Psion-organiser computer was set up by the Kiel group in the project. The time resolution chosen was one hour, as in all the time-resolved equipment.

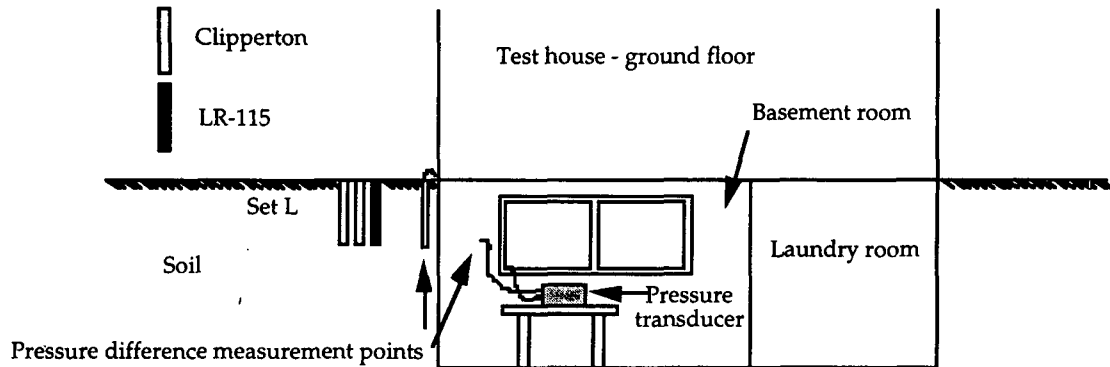


Fig. 5.9: Installation of the pressure transducer in the test house to measure continuously the pressure difference between the lateral soil and the basement room.

Fig. 5.2 shows the distribution the different sensors and detectors installed in the test house for the experimental study.

5.2.2.5. Permeability device.

The gas-permeability of the soil of the test house garden was measured in situ by means of the RADON-JOK portable equipment, manufactured by the Czech company RADON v.o.s. corp⁴. The principle of the measurement consists of air withdrawal by means of negative pressure: the air is pumped from the soil under a constant pressure through a specially designed probe with a constant surface of contact between the probe head and the soil. The soil-air pumping is performed with a special rubber sack that has one or two weights incorporated. Thus, the measurement of the pumping time required to inflate the rubber sack up to a known air volume, allows the estimation of the soil-gas permeability. The equation used is based on the Darcy's equation, assuming the soil to be homogeneous and isotropic, and the soil air to be incompressible. This portable and simple single-probe technique allows to perform fast measurements independently of any source of energy.

⁴ RADON, v.o.s. corp. Za koncem 1380. 289 22 Lysá nad Labem. Czech Republic.

This equipment was available only in the Leipzig group. Within the frame of the coordinated activities in the European project, the equipment was sent round among the different laboratories to carry out gas-permeability measurements in the different test-houses. In our case, we used it for two days in the Barcelona test house garden. Fig. 5.10 shows the equipment under operation in the test house garden.

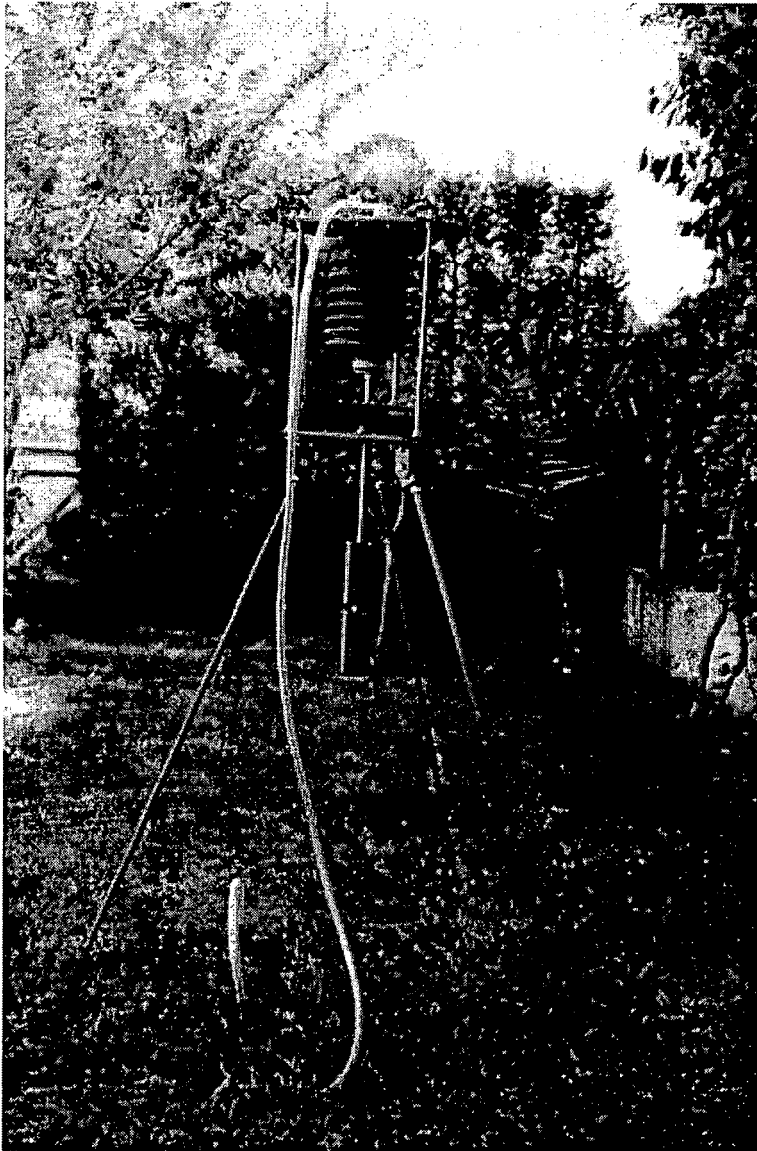


Fig. 5.10: The portable RADON-JOK instrument used to measure the soil-gas permeability of the test house garden soil.

5.3. Calibration and intercomparison activities

In this section we report on the calibration and intercomparison activities performed to check the quality of the different equipment and radon detectors used in the experimental study.

5.3.1. Radon detectors

5.3.1.1. Passive detectors.

When the Grup de Física de les Radiacions (GFR) of the Universitat Autònoma de Barcelona (UAB) started using the Makrofol-based dosimeter to measure indoor radon concentration, we sent a set of dosimeters to the Environmental Chamber at the National Radiological Protection Board (NRPB) Chilton Laboratory for calibration. The Makrofol plates showed a linear response over the exposure range 100 - 1000 kBq·m⁻³·h (Gutiérrez et al. 1992, Font 1993). The sensitivity value obtained has been checked every year at the NRPB radon chamber, and no change of its value has been observed, taking into account its uncertainty. Moreover, the GFR participates in the periodical European Union Intercomparisons of Passive Radon Detectors (Whysall et al. 1996, Miles et al 1996) funded by the Commission of the European Communities.

Within the frame of the EU-project, two intercomparisons of Solid State Nuclear Track Detectors (SSNTDs) have been carried out. The first one took place in the SRPI (Swedish Radiation Protection Institute) radon room in Stockholm, and allowed us to confirm the sensitivity of the Makrofol dosimeters (Baixeras et al. 1996a). The second one was done in the ENEA (Ente per le Nuove Tecnologie, l'Energia e l'Ambiente) radon room in Rome. In this intercomparison, we exposed for the first time the LR-115 soil radon detectors to a known radon exposure, so that the exercise allowed us to calibrate this dosimeter. The sensitivity obtained is given in table 5.2. In both intercomparison exercises, a set of ten dosimeters were used to determine the sensitivity and three as a transit control. Moreover, we have recently sent 3 sets of 10 LR-115 soil radon dosimeters to the NRPB radon chamber to be exposed at three different radon exposures in order to better determine the sensitivity of the detector.

The Detection Limit L_D is defined as $L_D = 2.71 + 3.29 \cdot \sigma_b$ (Currie, 1968), where σ_b is the background standard deviation. The radon Minimum Detectable Concentration (MDC) corresponds to L_D expressed in activity concentration units and depends on the exposure time. In table 5.2 we present the values of the sensitivity, background track density and MDC obtained for the Makrofol and LR-115 passive radon dosimeters, as a consequence of the calibration and intercomparison activities. The MDC has been calculated considering the exposure time used in the experimental study. Currently, we are participating in the 1997 EC passive radon detectors with both Makrofol and LR-115 detectors. The uncertainty associated to the radon concentration measurement with the Makrofol dosimeter found in both SRPI and ENEA intercomparisons is 10%, in agreement with the value already estimated in Ortega et al. (1996). The uncertainty obtained in the ENEA intercomparison for the LR-115 dosimeter is 22%.

Table 5.2: Sensitivity, Minimum Detectable Concentration (MDC), and background track density obtained for the radon passive detectors.

Detector material	Sensitivity (Tr·cm ⁻²)/(kBq·m ⁻³ ·h)	MDC (Bq·m ⁻³)	Background (Tr·cm ⁻²)
Makrofol (indoor radon)	0.89±0.08	4 ^a	7±2
LR-115 (soil radon)	0.9±0.2	87 ^b	13±8

^a Value corresponding to a 3 month exposure. ^b Value corresponding to a 2 week exposure.

5.3.1.2. Active detectors.

The PRASSI monitor was calibrated in the factory with a Ra-226 source having certified emission of Rn-222. The SILENA company provides the purchaser with a calibration certificate. The calibration parameters corresponding to our PRASSI monitor are given in table 5.3. The Clipperton probes were set up by the Montpellier group, and they found a calibration factor of 0.14 kBq·m⁻³/cph. Then, both active radon detectors were already calibrated and our efforts have been focused on intercomparing these detectors with the passive ones.

Table 5.3: PRASSI calibration parameters (from the calibration certificate)

Operating high voltage	900 V
Radon gas efficiency (continuous mode)	20.7 cpm/Bq
Grab sampling efficiency (grab sampling mode)	103 cpm/Bq
Background (measured with pure N ₂)	1.31 cpm

The PRASSI monitor was used to measure the time-evolution of radon concentration in the basement room of the test house, where a Makrofol dosimeter was installed as well. According to the EU-project coordinated pattern of exposure, the Makrofol dosimeters have been exposed in the test house rooms for consecutive periods of three months approximately, replacing a dosimeter when installing the following one. As we have said in section 5.2.2.2.1, we have had the possibility of measuring continuously the basement room radon concentration for a limited period of time. In table 5.4 we present the mean radon concentration obtained with the PRASSI monitor in the basement room of the test house for the two periods of time that best coincide with the exposure period of Makrofol dosimeters. The good agreement between both radon detectors obtained confirms their calibration and shows also that they are appropriate for the measurement of low radon concentration levels in air.

In order to intercompare the response of clipperton and LR-115 soil radon detectors, we carried out an experiment in the campus of the Autonomous University of Barcelona (UAB). We dug a hole of 31 cm diameter and 1.30 m deep. At the bottom there is a 50 cm layer of porex to homogenise radon concentration in the hole air. At the top of this 50 cm layer, we placed a 3 cm cork layer in which 5 holes were made to place 1 clipperton and 4 LR-115 dosimeters. Close to the top of the hole, we stuck 2 PVC bars to place the clipperton batteries on. The top is covered

with a screw-top. A diagram of the experimental arrangement is shown in Fig. 5.11. We exposed three sets of 4 LR-115 dosimeters in three consecutive periods; two two-week long and the third 5-day long. The radon concentration was almost constant during the consecutive periods. In all cases, we found a that the LR-115 dosimeters systematically overestimate (150%) the radon concentration with respect to the clipperton probes. This result shows that further calibration exercises are required: as we said in section 5.3.1.1, we are now calibrating the LR-115 dosimeter at the NRPB radon chamber. The mean radon concentration obtained with the clipperton and the LR-115 detectors for the three exposure periods are given in table 5.5, were the uncertainty associated to the LR-115 dosimeters correspond to the standard deviation of 4 dosimeters that measured the same, while the scattering of clipperton shows the variation of radon levels found with the detector during the exposure period. The relative discrepancy between both detector types is also given in table 5.5.

Table 5.4 Comparison of mean radon concentration obtained in the basement room with the Makrofol (passive, time-integrating) and PRASSI (active, time-resolved) radon detectors.

	Makrofol	PRASSI	Makrofol	PRASSI
Exposure period	13-6-95 to 17-10-95	19-6-95 to 17-10-95	17-10-95 to 23-1-96	17-10-95 to 6-1-96
Mean radon concent. (Bq·m ⁻³)	46±6	54	58±5	49

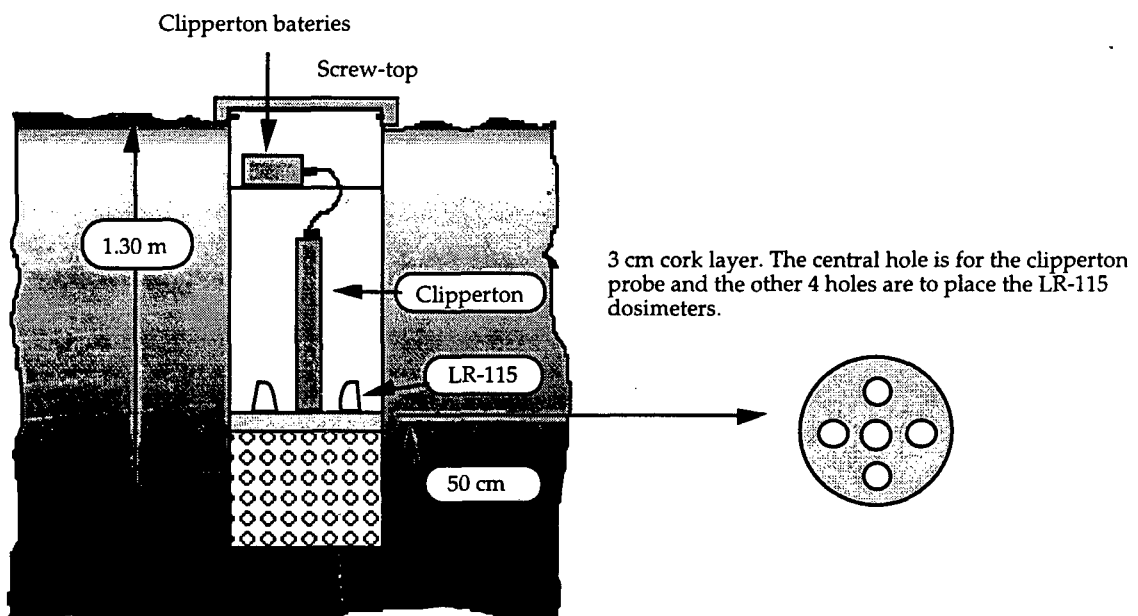


Fig 5.11: Diagram of the experimental arrangement set up to intercompare passive (LR-115) and active (clipperton) soil radon dosimeters when exposed at the same conditions.

Table 5.5: Mean soil radon concentration obtained in three consecutive periods with the clipperton probe and 4 LR-115 dosimeters exposed in the UAB hole. The Relative Discrepancy (RD) is defined as the ratio between the radon concentration values obtained with LR-115 and Clipperton radon detectors..

Exposure number	Exposure time (h)	Radon concentration (kBq·m ⁻³)		RD (dimensionless)
		LR-115	Clipperton II	
1	336.4	13.7±2.6	8.6±2.3	1.59
2	335.0	12.0±3.3	8.6±1.6	1.40
3	115.3	11.1±1.6	7.1±1.52	1.56
Mean		12.3	8.1	1.52

Fig. 5.12 shows the time-evolution of the soil radon concentration obtained during the experiment together with the LR-115 results. The sudden falls of radon concentration monitored with the clipperton probe correspond to the instant when the screw-top is opened to remove the LR-115 detectors and to install the following ones. The increase on the soil radon concentration inside the tube until reaching the steady-state is clearly seen.

We have found in the regular field measurements of soil radon concentration with the clipperton probes some humidity problems that can be minimised by protecting the probes with a membrane or a polythene bag. In the regular test-house garden we have used bare probes, latex membranes, and polythene bags. In order to study the influence of the different protections used, we performed a two-step experiment at the UAB hole. The first step consisted on exposing together the five clippertons used in the test house garden without any protection (bare) to see their relative agreement. The second step consisted on choosing three clippertons, one bare, one with a latex membrane, and the last with a polythene bag, which were exposed at the same conditions at the UAB hole.

The radon concentration time-behaviour obtained in the first step of the experiment with the four bare clipperton probes is shown in Fig. 5.13, where the curves have been smoothed by averaging each value with the preceding four values and the following four values to better differentiate the curves. No relevant differences have been observed between the four probes, leading to the conclusion that all the measurements are consistent. All the clipperton probes show the same initial increase on radon concentration, reaching an steady-state in 5 days approximately, which corresponds to the achievement of the equilibrium between the soil gas radon and the tube air radon. The short-term discrepancies observed between the different clipperton probes are interpreted as statistical fluctuations of the probes, so that this experiment allowed us to estimate that when the radon concentration is approximately constant, the statistical fluctuations of the clipperton probes are less than 15%. In table 5.6 the mean radon concentration, standard deviation and relative standard deviation obtained with each probe when the steady-state is reached, are given.

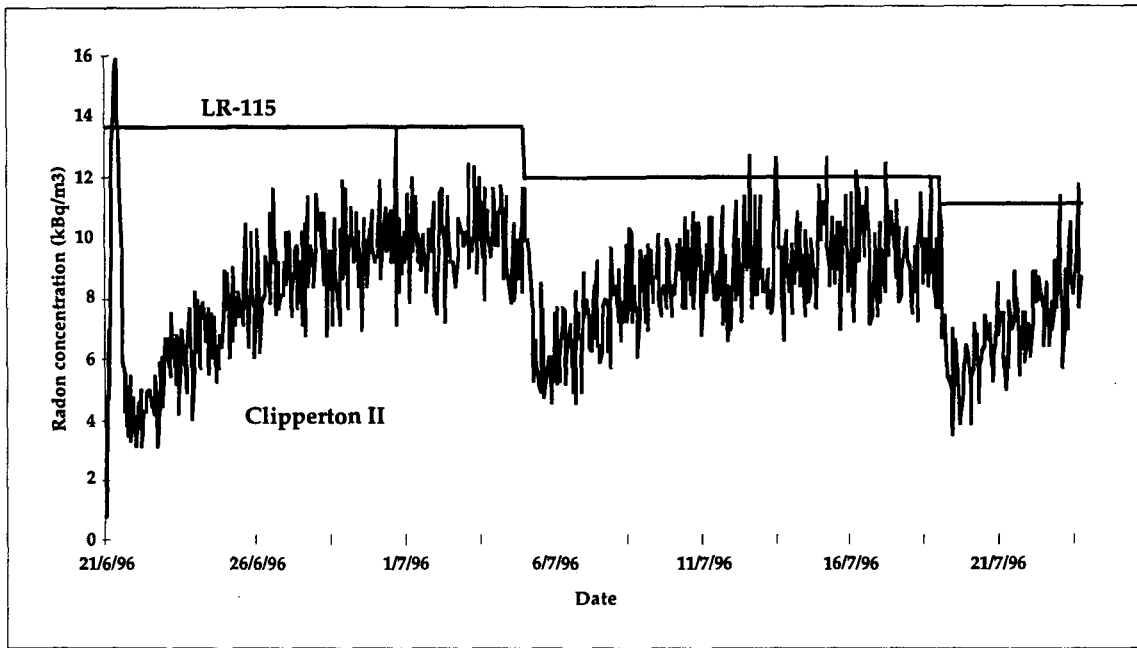


Fig. 5.12: Comparison of LR-115 and clipperton II soil radon detectors exposed in the same hole at the UAB campus.

Table 5.6: Mean radon concentration, standard deviation (SD) and relative standard deviation (RSD) obtained with the 5 clipperton probes exposed at the same conditions without any protection.

	Clipperton code				
	L1	L2	L3	L4	L5
Mean (kBq·m ⁻³)	9.8	9.4	10.9	11.3	9.4
SD (kBq·m ⁻³)	1.2	1.2	1.3	1.4	1.4
RSD (%)	12.6	13.2	12.1	12.6	15.1

Fig. 5.14 shows the results obtained in the second step of the experiment. The letters B, P and C of the clipperton probe codes correspond to the bare, polythene bag and latex membrane configuration respectively. The data has been smoothed in the same way as the first step. It can be seen that, excluding an initial radon concentration peak obtained with the clipperton that has the polythene bag incorporated and that we cannot explain, the three clippertons tend to the same equilibrium value, as it happened in the first step of the experiment. The graph also suggests that the clipperton that had the latex membrane needs a longer to reach the equilibrium value. This delay might diminish the response of the probe to sudden soil radon variations.

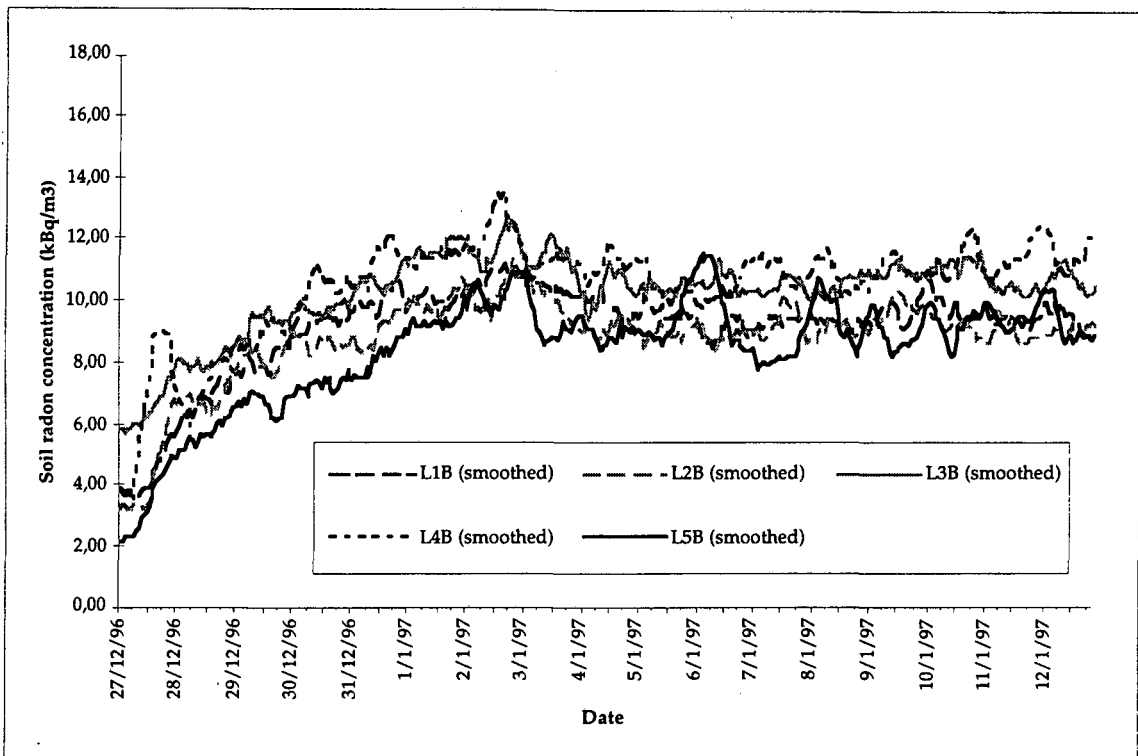


Fig. 5.13: Comparison of 5 bare clipperton probes exposed in the same hole at the UAB campus.

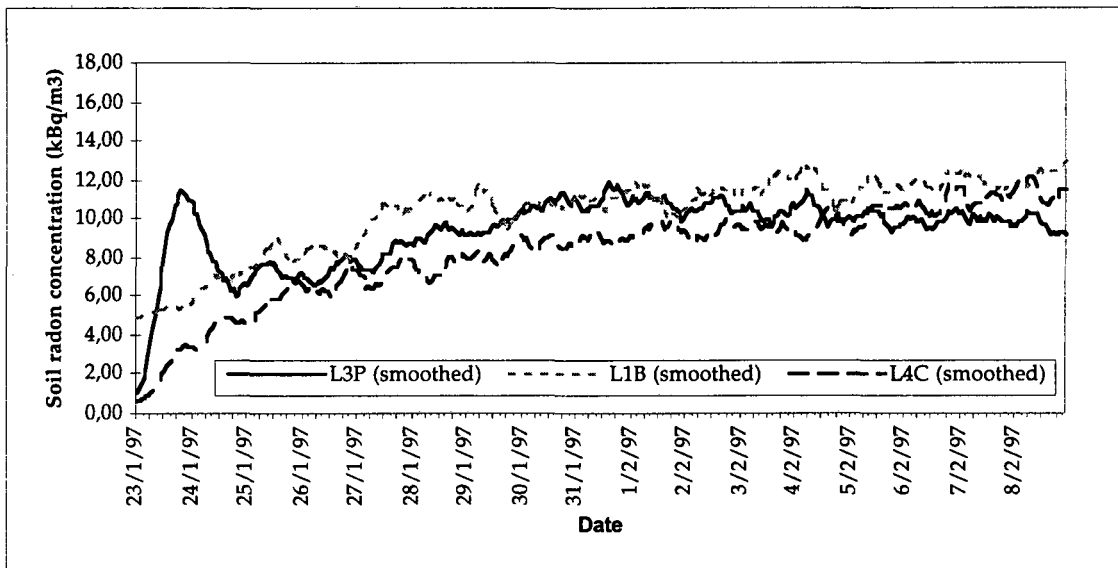


Fig. 5.14: Comparison of 3 clipperton probes exposed in the same hole at the UAB campus. Code L1B was bare, without protection; code L3P had a polythene bag, and code L4C had a latex membrane incorporated.

As a conclusion of this experiment we can say that the use of a protection in the clipperton probes doesn't seem to affect their readings and that the statistical fluctuations, due to electronic noise background can lead to 15% fluctuations of the clipperton counting.

5.3.2. Weather station

The different weather station components were checked at the laboratory before installing them in the test house. The only anomaly found was that the rain collector underestimates the rainfall for very high rainfall rates, being the maximum uncertainty associated 20%. The humidity, temperature and atmospheric pressure sensors were calibrated at the Laboratori General d'Assaigs i Mesures of the Generalitat de Catalunya, placed at the UAB campus.

5.3.3. Pressure differential transducer and permeability device

The calibration factor of the pressure differential pressure, that is, the relation bits-Pascal was carried out at the Kiel laboratory (Ghose, 1996). The determination of the number of bits stored for a zero pressure difference (zero adjustment) was necessary to obtain the bits-Pascal relation in the test house. To determine this zero adjustment bits value and also to check the stability of the sensor, we left the two pressure ports opened for 15 hours, with a time-step of one minute, such that the pressure difference was zero. The mean number of beats measured was 2423, with a standard deviation of 0.8. Then, the bits-Pascal relation is

$$y(Pa) = \frac{x(Bit) - 2423(Bit)}{16(Bit / Pa)}$$

The scattering found ($\sigma=0.8$) means then a fluctuation of 0.05 Pa around the zero value, which is a good stability and it is included in the precision of the sensor (1 bit = 0.06 Pa). Fig. 5.15 shows the results of the stability test of the pressure differential sensor.

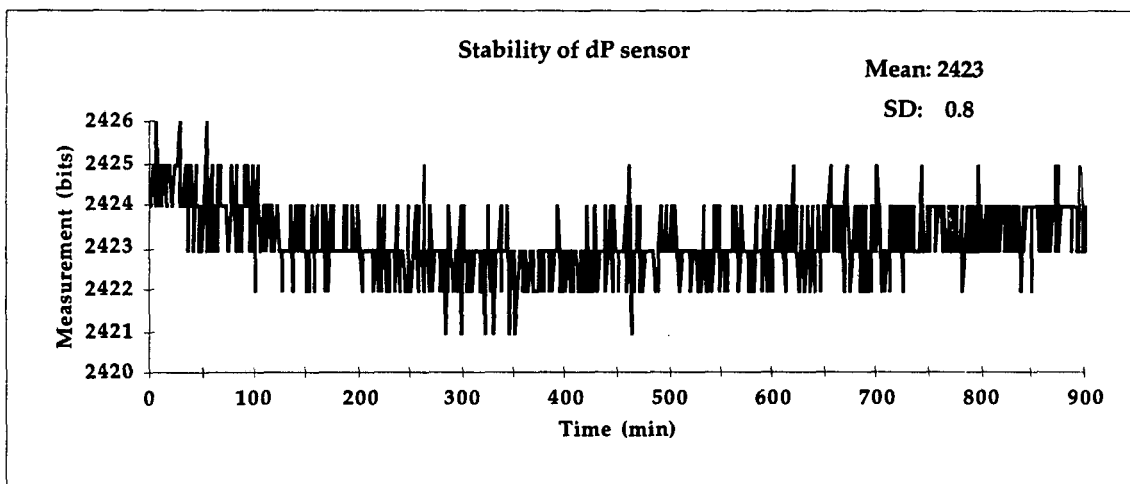


Fig. 5.15: Stability test of the pressure differential sensor. The mean bits measured correspond to a 0 Pa pressure difference.

Concerning the permeability device for in-situ measurements, its calibration factor was given by the manufacturing company.

6

Experimental results

This chapter reports on the one-year experimental results obtained in the test house within the EU project, from July, 1st 1995 to July, 1st 1996. The report is structured as follows: first, the radon data obtained with passive detectors is presented; second, we give the results corresponding to the time-resolved detectors, and finally, we show the results of measurements performed to characterise specifically the test house garden soil. The chapter finishes with a discussion of the experimental results obtained.

6.1 Time integrated data

6.1.1 Indoor radon data

The radon concentration values obtained in the different rooms of the test house with the Makrofol-based passive dosimeter are given in table 6.1. The first remark to these results is that in all cases the radon concentration values are similar to those obtained in the previous studies both in the test house and in the region, and that no high fluctuations are observed during the full year cycle. We also observe that the highest radon levels are achieved in the basement room and in the guest-room, which are the rooms less ventilated because they have not been permanently inhabited during the experience. A decrease of the radon level in the basement is appreciated from January 1996, when the room was equipped as an office and inhabited. This result suggests that, as an average, the influence of the ventilation is higher than the proximity of the room level to the soil.

Table 6.1. Indoor radon data obtained with the Makrofol passive dosimeter

Set	Exposure period	Radon concentration (Bqm ⁻³)					
		Basement	Living-room	Kitchen	Bathroom	Bedroom	Guest-room
1	13/6/95-17/10/95	46	17	21	19	15	29
2	17/10/95-23/1/96	58	38	39	52	37	52
3	23/1/96-25/4/96	37	48	28	38	43	53
4	25/4/96-24/7/96	28	33	27	16	26	33
MEAN		42	34	29	31	30	42

A closer view to the table 6.1 shows that the highest mean radon values in each room correspond to the winter time; when the manual ventilation is lower because the windows and doors are

kept closed a longer time. However, in the Mediterranean climate, the winter is very soft and this effect is not so high.

6.1.2. Soil radon data

The monthly averaged soil radon concentration values obtained with the LR-115 dosimeters of codes L3, B2 and F3 are given in Figs. 6.1, 6.2 and 6.3 respectively. In all cases, the data from the first three months are lost due to technical problems in the etching process.

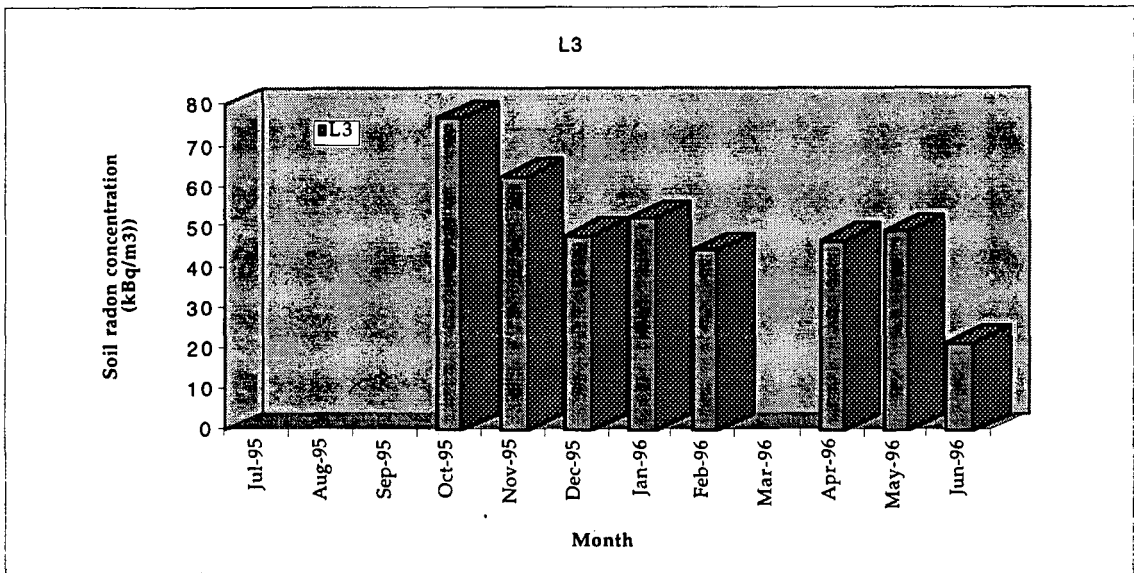


Fig. 6.1: Monthly averaged soil radon concentration obtained in the L3 measurement point with the LR-115 dosimeter.

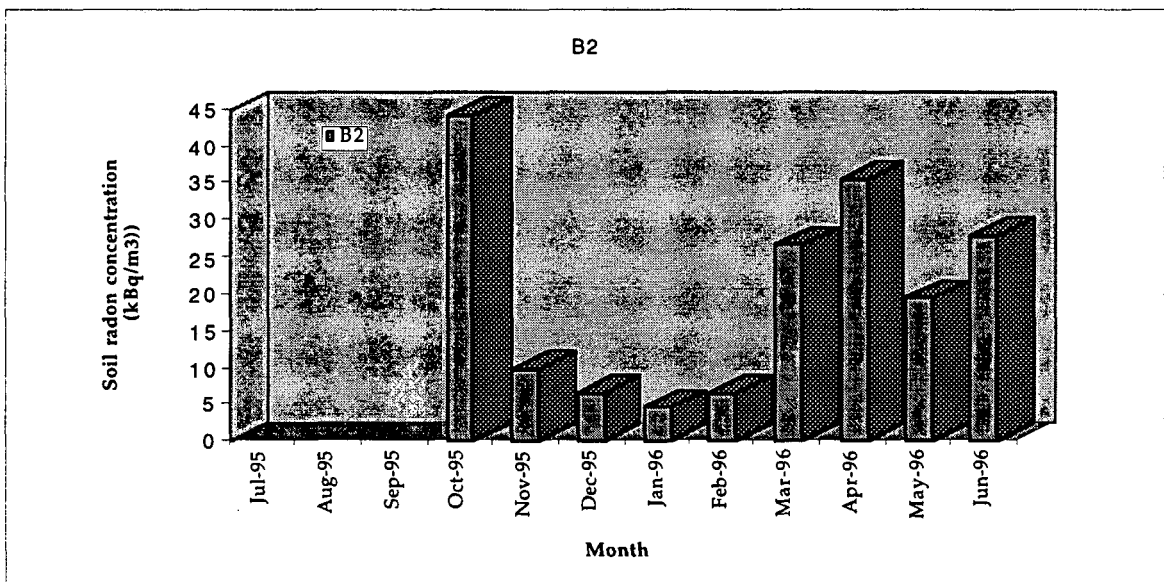


Fig. 6.2: Monthly averaged soil radon concentration obtained in the B2 measurement point with the LR-115 dosimeter.

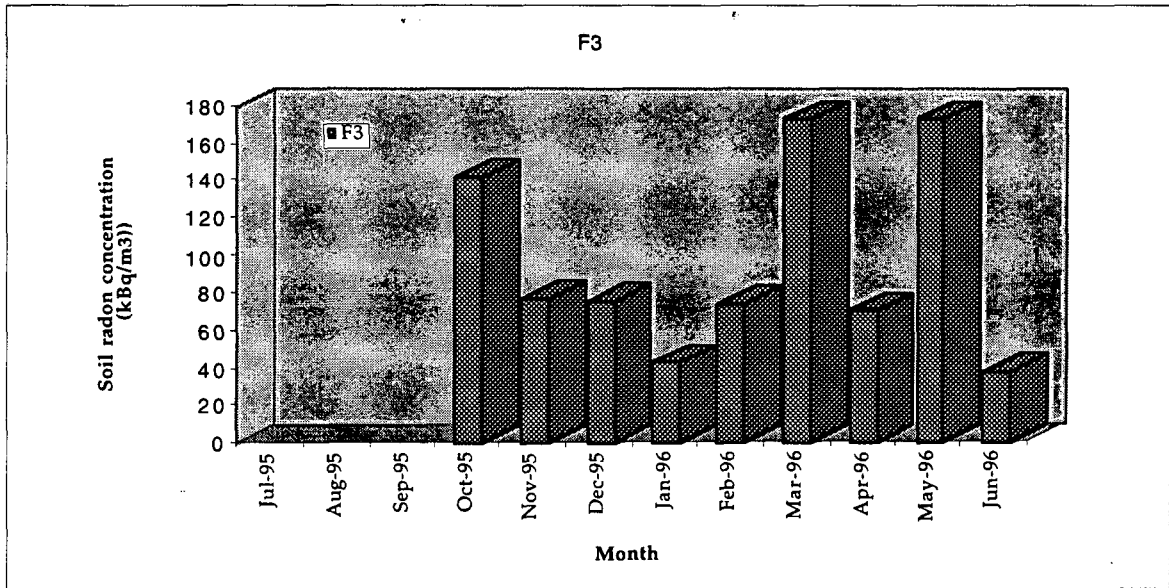


Fig. 6.3: Monthly averaged soil radon concentration obtained in the F3 measurement point with the LR-115 dosimeter.

The results obtained are very different from one measurement point to another; the mean values obtained in L3, B2 and F3 measurement points are respectively, 50.0, 20.2 and 96.1 kBq·m⁻³ such that the highest and lowest mean values differ a factor of 5. The dynamic behaviour is also different: the measurement point of code L3 do not present very high fluctuations, while F3 presented in October, Mars and May, a very high radon concentration value. The measurement point B3 presented a very clear minimum of radon concentration in the winter time, reaching very low radon concentration levels (about 5 kBq·m⁻³) compared to the typical values from the literature (20-80 kBq·m⁻³). This behaviour has been found also in the results of the B1 clipperton probe (see section 6.2.2) and we interpreted that the minimum is consequence of the presence of the opening very close to the set B detectors (see Figs. 5.5 and 5.9): the radon gas somehow migrates in the soil and reaches the open air through the opening concrete small cracks (we did not observe any big crack in the opening surface). The fact that the minimum is observed in winter time suggests that this process is sensitive to the external temperature and atmospheric pressure because, as it can be seen in section 6.2.3, these two meteorological parameters presented minimum values in winter time.

6.2 Time-resolved data

The data obtained with the time-resolved detectors correspond to one-year period with a time-resolution of 1 hour, which means that for each parameter we have over 8700 data points. As a general comment we would say that we do not have a complete one-year set of parameter values because the experimental study has been carried out in a real inhabited house instead of in a laboratory or test structure. Certainly, as we said in section 5.2.2.2.1, we only could use the

PRASSI monitor to measure continuously the basement room radon concentration for a limited period of time: from June, 19, 1995 to January, 6, 1996. Moreover, any unexpected accident was detected only when visiting the house. For example, someone could accidentally unplug the weather station control unit (children of guests, cleaning woman, etc.) and then the data is lost until the next visit to the house for data collecting and equipment control. The pressure difference sensor was installed in September 1996, after the end of the one-year cycle analysed in this work, because it was not available before. However, the soil-basement pressure difference data obtained in September 1996 will be very useful to estimate the previous pressure differences, as it is discussed in chapter 7. The time-resolved data is organised in 15-day graphs, in which we present the data obtained for that period. The complete set of data obtained for the period studied is given in annex 2 in the 15-day graph format; in this section we discuss the results obtained from the one-year point of view, looking at the one-year evolution of the parameters measured.

6.2.1. Indoor radon data

Indoor radon concentration was measured continuously with the PRASSI portable monitor. In addition to the basement room measurements for the period said above, we have also measured eventually radon concentration outdoors and in other rooms of the house. We have measured radon concentration in the bathroom both with the shower opened and closed to see if there is any contribution of the water supply. The same experiment has been performed in the laundry room, where the heating system is installed, to search for any contribution of the natural gas. In both cases we could not detect any increase on the radon concentration in the room as a consequence of the use of the shower or the natural gas and therefore, we conclude that the contribution of the water and gas supplies are negligible. Table 6.2 summarises the different indoor radon concentration measurements carried out in the test house with the PRASSI monitor.

Table 6.2: Mean radon concentration values obtained in the test house with the PRASSI portable monitor.

Room	Level	Measurement period	Data points	Mean Rn conc. (Bq·m ⁻³)	Range (Bq·m ⁻³)	Remarks
Guest-room	2	28/2/96-29-2-96	30	28±5	17-42	
Bathroom	1	24/2/96-25/2/96	51	20±8	4-39	No effect of the water supply use observed.
Laundry room	-1	26/2/96	7	16±10	7-34	No effect of the gas supply use observed.
Basement room	-1	19/6/95-6/1/96	4818	52±18	2-133	
Outdoors	0	23/2/96	14	2±2	0.2-5.3	

The mean radon concentration value obtained with the PRASSI monitor in the basement was already compared with the Makrofol-based dosimeter in section 5.3.1.2 (see table 5.4), where an

excellent agreement was found. The results obtained in the guest-room and in the bathroom with the PRASSI monitor are lower than those obtained with the Makrofol dosimeters; however, it must be taken into account that the PRASSI measurements correspond to a very short period compared to the exposure period of the Makrofol dosimeters, so that at the instant of the PRASSI measurements, the radon concentration was lower than the averaged value. It is also remarkable the low outdoor radon concentration measured at the surface level, which, considering that there was not appreciable wind at the moment of the measurement, seems to indicate a low exhalation rate from the soil. In Fig. 6.4 we present a typical 15-day pattern of the basement radon concentration evolution, where it can be seen that the fluctuations of the radon levels around $50 \text{ Bq}\cdot\text{m}^{-3}$ are not so high.

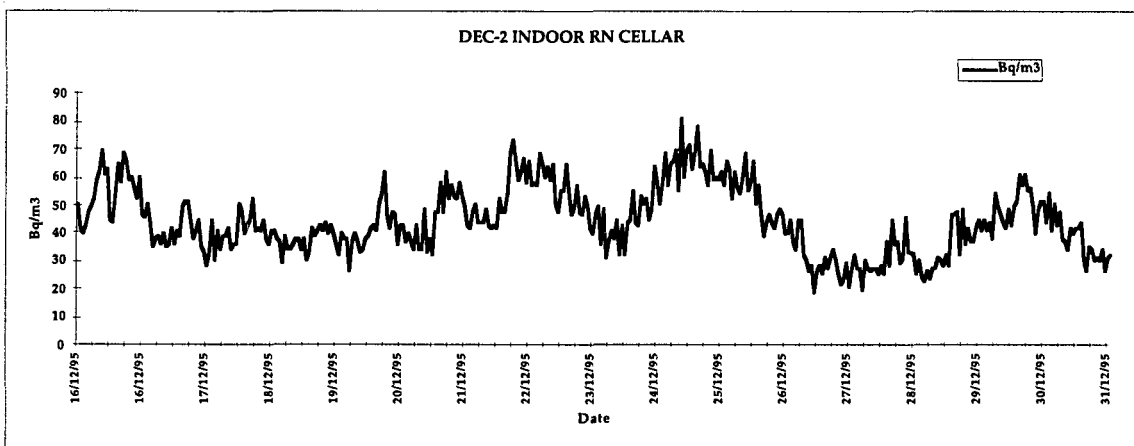


Fig. 6.4: Typical pattern of basement room radon fluctuations measured with the PRASSI portable radon monitor.

To better see the evolution of the basement radon concentration for the period measured, we present in Fig. 6.5 the monthly averaged values of the basement radon concentration.

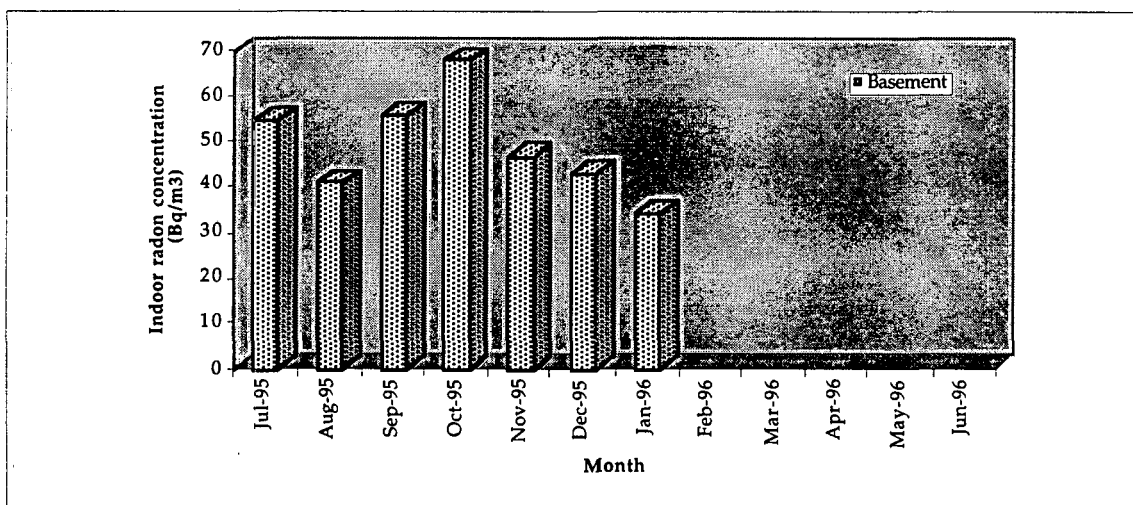


Fig. 6.5: Monthly-averaged radon concentration obtained in the basement with the PRASSI monitor. In January 1996 we had to stop the measurements not to disturb the inhabitants of the test house.

6.2.2. Soil radon data

Soil radon concentration was measured continuously with the Clipperton II probes in 5 points of the soil garden, as it was explained in section 5.2.2.1.2 (see Figs. 5.5 and 5.9). As in the indoor radon data, the complete set of measurements is given in annex 2. In general, the radon concentration values obtained with the Clipperton II probes are lower than those obtained with the LR-115 soil radon dosimeters, in accordance with the intercomparison between both type of soil radon detectors described in section 5.3.1.2.

As a general comment, we must say that in some cases some Clipperton II probes presented humidity problems, which produced an uncontrolled increase of the counting rate that led to data losses.

The behaviour of the different probes is very complex: in some periods, the radon levels of the probes of the same set, that is L1, L2 and F1, F2, which are separated by less than 20 cm in the soil, present similar values, and in others absolutely different; moreover, the dynamics can be very different as well, and consequently, no simple correlation can be found from the global point of view. Some clippertons have experimented in a given instant a sudden increase and decrease of counting rates which can not be easily associated with any meteorological parameter. These results show the complexity of the problem and how radon levels in a specific site of the soil might be disconnected from another site just 20 cm far. Thus, no simple correlation has been found between the different probes. A better agreement between the different probes is achieved when taking the averaged monthly value, as it can be seen in Figs. 6.6 and 6.7, where the soil radon concentration values obtained in the sets L and F respectively, are presented. It is observed that the monthly averaged soil radon concentration fluctuated in both sets around a mean value close to $17 \text{ Bq}\cdot\text{m}^{-3}$, and that the dynamics of the radon levels measured with the two probes is similar, specially in the set L, where we do not have significant losses.

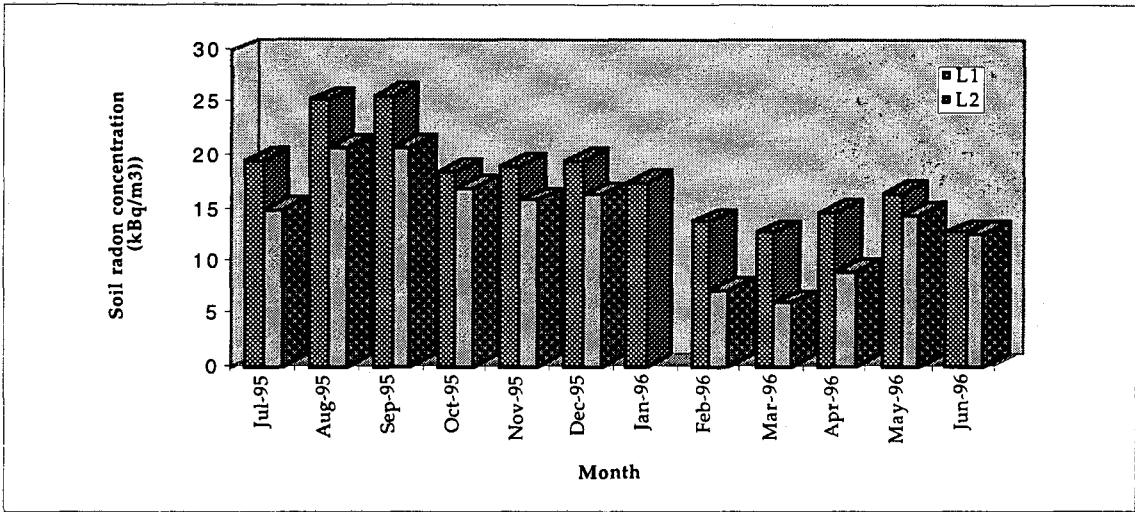


Fig. 6.6: Monthly averaged soil radon concentration obtained in the set L clipperton probes. Both probes present maxima and minima at the same instants.

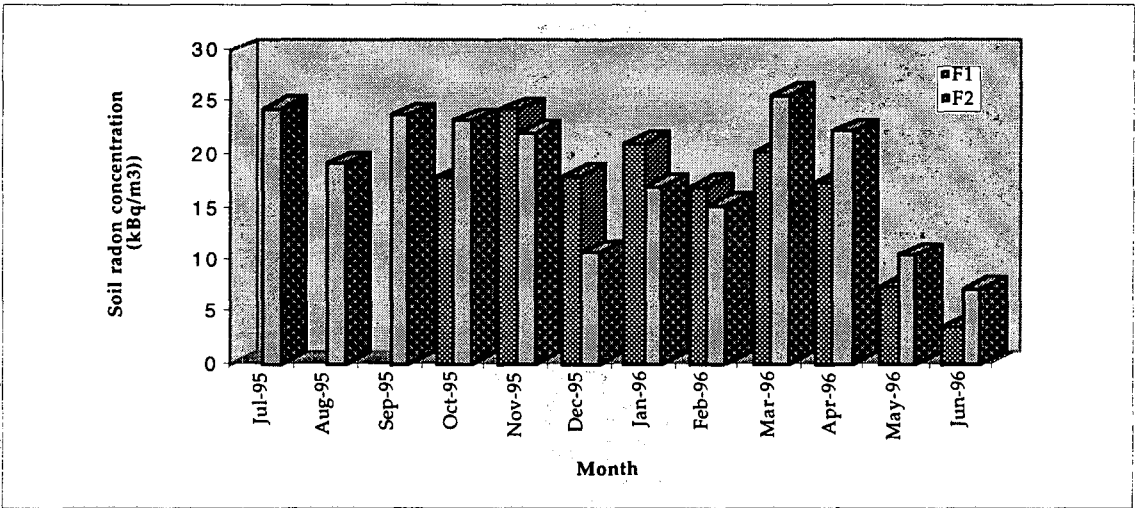


Fig. 6.7: Monthly averaged soil radon concentration obtained in the set F clipperton probes. A similar time-behaviour is obtained from November-95.

The most fluctuating soil radon concentration has been obtained in the B1 site, where a very clear minimum has been found during the winter period, as it can be seen in Fig. 6.8. The same behaviour has been observed and interpreted in section 6.1.2 with the LR-115 detectors in the measurement point B2.

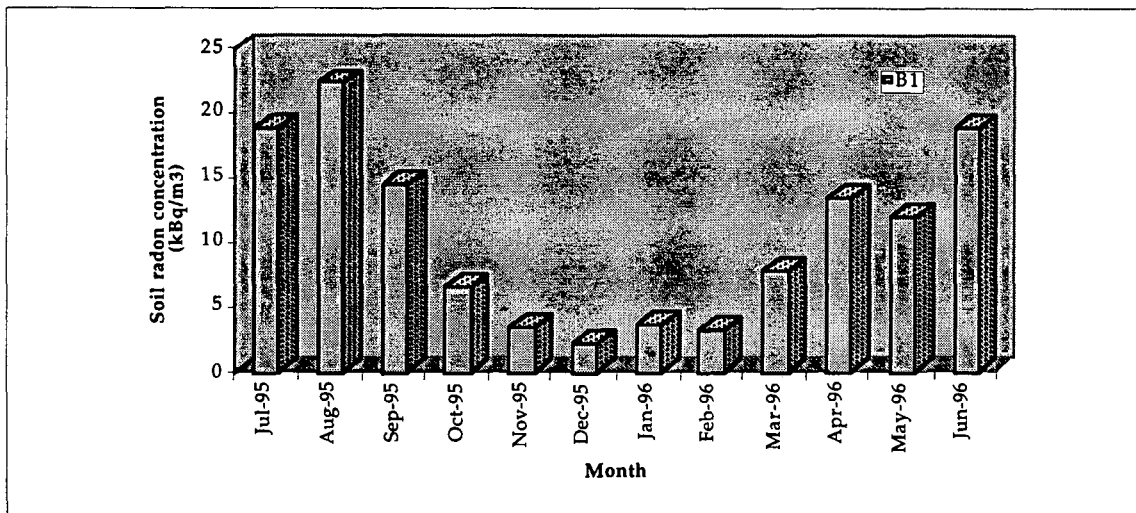


Fig. 6.8: Monthly averaged soil radon concentration obtained with Clipperton probe B1. the presence of the minimum is interpreted as a consequence of the escape of the soil radon gas through the opening nearby.

The annual averaged soil radon concentration values obtained with the clipperton probes are given in table 6.3. There is a good agreement between all the probes excepting B1, and therefore we conclude that the mean soil radon concentration in the test house garden is around 17 kBq·m⁻³.

Table 6.3: Annual averaged soil radon concentrations measured with the Clipperton probes.

	Clipperton II code				
	L1	L2	B1	F1	F2
Annual average (kBq·m ⁻³)	18.0	14.1	10.7	16.4	18.4

6.2.3. Weather station data

The complete data set of the relevant weather parameters is given in annex 2. The variation of the weather parameters obtained is typical for a Mediterranean climate. The monthly averaged values of indoor and outdoor temperature, atmospheric pressure and wind speed are shown in Fig. 6.9, 6.10 and 6.11 respectively, and the total rainfall per month is given in Fig. 6.12. The total annual rainfall was 579 mm and the mean wind speed 0.5 m·s⁻¹, and the mean indoor-outdoor temperature difference 5°C.

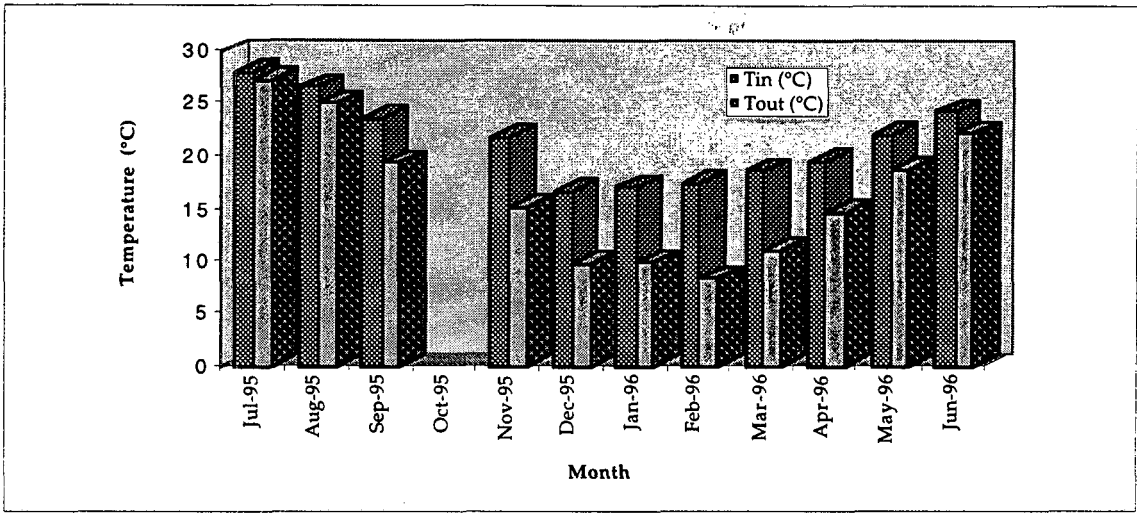


Fig. 6.9: Monthly-averaged indoor and outdoor temperature difference obtained with the weather station.

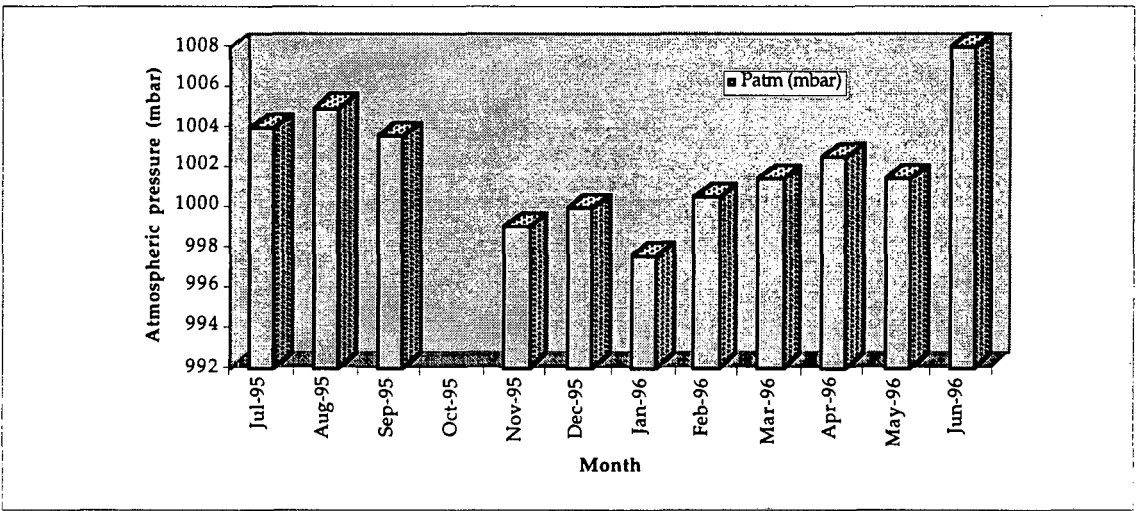


Fig. 6.10: Monthly-averaged atmospheric pressure measured with the weather station.

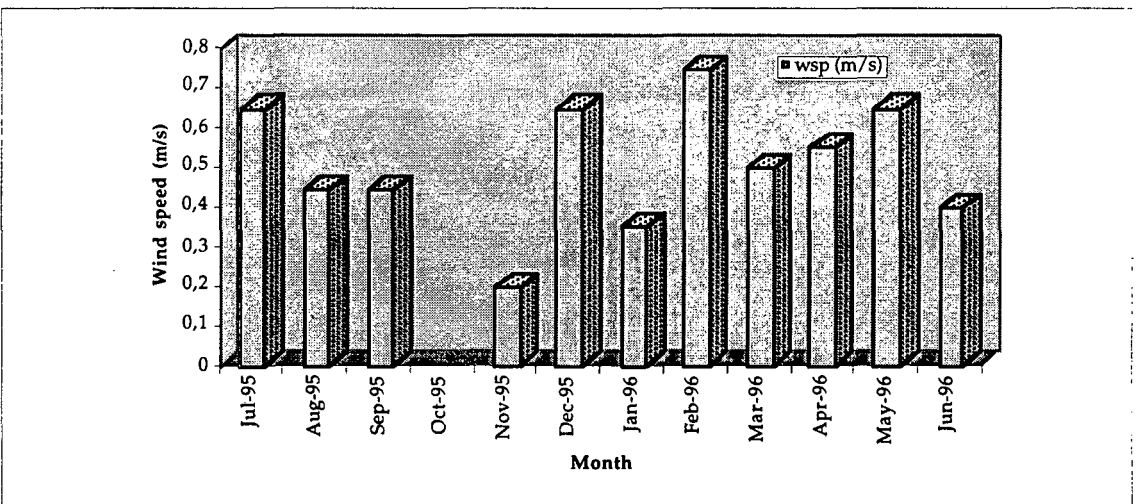


Fig. 6.11: Monthly-averaged wind speed measured with the weather station.

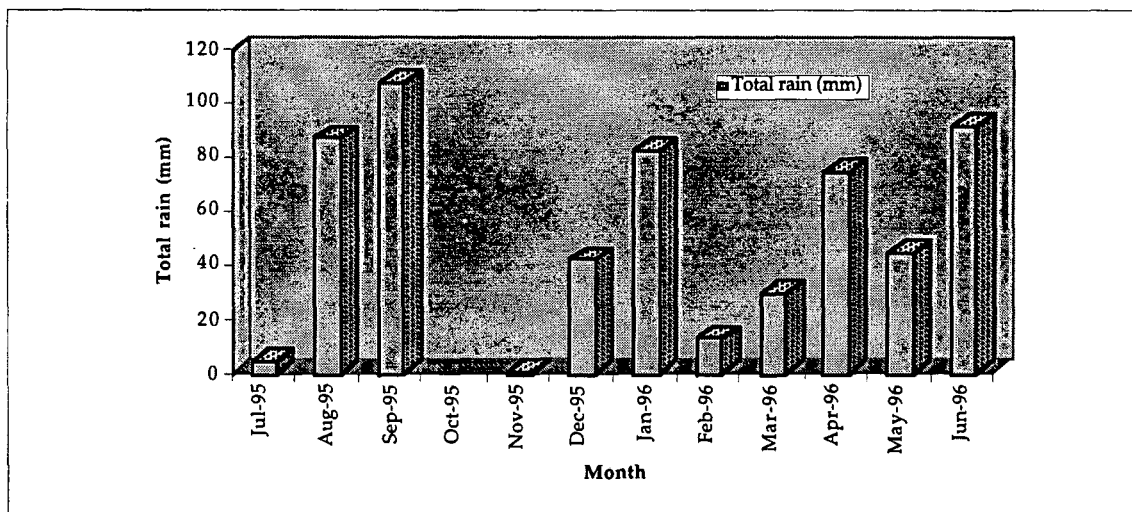


Fig. 6.12: total rain per month measured with the weather station.

6.2.4. Soil-indoor pressure difference data

We started measuring the soil-indoor pressure difference in September 1996. The EU project survey continued until December 1996 such that the weather station parameters were collected as well. The measurement of both soil-indoor pressure difference and meteorological parameters allowed us to model the dynamics of soil-indoor pressure difference as a function of meteorological parameters as it is explained in chapter 7. The one-month time-evolution of the pressure difference is shown in Fig. 6.13, where a periodic behaviour is observed around the mean value: 2.1 ± 0.4 Pa, meaning that the basement room is underpressured with respect to the soil.

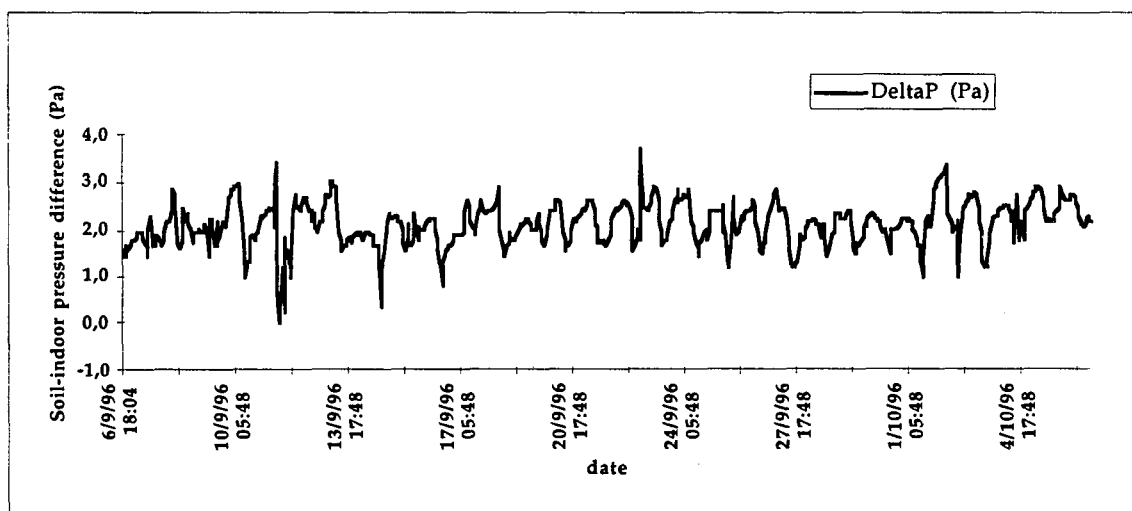


Fig. 6.13: One-month soil-indoor pressure difference dynamics measured in the test house. A positive value means indoors underpressured with respect to the soil.

6.3. Soil characterisation data

The specific characterisation of the test house soil has been carried out by determining the texture of the soil, its gas permeability and its radium content.

6.3.1 Texture

One soil sample at one meter depth was collected for each soil detector placement and sent to the Unitat de Geodinàmica Externa i Hidrogeologia of the UAB for texture analysis. The samples can be divided into two groups: the first one corresponds to code F samples, which have shown a higher consistency, while the second, corresponding to codes B and L, are constituted by heterogeneous materials, including rests of building materials. The results obtained suggest that the soil of the test house can be classified as "Yolo Light Clay" (Mas-Pla and Linares, 1997), which has the following characteristics:

Sand: 23.8%

Loam: 46.0%

Clay: 31.2%

Porosity: 0.495

6.3.2. Permeability

The permeability device available in the Leipzig group of the EU-project was used to measure, in two consecutive days, the gas-permeability of the test house soil. The measurements were performed at different points and depths of the test house garden. Fig. 6.14 shows the distribution of the measurement points in the test house garden, and the results obtained are given in table 6.5. It can be seen that a very high scattering was obtained, showing how inhomogeneous the soil can be with respect to the gas-permeability. In addition to the spatial scattering, a temporal variation of the gas-permeability might be expected as a consequence of the rainfall events. Most of the values obtained correspond to very low permeability soils. It is worthwhile to note that the points where local gas-permeability is higher are L and B, which are the points very close to the house walls and therefore, have rests of building materials that can produce local air bubbles in the soil.

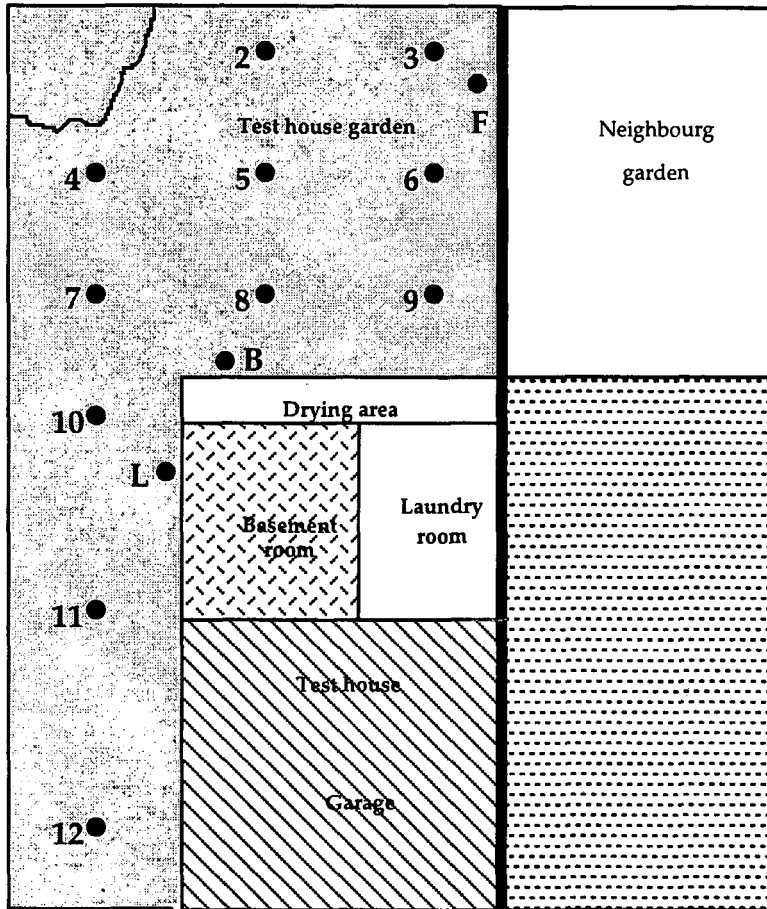


Fig. 6.14: distribution of the gas-permeability measurement points at the test house garden

Table 6.5: Gas-permeability results measured in the test house garden

Measurement point	Depth (cm)	Gas-Permeability (m^2)
2	77	$9.01 \cdot 10^{-14}$
3	72	$< 6.38 \cdot 10^{-15}$
4	80	$< 6.39 \cdot 10^{-15}$
5	80	$1.18 \cdot 10^{-14}$
6	79	$< 6.39 \cdot 10^{-15}$
7	79	$< 6.39 \cdot 10^{-15}$
8	80	$2.49 \cdot 10^{-14}$
9	81	$4.29 \cdot 10^{-14}$
10	78	$1.11 \cdot 10^{-12}$
11	79	$2.66 \cdot 10^{-13}$
12	86	$4.82 \cdot 10^{-13}$
L	26	$8.66 \cdot 10^{-15}$
L	45	$2.01 \cdot 10^{-12}$
L	84	$1.84 \cdot 10^{-11}$
B	45	$2.75 \cdot 10^{-11}$
B	70	$1.57 \cdot 10^{-12}$
B	85	$5.91 \cdot 10^{-14}$
F	47	$8.27 \cdot 10^{-15}$
F	65	$4.29 \cdot 10^{-15}$
F	75	$1.08 \cdot 10^{-14}$

6.3.3. Radium and uranium content

Within the coordinated activities of the EU project, we sent soil samples from all the measurement points of the survey corresponding to the test house and to the 10 control houses to the Leipzig group for gamma spectrometry analysis. The measurement technique and the results obtained (specific activities of Th-234, Ra-226, Pb-210, Ac-228, K-40 and the uranium and thorium contents) are presented in the EU project internal report given in annex 5 (Treutler and Freyer, 1995). The radium content values obtained in the locations of the test house garden are given in table 6.6 and can be considered as in the normal environmental level.

Table 6.6: Specific Ra-226 activity measured in the test house soil samples

Soil sample code	Ra-226 specific activity (Bq.m ⁻³)
L1	13 ± 1
L2	25 ± 2
L3	27 ± 2
B1	25 ± 2
B2	24 ± 1
F1	28 ± 2
F2	30 ± 2
F3	27 ± 3

6.4 Discussion

The results obtained with the time-resolved detectors have shown the complexity of the soil and indoor radon behaviour in an inhabited house, where most of the parameters cannot be controlled. We have seen that the soil radon dynamics can be very different from one point to another very close, making very difficult the detailed understanding of the radon dynamics. Climent (1996) also found this behaviour in different soil locations from the test house in Montpellier and obtained, with a Correlatory and Spectral Analysis, different correlations between soil radon concentration and meteorological parameters in the different measurement sites.

The measurements carried out with the Makrofol passive detectors are in excellent agreement with both previous studies and time-resolved measurements with the PRASSI monitor. In the case of soil passive detectors, based on LR-115, the mean soil radon concentration values obtained are higher than those collected with the clipperton probes. Even though the results are not directly comparable because the detectors have not been installed exactly in the same place, the systematic overestimation of radon concentration of the LR-115 dosimeters with

respect to the clipperton probes confirms the discrepancy observed in section 5.3.1.2. The determination of the soil porosity and radium content allows us the estimation of the soil radon concentration in secular equilibrium with radium. Considering an emanation fraction of 0.2, and a water saturation fraction of 0.5, we obtain a value of the soil radon concentration around 26 kBq·m⁻³. Considering that in an undisturbed soil the radon concentration at 1 meter depth is in equilibrium with radium, and that our measurements have been carried out in a depth of 0.8 - 1 m, we conclude that the values given by the clipperton probes are more reasonable. The calibration of the LR-115 detectors that is being currently carried out will hopefully solve this discrepancy.

The disturbing effect of the test house has been clearly seen in the measurements of the soil gas-permeability. All the values of gas-permeability in the measurement points far from the building shell were low and typical for a clayey soil, while very close to the building shell, higher values were found.

7

Model-experiment comparison

In the preceding chapter we have presented the data obtained in the experimental study carried out in this work. The purpose of this chapter is to use the RAGENA model to understand radon accumulation and dynamics in the test-house site, by adapting the model to the data available. The chapter is structured into two parts: in the first one, we describe the adaptation of the model to the test-house site, and in the second, we present the predictions obtained with the model and we compare them with the experimental results.

It is worthwhile to note that the comparison between the experimental data and the predictions of the RAGENA model does not constitute a validation of the model, because many parameters were neither controlled nor monitored. Strictly speaking, a validation of the model only can be performed under laboratory conditions, that is, in a test structure where the maximum number of parameters are continuously controlled and monitored. We do not have in our laboratory a test structure available; however, in this chapter we show how the model can be adapted to a specific situation in which the data set is limited, as it might occur in many real cases.

7.1 Adaptation of RAGENA model to the test-house

The test-house modelling work has been restricted to the basement room because it is the only room in which radon concentration was measured continuously for a long period of time with the PRASSI monitor, such that the radon dynamics obtained with the model can be compared directly with the PRASSI data.

To adapt the model to the basement room of the test house we have proceeded as follows: by default, the values of the parameters correspond to those chosen in the reference configuration described in chapter 4; in case of having experimental information on a given parameter, we use this direct information specific of the site instead of the reference configuration value; and finally, when it is possible, we consider reasonable assumptions on some parameter values according to the experimental data obtained. In the following sections we describe the parameter values assignment.

7.1.1 Geometry of the room

The roof, the floor, and two walls are made from concrete, and the other two are made from brick. The two concrete walls correspond to the building shell; one is in direct contact with the lateral soil where the set L of soil radon detectors are placed, and the other has a window and faces the opening (see Fig. 5.5) close to which the set B soil radon detectors are installed. One of the brick walls separates the basement room from the laundry room and has a door to the staircase, and the other wall separates the room from the garage. The values of the basement surface in direct contact with soil, total concrete surface, and brick surface, subtracting the contribution of the window and the door, are given in table 7.1 together with the rest of parameter values. There are not visible cracks in the room, so that a small fraction of the open area value has been selected. The concrete covering factor has been reduced because the lateral concrete wall has a metallic sheet incorporated to avoid moisture problems that is assumed to reduce greatly the radon exhalation from the concrete surface.

Table 7.1: Parameter values corresponding to the geometry of the room

Parameter	Value
Concrete surface	32.7 m ²
Brick surface	16.6 m ²
Surface in direct contact with soil	20 m ²
Volume of the basement room	26.1 m ³
Fraction of the open area	1·10 ⁻⁶
Concrete covering factor	0.3

7.1.2 Soil parameters

The values of the soil parameters are given in table 7.2. We have assigned to the disturbed soil the mean radium content of the sets L and B soil samples, which are close to the house, and to the undisturbed soil the mean radium content of the set F samples. The radium content of each sample is given in section 6.3.3. Due to the property of clays to strongly retain the water, we have chosen a water saturation fraction of 0.45 which is higher than the reference configuration value, but it is a typical value for a clayey soils, according to the soil classification as "Yolo Light Clay" (section 6.3). We have seen in section 6.3 that the in-situ local permeability measurements have shown a very big scattering. Considering only the measurements carried out close to the basement room, that is, in the disturbed soil (measurement points 8,10, 11, L and B (see Fig. 6.12), we obtain an averaged value of $5.7 \cdot 10^{-12}$ m². However, we are interested on describing the dynamics of the radon entry and accumulation indoors, and consequently, we should relate the soil gas-permeability to the water saturation fraction in order to relate it to

the rainfall. We have multiplied expression (3.10) by a correction factor of 0.5 to obtain a gas-permeability value with this expression very close to the experimental averaged value. The gas-permeability value given in table 7.2 corresponds to that obtained with the expression (3.10) corrected. Thus, under dynamic conditions, changes on the water saturation fraction will produce changes on the soil gas-permeability according to expression (3.10).

Table 7.2: Parameter values corresponding to the soil garden of the test house.

Parameter	Value
Disturbed soil radium content	22.8 Bq·kg ⁻¹
Undisturbed soil radium content	28.3 Bq·kg ⁻¹
Mean grain diameter	1·10 ⁻⁵ m
Porosity	0.495
Gas-permeability	6.45·10 ⁻¹² m ²
Water saturation fraction	0.45
Maximum emanation fraction	0.2

7.1.3 Soil-indoor pressure difference and ventilation rate

Two of the most relevant parameters found in chapter 4 are the soil-indoor pressure difference and the ventilation rate. The first was measured after the studied period, while the second was never measured. We also do not have any information on the air-exchange between the basement room, the laundry room, the garage, and the ground floor rooms. We assume that the radon concentration in the other basement rooms must be similar to the basement room and therefore, the air-exchange between the different rooms is not so relevant. This assumption seems reasonable because the results obtained with the passive detectors have shown that, as an average, there are not so high differences between radon levels in the test house rooms. Thus, we do not consider any inter-zone flow in our model adaptation.

The soil-indoor pressure difference started being measured in September 1996, when the experimental period studied in this work was finished. However, the fact that the meteorological parameters were measured simultaneously, allows us to obtain an expression to relate soil-indoor pressure difference with some meteorological parameters. According to Eq. (3.35), the total soil-indoor pressure difference is modelled as the sum of the contributions of the indoor-outdoor temperature differences, the wind speed, the atmospheric pressure changes, and the use of mechanical ventilation. In our case, there is not mechanical ventilation, so that we have fitted the one-month experimental data given in Fig. 6.13 to the expression

$$\Delta P = a + b \frac{T_i - T_o}{T_o} + cu^2 \quad (7.1)$$

were a, b , and c are the fitting parameters.

T_i and T_o are the indoor and outdoor temperature respectively ($^{\circ}\text{K}$).

u is the wind speed ($\text{m}\cdot\text{s}^{-1}$).

ΔP is the soil-indoor pressure difference.

The values obtained for the fitting parameters are $a=1.5$, $b=1.8$, $c=0.1$, and in Fig. 7.1 the comparison between the measured and the modelled pressure difference is given. The good agreement obtained with expression 7.1 suggests that there was not relevant contribution of the atmospheric pressure changes to the soil-indoor pressure difference, which is expected to have a high time-dependence, and that an undefined mechanism produces a permanent underpressure of the basement room with respect to the soil. The period modelled is long enough to consider the fitted expression as correct for previous periods. The dynamics of the soil-indoor pressure difference is clearly driven by the soil-indoor temperature difference and the wind speed. The mean soil-indoor pressure difference obtained experimentally and with expression (7.1) are 2.14 Pa and 2.07 Pa respectively.

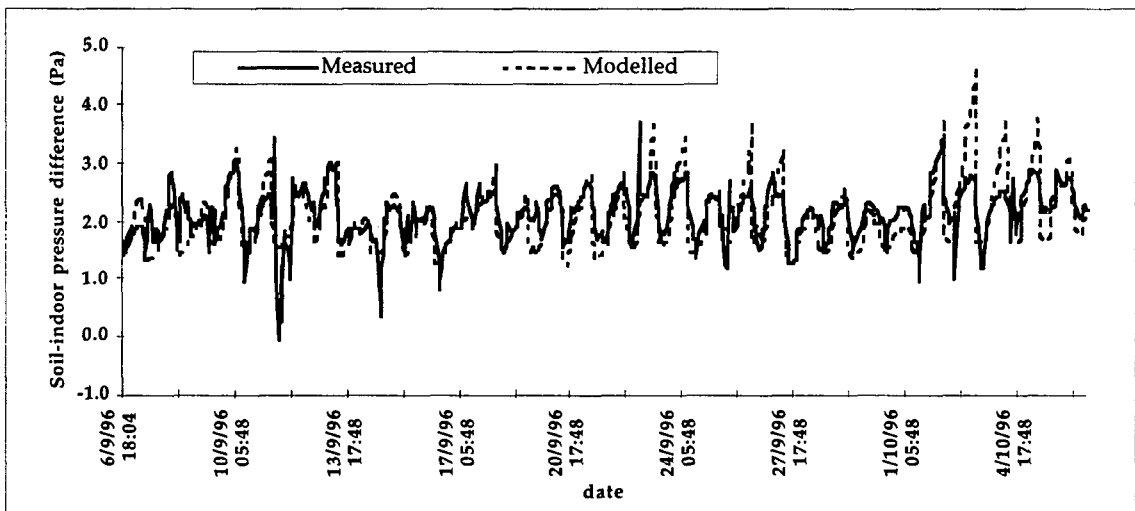


Fig. 7.1: Comparison between measured and modelled soil-indoor pressure difference.

Since the basement room was not inhabited during the measuring period, the window and the door were basically kept closed, so that infiltration was the main component of the ventilation rate. When there is not any mechanical ventilation, the infiltration and the unbalanced components of the ventilation rate are the same (see section 2.3). Therefore, due to the fact that we can properly estimate the soil-indoor pressure difference, we use Eq. (2.30) to estimate the ventilation rate of the room, where we have chosen $n=0.75$ and we have fitted the effective leakage area (A_0) to obtain reasonable values of ventilation rate: as it is said in section 2.3, typical values for infiltration rates are within the range $0.1\text{-}1\text{ h}^{-1}$. In Fig. 7.2 the dynamics of the

ventilation rate obtained in the first 15 day period of August 1995 is shown. The mean ventilation rate obtained is 0.45 h^{-1} .

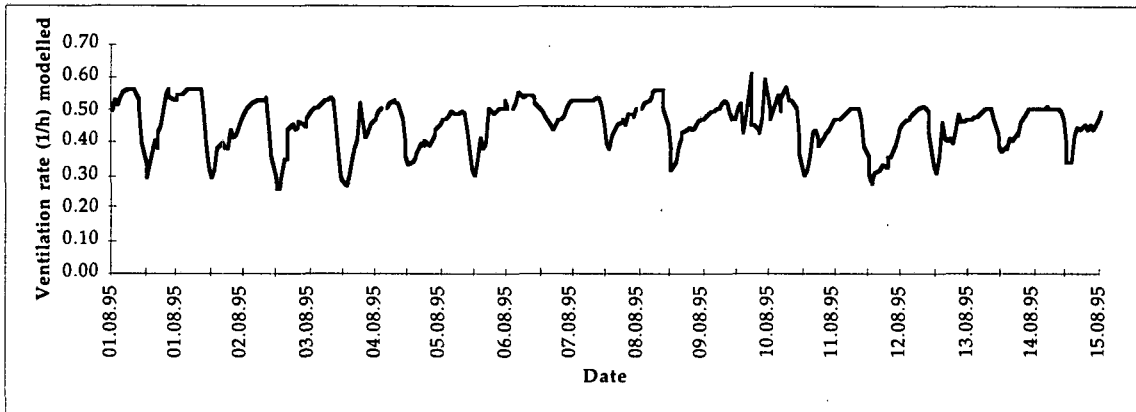


Fig. 7.2: Ventilation rate modelled in the first 15-day period of August 1995

7.1.4 Water saturation fraction

We have already assigned a mean typical value for clayey soils of 0.45 to the water saturation fraction. However, we have the possibility with the environmental parameters sector of the RAGENA model, to use a very simple model to relate the rainfall data with the water saturation fraction. As we said in section 3.3.7.1.5, we characterise the soil with two parameters: the remaining water saturation fraction, and the drying rate. The first one corresponds to the typical value of the water saturation fraction when it does not rain for a couple of weeks and the second is the rate at which the gravitational component of the soil water infiltrates downward. We have assumed that in 5 days, half of the gravitational soil water has infiltrated, that is, that the gravitational component of the soil water has a "half life" of 5 days. The water saturation fraction obtained in the first 15-day period of August 1995 is shown in Fig. 7.3.

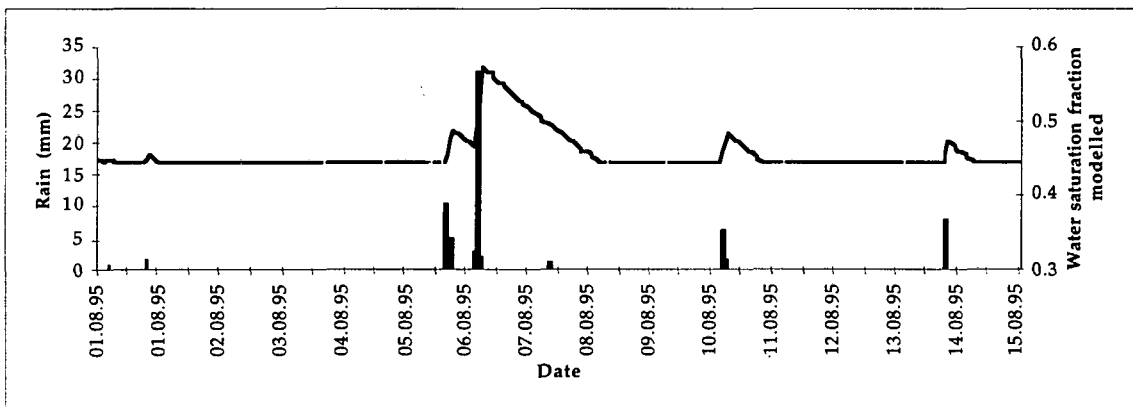


Fig. 7.3: Water saturation fraction modelled and rainfall measured for the first 15-day period of August 1995.

7.2 Comparison of RAGENA predictions with experimental results

The comparison of the RAGENA predictions with the experimental results is divided into two steps. First, we run the model under steady-state conditions to compare the RAGENA prediction with the results of the passive detectors; and second, we run the model for the 15-day periods in which we have both meteorological parameters and PRASSI data available.

7.2.1 Steady-state results

The values of the parameters chosen for the steady-state simulation are those given in tables 7.1 and 7.2, in the reference configuration, and in the case of the soil-indoor pressure difference and ventilation rate, the values chosen are the mean values obtained in section 7.1.3: 2.14 Pa and 0.45 h⁻¹ respectively. The steady-state results are given in table 7.3. It is observed that the mean indoor radon concentration obtained is of the same order than the annual radon concentration value measured with the Makrofol dosimeters (42 Bq·m⁻³). A better agreement is achieved if we consider only the two first values of Makrofol results (46 and 58 Bq·m⁻³), which correspond to the period when the basement was not inhabited and the contribution of manual ventilation was negligible. It is also observed that the soil radon concentrations are slightly higher than those measured with the Clipperton II probes. These results are very satisfactory, taking into account that there were many parameters no measured like, for instance, the concrete radium content, effective diffusion constant, the ventilation rate, etc. The results obtained with the model allow the characterisation of the radon entry into the basement:

- i) The soil is main source of radon entry into the basement, accounting for 67.3% of the total radon entry, being advection, with 43.5%, the dominant mechanisms.
- ii) The contribution of the radon exhalation from concrete is very similar to the contribution of the diffusion from the soil.
- iii) The less relevant radon source are the brick walls.

Table 7.3: Steady-state results of the RAGENA model applied to the basement room of the test-house

Output parameter	Value	Percentage
Radon concentrations:		
Undisturbed soil radon concentration	25777 Bq·m ⁻³	
Disturbed soil radon concentration	25767 Bq·m ⁻³	
Basement room radon concentration	57 Bq·m ⁻³	
Radon entry rates into the basement room from:		
Concrete	0.121 Bq·s ⁻¹	25.5%
Brick	0.034 Bq·s ⁻¹	7.2%
Soil (advection)	0.206 Bq·s ⁻¹	43.5%
Soil (diffusion)	0.113 Bq·s ⁻¹	23.8%
Radon entry flows into the basement room:		
Concrete (exhalation rate)	3.71·10 ⁻³	
Brick (exhalation rate)	2.34·10 ⁻³	
Soil (advection)	1.03·10 ⁻²	
Soil (diffusion)	5.64·10 ⁻³	

7.2.2 Dynamic results

The time-evolution of the disturbed soil radon concentration calculated with the RAGENA model is compared to the radon dynamics obtained with the clipperton probes L1 and L2, which are those closest to the basement room, and the modelled basement radon concentration is compared to the PRASSI results. We have modelled the 3 month period July 95 - September 95 because it is the period in which we have simultaneously available PRASSI, clipperton and meteorological parameter data. The results of the comparison are given in the 15-day graph format at the end of annex 2. As a general comments to the model-experiment comparison results we can say that a very similar periodical behaviour is obtained in both modelled and experimental results. In the soil radon dynamics, the model predicts higher radon values, as we have seen in the steady-state comparison, and also in some cases predicts the existence of radon concentration peaks of a higher amplitude than observed. However, it must be noted that also the clipperton probes show different amplitudes in the radon concentration peaks. A better agreement with the mean values occurs in the basement radon simulations; were it can be seen that the fluctuations predicted by the model are smaller than those measured. It is clear than a sudden decrease of the indoor radon level due to the opening of the window would have been reflected in the experimental data, but not in the model, as we only have considered infiltration. In some cases, we have observed experimentally a sudden increase of basement radon concentration that it is not reproduced by the model.

In Figs. 7.4 and 7.5 we present the results of the model-experiment comparison corresponding to the second 15-day period of September 1995 and the environmental parameter data respectively. The periodicity of the RAGENA simulation results is due to the fact that the time-dependent parameters are modelled as a function of meteorological parameters. In the soil comparison, a very high peak is obtained with the RAGENA model. This peak is clearly a consequence of the extreme hard rain it happened on September, 19 (50 liters per m² in one hour), showing that the simple rainfall - water saturation fraction model we have developed overestimates the effect of a hard rain and therefore, it must be reviewed. For the rest of the period, it exists an agreement between the modelled dynamics and the measured dynamics of probe L1, while the L2 probe presents another dynamic behaviour. In this period, the comparison of basement radon dynamics shows that the modelled radon concentration follows the experimental dynamics in all the period excepting two sudden falls probably due to the opening of the window, and two peaks at the beginning and the end of the period.

We conclude that the model-experiment comparison has led to satisfactory results, showing that the RAGENA model is appropriate to describe the dynamics of the soil and indoor radon concentration and to characterise the radon entry processes into the test house basement room.

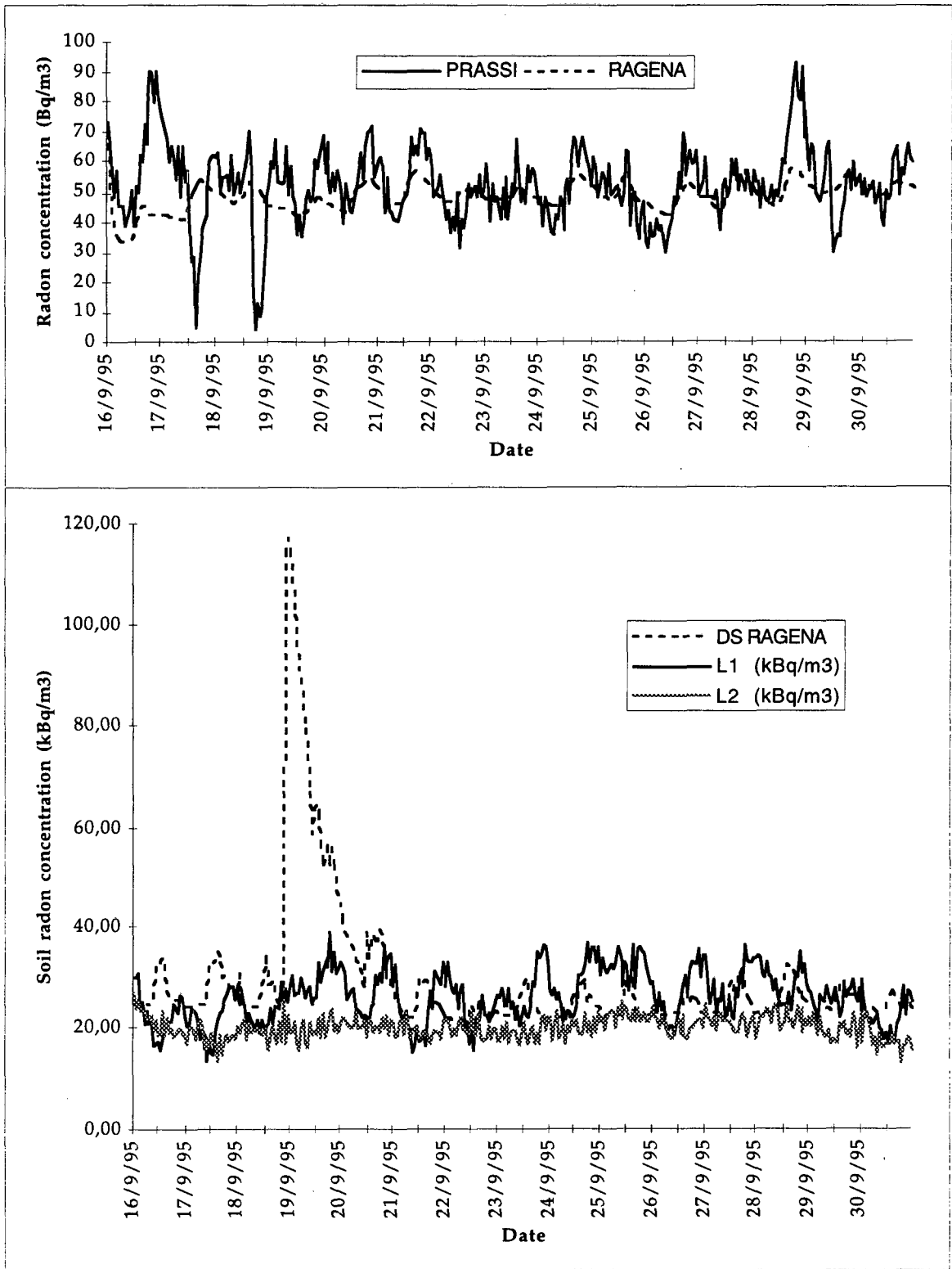


Fig. 7.4: Model-experiment comparison of basement and soil radon concentration corresponding to the second half of September 1995.

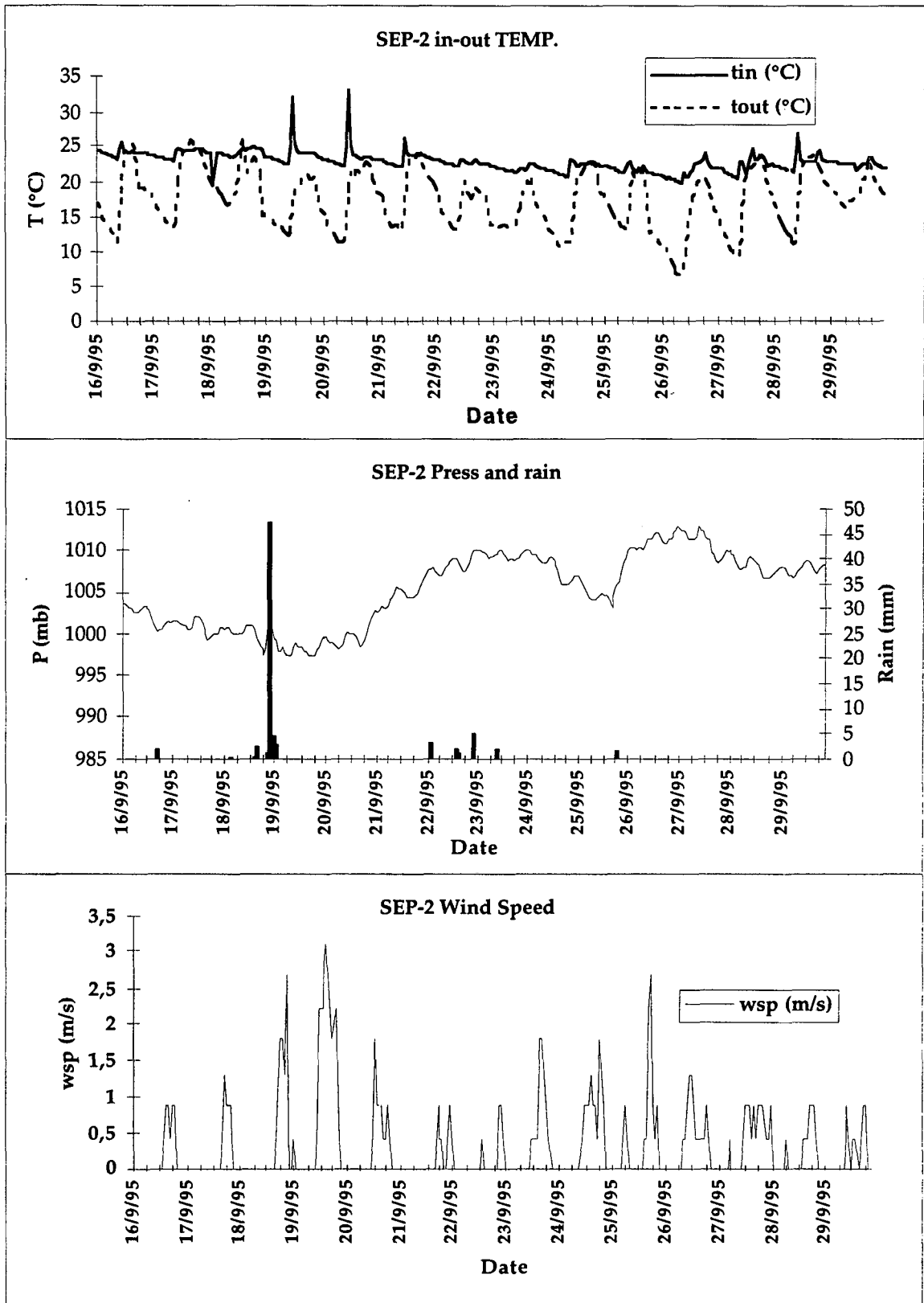


Fig. 7.5: Meteorological parameter dynamics corresponding to the second half of September 1995.

8

Conclusions

8.1 Results obtained

1- The review of the most relevant parameters and processes affecting indoor radon concentration has shown that the behaviour of soil and indoor radon concentration depends on a lot of parameters and that the values of these parameters found in the literature can span a very wide range. Therefore, it is necessary to characterise the source, the interface source-indoor and the indoor media considering simultaneously all the relevant parameters, especially those driving the dynamics.

2- A global, sectorial and dynamic model of radon generation in the source, entry into, and accumulation in a multi-zone house (RAGENA) has been designed, developed and set up. The main characteristics of the RAGENA model are:

- 2a) It has been built with the STELLA II software and solves a set of first-order coupled differential equations by the 4th order Runge-Kutta numerical method.
- 2b) All the radon sources and processes affecting indoor radon dynamics are taken into account.
- 2c) It can be easily adapted to a wide range of situations, without the need of a very detailed description of the site.
- 2d) It is adaptable to any time-scale.
- 2f) The input parameters can be either constant values, assumed probabilistic distributions, or time series data collected experimentally.
- 2g) It has not spatial resolution: rather than a complete description of the system, the model is more concerned with its dynamic behaviour.
- 2h) Its structure allows to incorporate a more detailed description of the system.

The RAGENA model has been applied to a reference configuration, corresponding to a generic single family house, under both static and dynamic conditions and the following conclusions have been found:

3- Under steady-state conditions the model gives reasonable outputs, characterising the radon generation, entry and accumulation processes in a multi-zone house.

A variability analysis around the reference configuration has shown that:

- 4- The model can be applied to a very wide range of situations without mathematical problems.
- 5- The impact of each parameter on indoor radon concentration depends on the values of the rest of the parameters, and therefore, any statement about the relative importance of a given parameter must be understood as valid for the given situation.
- 6- In the generic reference configuration, the impact of each input parameter has been quantified by the Variability Index. The most relevant parameters found are: the mean soil grain diameter, due to its influence on the soil permeability, the ventilation rate of the rooms, the air-exchange rate between the basement and the room 2, the soil-indoor pressure difference, the open area and the concrete radium content.
- 7- The highest entry rates are achieved when the soil gas-permeability is high ($> 10^{-10} \text{ m}^2$), showing that advection is the dominant mechanism in this situation.
- 8- The maximum entry rate into a structure from the soil is achieved for an intermediate value of the soil water saturation fraction. The value of water saturation fraction corresponding to the maximum radon entry rate increases with the mean grain diameter.
- 9- The relative importance of diffusive and advective radon entry rate from soil depends on both the soil type and the water saturation fraction.
- 10- An increase of the ventilation rate when it is low ($< 1\text{h}^{-1}$) has a large impact on indoor radon levels and can reduce them very much.
- 11- The increase of the air-exchange rates between the rooms redistributes the radon concentration in the house, tending to homogenise their radon levels.
- 12- The contribution of the brick walls as radon source has been found negligible. The contribution of the concrete walls increases with the height of the room level.
- 13- Indoor radon concentration is proportional to the Ra-226 content in of the soil and of the building materials.
- 14- The radon entry from soil is proportional to the open area.

15- The results obtained with the sensitivity analysis reflect a good behaviour of the model, in the sense that its predictions can be imputed to the physical system rather than to any mathematical problem, except in the case of great soil-indoor pressure difference variations, which produce too high soil radon concentration fluctuations.

16- The uncertainty of the model predictions can be obtained from any assumption of the input parameter distributions: assuming a normal distribution of all the input parameters with a relative standard deviation (RSD) of 10%, the model outputs present a RSD in the range [17-22] %.

17- Within the frame of an EU-project, an experimental study has been carried out in which, for the first time in Spain, a characterisation of a real inhabited and typical house from the radon point of view is presented.

18- The equipment necessary to monitor the weather parameters and the indoor and soil radon has been set up in the test house.

19- Calibration and intercomparison activities have been performed to check the quality of the measurements, and the main conclusions are:

19a) The previous value of the indoor radon passive detectors has been confirmed and an agreement with the indoor radon PRASSI monitor has been found.

19b) The passive soil radon dosimeters based on LR-115 detector present higher soil radon concentration values than the Clipperton II probes when exposed to the same conditions. The analysis of the experimental field results indicates that the Clipperton II results are more reasonable.

19c) No effect of using a latex membrane or a plastic bag to protect the Clipperton probes against humidity has been found.

19d) The uncertainties associated to the radon concentration measurements performed with Makrofol, LR-115 and Clipperton II probes are, respectively, 10%, 22% and 15%.

20- The characterisation of indoor and soil radon concentration dynamics is very complicated, specially in an experimental site where most of the parameters can not be controlled: no simple correlation between meteorological parameters and radon dynamics has been found.

21- The radon concentration value obtained indoors is in agreement with previous studies in both the test house and the region.

22- No effect of the use of water and natural gas supplies has been observed in the test house.

23- The influence of the ventilation on indoor radon levels has been observed by finding higher radon levels in the rooms less ventilated.

24- In general, no seasonal effects have been observed in soil radon levels.

25- The basement of the test house is permanently underpressured with respect to the soil, presenting the soil-indoor pressure difference daily fluctuations within the range [0.0 - 3.5] Pa and around the mean value 2.1 Pa.

The RAGENA model has been adapted to the basement room of the test house by incorporating the experimental data available and the main findings are:

26- The variations of the soil-indoor pressure difference are driven by the indoor-outdoor temperature difference and the wind speed. No transient soil-indoor pressure differences due to the barometric pressure changes have been found.

27- The main findings obtained with the model under steady-state conditions are:

27a) The basement radon concentration predicted by the model is in excellent agreement with the experimental results.

27b) The annual averaged soil radon concentration obtained with the Clipperton II probes is 35% lower than the prediction of the RAGENA model.

27c) The soil is the main source of radon entry into the basement, accounting for 67% of the total radon entry, being advection, with 43%, the dominant mechanism.

27d) The contribution of the radon exhalation from concrete is of the same order than the contribution of the diffusion from the soil (around 25%).

27e) The less relevant radon source are the brick walls, which account for 7% of the total radon entry into the basement.

28- The dynamic behaviour predicted with the model in both the soil and the basement presents the same 24 hour periodicity as observed experimentally. However, the model predicts, in general, radon concentration fluctuations smoother than observed.

29- It has been found that in the case of a hard rainfall event, the RAGENA model overestimates its effect on soil radon concentration.

30- The dynamics of the basement radon concentration predicted with the RAGENA model describes the experimental behaviour obtained in a three months period when the basement window and door were almost kept closed.

Consequently, the main conclusion of the adaptation of the model to the experimental site is that

31- The RAGENA model has been appropriate to characterise the radon generation, entry and accumulation in the basement of the test house and to describe its dynamics.

8.2 Perspectives for future work

In this PhD dissertation a new concept of global radon model has been presented, and therefore, a new research line has been opened. The main perspectives for future work are:

i) To improve the model, trying to solve the problems detected: the high sensitivity of soil radon concentration to soil-indoor pressure difference and to hard rainfall.

ii) In order to validate the model, a test structure in which all the parameters are controlled and measured can be designed and set up.

iii) To apply the model to the rest of the test houses of the EU project in order to describe the main differences as a function of the climate, the house construction, the geology of the site, and the inhabitants habits.

iv) To perform additional simulations trying to reproduce situations likely to be found in the Nature with the aim to find out the best remedial actions to reduce radon levels.

v) The sectorial structure of the model allows to add in the future new sectors describing any missing aspect like, for instance: the air circulation inside a multi-zone house as a function of the meteorological parameters, inhabitants habits, and the design of the Heating, Ventilation and Air-Conditioning systems, or the dynamics of short-lived radon daughters.

References

- Andersen, C.E. Entry of soil gas and radon into houses. PhD dissertation. ISBN-87-550-1804-1 Risø National Laboratory, Roskilde, Denmark. 1992
- Arvela, H.; Voutilainen, A.; Mäkeläinen, I.; Castren, O. and Winqvist, K. Comparison of predicted and measured variations of indoor radon concentration. *Radiat. Prot. Dosim.* 24:231-235; 1988.
- Baixeras, C.; Garcia, I.; Fernández, F.; Domingo, C.; Vidal-Quadras, A. and Piesch, E. Indoor radon concentration measurements in some Spanish houses and dwellings with plastic nuclear track etch detectors. *Nucl. Tracks Radiat. Meas.* 19:279-282; 1991.
- Baixeras, C.; Font, Ll.; Sánchez-Cabeza, J. A.; Pujol, Ll.; Fernández, F. and Domingo, C. A comparative study of different methods for measuring radon concentration. *Env. Geochem. Health*, 16:489-497; 1995.
- Baixeras, C.; Bacmeister, G. U.; Climent, H.; Albarracín, D.; Enge, W.; Freyer, K.; Treutler, H.-C.; Jónsson, G.; Ghose, R.; Monnin, M. M.; Font, L.; Devantier, R.; Seidel, J.-L. and Schiocchetti, G. Report on the first phase activity of an EU-project concerning coordinated radon measurements in five european countries. *Environment International*, 22:S687-S697; 1996a.
- Baixeras, C.; Climent, H.; Font, Ll.; Bacmeister, G. U.; Albarracín, D. and Monnin, M. M. Using passive detectors in soil and indoors in two Mediterranean locations for radon concentration measurements. Accepted for publication in *Radiat. Measurements*; 1996b.
- Baixeras, C.; Font, Ll.; Robles, B. and Gutiérrez, J. Indoor radon survey in the most populated areas in Spain. *Environment International*, 22:S671-S676; 1996c.
- Baixeras, C.; Font, Ll.; Fernández, F. and Domingo, C. Indoor radon levels in a public school and some dwellings from the village of Teià, Catalonia (Spain). *Proceedings of the 1996 International Congress on Radiation Protection*. Vienna, Austria, April 14-19; 1996d.
- Bonnefous, Y. C.; Gadgil, A. J.; Fisk, W. J.; Prill, R. J. and Nematollahi, A. R. Field study and numerical simulation of subslab ventilation systems. *Environ. Sci. Technol.* 26:1752-1759; 1992.
- Bonnefous, Y. C.; Gadgil, A. J. and Fisk, W. J. Impact of subslab ventilation technique on residential ventilation rate and energy costs. *Energy and buildings*, 21:15-22; 1994.
- Bonnefous, Y. C.; Richon, P.; Tarlay, V.; Arnautou, J.-C.; Sabroux, J.-C. and Goutelard, F. Subslab ventilation system: installation and follow up in a high radon house in Brittany, France. *Environment International*, 22:S1069-S1072; 1996.
- Capra, D.; Silibello, C. and Queirazza, G. Influence of ventilation rate on indoor radon concentration in a test chamber. *Radiat. Prot. Dosim.* 56: 15-18; 1994.
- Cavallo, A.; Gadsby, K.; Reddy, T. A. and Socolow, R. The effect of natural ventilation on radon and radon progeny levels in houses. *Radiat. Prot. Dosim.* 45:569-574; 1992.
- Cavallo, A.; Gadsby, K. and Reddy, T. A. The use of computed radon entry rates to understand radon concentration in buildings. *Health Phys.* 66:178-184; 1994.

- Chen, C.-J; Weng, P.-S. and Chu, T.-C. Radon exhalation rate from various building materials. *Health Phys.* 64:613-619; 1993.
- Chen, C. and Thomas, D. M. Modeling of radon transport in unsaturated soil. *J. Geophys. Res.*, 100:15517-15525, 1995.
- Cliff, K. D.; Naismith, S. P.; Scivier, C. and Stephen, R. The efficacy and durability of radon remedial measures. *Radiat. Prot. Dosim.* 56:65-69; 1994.
- Climent, H. Transport du radon à l'interface soil-air: étude de l'influence des paramètres externes. PhD dissertation. Report 96 mon2 167. Université Montpellier II; 1996.
- Cripps, A. Time-dependent modelling of soil-gas flow rates. *Environment International*, 22:S499-S507; 1996.
- Currie, L. Limits for qualitative detection and quantitative determination. *Analytic chemistry*, 40:586-592; 1968.
- De Meijer, R. J.; Stoop, P. and Put, L.W. Contribution of radon flows and radon sources to the radon concentration in a dwelling. *Radiat. Prot. Dosim.* 45: 439-442; 1992.
- Ennemoser, O.; Oberdorfer, E.; Brunner, P.; Schneider, P. ; Purtscheller, F.; Stingl, V. and Ambach, W. Mitigation of indoor radon in an area with unusually high radon concentrations. *Health Phys.* 69:227-232; 1995.
- Fisk, W. J.; Prill, R. J.; Wooley, J.; Bonnefous, Y. C.; Gadgil, A. J. and Riley, W. J. New methods of energy efficient radon mitigation. *Health Phys.* 68:689-698; 1995.
- Font, Ll. Determinació de la concentració de radó en l'interior d'edificis amb detectors plàstics de traces. Master thesis. Universitat Autònoma de Barcelona; 1993.
- Garbesi, K. Toward resolving model-measurement discrepancies of radon entry into houses. Lawrence Berkeley Laboratory, Berkeley, CA, USA, report LBL-34244. PhD. Dissertation; 1993.
- Gadd, M. S. and Borak, T. B. Partitioning of Rn-222 entry into a structure surrounded by soil. *Health Phys.* 67:53-59; 1994.
- Gadd, M. S. and Borak, T. B. In situ determination of the diffusion coefficient of Rn-222 in concrete. *Health Phys.* 68:817-822.
- Gadgil, A. J. Models of Radon Entry. *Radiat. Prot. Dosim.* 45:373-380; 1992.
- Geneviève, 1994.
- Ghose, R. Instructions to set up the effa SK1T12 differential pressure transmitter. EU project ERB-CHRX-CT 930422 internal report; 1996.
- Gutiérrez, J.; Baixeras, C.; Robles, B.; Saez, J. C. and Font, Ll. Indoor radon levels and dose estimation in two major Spanish cities. *Radiat. Prot. Dosim.* 45:495-498; 1992.
- Hannon B. and Ruth, M. Dynamic modelling. Springer-Verlag New York, Inc. 1994 ISBN 0-387-94309-3 (New York).
- Henschel, D. B. Analysis of radon mitigation techniques used in existing US houses. *Radiat. Prot. Dosim.* 56:21-27; 1994.

- HPS (High Performance Systems, Inc.). Stella II technical documentation. HPS 1994. Hanover NH 03755.
- Hintenlang, D. E. and Al-Ahmady, K. K. Pressure differentials for radon entry coupled to periodic atmospheric pressure variations. *Indoor air*, 2:208-215; 1992.
- Hintenlang, D. E. and Al-Ahmady, K. K. Influence of ventilation strategies on indoor radon concentrations based on a semiempirical model for Florida-style houses. *Health Phys.* 64:427-432; 1994.
- Holkko, J. and Liukkonen, S. Radon diffusion in model tests on Finnish esker and till soils. *Health Phys.* 64:132-140; 1993.
- Holub, R. F. and Killoran, L. K. Is diffusion or forced flow the main mechanism of radon infiltration into underground openings? A theoretical study. *Radiat. Prot. Dosim.* 56:161-165; 1994.
- Hubbard, L. M.; Hagberg, N. and Enflo, A. Temperature effect on radon dynamics in two Swedish dwellings. *Radiat. Prot. Dosim.* 45:381-386; 1992.
- IAEA (International Atomic Energy Agency). Measurement and calculation of radon releases from uranium mill tailings. Technical reports series 333. IAEA, Vienna; 1992.
- Jönsson, G.; Baixeras, C.; Enge, W.; Freyer, K.; Treutler, H.-C.; Monnin, M. M. and Sciocchetti, G. Criteria for indoor radon concentration - an experimental study considering especially the Leipzig-Halle brown coal area. *Radiat. Measurements*, 25:627-630; 1995.
- Jönsson, G.; Albarracín, D.; Bacmeister, G. U.; Baixeras, C.; Climent, H.; Devantier, R.; Enge, W.; Freyer, K.; Font, Ll.; Ghose, R.; Monnin, M. M.; Sciocchetti, G.; Seidel, J.-L. and Treutler, H.-C. Comparison of radon measurements done by solid state nuclear track detectors and electronic devices in the frame of an EU-radon project. Accepted for publication in *Radiat. Measurements*; 1996.
- Loureiro, C. O. Simulation of the steady-state transport of radon from soil into houses with basements under constant negative pressure. Lawrence Berkeley Laboratory, Berkeley, CA, USA, LBL-24378. PhD. Dissertation, 1987.
- Markkanen, M. and Arvela, H. Radon emanation from soils. *Radiat. Prot. Dosim.* 45:269-272; 1992.
- Mas-Plà, J. and Linares, R. Característiques geològiques i hidrogeològiques dels materials no-saturats de la zona experimental de Cerdanyola del Vallès. Internal report. Universitat Autònoma de Barcelona; 1997.
- Miles, J.C.H.; Algar, R.A.; Howarth, C.B.; Hubbard, L.M.; Risica, S.; Kies, A. and Poffijn, A. Results of the 1995 European Commission intercomparison of passive radon detectors. Report EUR 16949. ISBN 92-827-7892-4; 1996.
- Morin, J. P.; Seidel, J.-L. and Monnin, M. M. A tridimensional model for radon transport in a porous medium. *Nucl. Tracks Radiat. Meas.* 22:415-418; 1993.
- Morris, R. C. and Fraley, L. Jr. Soil permeability as a function of vegetation type and soil water content. *Health Phys.* 66:691-698, 1994.
- Nazaroff, W. W.; Nero, A. V., eds. Radon and its decay products in indoor air. New York: John Wiley and sons; ISBN 0-471-62810-7, 1988.

- Nazaroff, W. W.; Moed, B. A. and Sextro, R. G. Soil as a source of indoor radon: Generation, migration and entry. In: Nazaroff, W. W.; Nero, A. V., eds. Radon and its decay products in indoor air. New York: John Wiley & sons; 1988: 57-112.
- Nero, A. V. Radon and its decay products in indoor air: an overview. In: Nazaroff, W. W.; Nero, A. V., eds. Radon and its decay products in indoor air. New York: John Wiley & sons; 1988: 1-53.
- Nielson, K. K.; Rogers, V. C. and Holt, R. B. The RAETRAD model of radon generation and transport from soils into slab-on-grade houses. *Health Phys.* 67:363-377; 1994.
- Novell, M. and Font, Ll. Estudio del impacto radiológico ambiental producido por las emisiones naturales de radón en recintos cerrados. Internal report. 1997.
- Ortega, X.; Novell, M.; Vargas, A.; Baixeras, C. and Font, Ll. Study of the variation of ^{222}Rn indoor concentration with several passive detectors and an active detection system. *Environment International*, 22:S601-S606; 1996.
- Peter, J. E.; Haider, B. and Ferron, G. A. Stabilisation characteristics of ventilation in buildings. *Radiat. Prot. Dosim.* 56: 193-196; 1994.
- Porstendörfer, J.; Butterweck, G. and Reineking, A. Daily variation of the radon concentration indoor and outdoors and the influence of meteorological parameters. *Health Phys.* 67: 283-287; 1994.
- Renken, K. J. and Rosenberg, T. Laboratory measurements of the transport of radon through concrete samples. *Health Phys.* 68: 800-808; 1995.
- Revzan, K. L.; Fisk, W. J. and Sextro, R. G. Modeling radon entry into Florida slab-on-grade houses. *Health Phys.* 65:375-385; 1993.
- Robinson, A. L. and Sextro, R. G. The influence of a subslab gravel layer and open area on soil-gas and radon entry into two experimental basements. *Health Phys.* 69: 367-377; 1995.
- Ródenas, C. Estudio de las fuentes de radiación natural en España. Estimación de dosis a la población. PhD dissertation. Universidad de Cantabria; 1995).
- Roelofs, L. M. M. and Scholten, L. C. The effect of aging, humidity, and fly-ash additive on the radon exhalation from concrete. *Health Phys.* 67:266-271; 1994.
- Rogers, V. C. and Nielson, K. K. Multiphase radon generation and transport in porous materials. *Health Phys.* 61:225-230; 1991.
- Rogers, V. C. and Nielson, K. K. Data and models for radon transport through concrete. Proceedings of the 1992 International Symposium on Radon and Radon Reduction Technology. Vol. 1. Washington DC: U.S. EPA; EPA-600/R-93-083a; 1993:6-41.
- Rogers, V. C.; Nielson, K. K.; Holt, R. B. and Snoddy, R. Radon diffusion coefficient for residential concretes. *Health Phys.* 67:261-265; 1994.
- Rogers, V. C., Nielson, K. K. and Holt, R. B. Radon diffusion coefficients for aged residential concretes. *Health Phys.* 68:832-834; 1995.
- Rutherford, P. M.; Dudas, M. J. and Arocena, J. M. Radon emanation coefficients for phosphogypsum. *Health Phys.* 69: 513-520; 1995.

- Schell, W. R.; Linkow, I.; Myttenaere, C. and Morel, B. A dynamic model for evaluating radionuclide distribution in forests from nuclear accidents. *Health Phys.* 70:318-335; 1996.
- Schery, S. D., Gaeddert, D. H. and Wilkening, M. H. Factors affecting exhalation of radon from a gravelly sandy loam. *J. Geophys. Res.* 89:7299-7309; 1984.
- Scott, A. G. Preventing radon entry. In: Nazaroff, W. W.; Nero, A. V., eds. *Radon and its decay products in indoor air*. New York: John Wiley; 1988:407-433.
- Scott, A. G. Radon sources, radon ingress and models. *Radiat. Prot. Dosim.* 56: 145-149; 1994.
- Stoop, P.; Aldenkamp, F. J.; Loos, E. J. T.; de Meijer, R. J. and Put, L. W. Measurements and modeling of radon infiltration into a dwelling. In: *Proceedings of the 1992 International Symposium on Radon and Radon Reduction Technology*. Philadelphia: U.S. EPA; 1993.
- Stranden, E.; Kolstad, A. K. and Lind, B. The influence of moisture and temperature on radon exhalation. *Radiat. Prot. Dosim.* 7:55-58; 1984.
- Stranden, E. Building materials as a source of indoor radon. In: Nazaroff, W. W.; Nero, A. V., eds. *Radon and its decay products in indoor air*. New York: John Wiley; 1988:113-130.
- Strong, K. P. and Levins, D. M. Effect of moisture content on radon emanation from uranium ore and tailings. *Health Phys.* 42:27; 1982.
- Sun, H. Monte Carlo simulation of radon emanation from dry building materials. *Health Phys.* 68:553-560; 1995.
- Tanner, A. B. The role of diffusion in radon entry into houses. In *Proc. 1990 Int. Symp. on Radon and Radon Reduction Technology*. Vol. III (Research Triangle Park: US Environmental Protection Agency) EPA/600/9-90/005c, 1991.
- Treutler, H.C. and Freyer, K. Measurement of radionuclides in soil samples from surroundings of the test house in Barcelona by gamma spectrometry. EU project ERB-CHRX-CT 930422 internal report; 1995.
- Tso, M. W., Chor-yi Ng and Leung, J. K. Radon release from building materials in Hong Kong. *Health Phys.* 67:378-384; 1994.
- Tsang, Y. W. and Narashiman, T. N. Effects of periodic atmospheric pressure variation on radon entry into buildings. *J. Geophys. Res.* 97:9161-9170; 1992.
- Turk, B. H.; Grumm, D.; Li, X. and Schery, S. D. Soil gas and radon entry potentials for slab-on-grade houses. In: *Proceedings of the 1991 International Symposium on Radon and Radon Reduction Technology*. Vol. 3: V-5 Philadelphia: U.S. EPA; 1992.
- UNSCEAR (United Nations Scientific Committee on the Effects of Atomic Radiation). *Sources, effects and risks of ionizing radiation*; 1993. UNSCEAR, New York, NY.
- Vand der Graaf, E. R., Witteman, G. A. A., van der Spoel, W. H., Andersen, C. E. and de Meijer, R. J. Measurements on, and modelling of diffusive and advective radon transport in soil. *Radiat. Prot. Dosim.* 56:167-170, 1994.
- Ward, D. C.; Borak, T. B. and Gadd, M. S. Characterization of Rn entry into a basement structure surrounded by low-permeability soil. *Health Phys.* 65:1-11; 1993.
- Washington, J. W. and Rose, A. W. Temporal variability of radon concentration in the interstitial gas of soils in Pennsylvania. *J. Geophys. Res.* 97:9145-9159; 1992.

Whysall, K.; Miles, J.C.H., and Olast, M. Results of the 1991 CEC Intercomparison of Passive Radon Detectors. Commission of the European Communities/DG XII Report, Brussels, Belgium (in press); 1996.

Yu, K.N. The effects of typical covering materials on radon exhalation rate from concrete surfaces. Radiat. Prot. dosim. 48: 367-370; 1993.

List of Figures and Tables

Figures

- Fig. 2.1:** Typical soil permeability values (m^2). 9
- Fig. 2.2:** Soil gas entry routes into a house. 19
- Fig. 2.3:** Radon concentration profile in a concrete sample that has the parameter values given in table 2.5. C_l and C_r are the value of the radon concentration at the left and right side of the material respectively. Horizontal arrows represent the exhalation rate at the surface in the cases i) $C_r=C_l=0$, ii) $C_r=200$, $C_l=30000$ and iii) $C_r=500$, $C_l=100000$ The concentrations are expressed in $\text{Bq}\cdot\text{m}^{-3}$ 24
- Fig. 3.1:** Global structure of the RAGENA dynamic model of radon generation, entry, and accumulation indoors. 38
- Fig. 3.2:** Separation of the soil underneath the house into the disturbed and the undisturbed soils. M_d is the radon migration distance, defined in equation 2.17. 39
- Fig. 3.3:** Dependence of gas-permeability, effective diffusion constant and relative emanation fraction on the water saturation fraction for clay, silt and sand, where the values of porosity and mean grain diameter are, respectively, 0.6 and 10^{-6} for clay, 0.5 and 10^{-5} for silt, and 0.4 and 10^{-4} for sand. 42
- Fig. 3.4:** Radon migration distance in the soil as a function of the gas-permeability for pressure gradients of 10, 17, 33 and 100 Pa m^{-1} . Soil effective diffusion constant, porosity and dynamic viscosity have been taken respectively, as $10^{-6} \text{ m}^2\text{s}^{-1}$, 0.5, and $18 \times 10^{-6} \text{ Pa}\cdot\text{s}$. The radon concentration in the deep soil and in the basement are respectively 30000 and $200 \text{ Bq}\cdot\text{m}^{-3}$. 45
- Fig. 4.1:** Diagram of the reference configuration house. 56
- Fig 4.2:** Patterns of one week dynamics of soil-basement and soil-room 1 pressure differential, ventilation rates of rooms 1 and 2, and rooms 3 and 4, inter-zone air exchange rates between basement and room 2 and between rooms 2 and 3, inter-zone air exchange rates between rooms 1 and between rooms 3 and 4, soil water saturation fraction, and water use rate. 60
- Fig. 4.3:** Variation of soil emanation fraction, fraction of emanated radon atoms that reach the gas-filled volume, soil effective diffusion constant and soil permeability, during the one-week simulation period. 61

Fig. 4.4a: Evolution of basement and rooms, radon concentration obtained for the reference configuration under steady conditions.	62
Fig. 4.4b: Evolution of disturbed soil and undisturbed soil radon concentrations obtained for the reference configuration under steady conditions.	62
Fig. 4.5a: The influence of initial soil radon concentration on basement radon concentration.	66
Fig. 4.5b: The influence of initial concrete radon concentration on basement radon concentration.	66
Fig. 4.6: Basement radon concentration as a function of soil radon concentration when soil-type and water saturation fraction are kept constant. The Radon Entry Efficiency (REE) is the slope (in percentage) of the line.	70
Fig. 4.7: Diffusive and advective radon entry from soil into the basement as a function of the water saturation fraction, where clay, silt and sand correspond to those given in Fig. 3.3.	71
Fig. 4.8: Soil radon concentration as a function of the water saturation fraction, where clay, silt and sand correspond to those given in Fig. 3.3.	72
Fig. 4.9: Basement radon concentration as a function of the water saturation fraction, where clay, silt and sand correspond to those given in Fig. 3.3.	72
Fig. 4.10: Basement radon concentration as a function of soil gas-permeability.	73
Fig. 4.11: Indoor radon concentrations as a function of the concrete radon concentration.	74
Fig. 4.12: Influence of the ventilation rate of rooms 1 and 2 on the radon concentration in the basement and in rooms 1 and 2.	76
Fig. 4.13: Response of the indoor radon concentrations to a sudden change of the soil water saturation fraction.	77
Fig. 4.14: Response of the indoor radon concentrations to a pulse pattern of rooms 1 and 2 ventilation rates: beginning at the instant $t=100$ h, a sudden raise and descend of ventilation rate from 1 to 9 (1/h) happens every 24 hours.	79
Fig. 4.15: Response of the indoor radon concentrations to a pulse pattern of the air-exchange rate between the basement and the room 2: beginning at the instant $t=100$ h, a sudden raise and descend of the air-exchange rate from 0.2 to 8.2 (1/h) occurs every 24 hours.	81
Fig. 4.16: Response of the indoor radon concentrations to a sinwave pattern of the soil-indoor pressure difference, with an amplitude of 2 Pa and a period of 24 hours, which has been added to a constant baseline of 2 Pa.	82

Fig. 4.17: Response of the indoor radon concentrations to a sinwave pattern of the soil-indoor pressure difference, with an amplitude of 2 Pa and a period of 12 hours, which has been added to a constant baseline of 2 Pa.	84
Fig. 4.18: One-week dynamics of the basement radon concentration when the soil-basement pressure difference, ventilation rates, inter-zone air-exchange rates, water saturation fraction of the soil, and water use rate follow the patterns given in Fig. 4.3	86
Fig. 4.19: One-week dynamics of rooms 1 and 2 radon concentration when the soil-basement pressure difference, ventilation rates, inter-zone air-exchange rates, water saturation fraction of the soil, and water use rate follow the patterns given in Fig. 4.3.	87
Fig. 4.20: One-week dynamics of rooms 3 and 4 radon concentration when the soil-basement pressure difference, ventilation rates, inter-zone air-exchange rates, water saturation fraction of the soil, and water use rate follow the patterns given in Fig. 4.3.	87
Fig. 5.1: Distribution of soil radon detectors in the test house garden (top view). The rooms of the test house are those placed at the basement level.	93
Fig. 5.2: Distribution of the different equipment installed in the test house for the experimental study.	94
Fig. 5.3: Diagram of the LR-115 soil radon dosimeter.	95
Fig. 5.4: Exposure of the LR-115 soil radon dosimeter .	96
Fig. 5.5: Diagram of the semiautomatic counting system. The Microscope is used for track counting the LR-115 foils, while the Photo Videocamera is used for the Makrofol foils.	97
Fig. 5.6: Exposure of the Clipperton II probe to measure soil radon.	98
Fig. 5.7: The portable radon monitor PRASSI.	101
Fig. 5.8: The indoor radon dosimeter (based on Makrofol ED) and its components.	100
Fig. 5.9: Installation of the pressure transducer in the test house to measure continuously the pressure difference between the lateral soil and the basement room.	102
Fig. 5.10: The portable RADON-JOK instrument used to measure the soil-gas permeability of the test house garden soil.	103
Fig 5.11: Diagram of the experimental arrangement set up to intercompare passive (LR-115) and active (clipperton) soil radon dosimeters when exposed at the same conditions.	106

Fig. 5.12: Comparison of LR-115 and clipperton II soil radon detectors exposed in the same hole at the UAB campus.	108
Fig. 5.13: Comparison of 5 bare clipperton probes exposed in the same hole at the UAB campus.	109
Fig. 5.14: Comparison of 3 clipperton probes exposed in the same hole at the UAB campus. Code L1B was bare, without protection; code L3P had a polythene bag, and code L4C had a latex membrane incorporated.	109
Fig. 5.15: Stability test of the pressure differential sensor. The mean bits measured correspond to a 0 Pa pressure difference.	110
Fig. 6.1: Monthly averaged soil radon concentration obtained in the L3 measurement point with the LR-115 dosimeter.	114
Fig. 6.2: Monthly averaged soil radon concentration obtained in the B2 measurement point with the LR-115 dosimeter.	114
Fig. 6.3: Monthly averaged soil radon concentration obtained in the F3 measurement point with the LR-115 dosimeter.	115
Fig. 6.4: Typical pattern of basement room radon fluctuations measured with the PRASSI portable radon monitor.	117
Fig. 6.5: Monthly-averaged radon concentration obtained in the basement with the PRASSI monitor. In January 1996 we had to stop the measurements not to disturb the inhabitants of the test house.	117
Fig. 6.6: Monthly averaged soil radon concentration obtained in the set L clipperton probes. Both probes present maxima and minima at the same instants.	119
Fig. 6.7: Monthly averaged soil radon concentration obtained in the set F clipperton probes. A similar time-behaviour is obtained from November-95.	119
Fig. 6.8: Monthly averaged soil radon concentration obtained with Clipperton probe B1. the presence of the minimum is interpreted as a consequence of the escape of the soil radon gas through the opening nearby.	120
Fig. 6.9: Monthly-averaged indoor and outdoor temperature difference obtained with the weather station.	121
Fig. 6.10: Monthly-averaged atmospheric pressure measured with the weather station.	121
Fig. 6.11: Monthly-averaged wind speed measured with the weather station.	121
Fig. 6.12: Total rain per month measured with the weather station.	122
Fig. 6.13: One-month soil-indoor pressure difference dynamics measured in the test house. A positive value means indoors underpressured with respect to the soil.	122

Fig. 6.14: Distribution of the gas-permeability measurement points at the test house garden.	124
Fig. 7.1: Comparison between measured and modelled soil-indoor pressure difference.	130
Fig. 7.2: Ventilation rate modelled in the first 15-day period of August 1995.	131
Fig. 7.3: Water saturation fraction modelled and rainfall measured for the first 15-day period of August 1995.	131
Fig. 7.4: Model-experiment comparison of basement and soil radon concentration corresponding to the second half of September 1995.	135
Fig. 7.5: Meteorological parameter dynamics corresponding to the second half of September 1995.	136

Tables

Table 2.1: Radon solubility in water as function of temperature.	6
Table 2.2: Parameters related with radon generation and migration in soil.	13
Table 2.3: Literature review of soil radon generation and migration parameters data.	13-15
Table 2.4: Building material data from literature.	16-18
Table 2.5: Radon exhalation rate from concrete for different boundary conditions	24
Table 2.6: Radon entry data from literature. The entry flow from building materials correspond to the so-called exhalation rate.	26-28
Table 4.1: Building design parameters.	56
Table 4.2: Building materials' parameters.	57
Table 4.3 Building material surface values for the reference configuration. All walls made from brick have the same surface (S_{br}).	57
Table 4.4: Soil parameters.	57-58
Table 4.5: Mean value of steady-state entry parameters.	58
Table 4.6 The steady-state results of the model for the reference configuration .	63
Table 4.7: Contribution of each source to the radon concentration in each room.	64
Table 4.8: Radon concentration in soil and building materials for the reference configuration.	65
Table 4.9: The range of variation and the Variability Index in each room corresponding to each parameter around the reference configuration.	68
Table 4.10: Response time (RT), new steady-state values of radon concentration C (in $Bq \cdot m^{-3}$) and percentage of variation (PV) obtained with the step functions for each studied parameter in each room. The PV is calculated as $PV = (New\ value - old\ value) * 100 / old\ value$.	78

Table 4.11:	Mean radon concentrations (in Bq·m ⁻³) obtained with a constant 2 Pa indoor underpressurisation and with two sinwave pressure difference patterns , added to a constant baseline of 2 Pa. Notation: in the sinwave function, the first number in brackets is the amplitude (in Pa) and the second is the period (in hours).	83
Table 4.12:	Descriptive statistics of the indoor radon concentrations (in Bq·m ⁻³) obtained when all the input parameters are given by a normal distribution of 10% relative standard deviation around the reference configuration value.	85
Table 4.13:	Radon concentration values (in Bq·m ⁻³) averaged over the one-week dynamics compared with the steady-state results. The relative difference is defined as (averaged value - steady-state value)*100/steady-state value.	88
Table 5.1:	Distribution of the rooms in the three floor levels of the test house. The level 0 corresponds to the ground-floor.	92
Table 5.2:	Sensitivity, Minimum Detectable Concentration (MDC), and background track density obtained for the radon passive detectors.	105
Table 5.3:	PRASSI calibration parameters (from the calibration certificate).	105
Table 5.4	Comparison of mean radon concentration obtained in the basement room with the Makrofol (passive, time-integrating) and PRASSI (active, time-resolved) radon detectors.	106
Table 5.5:	Mean soil radon concentration obtained in three consecutive periods with the clipperton probe and 4 LR-115 dosimeters exposed in the UAB hole. The Relative Discrepancy (RD) is defined as the ratio between the radon concentration values obtained with LR-115 and Clipperton radon detectors.	107
Table 5.6:	Mean radon concentration, standard deviation (SD) and relative standard deviation (RSD) obtained with the 5 clipperton probes exposed at the same conditions without any protection.	108
Table 6.1.	Indoor radon data obtained with the Makrofol passive dosimeter,	113
Table 6.2:	Mean radon concentration values obtained in the test house with the PRASSI portable monitor.	116
Table 6.3:	Annual averaged soil radon concentrations measured with the Clipperton probes.	120
Table 6.5:	Gas-permeability results measured in the test house garden.	124
Table 6.6:	Specific Ra-226 activity measured in the test house soil samples.	125
Table 7.1:	Parameter values corresponding to the geometry of the room.	128
Table 7.2:	Parameter values corresponding to the soil garden of the test house.	129

Table 7.3: Steady-state results of the RAGENA model applied to the basement room of the test-house.

133

GLOSSARY OF THE PRINCIPAL SYMBOLS

Symbol	Name of the parameter	Units
A_{Ra}	Radium content of a solid medium	$\text{Bq}\cdot\text{kg}^{-1}$
β_p	Pressure coefficient	Dimensionless
$C_g, C_w, C_i, C_0, C_m, C_{av}$	Radon activity concentration in the soil-gas, water, at deep soil, at the interface soil-open air, in the building material, and the contribution of water use, respectively	$\text{Bq}\cdot\text{m}^{-3}$
$c_{US}, c_{DS}, c_i, c_{BM}, c_o, c_w, c_g$	Radon concentration in the undisturbed soil, disturbed soil, room i , building material, outdoors, water, and natural gas	$\text{atoms}\cdot\text{m}^{-3}$
D, D_e	Bulk and effective radon diffusion coefficient in a solid medium	$\text{m}^2\cdot\text{s}^{-1}$
D_0	Diffusion coefficient of radon in open air	$\text{m}^2\cdot\text{s}^{-1}$
DER	Diffusive entry rate from soil into the house	$\text{atoms}\cdot\text{s}^{-1}$
DEF	Diffusive entry flow from soil into the house	$\text{atoms}\cdot\text{s}^{-1}\cdot\text{m}^{-2}$
d	Mean soil grain diameter	m
D_p	"Diffusion coefficient" for pressure disturbances in soil	$\text{m}^2\cdot\text{s}^{-1}$
ΔP_f	Indoor-outdoor pressure difference across the lower part of a building	Pa
$\Delta P_{mv,u}$	Indoor-outdoor pressure difference generated by unbalanced mechanical ventilation	Pa
ΔP	Average indoor-outdoor pressure difference across the building shell	Pa
ΔP_{s-in}	Soil-indoor pressure difference	Pa
$\Delta P_{s-in,t}$	Transient soil-indoor pressure difference	Pa
Δt	Step size on RAGENA simulations	s
ϵ	Porosity of the medium	dimensionless
$\epsilon_\gamma, \epsilon_w$	Gas-porosity and water-porosity of the medium	dimensionless
E, E'	Emanation and effective emanation rates in the medium	$\text{atoms}\cdot\text{s}^{-1}$
f	Emanation coefficient in the medium	dimensionless
f_{max}	Maximum emanation coefficient in the medium	dimensionless
F	Fraction of radon atoms emanated into the pore volume that reach the gas volume	dimensionless
F_{io}, F_{ij}	Net radon atoms exchange rate between room i and outdoors, and between room i and j .	$\text{atoms}\cdot\text{s}^{-1}$

Symbol	Name of the parameter	Units
F_w, F_g	Radon atoms entry rate from water and from natural gas	atoms·s ⁻¹
Φ_d	Diffusive flow density of radon activity per unit pore area of soil	Bq·m ⁻² ·s ⁻¹
Φ_a	Advective flow density of radon activity per unit pore area of soil	Bq·m ⁻² ·s ⁻¹
G	Radon generation term in the medium	Bq·m ⁻³ ·s ⁻¹
G_{gr}	Total natural gas use-rate	m ³ ·s ⁻¹
g	Acceleration of gravity	m·s ⁻²
h	Forchheimer term	s·m ⁻¹
k	Gas-permeability of the soil	m ²
K_{US}	Undisturbed soil transfer coefficient	m ³ ·s ⁻¹
K_D	Diffusion transfer coefficient of the medium	m ³ ·s ⁻¹
K_A	Advection transfer coefficient of the medium	Pa ⁻¹ ·s ⁻¹ ·m ³
L	Coefficient of solubility of radon in water	Dimensionless
l_d	Diffusion length of the medium	m
l_a	Advection length of the medium	m
l_p	Distance that the pressure difference propagates in soil	m
λ_{Rn}	Radon decay constant	s ⁻¹
λ_v	Ventilation rate of the residence	s ⁻¹
$\lambda_{v,i}$	Infiltration component of the ventilation rate	s ⁻¹
$\lambda_{v,u}$	Unbalanced component of the ventilation rate	s ⁻¹
$\lambda_{v,m}$	Manual component of the ventilation rate	s ⁻¹
$\lambda_{v,me}$	Mecanical component of the ventilation rate	s ⁻¹
λ_{io}	Ventilation rate of room i	s ⁻¹
λ_{ij}	Air-exchange rate from room i to room j	s ⁻¹
μ	Dynamic viscosity of the gas-phase of soil pores	Pa·s
M_d	Radon migration distance in soil	m
m	Fraction of water saturation in soil	dimensionless
N	Number of radon atoms in the medium	atoms
P	Pressure field in the medium	Pa
q_{io}	Air current from room i to outdoors	m ³ ·s ⁻¹
q_{ij}	Air current from room i to room j	m ³ ·s ⁻¹
$\rho_{gr}, \rho_a, \rho_m,$		
ρ_w	Density of soil grains, air, building material, and water	kg·m ⁻³
ρ_{ws}	Density of the wet soil (bulk density)	kg·m ⁻³

Symbol	Name of the parameter	Units
R	Resistance of the medium to an advective flow	$\text{Pa}\cdot\text{s}\cdot\text{m}^{-3}$
S_{is}	Building surface in direct contact with soil	m^2
σ	Fraction of the open area	dimensionless
τ_{Rn}	Radon mean-life	s
t_w	Transfer efficiency of radon from water to indoor air	dimensionless
t	Transfer factor from radon in water to radon in air	dimensionless
t_g	Transfer efficiency of radon from gas to indoor air	dimensionless
T	Air temperature	K
u	Wind speed	$\text{m}\cdot\text{s}^{-1}$
v	Superficial velocity vector in the soil	$\text{m}\cdot\text{s}^{-1}$
V_r	Volume per resident of the dwelling	m^3
V	Volume of the medium	m^3
V_p, V_g, V_w	Pore, gas-filled, and water-filled volumes of the medium	m^3
$w_{1/2}$	Half-width of the medium	m
w	Width of the medium	m
W_r	Water use-rate per resident	$\text{m}^3\cdot\text{person}^{-1}\cdot\text{s}^{-1}$
W_{ur}	Total water use-rate	$\text{m}^3\cdot\text{s}^{-1}$
y_w	Wind parameter	dimensionless
y_s	Stack parameter	dimensionless

Annexes

ANNEX 1

Derivation of Eqs. (2.11), (2.12), (2.14), (2.15), (2.16) and (2.17)

The one-dimensional steady-state transport equation obtained from Eq. (2.9) is

$$\frac{d^2 C_g}{dx^2} - \frac{v}{\epsilon D_e} \frac{dC_g}{dx} - \frac{\lambda_{Rn}}{D_e} C_g = -\frac{G}{D_e} \quad (\text{A1.1})$$

where

$$v = -\frac{k}{\mu} \frac{dp}{dx} \quad (\text{A1.2})$$

Following, we consider different idealised situations:

i) Only diffusion

Eq. (A1.1) becomes

$$\frac{d^2 C_g}{dx^2} - \frac{\lambda_{Rn}}{D_e} C_g = -\frac{G}{D_e} \quad (\text{A1.3})$$

The general solution of this equation (C_g) can be expressed as the sum of the general solution of the reduced equation ($C_{g,r}$) and a particular solution of the general equation ($C_{g,p}$). The general solution of the reduced equation has the form

$$C_{g,r} = Ae^{m_1 x} + Be^{m_2 x} \quad (\text{A1.4})$$

if m_1 and m_2 are real single roots of the characteristic equation

$$m^2 - \frac{\lambda_{Rn}}{D_e} = 0 \quad (\text{A1.5})$$

Then, the general solution of the reduced equation is

$$C_{Rn,r} = A \exp\left\{\left(\frac{\lambda_{Rn}}{D_e}\right)^{1/2} x\right\} + B \exp\left\{-\left(\frac{\lambda_{Rn}}{D_e}\right)^{1/2} x\right\} \quad (\text{A1.6})$$

A particular solution of the general equation can be obtained easily trying a constant as a solution

$$C_{g,r} = C \quad (\text{A1.7})$$

Substituting Eq. A1.7 into Eq. A1.3 we obtain

$$C = \frac{G}{\lambda_{Rn}} \quad (\text{A1.8})$$

and the general solution of Eq. A1.3 is

$$C_g = A \exp\left\{\left(\frac{\lambda_{Rn}}{D_e}\right)^{1/2} x\right\} + B \exp\left\{-\left(\frac{\lambda_{Rn}}{D_e}\right)^{1/2} x\right\} + \frac{G}{\lambda_{Rn}} \quad (\text{A1.9})$$

To determine the value of constants A and B we need two boundary conditions. Assuming that at high depths the soil radon is in secular equilibrium with radium ($C_\infty = G/\lambda_{Rn}$) and that the atmospheric radon concentration is zero ($C_0 = 0$) we obtain $A = 0$ and $B = -G/\lambda_{Rn}$, so that the solution of the equation under these boundary conditions is

$$C_g = C_\infty \left(1 - \exp\left(-\frac{x}{l_d}\right)\right) \quad (\text{2.11})$$

where

$l_d = \left(\frac{D_e}{\lambda_{Rn}}\right)^{1/2}$ is the so-called diffusion length, defined as the depth at which radon concentration is reduced a factor $(1-e^{-1})$ with respect to the deep-soil radon concentration.

ii) Only advection

In this case Eq. (A1.1) becomes

$$\frac{dC_g}{dx} + \lambda_{Rn} \frac{\varepsilon}{v} C_g = \frac{\varepsilon}{v} G \quad (\text{A1.10})$$

In general, the Darcy's velocity (i.e., the pressure gradient and the permeability) change in depth and the general solution of this first-order differential equation can be obtained directly from expression (A1.11) in case of knowing the dependence of v on x , $v = v(x)$.

$$C_g = \left\{ A + \int dx \varepsilon G v(x)^{-1} \exp[\lambda_{Rn} \varepsilon \int v(x)^{-1} dx] \right\} \exp[-\lambda_{Rn} \varepsilon \int v(x)^{-1} dx] \quad (A1.11)$$

Assuming a constant Darcy's velocity, expression A1.11 becomes much simpler

$$C_g = A \exp\left(-\frac{\lambda_{Rn} \varepsilon}{v} x\right) + C_\infty \quad (A1.12)$$

Adopting again the boundary condition that the atmospheric radon concentration is zero, the constant A is determined and the solution of Eq. A1.11 becomes

$$C_g = C_\infty \left(1 - \exp\left(-\frac{\lambda_{Rn} \varepsilon}{v} x\right) \right) \quad (A1.13)$$

This expression is very similar to (2.11) and suggests the use of the term "advection length" in a similar way as the diffusion length, defined as

$$l_a = \frac{v}{\varepsilon} \frac{1}{\lambda_{Rn}} = \frac{v}{\varepsilon} \tau_{Rn} \quad (2.13)$$

where τ_{Rn} is the radon mean life. Then, expression (A1.13) can be re-written

$$C_g(x) = C_\infty \left(1 - \exp\left(-\frac{x}{l_a}\right) \right) \quad (2.12)$$

iii) Diffusion and advection

Now we assume that both transport mechanisms are important. To obtain the general solution we proceed in a similar way as in case of diffusion-dominated soil, considering the Darcy's velocity constant.

The characteristic equation correspondig to Eq. A1.1 is

$$m^2 - \frac{v}{\varepsilon D_e} m - \frac{\lambda_{Rn}}{D_e} = 0 \quad (\text{A1.14})$$

which has two single real solutions:

$$m = \frac{v}{2\varepsilon D_e} \pm \sqrt{\left(\frac{v}{2\varepsilon D_e}\right)^2 + \frac{\lambda_{Rn}}{D_e}} \quad (\text{A1.15})$$

A particular solution of the general equation is

$$C_{g,p} = \frac{G}{\lambda_{Rn}} = C_\infty \quad (\text{A1.16})$$

and therefore, the general solution of Eq. A1.1 is

$$C_g = A \exp\left[\left(\frac{v}{2\varepsilon D_e} + \sqrt{\left(\frac{v}{2\varepsilon D_e}\right)^2 + \frac{\lambda_{Rn}}{D_e}}\right)x\right] + B \exp\left[\left(\frac{v}{2\varepsilon D_e} - \sqrt{\left(\frac{v}{2\varepsilon D_e}\right)^2 + \frac{\lambda_{Rn}}{D_e}}\right)x\right] + C_\infty \quad (\text{A1.17})$$

assuming again the same boundary conditions and noting that

$$\left| \sqrt{\left(\frac{v}{2\varepsilon D_e}\right)^2 + \frac{\lambda_{Rn}}{D_e}} \right| > \left| \frac{v}{2\varepsilon D_e} \right| \quad (\text{A1.18})$$

we obtain the following general solution

$$C_g = C_\infty \left\{ 1 - \exp\left[\left(\frac{v}{2\varepsilon D_e} - \sqrt{\left(\frac{v}{2\varepsilon D_e}\right)^2 + \frac{\lambda_{Rn}}{D_e}}\right)x\right] \right\} \quad (\text{A1.19})$$

which, using the already defined diffusion and advection lengths, can be re-written as

$$C_g(x) = C_\infty \left\{ 1 - \exp\left[\frac{1}{2l_d^2} (l_a - \sqrt{l_a^2 + 4l_d^2})x\right] \right\} \quad (2.14)$$

and we define therefore the "migration distance" as a typical distance that radon can migrate in the soil and in which radon concentration is reduced a factor $(1-e^{-1})$ compared with the deep soil radon concentration.

$$M_d = \frac{1}{2} \left(l_a + \sqrt{l_a^2 + 4l_d^2} \right) \quad (2.15)$$

If, to be more realistic, we impose that radon concentration at $x=0$ has a given value, C_0 , different than zero, we obtain the following values for the coefficients A and B from expression (A1.17):

$$A=0 \quad ; \quad B=C_0 - C_\infty \quad (A1.20)$$

so that the solution of Eq. A1.1 and the migration distance are

$$C_g(x) = (C_0 - C_\infty) \exp \left[\frac{1}{2l_d^2} \left(l_a - \sqrt{l_a^2 + 4l_d^2} \right) x \right] + C_\infty \quad (2.16)$$

$$M_d = \left(1 - \frac{C_0}{C_\infty} \right) \frac{1}{2} \left(l_a + \sqrt{l_a^2 + 4l_d^2} \right) \quad (2.17)$$

A1.2 Derivation of Eqs. (2.19), (2.20), (2.24), (2.25) and (2.26)

In the case of the transport through the building materials, only diffusion is a relevant mechanism, so that the steady-state one dimensional transport equation for radon in building materials is (A1.3), which, using the diffusion length of the material ($l_{d,m}$), can be written as

$$\frac{d^2 C_m}{dx^2} - \frac{1}{l_{d,m}^2} C_m = - \frac{G_m}{\lambda_{Rn}} \frac{1}{l_{d,m}^2} \quad (2.18)$$

where G_m is the generation term in the material ($\text{Bq} \cdot \text{m}^{-3} \cdot \text{s}^{-1}$)

$$G_m = \frac{A_{Ra,m} \rho_m f_m}{\varepsilon_m} \lambda_{Rn} \quad (A1.21)$$

C_m is the interstitial radon concentration in the material ($\text{Bq} \cdot \text{m}^{-3}$).

$A_{Ra,m}$ is the radium content of the material ($\text{Bq} \cdot \text{kg}^{-1}$).

ρ_m is the bulk density of the material ($\text{kg} \cdot \text{m}^{-3}$).

f_m is the emanation coefficient of the material (dimensionless).

ε_m is the porosity of the material (dimensionless).

The general solution of this equation is (see expression (A1.9))

$$C_m = A \exp\left\{\frac{x}{l_{d,m}}\right\} + B \exp\left\{-\frac{x}{l_{d,m}}\right\} + \frac{G_m}{\lambda_{Rn}} \quad (\text{A1.21})$$

We define the coordinate system such that its origin is in the middle of the building material, as shown in Fig. A1.1. The material width is $2 \cdot w_{1/2}$.

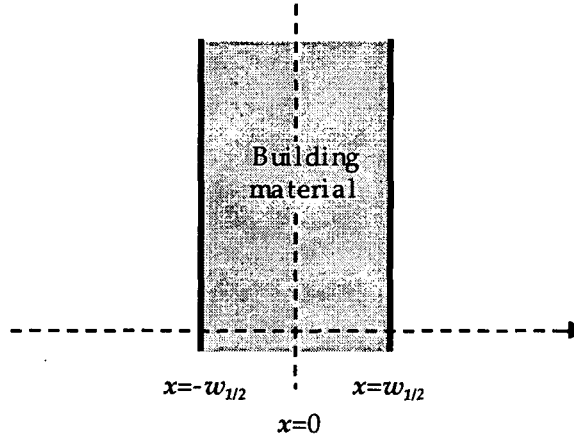


Fig. A1.1: Coordinate system used to describe radon transport in a building material sample

The values of constants A and B depend on the boundary conditions. Following we consider two cases:

i) Radon concentration at both sides of the building material is zero:

$$C_m(w_{1/2}) = C_m(-w_{1/2}) = 0$$

These boundary conditions lead to the system of equations

$$\left. \begin{aligned} A \exp\left(\frac{w_{1/2}}{l_{d,m}}\right) + B \exp\left(-\frac{w_{1/2}}{l_{d,m}}\right) + \frac{G_m}{\lambda_{Rn}} &= 0 \\ A \exp\left(-\frac{w_{1/2}}{l_{d,m}}\right) + B \exp\left(\frac{w_{1/2}}{l_{d,m}}\right) + \frac{G_m}{\lambda_{Rn}} &= 0 \end{aligned} \right\} \quad (\text{A1.22})$$

The solution of this system is

$$A = B = -\frac{G_m}{\lambda_{Rn}} \frac{1}{\exp\left(\frac{w_{1/2}}{l_{d,m}}\right) + \exp\left(-\frac{w_{1/2}}{l_{d,m}}\right)} \quad (\text{A1.23})$$

Then, the general solution of Eq. (2.18) is

$$C_m = \frac{G_m}{\lambda_{Rn}} \left[1 - \frac{\exp\left(\frac{x}{l_{d,m}}\right) + \exp\left(-\frac{x}{l_{d,m}}\right)}{\exp\left(\frac{w_{1/2}}{l_{d,m}}\right) + \exp\left(-\frac{w_{1/2}}{l_{d,m}}\right)} \right] = \frac{G_m}{\lambda_{Rn}} \left[1 - \frac{\cosh\left(\frac{x}{l_{d,m}}\right)}{\cosh\left(\frac{w_{1/2}}{l_{d,m}}\right)} \right] \quad (2.19)$$

The exhalation rate (E) at the surface of the building material can be obtained by applying the Fick's law:

$$\begin{aligned} E(x=w_{1/2}) &= -D_e \varepsilon_m \frac{dC_m}{dx} \Big|_{x=w_{1/2}} = -l_{d,m}^2 \lambda_{Rn} \varepsilon_m \frac{G_m}{\lambda_{Rn}} \left(-\frac{\sinh\left(\frac{x}{l_{d,m}}\right)}{\cosh\left(\frac{x}{l_{d,m}}\right)} \right) \frac{1}{l_{d,m}} \Big|_{x=w_{1/2}} = \\ &= l_{d,m} \varepsilon_m G_m \tanh\left(\frac{w_{1/2}}{l_{d,m}}\right) = l_{d,m} \rho_m A_{Ra,m} f_m \lambda_{Rn} \tanh\left(\frac{w_{1/2}}{l_{d,m}}\right) \end{aligned} \quad (2.24)$$

The exhalation rate at the other side ($x=-w_{1/2}$) has the same value but an opposite sign, according to the coordinate system chosen.

ii) Radon concentrations at both sides of the building material are different than zero:

$$C_m(w_{1/2}) = C_R; \quad C_m(-w_{1/2}) = C_L$$

Now the system of equations to be solved is

$$\left. \begin{aligned} A \exp\left(\frac{w_{1/2}}{l_{d,m}}\right) + B \exp\left(-\frac{w_{1/2}}{l_{d,m}}\right) + \frac{G_m}{\lambda_{Rn}} &= C_R \\ A \exp\left(-\frac{w_{1/2}}{l_{d,m}}\right) + B \exp\left(\frac{w_{1/2}}{l_{d,m}}\right) + \frac{G_m}{\lambda_{Rn}} &= C_L \end{aligned} \right\} \quad (A1.24)$$

and its solution is

$$A = \frac{1}{2 \cosh\left(\frac{w_{1/2}}{l_{d,m}}\right)} \left[\frac{C_R + C_L}{2} - \frac{G_m}{\lambda_{Rn}} \right] + \frac{1}{2 \sinh\left(\frac{w_{1/2}}{l_{d,m}}\right)} \frac{C_R - C_L}{2} \quad (A1.25)$$

$$B = \frac{1}{2 \cosh\left(\frac{w_{1/2}}{l_{d,m}}\right)} \left[\frac{C_R + C_L}{2} - \frac{G_m}{\lambda_{Rn}} \right] - \frac{1}{2 \sinh\left(\frac{w_{1/2}}{l_{d,m}}\right)} \frac{C_R - C_L}{2} \quad (\text{A1.26})$$

substituting in (A1.21) the radon concentration field obtained in the material is

$$C_m(x) = \frac{C_R}{2} \left[\frac{\cosh\left(\frac{x}{l_{d,m}}\right) + \sinh\left(\frac{x}{l_{d,m}}\right)}{\cosh\left(\frac{w_{1/2}}{l_{d,m}}\right) + \sinh\left(\frac{w_{1/2}}{l_{d,m}}\right)} \right] + \frac{C_L}{2} \left[\frac{\cosh\left(\frac{x}{l_{d,m}}\right) - \sinh\left(\frac{x}{l_{d,m}}\right)}{\cosh\left(\frac{w_{1/2}}{l_{d,m}}\right) - \sinh\left(\frac{w_{1/2}}{l_{d,m}}\right)} \right] + \frac{G_m}{\lambda_{Rn}} \left[1 - \frac{\cosh\left(\frac{x}{l_{d,m}}\right)}{\cosh\left(\frac{w_{1/2}}{l_{d,m}}\right)} \right] \quad (\text{2.20})$$

and finally, applying again the Fick's law, we obtain expressions (2.25) and (2.26)

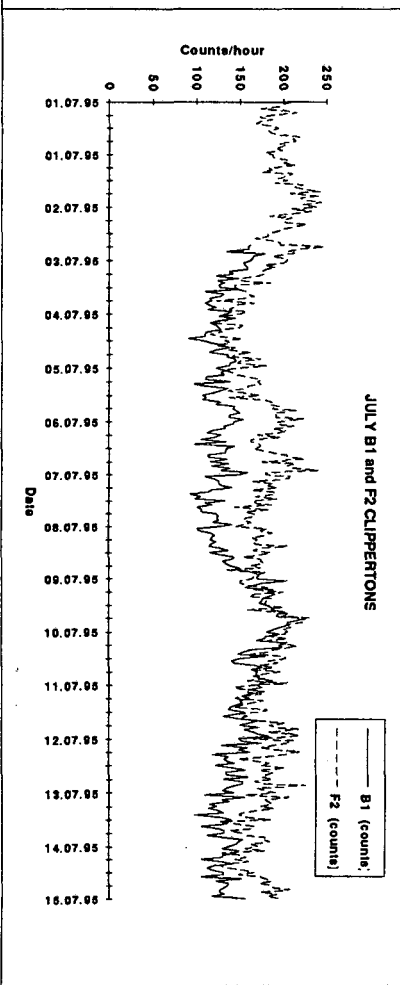
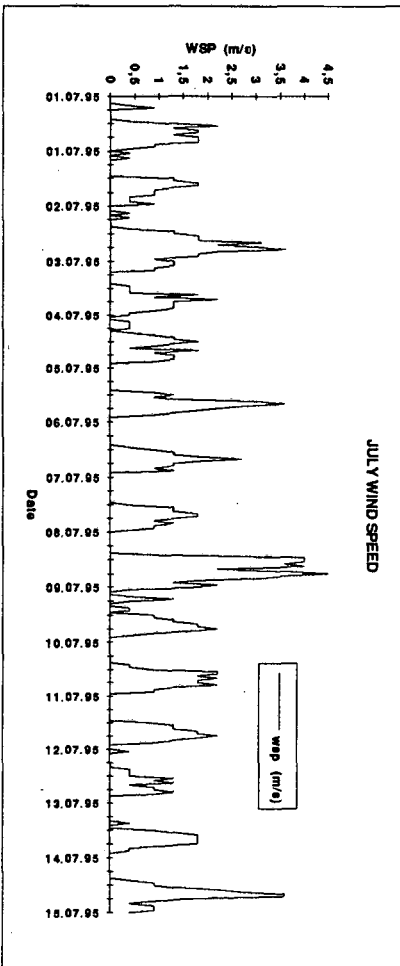
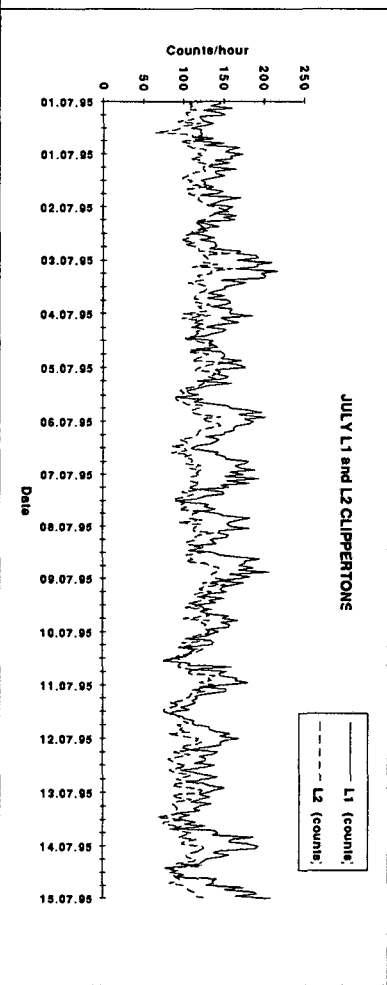
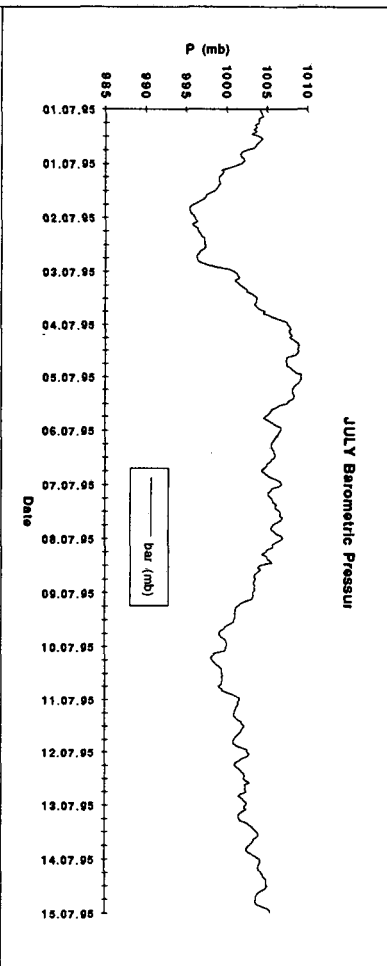
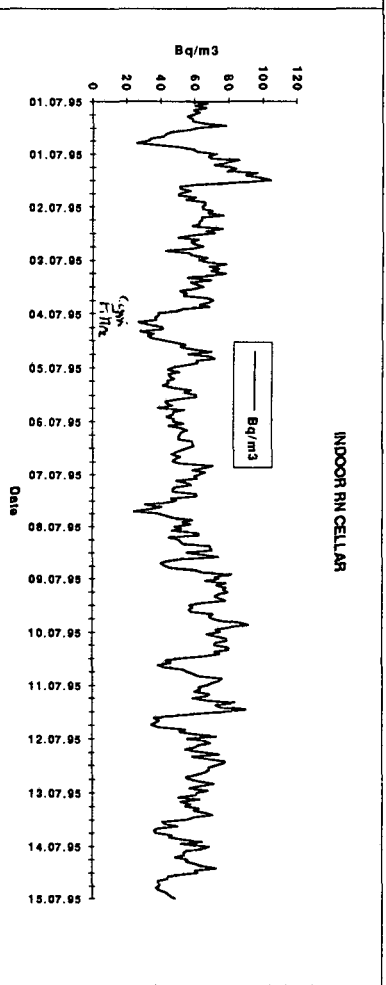
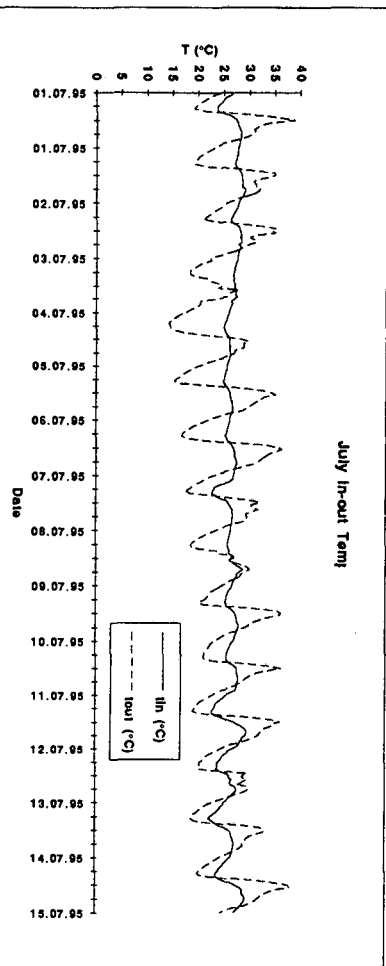
$$E(x = w_{1/2}) =$$

$$= \lambda_{Rn} A_{Ra,m} \rho_m f_m l_{d,m} \tanh\left(\frac{w_{1/2}}{l_{d,m}}\right) - l_{d,m} \lambda_{Rn} \epsilon_m \left[\left(\frac{C_R + C_L}{2}\right) \tanh\left(\frac{w_{1/2}}{l_{d,m}}\right) + \left(\frac{C_R - C_L}{2}\right) \cot \operatorname{anh}\left(\frac{w_{1/2}}{l_{d,m}}\right) \right] \quad (\text{2.25})$$

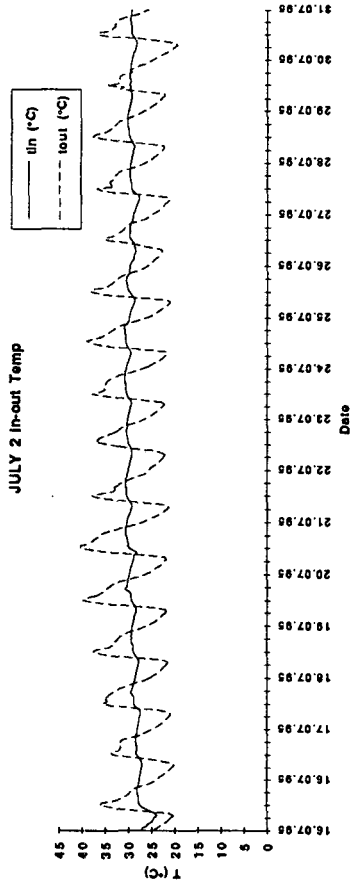
$$E(x = -w_{1/2}) =$$

$$= \lambda_{Rn} A_{Ra,m} \rho_m f_m l_{d,m} \tanh\left(\frac{w_{1/2}}{l_{d,m}}\right) - l_{d,m} \lambda_{Rn} \epsilon_m \left[-\left(\frac{C_R + C_L}{2}\right) \tanh\left(\frac{w_{1/2}}{l_{d,m}}\right) + \left(\frac{C_R - C_L}{2}\right) \cot \operatorname{anh}\left(\frac{w_{1/2}}{l_{d,m}}\right) \right] \quad (\text{2.26})$$

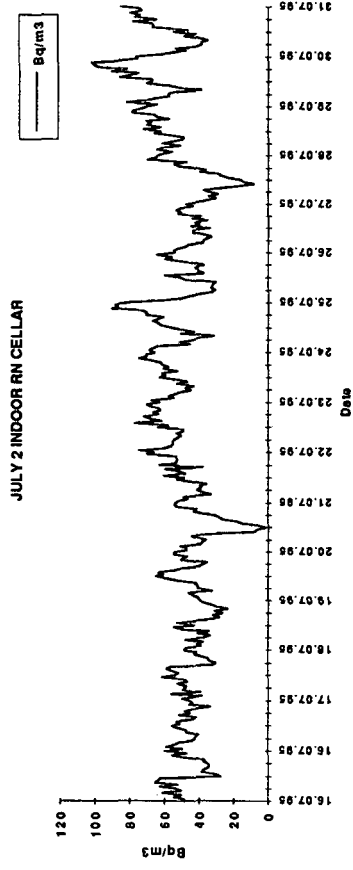
ANNEX 2



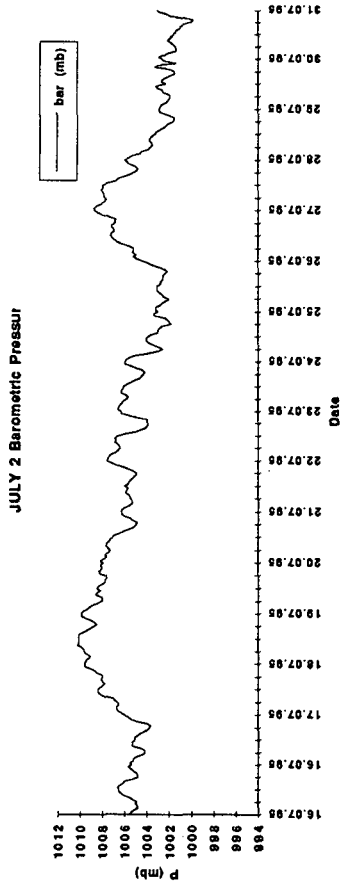
JULY 2 In-out Temp



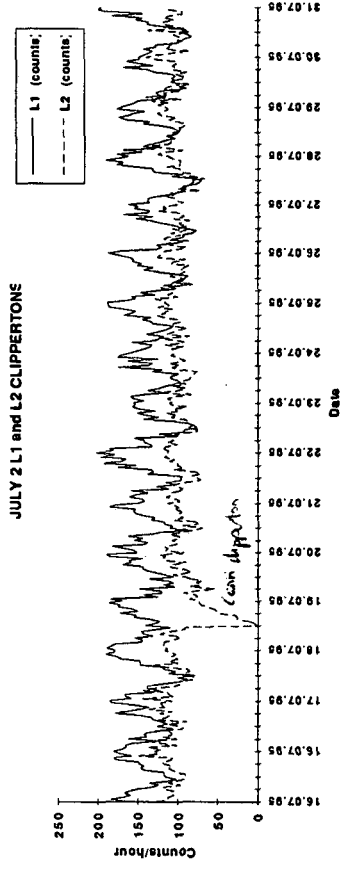
JULY 2 INDOOR RN CELLAR



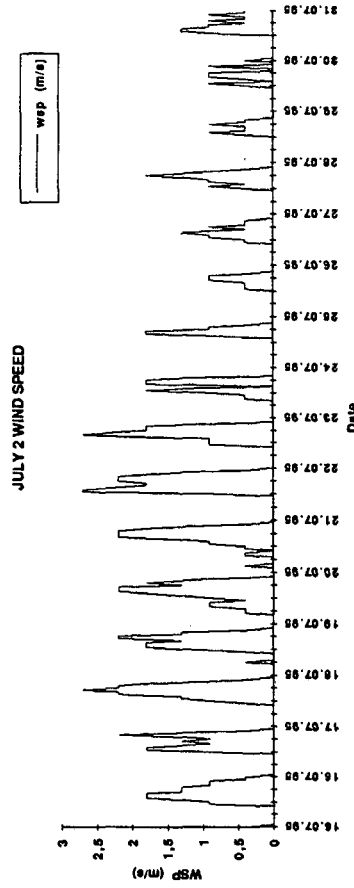
JULY 2 Barometric Pressur



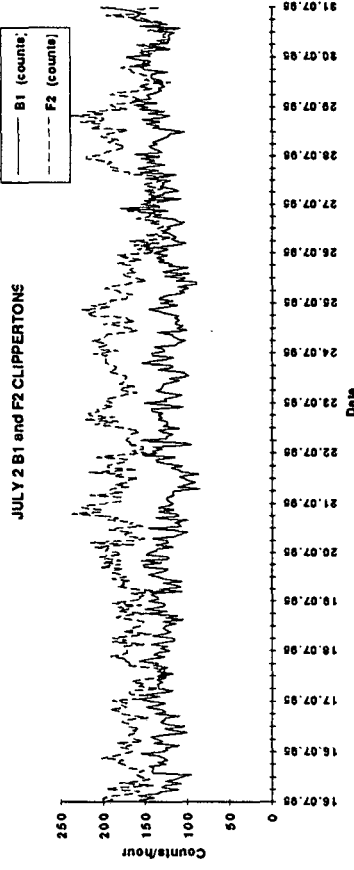
JULY 2 L1 and L2 CLIPPERTONS

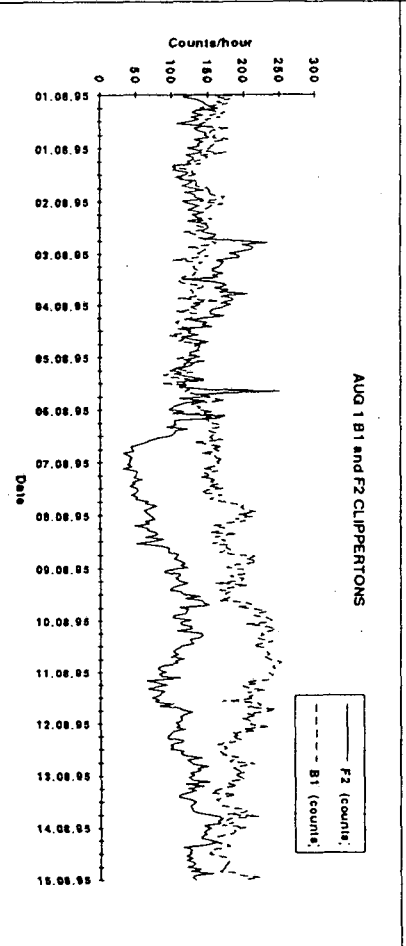
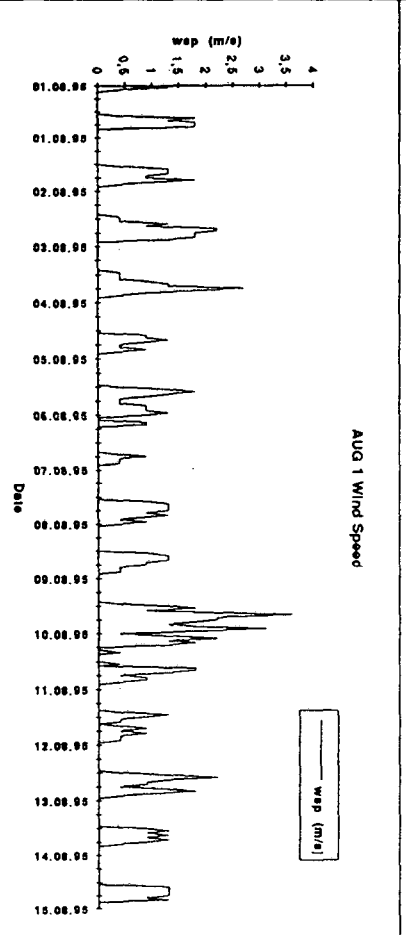
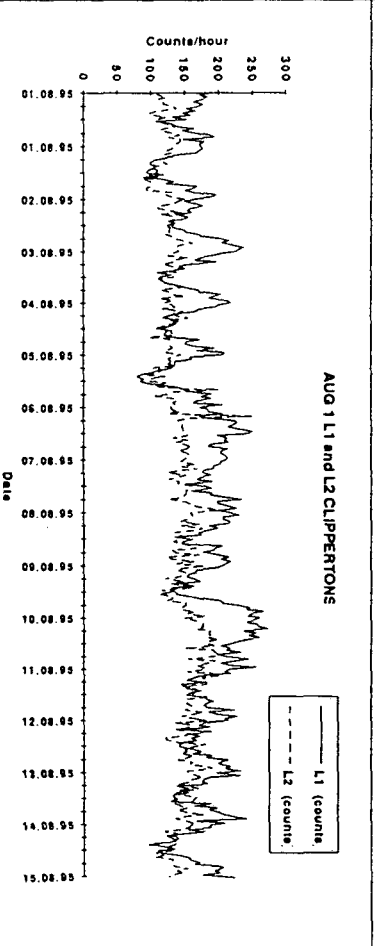
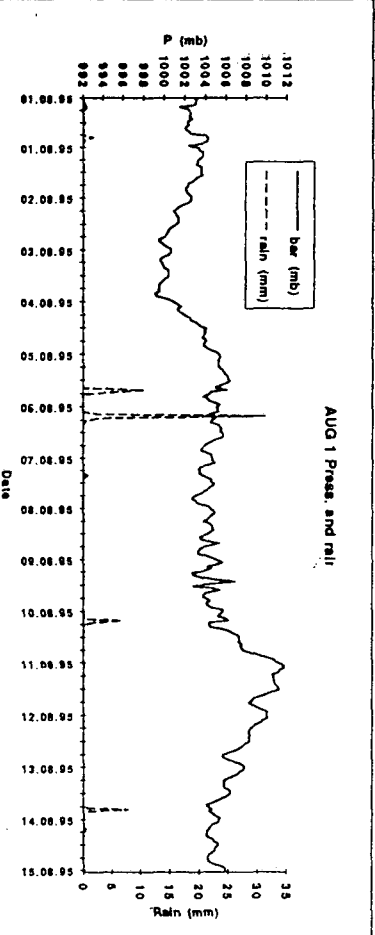
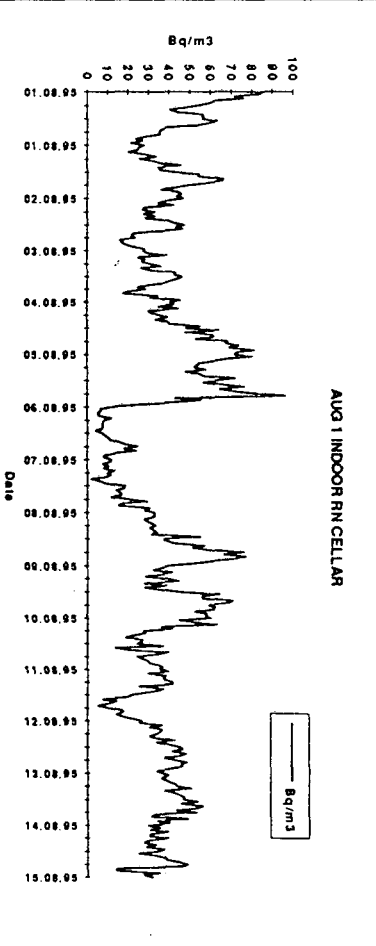
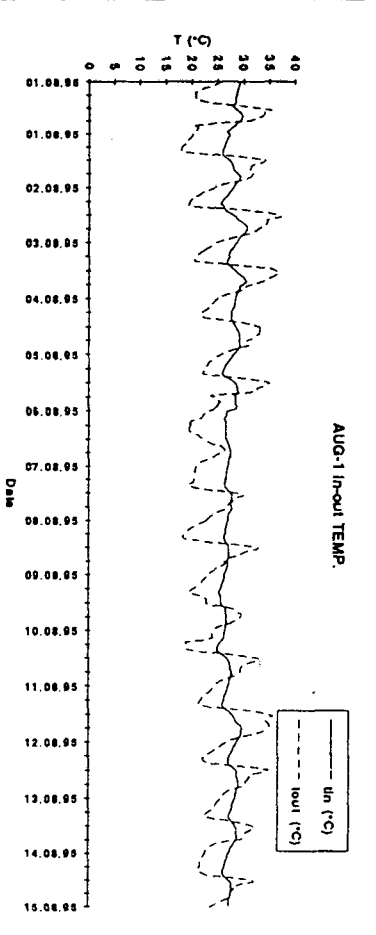


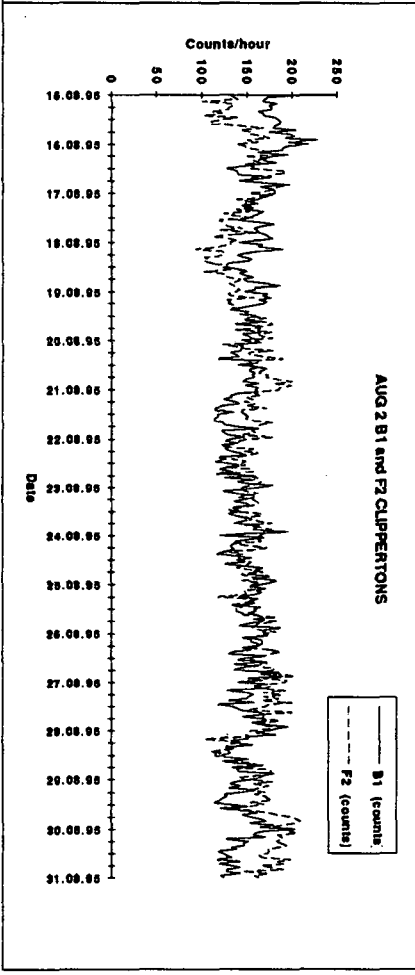
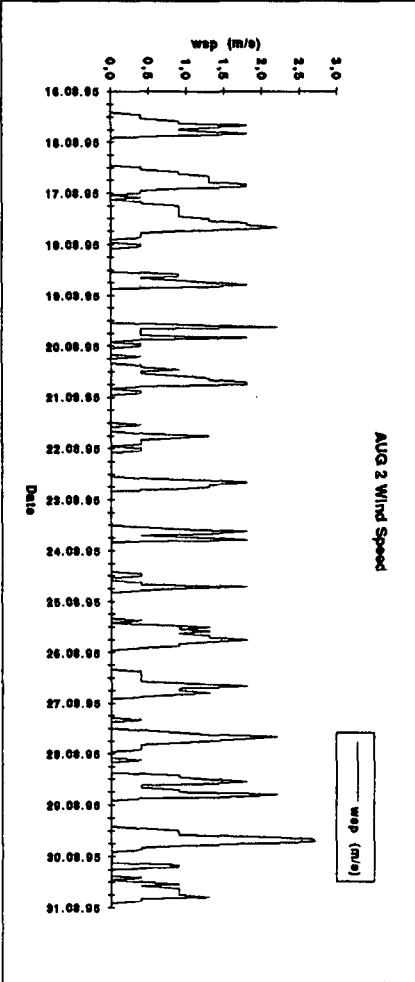
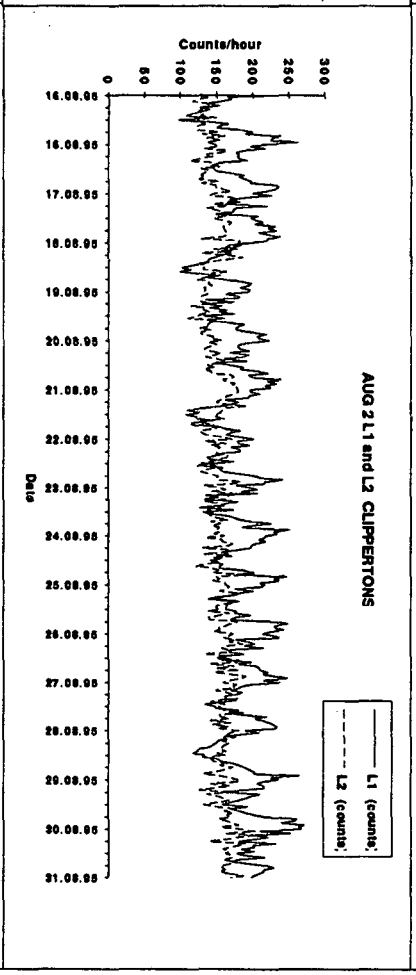
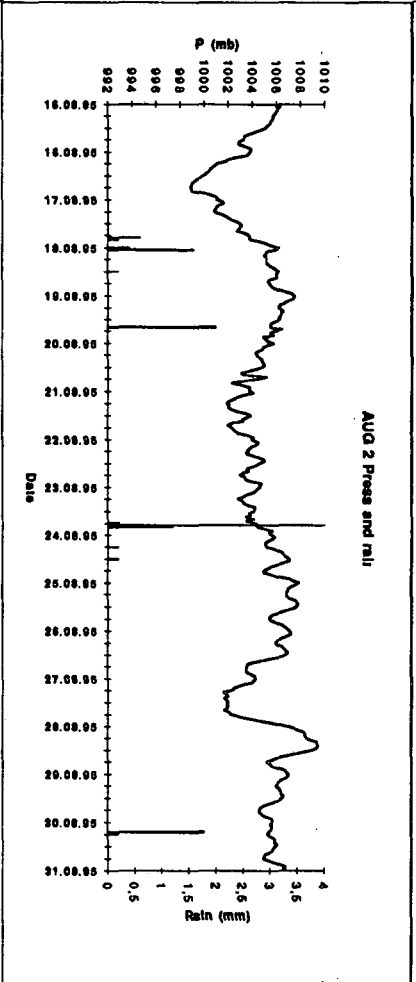
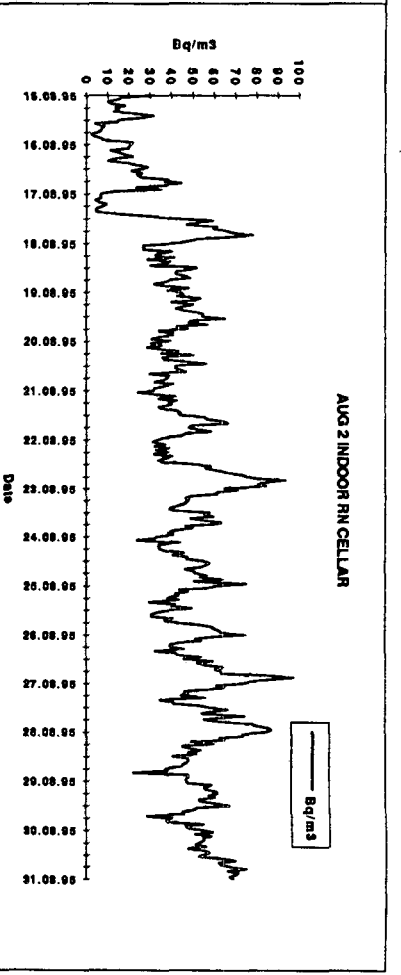
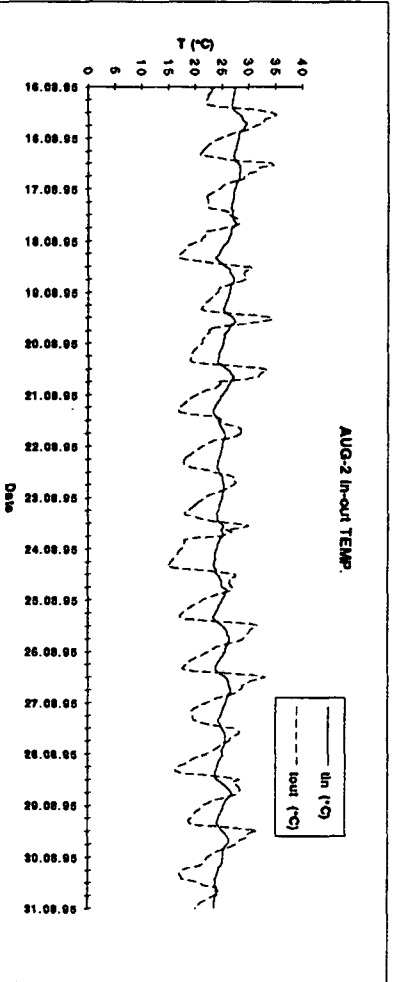
JULY 2 WIND SPEED

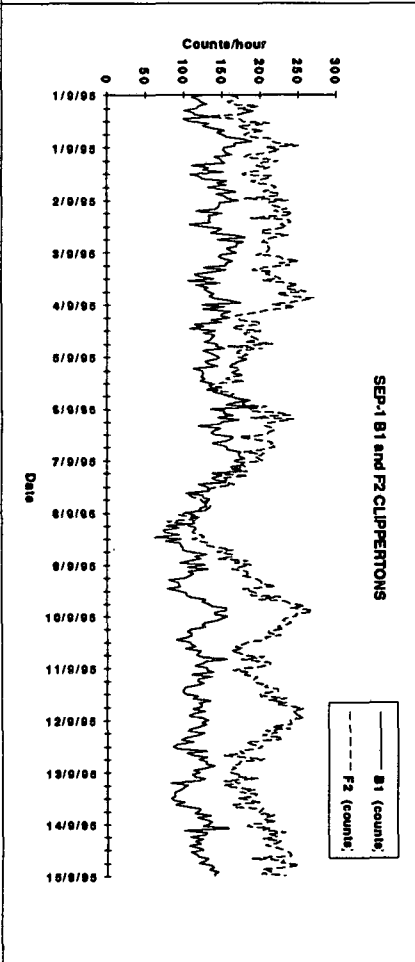
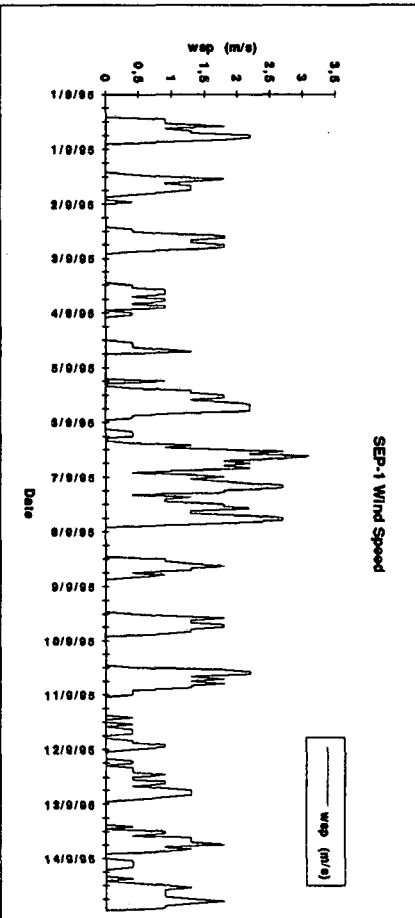
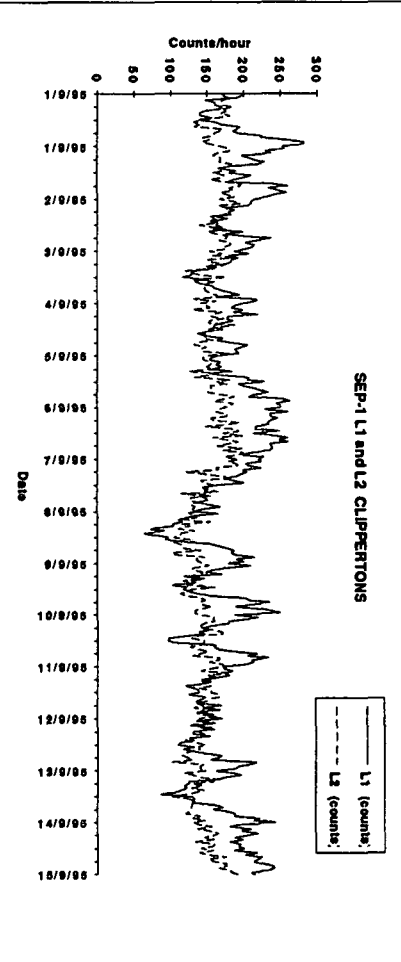
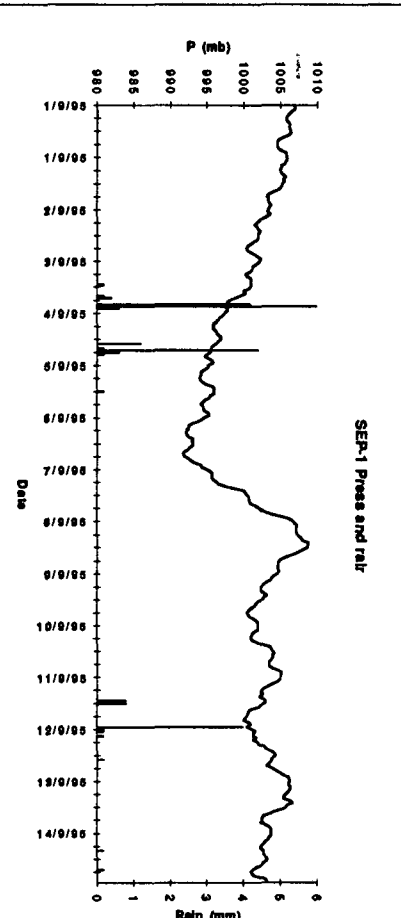
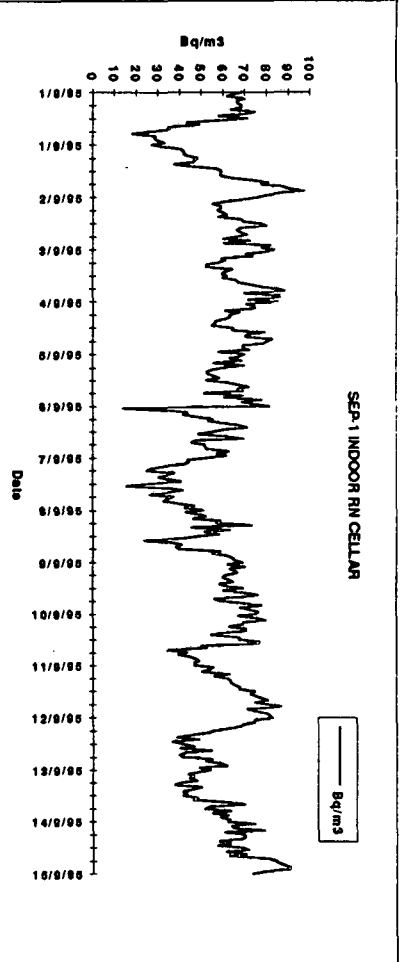
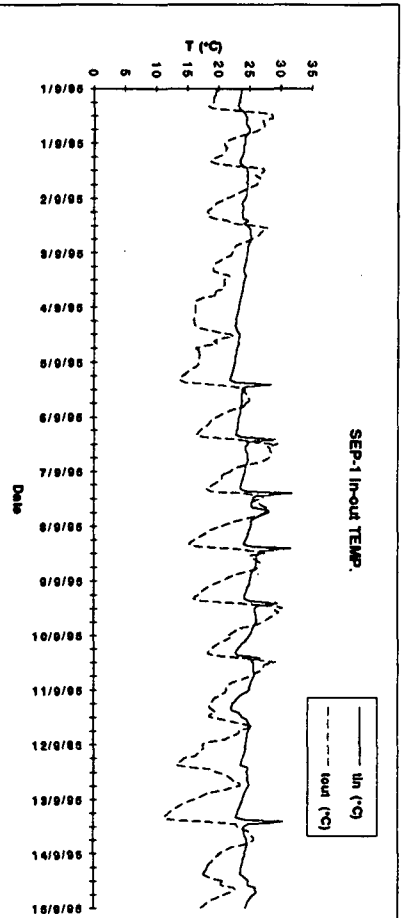


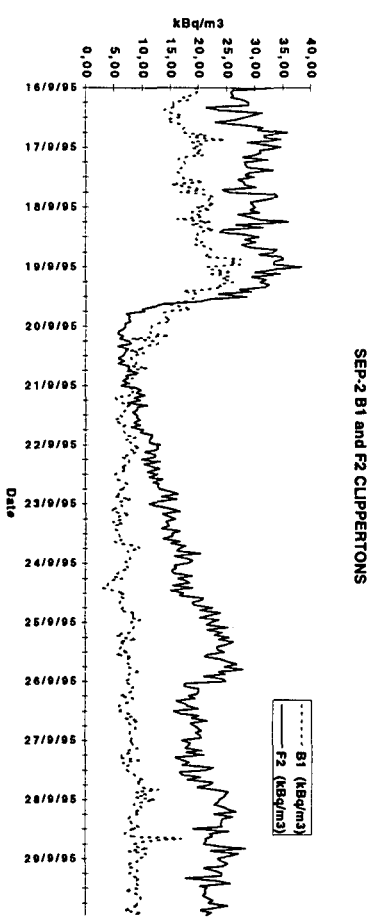
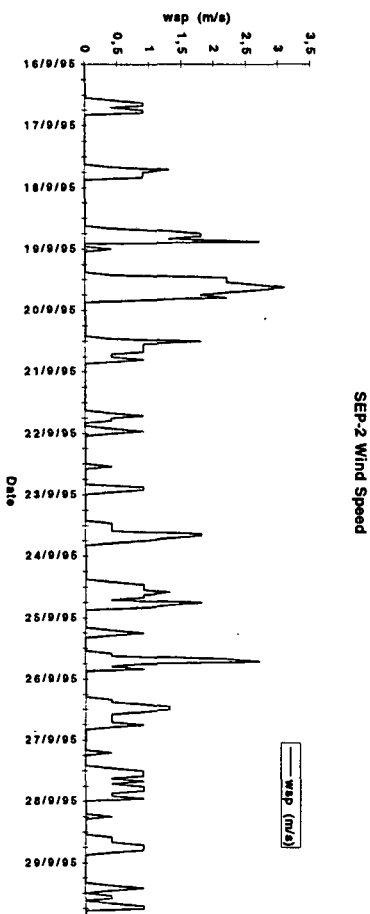
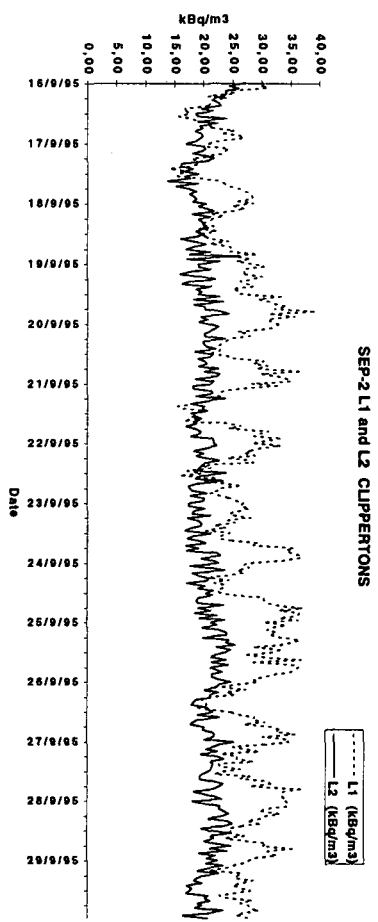
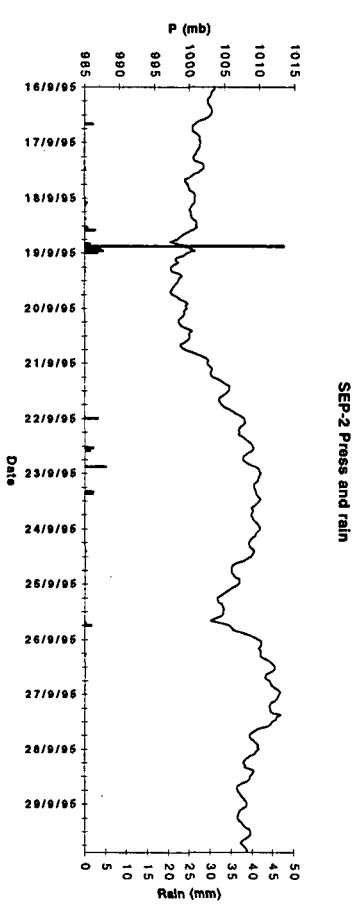
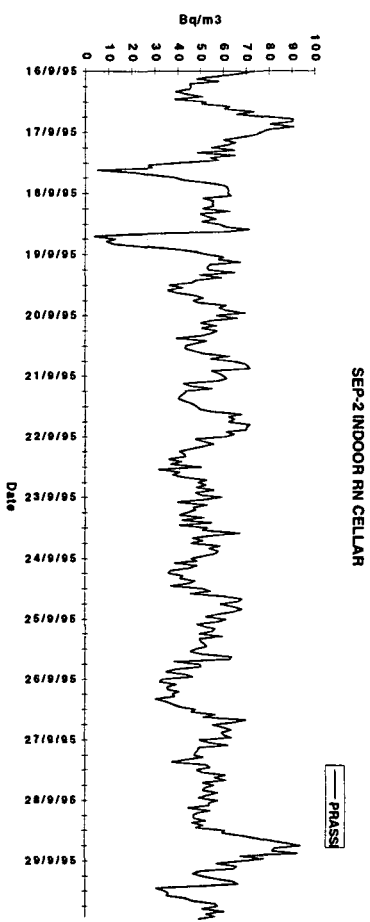
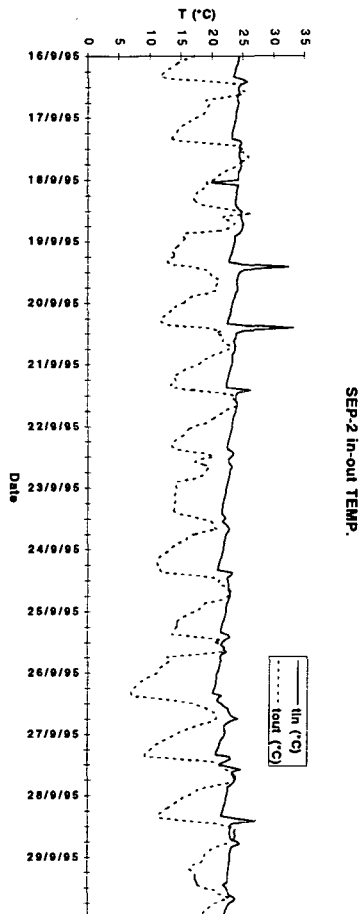
JULY 2 B1 and F2 CLIPPERTONS



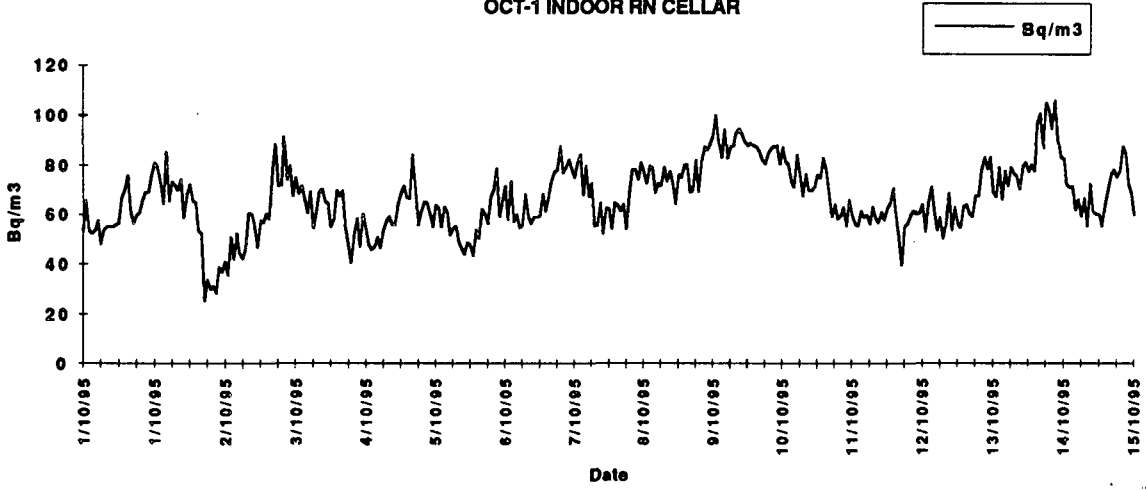




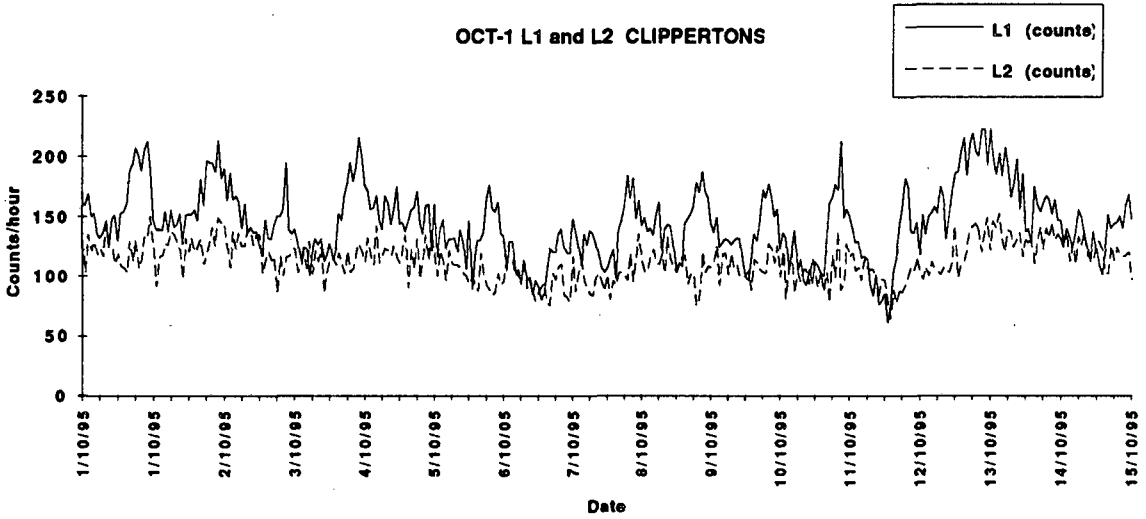




OCT-1 INDOOR RN CELLAR



OCT-1 L1 and L2 CLIPPERTONS



OCT-1 B1 and F2 CLIPPERTONS

